“Isotopes don’t lie; it is our interpretations of them where we tend to disagree.”

James Ehleringer

Supervisors:	Prof. dr. ir. Niko E. C. Verhoest Department of Forest and Water management Ghent University, Belgium
	Prof. dr. ir. Pascal Boeckx Department of Applied Analytical and Physical Chemistry Ghent University, Belgium
Jury Members:	Prof. dr. Anita Van Landschoot (Chairperson) Department of Applied Biosciences Ghent University, Belgium
	Prof. dr. ir. Kathy Steppe Department of Applied Ecology and Environmental Biology Ghent University, Belgium
	Prof. dr. ir. Kristine Walraevens Department of Geology Ghent University, Belgium
	Prof. dr. ir. Wim Cornelis Department of Soil Management Ghent University, Belgium
	Prof. dr. Carlos Oyarzún Instituto de Ciencias de la Tierra Universidad Austral de Chile, Chile
	Prof. dr. Nicolas Brüggemann Institute of Bio- and Geosciences, Agrosphere (IBG-3), Jülich Forschungszentrum, Germany
Dean:	Prof. dr. ir. Marc Van Meirvenne
Rector:	Prof. dr. Anne De Paepe

MSc. Pedro Hervé Fernández

Ecohydrological assessment of catchments covered with old-growth native evergreen forest and eucalyptus plantations in south-central Chile

Thesis submitted in fulfilment of the requirements for the degree of

Doctor (Ph. D.) of Applied Biological Sciences

Academic year 2016-2017

Dutch translation of the title:

Ecohydrologische beoordeling van stroomgebieden bedekt met oude immergroene inheemse bossen en eucalyptus plantages, in zuid-centraal Chili

Please refer to this work as follows:

Pedro Hervé-Fernández (2017). Ecohydrological assessment of catchments covered with old-growth native evergreen forest and eucalyptus plantations, in south-central Chile, Ph. D. Thesis, Faculty of Bioscience Engineering, Ghent University, Ghent, Belgium.

Cover: Bonifacio hill top, Coastal mountain range, Región de los Rios, Chile (2011).

ISBN: 978-90-5989-998-8

Acknowledgements

This dissertation was possible through the collaboration of a number of people from the Laboratory of Hydrology and Water Management, Isotope Bioscience laboratory and Instituto de Ciencias Ambientales y Evolutivas, Universidad Austral de Chile. These lines are devoted to all of them.

My truthful thankfulness goes to my promoters, prof. dr. ir. Niko Verhoest and prof. dr. ir. Pascal Boeckx. I am very grateful for their timely and proficient reviews, heated discussions, advice, ideas and suggestions during the course of my PhD studies. I would like to put especial emphasis on their support, which despite differences in opinion, I could always count on both of them, and it was always the best. Thanks also for their patience. To Prof. Carlos Oyarzun, for constant advice during the course of this work and for giving me the opportunity to participate on the formulation of the FONDECYT project, which turned up in my PhD. Dr. Dries Huygens for helping with the formulation of the project and during manuscript preparation. I would like to thank also to Christophe Brumbt, Chris, was the one in charge of the the sampling, sample processing during my absence…and joining me during field campaigns during dry season, without his efforts this work would have not been the same. To Jorge Morgestern who helped in this work. Thanks for everything.

To my collegues in my (old and new) office, Tu, Lien, Jasper, Niels, Brecht, Katrien, Alexandra, Lisa, Frederick, Douglas, Hans, Diego, Hendrik, Wouter, Matthias, Dominik, Anabelle, Davy and Rudi. Each one of you helped me when I asked for your help, whether super simple math, how to do something, withstand all my “explicit Chilean lenguage” when things did not went as expected, inviting me to field campaigns, course trips or just being there to hear. You cannot imagine how important were all of you.

To my collegues in the lab, my time there was incredible!. Marco, Hari, Marijn, Sebastian, Heather, Steijn, Eric (always giving advice when I asked for it), and Saskia, for all trouble caused by having a shared Ph.D. student and other details. To Jan Vermeulen, who tought me how to use the Picarro…I still remember the day you left, next day the analyser failed and stopped for a week...a circuit board burnt!. However, we (a royal we!) managed to put it up and running again.

A special mention goes to ‘big sister ’Katja and ‘big brother’ Samuel. Both have been a real backbone for me and solved the weirdest questions in “the question of the day”. Katja adopted us in a way I really have no words to thank everything you have done for this thesis, Inés, Catalina and me, of course!.

A los latinos que me (nos) hemos encontrado en Gante y en los lugares mas raros de Bélgica. Andrés y Blanche (i.e. Los Ritter), Ricardo, Mariuxi, Bernardo,

Miguel y Lesle (i.e. Los Arato), Julio, Dora, Mario y Vicky (i.e. Los Veloso) gracias por hacer de esta estadia más agradable con diversas actividades gastronomicas y turisticas. Agradecimientos especiales para los Van-Castillo (Thomas y Catalina), sin su ayuda, esta odisea hubiese tomado un camino muy distinto…probablemente aun estaria navegando…In addition, I would like to thank the Pala's (Mehmet and Melike), you cant imagine the important you have been to me and Inés, you make true the saying "always ready, no matter what!". Por ultimo, me gustaria agradecer a los Hervé-Navarrete (Luispa y Coté) por recibirme(nos) en su casa en aquellos veranos de muestreos con tardes ludicas y gastronomicas. Muchas gracias chiquillos!

Thanks you all, for your help given through this/these odyssey(s).

People I have met in different courses and scientific meetings throughout this period (Lucile Verrot, Natalie Orlowski, Alicia Correa, Jaivime Evaristo…this list could really go forever…). They have been always open to discuss, collaborate and give opinion on the sparsest isotopic topics. Also to the isotope experts which with the best intentions took their time to answer long emails, sent hardcopies of papers and/or simply gave their time to talk in front of a poster, small drawing, listening a presentation and then telling their opinion. Thanks Dr. Jeff McDonnell, Dr. K. Rozanski, Dr. R. Gonfiantini, Dr. J. Gibson, Dr. D. Tetzlaff and Dr. S. Terzer. An especial mention goes to Dr. Joel Gat, who gave a tremendous morale boost when starting with the subject of isotope hydrology (as agreed before, I didn't and will never forget. Thanks!). Their words and comments have been a real beacon during this/these odyssey(s).

To Maria Poca, Lien De Wispelare, Hannes De Deurwaerdeer, Bashar Al-Barri, Shihab Uddin, Jeroen Schreel and Felipe Benavides. I thank all of you for discussing your data, work, or came with questions. You can't imagine how much I have learned discussing your data, and making that this odyssey turned into many nice oddyseys, Thanks indeed!!!.

To my parents (mine and in law: Marcelo, Mónica; Freddy and María Adela), my brothers (real and non-real: Marcelo, Nico, Pelayo; Rodrigo, Mario, Manuel and Cesar), for being there always when needed advice or going to Mordor "no-questions asked" and put their best efforts and comprehension when I needed them most. Thanks a lot for everything.

Finally, I would like to thank my wife Inés Paula who has been always there for discussions on data and countless advice. Además de achichar constantemente in this small boat, despite the many storms we have been through this time. Thanks for always believing in me, and your support. Without it, I wouldn't have finished at all.

This work is dedicated to Catalina, my daughter.

Table of Contents

List of acronyms and symbols in alphabetical order

Acronym/Symbol	Unit	Description
$[^{16}O]$	mol	Oxygen-16 concentration
$[^{18}O]$	mol	Oxigen-18 concentration
$[^{1}H]$	mol	Protium concentration
$[^{2}H]$	mol	Deuterium concentration
^{16}O		Oxygen-16
^{18}O		Oxygen-18
^{1}H		Protium
^{2}H		Deuterium
^{3}H		Tritium
AMU		Atomic mass unit
API	mm	Antecedent Precipitation Index
API_7	mm	7 days Antecedent Precipitation Index
API_{14}	mm	14 days Antecedent Precipitation Index
Bp_x	$kg \cdot ha^{-1} \cdot yr^{-1}$	Bulk precipitation concentration of a nutrient
B_x	$kg \cdot ha^{-1} \cdot yr^{-1}$	Balance, where subscript x is the nutrient species
C_k	unitless	Kinetic resistance
D	$mol \cdot m^{-2} \cdot s^{-1}$	Diffusion of the common species (e.g. $^{1}H_2{}^{16}O$)
d-excess	‰	Deuterium excess
D_i	$mol \cdot m^{-2} \cdot s^{-1}$	Diffusion of the rare species (e.g. $^{2}H_2{}^{16}O$ $^{1}H^{2}H^{16}O$ and $^{1}H_2{}^{18}O$)
DIN	$\mu g \cdot L^{-1}$; $kg \cdot ha^{-1} \cdot yr^{-1}$	Dissolved Inorganic Nitrogen
DNRA		Dissimilatory Nitrate Reduction to Ammonium
DON	$\mu g \cdot L^{-1}$; $kg \cdot ha^{-1} \cdot yr^{-1}$	Dissolved Organic Nitrogen
DV	$kg \cdot ha^{-1} \cdot yr^{-1}$	Dominant Vegetation
EL		Evaporation Line
EL_{sl}	unitless	Evaporation Line slope
EP		*Eucalyptus* plantation

Er_x	unitless	Enrichment ratio
Es	mm	Soil evaporation
ET	mm	Evapotranspiration
f	unitless	Fraction
FGES		Fast Growing Exotic Species
f_{wi}	unitless	Fraction of initial water ($f = 1$)
f_{wr}	unitless	Fraction of water remaining ($f < 1$)
GMWL		Global Meteoric Water Line
GNIP		Global Network of Isotopes in Precipitation
GNIR		Global Network if Isotopes in Rivers
H		Hydrogen
h	unitless	Normalized air humidity to evaporating surface temperature
I		Number of a common molecular or isotopologue when t > 0
I_0		Number of a common molecular or isotopologue when t = 0
Ic	mm	Canopy interception
I_i		Number of a rare molecular species or isotopologue when t > 0
$I_{i,0}$		Initial number of a common molecular isotopologue at t = 0
In_x	$kg \cdot ha^{-1} \cdot yr^{-1}$	Nutrient inputs, where subscript x is the nutrient species
IRIS		Infrared Isotope Spectrometers
kPa	$kg \cdot m^{-1} \cdot s^{-2}$	kilopascal
K-W		Kruskall-Wallis
K_{w-v}	unitless	Thermodynamic reaction constant from vapor to water
LAI	$m^2\ m^{-2}$	Leaf Area Index
lc-excess	‰	Line conditioned excess
lc-excess*	unitless	Line conditioned excess, divided by standard deviation of the measurement
LMWL		Local Meteoric Water Line
$LMWL_{int}$	‰	Local Meteoric Water Line intercept
$LMWL_{sl}$	unitless	Local Meteoric Water Line slope

m	mol	Molar mass of the common atom or isotopologues
m a.s.l.	m	Meters Above Sea Level
MCM		Micro Combustion Module
m_G	mol	Molar mass of a gas (i.e. earth atmosphere 28.8 $g \cdot mol^{-1}$)
m_i	mol	Molar mass of the rare atom or isotopologues
M-W		Mann-Whitney
MWL		Meteoric Water Line
N		Nitrogen
n	unitless	Turbulence parameter
N^0	AMU	Neutrons
NF		Native Evergreen Forest
NH_4^+-N	$\mu g \cdot L^{-1}$; $kg \cdot ha^{-1} \cdot yr^{-1}$	Nitrogen in the form of ammonium
NO_2^--N	$\mu g \cdot L^{-1}$	Nitrogen in the form of nitrite
NO_3^--N	$\mu g \cdot L^{-1}$; $kg \cdot ha^{-1} \cdot yr^{-1}$	Nitrogen in the form of nitrate
O		Oxygen
OLR		Ordinary Linear Regression
Org-N	$\mu g \cdot L^{-1}$; $kg \cdot ha^{-1} \cdot yr^{-1}$	Organic nitrogen
Out_x	$kg \cdot ha^{-1} \cdot yr^{-1}$	Nutrient output, where subscript x is the nutrient species
P		Phosphorus
P^+	AMU	Protons
Pp	mm	Precipitation
PTFE		Polytetrafluoroethylene
Q	mm	Catchment discharge
R	unitless	Ratio of heavy to light isotope
R_A	unitless	Atmospheric water O- or H-isotope ratio
R_{iv}	unitless	Initial gaseous water (i.e. water vapor) O- or H-isotope ratio (i.e.t = 0)
R_{iw}	unitless	Initial liquid water O- or H-isotope ratio (i.e. t = 0)
R_L	unitless	Liquid water O- or H-isotope ratio
RMA		Reduced major axis linear regression

R_{rv}	unitless	Remaining gaseous water (i.e. water vapor) O- or H-isotope ratio
R_{rw}	unitless	Residual liquid water O- or H-isotope ratio
R_S	unitless	Evaporating liquid surface O- or H-isotope ratio
R_v	unitless	Water vapor O- or H-isotope ratio
R_w	unitless	Liquid water O- or H-isotope ratio
SEL		Soil Evaporation Line
SMOW	‰	Standard Mean Ocean Water
SRP	$\mu g \cdot L^{-1}$; $kg \cdot ha^{-1} \cdot yr^{-1}$	Soluble reactive phosphorus
T	mm	Transpiration
TF	mm	Throughfall
TF_x	$\mu g \cdot L^{-1}$	Throughfall precipitation concentration of a nutrient
TN	$\mu g \cdot L^{-1}$; $kg \cdot ha^{-1} \cdot yr^{-1}$	Total nitrogen
TP	$\mu g \cdot L^{-1}$; $kg \cdot ha^{-1} \cdot yr^{-1}$	Total phosphorus
TWW		Two Water Worlds
VSMOW	‰	Vienna Standard Mean Ocean Water
VSMOW2	‰	Vienna Standard Mean Ocean Water since 2009
WS-CRDS		Wave Scanned Cavity Ring Down Spectrometer
WVC	$kg \cdot ha^{-1} \cdot yr^{-1}$	Weighted Vegetation Cover
XWL		Xylem Water Line
ZPE	$Kcal \cdot mole^{-1}$	Zero point energies
α	unitless	Equilibrium fractionation factor
$\alpha^{*}_{v\text{-}w}$	unitless	Equilibrium fractionation factor used for evaporation, from water to vapour
$\alpha^{+}_{w\text{-}v}$	unitless	Equilibrium fractionation factor used for condensation, from vapor to water
$\alpha^{18}O_{v\text{-}w}$	unitless	Equilibrium fractionation factor for ^{18}O for the evaporation process (i.e. from water to vapor)
$\alpha^{18}O_{w\text{-}v}$	unitless	Equilibrium fractionation factor for ^{18}O for the condensation process (i.e. from vapor to water)
α_K	unitless	Kinetic fractionation factor, only used for non-equilibrium processes

$\delta^{18}O_s$	‰	$\delta^{18}O$ sample signature
$\delta^{2}H_s$	‰	$\delta^{2}H$ sample signature
δ_A	‰	Atmospheric water isotopic signature
δ_L	‰	Water column O- or H- isotopic signature
δ_P	‰	Precipitation O- or H- isotope signature
ΔS	mm	Soil compartment water storage
δ_S	‰	Isotopic signature at the evaporating surface
δ_{wi}	‰	Isotope signature of initial water
δ_{wr}	‰	Isotope signature of remaining water
$\delta+$ or δ^-		Positive or negative charge, respectively
$\Delta\varepsilon$	‰	Non-equilibrium enrichment under variable air moisture
$\varepsilon^*_{v\text{-}w}$	‰	Enrichment under equilibrium conditions for evaporation (i.e. from water to vapor)
$\varepsilon^+_{w\text{-}v}$	‰	Enrichment under equilibrium conditions for condensation (i.e. from vapor to water)
ε_K	‰	Kinetic enrichment, only for non-equilibrium processes
ε^T	‰	Total enrichment (i.e. $\Delta\varepsilon + \varepsilon^*_{v\text{-}w}/\alpha^+_{w\text{-}v}$)
θ	unitless	Air moisture weighing factor
ρ	unitless	Resistance coefficient for the common isotope or isotopologues
ρ_i	unitless	Resistance coefficient for the rare isotope or isotopologues
ρ_M	unitless	Resistance coefficient at the laminar layer
$\rho_{M,i}$	unitless	Resistance coefficient at the laminar layer for the rare isotopes or isotopologues
ρ_T	unitless	Resistance coefficient at the turbulent layer
$\rho_{T,i}$	unitless	Resistance coefficient at the turbulent layer for the rare isotopes or isotopologue
Γ	cm	Collision diameter of the common atom or isotopologues
Γ_G	cm	Collision diameter of the common atom or isotopologues in the gaseous phase (i.e. atmosphere)
Γ_i	cm	Collision diameter of the rare atom or isotopologues

Samenvatting

Wijzigingen in landbedekking zijn één van de grootste bedreigingen voor zowel de waterkwaliteit (i.e. de chemische kwaliteit), als de waterkwantiteit (i.e. de waterbalans op stroomgebiedsschaal). Desondanks is er nog steeds weinig kennis over de effecten van deze wijzigingen op de hydrologie van het stroomgebied. In Chili vonden reeds grote veranderingen in landbedekking plaats sinds het begin van de 20ste eeuw, toen kolonisten land vrijmaakten om aan landbouw- en andere economische activiteiten – zoals bosbouw – te kunnen doen. In het begin van de jaren '70 was erosie een groot probleem, vooral in landbouwgebied. Met het oog op het terugdringen van bodemverlies en het herstellen van de bodemorganische lagen werden snelgroeiende exotische boomsoorten geïntroduceerd onder de vorm van industriële plantages. Deze veranderingen in landbedekking hadden echter een impact op zowel de waterkwaliteit als –kwantiteit. Deze impact werd al bestudeerd sinds de eerste hydrologische en biogeochemische studies op stroomgebiedsniveau. In dit onderzoek werd nagegaan hoe de nutriëntenexport (stikstof- en fosforverbindingen) en het watergebruik verschillen tussen natuurlijke immergroene bossen en stroomgebieden beplant met *Eucalyptus nitens*. Voor de nutriëntenexport wordt vooral gekeken naar stikstof- en fosforverbindingen, omdat hoge uitstroom hiervan stroomafwaarts vervuiling kan veroorzaken. De verschillen in watergebruik omvatten de evapotranspiratie op schaal van het stroomgebied en het onderscheid tussen gebruik van regenwater en grondwater. In deze studie werd gebruik gemaakt van stabiele isotopen van water en de chemische analyses van nutriënten in het water.

Deel 1: Probleemstelling:

Hoofdstuk 2 bestaat uit een studie die de basis vormt voor alle vragen en hypotheses die behandeld worden in dit doctoraat. Om het effect van wijzigingen in landbedekking op stikstof- (nitraat (NO_3^--N), ammoniak (NH_4^+-N), organisch stikstof (Org-N), totale stikstof (TN) en fosforverbindingen (oplosbare reactieve fosfor (SRP) en totale fosfor (TP) te analyseren, worden de volumes en de concentraties van doorval en afvoer in het stroomgebied bestudeerd. De studie werd uitgevoerd in drie stroomgebieden die bedekt zijn met natuurlijk bladverliezend bos (D), natuurlijk

immergroen bos (E) en een exotische *Eucalyptus globulus* plantatie (EP). Stalen van bulkneerslag, doorval en stroomafvoer werden genomen op basis van verschillende stormevents in E en EP, gedurende de periode Juni 2009 – Maart 2011; in D daarentegen werden de stalen genomen in de periode Oktober 2009 – Maart 2011. In vergelijking met de bulkneerslag is de doorvalcomponent doorgaans aangerijkt is met nutriënten, met uitzondering van NO_3^--N, dat typisch weerhouden wordt in het bladerdek. Verschillen in nutriënteninput in de verschillende stroomgebieden worden toegewezen aan een verschillende aanrijking van nutriënten wanneer het water door het bladerdek van de bomen druppelt; naar dit laatste proces zal verder in deze tekst verwezen worden als doorvalverrijking. De oorzaak van deze verschillen ligt in de hoge stratificatiegraad in inheemse immergroene en bladverliezende bossen. Beide stroomgebieden met de inheemse bedekking vertonen de hoogste retentie van TN en TP, in contrast met de *Eucalyptus* plantage, waar een nettoverlies aan TN en TP werd waargenomen. Door problemen met landeigenaars zijn de verdere analyses in de volgende hoofdstukken gebaseerd op nabijgelegen sites. Alle studiegebieden zijn echter dicht bij elkaar gesitueerd (i.e. op een afstand kleiner dan 25 km) en gelegen in de bergketens langs de kust. De vergelijkbaarheid tussen de verschillende studiegebieden kon niet worden nagegaan. De resultaten van de verschillende studiegebieden moeten dus met voorzichtigheid vergeleken worden en niet zomaar gezien worden als herhalingen.

Deel 2: De thesis:

In hoofdstukken 4, 9 en 10 worden de resultaten bekomen in dit PhD onderzoek beschreven. Hoofdstukken 5, 6, 7 en 8 beschrijven in detail hoe de signatuur van stabiele isotopen van de watermolecule kan wijzigen, en hoe deze kan gemodelleerd worden met het oog op verschillende toepassingen. In Appendices A tot en met J worden de wiskundige vergelijkingen, gebruikt in deze thesis, afgeleid. Gebaseerd op de resultaten uit hoofdstuk 2, wordt in hoofdstuk 4 specifiek nutriëntenexport en de scheiding van stroomafvoer in ‘oud’ water (grondwater) en ‘nieuw’ water (regenwater en water van oppervlakkige afvoer) bestudeerd op basis van een neerslagevent op het einde van het droge seizoen en een event in het midden van het natte seizoen. Het gedrag van de verschillende nutriëntenconcentraties (NO_3^--N, NH_4^+-N, Org-N, TN

and TP) gedurende deze twee events zal in dit hoofdstuk worden beschreven. De resultaten in hoofdstuk 4 tonen dat de concentratie van NO_3^--N wordt verdund indien de afvoer toeneemt, wat een duidelijke aanwijzing is dat het geëxporteerde NO_3^--N moeilijk beschikbaar is voor zowel oud of nieuw water; of dat het volume van de NO_3^--N bron relatief klein is. Org-N en TP vertoonden echter het tegenovergestelde gedrag, wat aangeeft dat beiden hydrologisch beschikbaar zijn. De belangrijkste conclusie van dit hoofdstuk is dat gedurende neerslagevents nitraat niet hydrologisch beschikbaar is, terwijl organisch stikstof dit wel is. Deze beschikbaarheid kan gelinkt worden aan de grootte van de bodemporiën, wat verder gelinkt is aan bronnen waaruit bomen hun water tappen. Dit laatste wordt geanalyseerd in hoofdstuk 9.

Uit welke bodemcompartimenten bomen hun water halen is een van de grote kennishiaten in de (eco)hydrologie en ecofysiologie. Recente studies tonen aan dat bomen water tappen uit verschillende compartimenten in de bodem. De hierop gebaseerde “twee-water-werelden” hypothese (TWW) suggereert dat planten water opnemen dat gebonden is aan bodempartikels, terwijl stromen en grondwater gevoed worden uit een tweede compartiment, typisch benoemd als “plant-beschikbaar water” of het mobiele water. Door gebruik te maken van een “*dual stable isotope*” benadering (i.e. $\delta^{18}O$ en $\delta^{2}H$), wordt in hoofdstuk 9 de “twee-water-werelden” hypothese getest door de seizoenale oorsprong van neerslagwater onttrokken door een oud inheems immergroen bos en een *Eucalyptus nitens* plantage te analyseren.

In het laatste hoofdstuk van deze thesis (hoofdstuk 10) wordt de schatting van verdamping uit de bodem, en zijn scheiding van de totale evapotranspiratie component op stroomgebiedsniveau beoogt. Evapotranspiratie is de moeilijkste component van de waterbalans op stroomgebiedsniveau om te schatten, meten of modelleren. Dit kan best gebeuren aan de hand van modellen, maar daarvoor moeten grote hoeveelheden data verzameld worden met een hoge frequentie en over lange tijdsperiodes. Het voordeel aan modellen is echter dat het mogelijk is om dagelijkse schattingen van zowel verdamping uit de bodem als transpiratie te bekomen. In deze thesis wordt een methode voorgesteld gebaseerd op de Rayleigh vergelijking, als een goedkoop en repliceerbaar alternatief, voor de schatting van de verdamping uit de bodem om stroomgebiedsschaal.

Summary

Land cover changes pose the biggest threat to water quality (i.e. water chemistry) and water quantity (i.e. catchment water balance), yet these effects are still poorly understood. In Chile, land cover changes have taken place since the early 1900's, where colonists cleared land to develop agriculture and other economic activities such as forestry. At the beginning of the 1970's erosion was a big problem and most of agricultural lands were heavily eroded. In this sense, in order to reduce soil losses and regenerate soil organic layers, hence promoting soil protection, fast growing exotic species were introduced for industrial plantations. However, these land cover changes affected water quality and quantity. Land cover changes effects have been observed since the early days of hydrological and biogeochemical studies at catchment level. The effects on water quality have been various; among them, this work is focussed on nutrient (nitrogen and phosphorus species) export, which pollutes ecosystems downstream. Therefore, the main driver of this work has been the before mentioned differences found on nutrient exportation and catchment evapotranspiration (i.e. evaporation at catchment level and tree water sources) in old growth native evergreen forests and *Eucalyptus nitens* covered catchments. In order to assess these differences, in this work, we use stable isotopes found in the water molecule and nutrient water chemistry.

Part 1: The problem:

In chapter 2, a study is presented which was the start of all questions and hypotheses addressed in this Ph. D. thesis. In order to study the effect of land cover on nitrogen (nitrate (NO_3^--N), ammonia (NH_4^+-N), organic nitrogen (Org-N), total nitrogen (TN)) and phosphorus species (soluble reactive phosphorus (SRP) and total phosphorus (TP)), concentrations and fluxes in throughfall precipitation and stream discharge are assessed. This study was made in a deciduous (D), evergreen (E) (both Chilean native forests), and exotic *Eucalyptus globulus* plantation (EP) covered catchments. Bulk and throughfall precipitation and stream water was sampled on a storm event basis in E and EP, during the period June 2009–March 2011, while in D, the sampling was made during October 2009–March 2011. Main results from this

study shows that most measured nutrients were enriched in throughfall, when compared to bulk precipitation. NO_3^--N was the only exception that was retained by tree canopies. Observed differences in nutrient inputs to studied catchments were attributed to nutrient enrichment when rainfall passes through tree canopies, referred to as throughfall enrichment further in the text. This is due to high multi-stratified canopies in evergreen and deciduous native forests. Both deciduous and evergreen native forest-covered catchments showed the highest retention of TN and TP, in contrast to *Eucalyptus* covered plantation, which showed a net nutrient loss for TN and TP. Unfortunately, due to problems with the landlord further chapters are based on another nearby field site. Even though, all sites are within the coastal mountain range and close to each other (i.e. less than 25 km approx.). The comparability of sites was not especially tested. Hence, results from studied sites should be taken with caution, and not as exact replicates.

Part 2: The thesis:

In chapters 4, 9 and 10 results obtained in this PhD thesis are shown. Chapters 5, 6, 7 and 8 are there to fully explain in detail how stable isotope signatures in the water molecule is altered or changes and can be modelled for its different applications. Appendices from A to J are also included at the end of this thesis, to show how each of the equations and models have been derived. Based on what has been observed in chapter 2, chapter 4 specifically assesses nutrient exportation and separate catchment discharge fluxes into old (i.e. groundwater) and new (i.e. event) water, during storm events at the end of the dry season and another in the middle of the wet season. During these events, the behavior of measured nutrient species (NO_3^--N, NH_4^+-N, Org-N, TN and TP) concentrations is described. Chapter 3 results show that NO_3^--N concentration is diluted as discharge increases, clearly suggesting that exported NO_3^--N is not easily hydrologically accessible to either old or new water; or that the NO_3^--N pool size is limited. Org-N and TP showed the opposite behavior. This suggests that both are hydrologically accessible. Briefly, the importance of this chapter is that during storm events, nitrate is not hydrologically accessible, while organic nitrogen is. This accessibility is linked to small pores (hydrologically inaccessible) and

big pores (hydrologically accessible). This is linked to tree water sources and from where trees are withdrawing water from the soil. This is assessed in chapter 9.

Tree water sources, remain one of the biggest unknowns in current hydrological, ecohydrological and tree physiological knowledge. Recent studies have shown that trees and streams rely on different water compartments within soils. Briefly, the 'two water worlds' (TWW) hypothesis suggests that plants transpire water that is bound to soil particles. While a second compartment, referred to as "plant available water" or mobile water compartment, feeds streams and recharges groundwater. In chapter 9, using a dual stable isotope approach (i.e. $\delta^{18}O$ and $\delta^{2}H$), the 'two water worlds' hypothesis is tested along the seasonal origin of precipitation water being withdrawn by old growth native evergreen trees and *Eucalyptus nitens*.

In the final chapter of this thesis (chapter 10), we assess the estimation of soil evaporation and its separation from the evapotranspiration term in the catchment water balance. As such, evapotranspiration is the most difficult compartment of the catchment water balance to assess, measure or model. Modelling approaches provide a great tool to understand and estimate evaporation and transpiration on a separate basis. However, for that a great amount of data needs to be collected with high frequency and for a long time. Modelling approaches have the advantage that, if soil evaporation is known, it is possible to get daily evaporation and transpiration values. In this thesis, a method based on the Rayleigh equation is porposed as a cheaper and highly replicable method for the estimation of evaporation from soil at catchment scale.

1. Chapter 1: Introduction

Land cover changes play important roles in socio-economic and ecological processes (Mickler *et al.*, 2002; Feddema *et al.*, 2005; Ostrom, 2009; Le Quéré *et al.*, 2013). Water quality (Boeckx *et al.*, 2005; de la Crétaz and Barten, 2007; Oyarzún *et al.*, 2007; Hervé-Fernández *et al.*, 2016a) and quantity (Little *et al.*, 2009; Huber *et al.*, 2010; Zhang, 2012; Iroumé and Palacios, 2013; Frêne *et al.*, 2014) have been linked to land cover changes. These have also affected other ecosystems services (Costanza *et al.*, 1997; Jansson *et al.*, 1999) such as biodiversity in various regions of the world (Sala *et al.*, 2000; Schwartz *et al.*, 2000; Solan *et al.*, 2010).

Even though catchment nutrient and water yields are major ecosystem services for agriculture and economy, these have been dramatically altered by anthropic forcing, such as landscape management, agriculture and climate change (Di Paolo *et al.*, 2001; Farley *et al.*, 2005; Ellison *et al.*, 2012). Sustaining key ecosystem services, while providing a reliable and good quality fresh water supply for agriculture and urban needs is a major challenge faced by managers of anthropic activities dominated catchments (Barbier, 2004; Cao and Zhang, 2014). Water is mainly used by vegetation during the transpiration process (Taiz and Zeiger, 2010; Aemisegger *et al.*, 2013; Jasechko *et al.*, 2013). The used amount is strongly dependent on vegetation physiological characteristics (i.e. leaf area, transpiration capacity, stomatal conductance among others), nutrient constrains (Caldwell *et al.*, 1998; Jeddi *et al.*, 2009; Forrester *et al.*, 2010; Taiz and Zeiger, 2010) and meteorological conditions (Cannell, 1999; Almeida *et al.*, 2007; Farquhar *et al.*, 2007; Seibt *et al.*, 2008; Manzoni *et al.*, 2013). Therefore, altering upstream land cover affects catchment ecosystem services such as catchment nutrient and water yields (Mark and Dickinson, 2008; Yang *et al.*, 2009; Ellison *et al.*, 2012; Ponette-González *et al.*, 2010; Hervé-Fernández *et al.*, 2016a). Modification of natural flow regimes changes the abundance and composition of native vegetation and biological communities, affecting ecosystem services such as nutrient cycling and water storage that depend on particular species or functional groups (Strange *et al.*, 1999; Sala, 2009). Complete restoration of natural hydrological pathways and processes is not an option, usually because those are largely unknown. There is a necessity to find and describe these pathways, in order

to apply specific amendments that are necessary to restore catchment ecosystem services (Strange *et al.*, 1999).

1.1. Catchment nutrient exportation

Land cover changes affect soil stability and hydrological pathways, enhancing nutrient loss and reducing nutrient retention. An important nutrient, nitrogen (N), is crucial to the health of ecological systems. In excess, N becomes a pollutant which can lead to downstream eutrophication of lakes and rivers (Galloway *et al.*, 2004). The rainy temperate forest ecosystems of southern Chile have efficient mechanisms of N retention, especially in the forms of ammonia (NH_4^+-N, to be read as N in the form of ammonium) and nitrate (NO_3^--N, to be read as N in the form of nitrate) (Oyarzún *et al.*, 2004, 2007; Boeckx *et al.*, 2005; Huygens *et al.*, 2007; Hervé-Fernández *et al.*, 2016a). Huygens *et al.* (2008) reported that biogeochemical processes such as heterotrophic nitrification, dissimilatory nitrate reduction to ammonium (DNRA), and a dissolved inorganic nitrogen (DIN) cycle that operates independently of dissolved organic nitrogen (DON) losses are some mechanisms responsible for N retention in Andean forests. Other studies in southern Chile, report that conversion of native forests to exotic fast-growing plantations is likely to decrease N retention on catchments (Oyarzún *et al.*, 2007), particularly that of NO_3^--N (Hervé-Fernández *et al.*, 2016a). Other studies have focused on the hydrological controls on chemical export from undisturbed old-growth (Hedin *et al.*, 1995; Salmon *et al.*, 2001) and second grown evergreen native forest and *E. globulus* plantation covered catchments (Hervé-Fernández, 2011) in south central, Chile.

Intriguingly, literature explaining N exportation and its fluxes remains largely inconsistent (Alexander *et al.*, 2002; Kirchner, 2003; Poor and McDonnell, 2007; Rinaldo *et al.*, 2015). It has been shown that land cover changes had a direct impact on nutrient exports to streams (Vitousek *et al.*, 1997; Peterson *et al.*, 2001; Merino *et al.*, 2005; Cuevas *et al.*, 2006; Little *et al.*, 2015; Hervé-Fernández *et al.*, 2016a). Campbell *et al*. (2004) reported that hydrology, forest cover and land use were the main factors controlling N retention in 24 watersheds in the north-eastern United States. Further, the authors conclude that catchments with thin or porous soils and

high infiltration rates have less capacity to retain N, and no clear relationship was found between vegetation and NO_3^--N and NH_4^+-N retention (Campbell *et al.*, 2004). Goodale *et al*. (2009) reported that NO_3^--N export from old-growth covered watersheds was greater than that of logged and burned watersheds in a region of the United States with moderate N deposition. In a recent study, however, Hervé-Fernández *et al.* (2016a, Chapter 2, in this thesis), describe exactly the opposite of what previously was described by Campbell *et al.* (2004) and Goodale *et al.* (2009) which is, native evergreen forest covered catchments show high soil water infiltration rates and N retention, while an *E. globulus* covered catchment, which showed lower water infiltration rates in soils and a poor N retention.

Usually, nutrient export studies use a simple grab sampling from the studied water body within a predetermined period. Although nutrient export throughout the year is important, it has been hypothesized that during storm events, nutrient concentrations increase (Petry *et al.*, 2002). While it is clear that land cover affects the magnitude of NO_3^--N and other nutrients exported from catchments, it is not clear how storm events affect nutrient dynamics or concentration patterns (Poor and McDonnell, 2007). Studies undertaken in forested catchments have shown that NO_3^--N can be either diluted, concentrated (Poor and McDonnell, 2007) or both in sequential events (Anderson *et al.*, 1997; Chen *et al.*, 2012; Billy *et al.*, 2013) as catchment discharge increases. Hence, there is no clear understanding on NO_3^--N source within soils or pathways leading to the stream (Soulsby *et al.*, 2003; Strahm and Harrison, 2006). A main tenant is that nutrients are mobilized by water (Van Herpe *et al.*, 2002; Chen *et al.*, 2012). Water movement in soils is often conceptualised as 'translatory flow' or 'piston flow' (Hewlett and Hibbert, 1966; Kirchner, 2003), which assumes that water entering the soil as precipitation displaces the water that is previously present, pushing it deeper into the soil and eventually into the stream, like a piston (Gazis and Feng, 2004). Therefore, since Hewlett and Hibbert (1966), water in soils have been considered as well-mixed, hence an homogeneous water compartment. This axiomatic paradigm is used in several hydrological and plant physiology studies. Hence, one could expect that water within a catchment is always connected to each other's compartment (i.e. hillslopes, riparian area, groundwater and stream). Yet, this long lasting axiom, that hydrological and/or ecohydrological connectivity between

vegetation, hill-slope, riparian area and stream is a continuum, has only occasionally been tested, and was rarely found (Ocampo *et al.*, 2006; Hopp and McDonnell, 2009; McGuire and McDonnell, 2010; Geris *et al.*, 2015a; van Meerveld *et al.*, 2015).

Nutrient cycling studies in forested ecosystems of southern Chile have focused on litterfall, litter decomposition and nitrogen mineralization in old-growth evergreen and secondary deciduous *Nothofagus* forests (Staelens *et al*. 2011), soil N dynamics in *Araucaria-Nothofagus* forest affected by severe fire (Rivas *et al.* 2011) and nutrient exportation hydrological controls in catchments with different land use history and vegetation cover (Hervé-Fernández, 2011). However, hydrological controls over nutrient export during individual rainfall events are still poorly known. Therefore, in order to understand and quantify nutrient exports, further insights into hydrological controls on nutrient, especially N species and phosphorus (P) exportation during storm events is needed.

Tracing of water within the water cycle in micro, meso or macro scales, provides information on the pathways and fluxes of water in the environment. These pathways and fluxes are highly sensitive to environmental changes, especially land cover changes (Geris *et al.*, 2015b). Usually, hydrologists and biogeochemists use the water molecule and its stable isotopes of hydrogen (^{2}H and ^{1}H, deuterium and protium, respectively) and oxygen (^{18}O and ^{16}O) to trace different water sources and pathways.

Seminal studies on how water was retained by soils using tritium (Horton and Hawkins, 1965; Zimmermann *et al.*, 1967) showed that not all water was draining and some was retained by soils. Dawson and Ehleringer (1991), using the deuterium to hydrogen content of soil water, stream and xylem waters, indicated that mature trees near a stream, were using water from deeper soil strata and not from the stream as previously hypothesized. A more recent study by Brooks *et al.* (2010) observed that two separate sets of water bodies with different isotopic characteristics exist in trees and streams, and concluded that complete mixing of water within the soil cannot be assumed, at least for Mediterranean regimes as has been done in the past by Hewlett and Hibbert (1966). This gave rise to the “two water worlds” (i.e. TWW) hypothesis, which is decribed as: “*one water world used by trees and seemingly not contributing*

to streamflow and a second, mobile water world related to infiltration, groundwater recharge, hillslope runoff, and streamflow that possessed a character unrelated to the water taken up by trees" (McDonnell, 2014).

1.2. Catchment water yield and balance

Numerous studies worldwide have demonstrated that changes in forest density cause changes in catchment water yields (Van Noordwijk *et al.*, 2014). In general, reducing forest cover increases water yield, while the opposite occurs when increasing forest cover. (Bosch and Hewlett, 1982; Andréassian, 2004; Bruijnzeel, 2004). Usually, hydrologists use a paired catchment approach (see Figure 1.1) to study the hydrological impacts of land cover changes (Bren and Hopmans, 2007) and forestry activities on plantation forest (Waterloo et al., 2007; Webb, 2009).

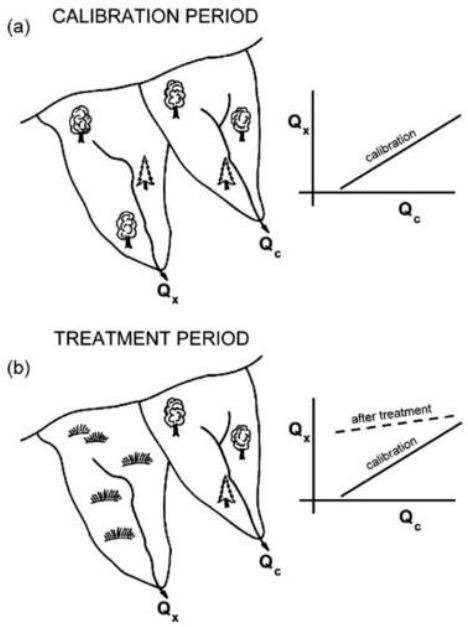

Figure 1.1: Sketch of a paired-watershed experiment. a) Calibration period, studied catchments water outputs are measured. b) Treatment period, where one of the catchments is "treated" (e.g. clear cut or another silvicultural treatment is applied), while the other one is used as a control (modified from Andréassian, 2004).

In a review of experimental paired catchments, Brown *et al*. (2005) concluded that reducing forest cover causes an increase in water yield and that coniferous and *Eucalyptus* spp. forest cover causes a larger increase in water yield when compared to hardwood species. Webb (2009) reported that monthly streamflow increased significantly due to a significant increase in baseflow in *Pinus radiata* (D. Don) plantations and native *Eucalyptus* spp. covered catchments after harvesting in south-eastern Australia.

The quantity of water consumed by plantations is mainly influenced by stand characteristics (i.e. species, age and management), precipitation regime, meteorological conditions (Guarnaschelli *et al.*, 2006; Jiménez-Castillo *et al.*, 2011; Zhang *et al.*, 2013), and soil water retention capacity (Warren *et al.*, 2005; Fritzsche *et al.*, 2006; Wenninger *et al.*, 2010). This last property is mainly important in areas with Mediterranean climate and where precipitation deficits are common during the summer season (David *et al.*, 2013; Barbeta *et al.*, 2014). The interactions of the different water compartments within a catchment are studied using a simple mass water balance method, explained further ahead in the text.

Precipitation has its source from condensed water vapor. Above the oceans, the main source of atmospheric water vapor are the oceans themselves. However, in the mainland, the main process generating water vapor fluxes to the atmosphere is transpiration (Gat and Matsui, 1991; Jasechko *et al.*, 2013; Schlesinger and Jasechko, 2014; Good *et al.*, 2015), although continental precipitation is also fed from other vapor sources, such as water evaporation from soils, water bodies (Gat *et al.*, 1994), water that is intercepted by vegetation land cover (i.e. canopy interception) (Gat, 1996), water vapor coming from the ocean that is transported inland (Gat *et al.*, 2003) and recycled water vapor (Salati *et al.*, 1979). All these sources of water vapor return an important amount of water to the atmosphere (see Figure 1.2), that eventually returns as meteoric water (i.e. snow, hail, rain or fog).

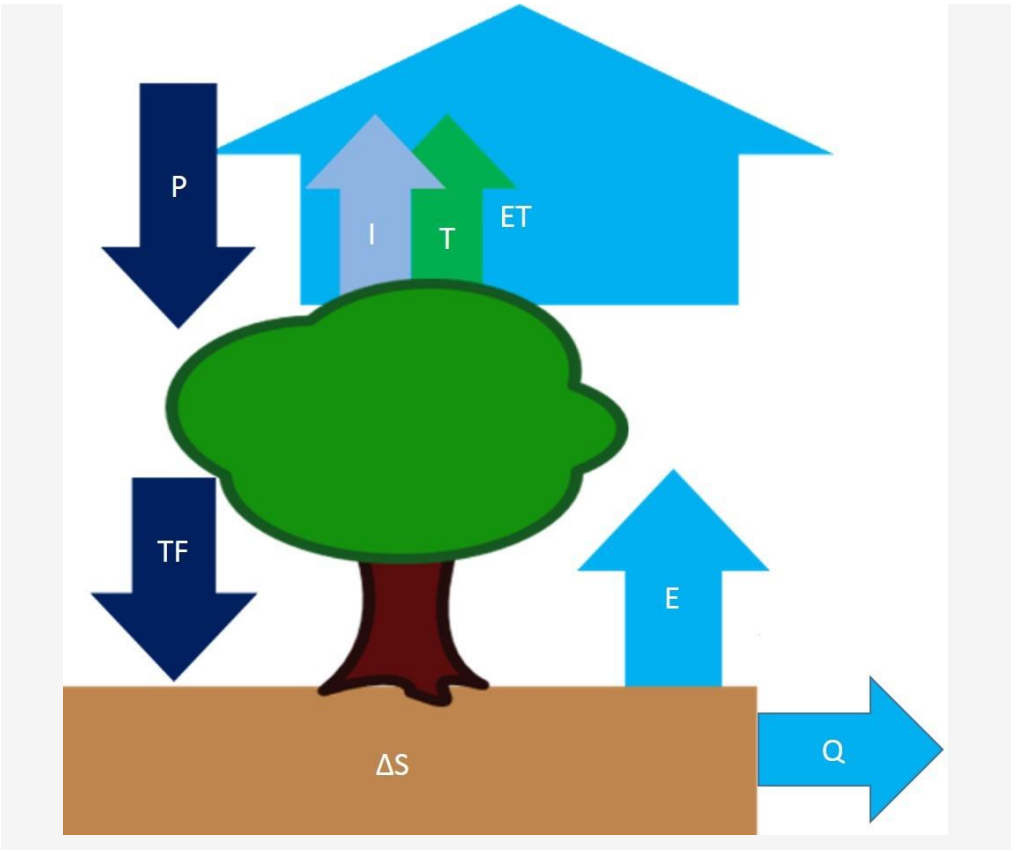

Figure 1.2: Forest hydrological cycle scheme. Where, precipitation (P); throughfall precipitation (TF); variation of soil water retention in time (ΔS); discharge (Q) and evapotranspiration (ET) compounded by: transpiration (T) canopy interception (Ic) and soil evaporation (E).

Since the measurement of vapor fluxes (i.e. transpiration and evaporation) is technically difficult, hydrologists developed a simpler way to study the water cycle within catchments by using the mass balance method (Thorntwaite, 1948; Xu and Singh, 1998; Huber *et al.*, 2010). The underlying assumption of this method is that all water inputs and outputs need to be quantified somehow. Briefly, this method consists of the quantification of: water inputs (as rain, P); outputs (catchment discharge, Q); variation of soil water retention in time, ΔS; and evapotranspiration, ET. In turn, ET is composed of three subcomponents: Canopy interception (Ic), transpiration (T), made by vegetation during photosynthesis and evaporation (E), which is water loss from soil and water bodies through evaporation. Considering all these components, the water balance becomes (Huber et al., 2010):

$$P = Q + (E + T + Ic) + \Delta S \quad (1.1)$$

The above method, however, has an important limitation. Evaporation (from soils and open water) and transpiration can only be estimated as part of a single component called evapotranspiration (or ET), only after solving Eq. (1.1) (Xu and Singh, 1998). Yet, this method fails to isolate transpiration and evaporation values. These are two of the most important components of the hydrological cycle. It allows linking the carbon and nutrient cycles to the catchment water balance (Prentice *et al.*, 2001; Buckley *et al.*, 2002; Cernusak *et al.*, 2003; Ferguson and Veizer, 2007; Freitag *et al.*, 2008), and dynamic process (40 times faster) than other components of the hydrological cycle (Gat and Airey, 2006). Yet, it has been shown that soil evaporation plays only a minor role in catchment water losses (Sutanto *et al.*, 2012; Or *et al.*, 2013; Good *et al.*, 2015). Hence, it is widely assumed that water is mostly lost/consumed by vegetation as transpiration (Jasechko *et al.*, 2013; Good *et al.*, 2015). As such, transpiration is dependent on vegetation physiological characteristics (i.e. leaf area, transpiration capacity, stomatal conductance) (Taylor *et al.*, 2001; Fritzsche *et al.*, 2006; Cernusak *et al.*, 2008; Taiz and Zeiger, 2010). Accordingly, upstream land cover changes along with the promotion of agricultural or forest plantation activities, affect catchment ecosystem services, such as soil water storage, water supply and nutrient cycling. Numerous studies worldwide have demonstrated that changes in forest area and density cause changes in catchment water yields.

In Chile, a conversion of native forest to fast growing exotic species (referred to as FGES) plantations started around 1974 with the introduction of subsidies for plantations and other incentives to private forestry (Little *et al.*, 2009; Iroumé and Palacios, 2013). Estimations indicate that between 1974 and 1992 about 200,000 ha of native forest was substituted by FGES (*Pinus radiata* and *Eucalyptus* spp.). Most of the conversion occurred in the Cordillera de la Costa area (Iroumé and Palacios, 2013; Zamorano-Elgueta *et al.*, 2015; Locher-Krause *et al.*, 2017) (Figure 1.3). In some regions of southern Chile, FGES stands have increased from 12,836 to 103,540 ha since 1985 (Locher-Krause *et al.*, 2017). Even though the forest sector accounts for 3.6% of Chile's gross domestic product, and 12.5% of total exports (INFOR, 2008),

afforestation with FGES has ended up being social, politically and ecologically questionable on the grounds of its supposed impact on the environment and water resources (Huber *et al.*, 1998, 2010; Cannell, 1999; Echeverría *et al.*, 2007; Little *et al.*, 2009; Belmar *et al.*, 2010; Iroumé and Palacios, 2013; Frêne *et al.*, 2014).

Figure 1.3: Typical landscape in the coastal mountain range in south-central Chile.

Oyarzún *et al*. (2011) compared soil hydrological properties, such as water infiltration rates among a second-grown native evergreen forest and a *Eucalyptus globulus* (Labill.) catchment. They found that soil water infiltration rates ranged from 703.3 ± 380 $mm \cdot h^{-1}$ to 76.9 ± 56.7 $mm \cdot h^{-1}$ for March and July, respectively in second-growth native evergreen forest; while under *E. globulus* plantation, soil water infiltration rates ranged from 23.0 ± 19.7 $mm \cdot h^{-1}$, to 6.7 ± 5 $mm \cdot h^{-1}$ for August and April, respectively. Oyarzún *et al*. (2011) concluded that the historical land cover changes, especially in the *E. globulus* plantation, was still reflecting a transition between prairie and plantation, which explains the observed differences in the soil water infiltration rates, when compared to those observed under the second-grown native forest.

Huber *et al*., (1998) compared three eight-year-old *E. nitens* (Deane & Maiden) Maiden. stand densities (1560, 850 and 663 $tree \cdot ha^{-1}$) and found that evapotranspiration was higher for stands with the highest tree density (79%, 75% and

71%, respectively for each density, of the total precipitation inputs). Iroumé and Huber (2000) compared catchment discharge from a *P. radiata* plantation, native evergreen and prairie covered catchments, in the Cordillera de los Andes. Their conclusion was that canopy interception losses reduced significantly catchment discharge during storm events. This effect was higher in the *P. radiata* plantation covered catchment, when compared to the native evergreen forest (Huber and Iroumé, 2001). It is important to state that, whenever interception losses are large, water use efficiency of the stand is inevitably low (Cannell, 1999). However, differences in transpiration among forest types, including *Eucalyptus* spp. are generally related to volume production, that is, given comparable climatic and nutritional conditions, the more water transpired, the greater growth rate of trees (Huber and Trecaman, 2004).

Evapotranspiration studies in the area have found that canopy interception is higher for native evergreen forest than for *Eucalyptus* sp. covered catchments (Huber and Iroumé, 2001; Soto-Schönherr and Iroumé, 2016). In addition, sap flux measurements show that some native trees have an equal or higher sap flow, when compared to *E. nitens* (Rivera, 2010; Jiménez-Castillo *et al.*, 2011). What these studies show, however, is to be interpreted with care, since the used methodology could be underestimating sap fluxes by 60% (Steppe *et al.*, 2010), although both studies used the same methodology. Despite all these similarities, native evergreen covered catchments are able to provide fresh water all year round, while FGES covered catchments does not (Belmar *et al.*, 2010; Iroumé and Palacios, 2013; Frêne *et al.*, 2014; Lara *et al.*, 2015).

The increase of fresh water supply from catchments is important due to the recent and projected growth in water demand in southern Chile for human consumption, irrigation, tourism, salmon farming and hydropower generation (Lara *et al.*, 2003). Studies on the economic value of native Chilean temperate forests emphasize their contribution to maintain a constant fresh water supply, which in turn supports water provision for other important activities, such as those mentioned above (Nahuelhual *et al.*, 2006; Frêne *et al.*, 2014; Lara *et al.*, 2015).

1.3. Hypothesis, research questions and overview

This work has emerged from the problems land cover changes are generating in catchment nutrient exportation and water balance as mentioned in the introduction. On all these topics, there is scattered information usually made on individual catchments, with few exceptions comparing different land covers. In order to assess these topics, suitable tools needed to be used. In this sense, stable isotopes in the water molecule present several advantages over other approaches.

The detailed hypothesis, general and specific objectives are presented below for each of the main topics:

1.3.1. What is the effect of land cover on nutrient input and export?

In order to understand N and P inputs, bulk, throughfall and stream chemistry was analysed. The working hypothesis is that, N and P species composition in throughfall and catchment discharge differs among catchments with different land cover. This is expected since leaf area index (LAI) is much higher in native forests compared to *Eucalyptus* spp. plantations

General objectives:

- Estimate the effect of native or exotic evergreen vegetation on N and P species inputs.
- Estimate N and P nutrient precipitation inputs and stream exports, in each studied catchment.

Specific objectives:

- Determine N and P wet inputs
- Determine N and P species throughfall nutrient enrichment ratios
- Determine stream nutrient loss

1.3.2. What is the relation of N species and catchment discharge?

In order to gain further knowledge on nutrient export from forested catchments, we need to understand its relation with catchment discharge. Therefore, the working hypothesis is the following: All nutrients, especially nitrate, will increase its concentration as catchment discharge increases during a storm event. Therefore, showing an enhanced hydrological access. This will be observed in *Eucalyptus nitens* H.Deane & Maiden covered catchment, but not in catchments covered with old growth native evergreen forest.

General objective:

- Find the relation of N species concentration and catchment discharge during storm events.

Specific objectives:

- Determine N species during storm events in stream water.
- Determine contribution of old and new water in catchment discharge during storm events.

1.3.3. Assessment of the 'two water worlds' hypothesis and tree water sources

The general assumption that vegetation only uses available or mobile water in soils is tested. As mentioned in the introduction and as will be shown in chapter 9 of this thesis, some studies using dual O- and H- stable isotope analysis have led hydrologists and plant physiologists to doubt this long-standing axiom. According to literature trees are not necessarily using the available or the mobile soil water as previously expected (Brooks *et al.*, 2010; Goldsmith *et al.*, 2011; Evaristo *et al.*, 2015, 2016; De Wispelaere *et al.*, 2017; Zhang *et al.*, 2017). Therefore, our working hypothesis is that that old-growth native evergreen tree species withdraw water from a different compartment than that of groundwater or stream water, while *E. nitens* withdraws water from groundwater/stream or a shared common water compartment.

General objective:

- Identify if the main tree source of water is static or mobile.

Specific objectives

- Isotopically characterize mobile water present in soils, in depth
- Characterize xylem water
- Characterize bulk soil water

1.3.4. Water evaporation from soil

Usually, soil evaporation is neglected in the catchment water balance, since it plays a minor role in the water vapor fluxes out of a catchment. Frequently, hydrological models are used for its estimation. However, the need of long-term datasets of several variables (temperature, relative humidity, radiation, etc…) which are usually not available for remote or new study sites. Our working hypothesis is the popular belief that evaporation from soil at catchment scale in *Eucalyptus nitens* covered catchments will be higher when compared to old-growth native evergreen forest.

General objective:

- Determine/estimate the importance of water evaporation from soil on catchments with different land cover.

Specific objectives:

- Determine stable isotope signatures of precipitation inputs.
- Determine stable isotope signature of catchment discharge.
- Determine soil and open water evaporation at catchment scale.

2. Chapter 2: Throughfall and stream nutrient chemistry

Adapted from Hervé-Fernández, P., C. Oyarzún and S. Woelfl. (2016). Throughfall enrichment and stream nutrient chemistry in small headwater catchments with different land cover in southern Chile. Hydrological Processes 30, 4944-4955.

2.1. Abstract

Land cover changes have a great impact on catchment nitrogen (N) and phosphorus (P) fluxes. In this study we wanted to compare different land covers: deciduous (2-Deciduous), evergreen (1-Evergreen) (both native forests) and exotic *Eucalyptus globulus* plantation (1-E. globulus), affected precipitation and stream discharge on N and P species concentrations and fluxes, under a low atmospheric deposition regime in south central Chile. Bulk and throughfall precipitation, and stream water were collected after 41 rainfall events in 1-Evergreen and 1-E. globulus (June 2009 – March 2011), and after 31 rainfall events in 2-Deciduous (October 2009 – March 2011). 2-Deciduous showed the highest throughfall enrichment for all N and P measured species. In contrast, 1-E. globulus showed minimum throughfall enrichment. Total nitrogen (TN) discharge in 1-E. globulus was about 8.6 times higher than that of 1-Evergreen and 2-Deciduous catchments. Stream NO_3^--N concentrations showed the biggest difference, and ranged from 3.4 ± 1.3 $\mu g \cdot L^{-1}$ (E) to 84.9 ± 16.7 and 134.7 ± 36.7 $\mu g \cdot L^{-1}$ (1-E. glublus and 2-Deciduous, respectively). Differences in nutrient throughfall enrichment are probably due to high multi-stratified canopies observed on native forests 1-Evergreen and 2-Deciduous, which also showed the highest retention of TN and TP, in contrast to *Eucalyptus* covered plantation.

2.2. Introduction

N and P are crucial to ecosystem productivity (Thomas *et al*., 2009; Vitousek *et al.*, 2010). Excess these nutrients lead to eutrophication of rivers and lakes (Rabalais *et al*., 2009; Smith 2003). Water quality control is a recognized ecosystem service provided by forests (Alexander *et al*., 2007). Several authors have found that different land cover (Cuevas *et al*., 2006; Oyarzún *et al,.* 2007; Vitousek *et al.,* 2010), forest type (De Schrijver *et al*., 2007) and hydrology (Campbell *et al.*, 2004) affects N and P

cycling in forests. These have a direct impact on nutrient exports to streams. For example, for coniferous and deciduous forest stands at comparable sites in Europe and south central Chile, it was observed that N deposition to the forest floor as well as N loss by leaching below the rooting zone was significantly higher in coniferous stands (Rothe *et al.*, 2002;Oyarzún *et al.,* 2005; De Schrijver *et al.,* 2007).

Native temperate rainforests of southern Chile represent an important global reserve of temperate forest with an extraordinary genetic, phytogeographic and ecological significance (Armesto *et al.*, 2010). These forests cover an area of 13.5 million ha. Native forests in the Valdivian eco-region (35° S through 48° S) have suffered anthropogenic disturbances due to inadequate logging practices, and to agricultural land or fast-growing exotic plantations (FGES) conversion. Historically, the coastal mountain range in south-central Chile (36° to 41° S) has gone through severe land use changes over time (Aguayo *et al*., 2009; Miranda *et al*., 2015). Once native evergreen forests, land changed to agricultural land, mainly as grazing grounds. Subsequently, FGES (mainly *Eucalyptus spp*. and *Pinus radiata*) replaced agricultural activities (Oyarzún *et al.*, 2011). Estimations indicate that between 1974 and 1992 about 200,000 ha of native forest were converted to exotic plantations of *Pinus radiata* and *Eucalyptus sp.* Native forest was replaced by plantations at a rate of 4.5 percent, per year, from 1975 to 2000 (Lara *et al.*, 2006) and most of the conversion was concentrated in the coastal mountain range area. Deciduous *Nothofagus obliqua* (Mirb.) Oerst. native forests also went through a drastic reduction in land cover and diversity reduction (San Martín *et al.,* 1991; Veblen *et al*., 1996). This forest type is poorly represented in the Chilean system of national parks and reserves (SNASPE) (Armesto *et al.*, 1998). However, these small areas have a great significance in biodiversity conservation (Armesto *et al.*, 2010), and probably also in the maintenance of surface and groundwater quality (Oyarzún *et al.*, 2005).

Temperate rain forest ecosystems of southern Chile have efficient mechanisms of retention of essential nutrients, especially ammonium and nitrate (Oyarzún *et al.*, 2004; Huygens *et al.*, 2007). Perakis and Hedin (2002) described that the dominant form of nitrogen in streams, was dissolved organic nitrogen (DON) in unpolluted native forests of southern Chile. However, native forest substitution is associated with rather

drastic logging practices with a large biomass removal, a variable quantity of logging slash on the forest floor, soil erosion and accelerated N mineralization (Fisk and Fakey 1990; Malmer 1993). These actions reduce TN retention within catchments. Oyarzún *et al*. (2007) described that TN stream export was higher than the TN inputs by open-field deposition in catchments converted to FGES. This represents an "opening" of the N cycle by forest conversion to FGES plantations as suggested by Huygens and Boeckx (2009). Since the surface area of eucalypt plantations have grown at an impressive rate, these actions will have a great impact over water provision, stream water quality and over nutrient budgets to maintain primary production in forests and downstream affected water bodies, despite the common assumption of hydrological connectivity between hillslopes and stream. Recent studies have addressed that this assumption is not valid, especially in catchments with a marked dry seasonality. Hillslope-groundwater/stream connectivity only occurs after high rainfall or during certain storm events during the year (Ocampo *et al.*, 2006; Hopp and McDonnell, 2009; McGuire and McDonnell, 2010; Geris *et al.*, 2015a; van Meerveld *et al.*, 2015). Therefore, nutrient balances estimated as done in previous studies could lead to doubtful results (Kirchner, 2003; Rinaldo *et al.*, 2015). However, this methodology still is useful as a level of comparison between catchments, although it assumes connectivity between water from hillslopes and groundwater/stream water throughout the year. In this study, the following hypothesis is tested, N and P species composition in throughfall and catchment discharge differs among catchments with different land cover. The objectives of this study are as follows: (a) to determine changes in the chemical composition of bulk precipitation (BP) while passing through canopies and (b) to determine the annual retention of nitrogen species (NO_3^-−N, NH_4^+−N, Dissolved inorganic nitrogen (DIN), organic-N, and total-N) and phosphorus species (soluble reactive phosphorous [SRP] and total-P) in headwater catchments with different land cover (deciduous and evergreen native forests, and *Eucalyptus globulus* plantation).

2.3. Material and Methods

2.3.1. Study area

For this study, three catchments were monitored at two different sites. On site 1, monitored headwater catchments were "1-Evergreen", covered by a second growth

native evergreen forest, with an area of 3.1 ha at 227-275 m a. s. l., and “1-E. globulus” covered with fast growing exotic species (FGES) cover of *Eucalyptus globulus* Labill., with an area of 5.6 ha at 250-297 m a.s.l. Both catchments were located 2 and 2.6 km (for 1-Evergreen and 1-E. globulus, respectively) from the pacific seashore, respectively. On site 2, the monitored headwater catchment “2-Deciduous” was covered with native deciduous *Nothofagus obliqua* (Birb.) Blume forest and a small area was covered by *Eucalyptus globulus* and *Acacia melanoxylon* R. Br. (20%, see Figure 2.1). This catchment had an area of 10.1 ha at 71-125 m a. s. l., 23.0 km from the coast. All sites were located within the coastal mountain range, southern Chile (39º 50´ S, 73º 10´ W, Figure 2.1). Please note that these sites were only used in this study.

According to (CIREN, 2003), soils in the study area are red clayish, derivatives from ancient volcanic ashes deposited over a metamorphic geological substratum, dominated by micaceous schist and quartz lenses. Soils at site 1 correspond to Asociación Tres Cruces, correponding to series Correltúe, while at site 2 to Serie Los Ulmos, soils are classified as mesic Andic Palehumults and mesic Typic Palehudults (both Ultisols) for site 1 and 2, respectively (CIREN, 2003; FAO, 2015). In general, soils were predominantly well drained, with moderate infiltration rates and predominantly deep (> 100 cm depth) (see Table 2.1). In 1-Evergreen and 1-*E. globulus,* soils were shallow (< 1.0 m depth), while in the deciduous covered catchment, soils were predominantly deep (> 1.0 m). Soils at 1-*E. globulus* catchment were mainly characterized by poor infiltration rates, while 1-Evergreen and 2-Deciduous catchments presented high water infiltration rates (Oyarzún *et al.,* 2011).

The climate in the area of study is rainy temperate. At the meteorological station Isla Teja (25 m a.s.l.), 30 to 40 km from the study sites, the mean annual temperature is 12 °C (January: 17 °C; July: 7.6 °C) and the mean annual precipitation is 1871 mm. Rainfall is concentrated during winter (May–August: 62% of total annual rainfall) and decreases strongly in the summer (January–March: 9%).

Table 2.1: Physical and chemical characteristics of the mineral soil at 1-Evergreen, 1-E. globulus and 2-Deciduous (n = 2 for each site), where, Bulk density was measured using the core method (Sandoval *et al*., 2011). Samples were 6 per horizon from two different soil pits, on each catchment; Infiltration rates measurements were 8, done on a monthly basis using a double ring infiltrometer. OM stands for Organic matter content measured using loss on ignition method at 550 °C for 4 hrs. Kjeldahl-N stands for N = NH_4^+-N + Org-N; while and Olsen-P for available phosphorus (see section 2.3.6.). nd = not determined.

Site	Depth (cm)	Bulk density ($g \cdot cm^{-3}$)	Porosity (%)	Infiltration rate ($mm \cdot hr^{-1}$)	pH	OM (%)	Kjeldahl-N ($mg \cdot kg^{-1}$)	Olsen-P ($mg \cdot kg^{-1}$)
1-Evergreen	0-29	0.53 ± 0.1	80.3 ± 3	236 ± 138	5.0 ± 0.03	19 ± 7.3	19 ± 1.25	1.7 ± 0.1
	29-65	0.76 ± 0.1	71.8 ± 4.7	nd	5.0 ± 0.02	8.1 ± 0.5	15 ± 0.87	1.5 ± 0.5
1-E. globulus	0-29	0.64 ± 0.1	75.8 ± 2.5	14.8 ± 10.6	5.0 ± 0.02	22 ± 0.2	nd	1.6 ± 0.3
	29-65	0.55 ± 0.1	79.5 ± 1.8	nd	5.0 ± 0.03	12 ± 1.2	nd	0.6 ± 0.1
2-Deciduous	0-20	0.66 ± 0.1	69.1 ± 2.8	196 ± 85.1	5.8 ± 0.04	17 ± 3.5	21 ± 1.47	2.4 ± 0.2
	20-40	0.77 ± 0.1	65.7 ± 1.8	nd	5.7 ± 0.02	7.5 ± 0.3	15 ± 1.34	2.0 ± 0.1

2.3.2. Forest cover

At catchment level, 1-Evergreen vegetation was classified as a second growth native evergreen forest, dominated by *Myrtaceae* spp., *Amomyrus luma* (Mol.) Legr. et Kaus (29%), *Amomyrtus meli* (Phil.) Legr. et Kaus (25%), *Laureliopsis phillipiana* (Mol.) Mol. (14%), *Myrceugenia planipes* (Hook. et Arn.) Berg. (13%), *Dyasaphillum diacanthoides* (Less.) Cabrera (7%), *Gevuina avellana* (Molina) Molina (6%), *Lomatia ferrugina* (Cav.) R. Br., *Persea lingue* (Ruiz et Pav.) Nees ex Koop. *Myrceugenia exucca* (DC.) Berg. (2%) and *Aextoxicon punctatum* Ruiz. et Pav. (1%). This catchment also functioned as a source of wood for local residents and as an occasional grazing ground for animals during the winter.

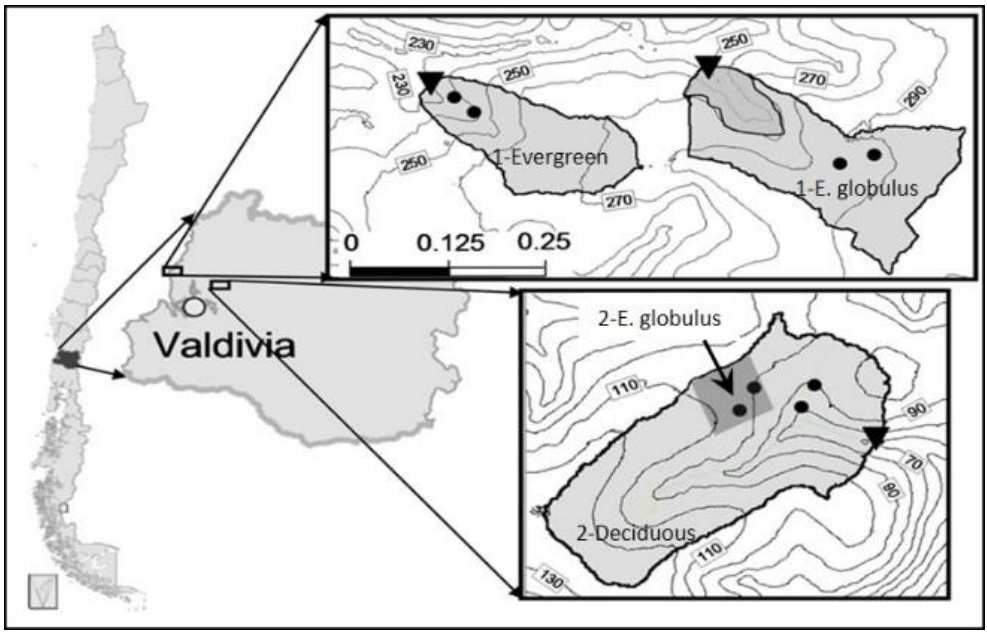

Figure 2.1: Location of study sites. Catchments at Site 1 have a second growth native evergreen forest (1-Evergeen) and *Eucalyptus globulus* plantation (1-E. globulus) land cover. At Site 2, the monitored catchment cover is deciduous native forest (2-Deciduous) and an area covered with *Eucalyptus globulus* (or 2-E. globulus). Black triangles denote catchment outlets, while black circles mark throughfall collector positions within each catchment. The dark area within 1-E. globulus marks a riparian native evergreen buffer strip, while in 2-Deciduous it marks the *E. globulus* area.

Catchment 1-E. globulus vegetation was composed of 80% exotic plantation of *E. globulus*, with a density of 1267 trees ha^{-1} and age of five-yeas-old, and of 20% native evergreen remnant vegetation as a buffer zone (*Berberis darwini* (Hooker), *Ovidia pillopillo* (Gray) Hohen ex Meissn, *Eucryphia cordifolia* Cav., *Lomatia ferruguinea* (Cav.) R. Br., *Dasyphyllum diacanthoides* (Less.) Cabrera., and *Raphitamnus spinosus* (Juss.) Mold. Originally, this catchment land cover was native evergreen forest. However, 40 years ago agricultural expansion (mainly grazing grounds) by means of slash and burn occurred in the study area. Recently (5 years ago, at the time of the study) the grassland was replaced by *E. globulus*.

At site 2, catchment 2-Deciduous was covered by a mixture of the deciduous species *Nothofagus obliqua* (Mirb.) Oerst. reaching a height of 35 m, which covers 63.3% of the catchment. Also, 13.8% and 7.9 % was covered by native secondary forests of *Gevuina avellana* and *Astrocedrus chilensis* planted in 1983 and 1982, respectively. This catchment also had 15% of its area covered by the fast-growing *Eucalyptus globulus* plantation (see Figure 2.1), also referred to in this document as 2-E. globulus. In this catchment, only throughfall was sampled. Understory trees include *Luma apiculate* (DC.) Burret, *Podocarpus salignus* D. Don, *Aextoxicon punctatum*, *Amomyrtus meli* (Phil.) D. Legrand & Kausel, *Gevuina avellana* (Molina) Gaertn and the exotic tree *Acacia melanoxylon* R. Br. Shrubs that reach heights over 3 m are mainly *Chusquea quila* Kunth with a 95% canopy cover up to 4 m height. Leaf area index (LAI) values were 6.5, 5.0 and 0.6 $m^2 \cdot m^{-2}$ for the deciduous, evergreen and *Eucalyptus* plantation, respectively (full canopy on January 2011) and 2.8, 2.5 and 0.5 $m^2\ m^{-2}$ on August 2010, respectively.

2.3.3. Water fluxes

At sites 1 and 2, rainfall was monitored continuously with a tipping bucket type gauge connected to a HOBO data logger (Ben Meadows, USA) installed on each site. The rain gauges were installed in open areas (no trees higher than 4 m were within a 20 m radius from the instruments). Throughfall water volumes were estimated using previously described canopy interception according to the literature, which was 30% for native evergreen and deciduous forests (Huber and Iroumé, 2001; Huber and

Oyarzún, 1992) and 5% for the young *Eucalyptus globulus* plantation (Oyarzún and Huber, 1999). These literature values corresponded to those of sites nearby of the selected catchments used in the present study. Water level recorders paired with baro divers (DIVER, Schulemberg Water Services, USA) were installed at the 60° V-notch weir in each catchment to measure water discharge (Figure 2.2).

Figure 2.2: 60° V-notch weir at 1-Evergreen. All other catchments V-notch weir setups were similar.

Discharge of all studied catchments was perennial and water samples were collected a few meters upstream from the V-notch weirs after storm events. Monthly precipitation and discharge is shown in Figure 2.4 for both sites. All samples were collected on a rainfall event basis. For site-1, 41 rainfall events were sampled for the period between June 2009 and March 2011; and 31 rainfall events at site 2 for the period between October 2009 and March 2011. The 41 and 31 rainfall events sampled represented 58.1% and 87.6% of the total rainfall at each site.

2.3.4. Atmospheric input and throughfall enrichment

Due to local variations in nutrient deposition to a forest stand, a large number of collectors would be often necessary. Rodrigo and Avila (2001) discussed the influence of sampling size in the estimation of throughfall and concluded that error is around 10% when 9 – 11 collectors are used. Puckett (1993) found that the total number of collectors necessary to estimate the mean concentration within 5 and 10% of the mean with 95% confidence ranged from 19 – 20 (for NO_3^- AND SO_4^{2-}) up to 309 (for NH_4^+) to be within 10% of the mean. In this study, due to economic and logistic constrains only two bulk precipitation (Bp) collectors were used on each site, and two throughfall (TF) collectors were installed under each land cover (evergreen, 1-Evergreen; deciduous, 2-Deciduous; and *Eucalyptus globulus* plantation, 1-E. globulus and 2-E. globulus for sites 1 and 2, respectively) (see Figure 2.3). Due to the low number of bulk and throughfall collectors (i.e. two) used in the present study, variability of concentrations could be as high as 50 to 60% (Puckett, 1991). Hence, presented results in this study should be taken cautiously.

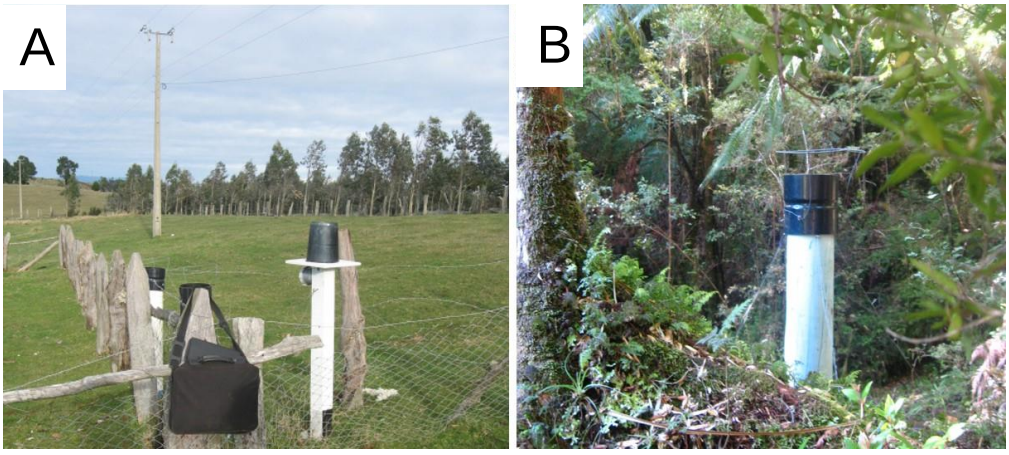

Figure 2.3: Bulk and throughfall collector under second growth native evergreen forest cover (A and B, respectively).

All collectors had a surface area of 254 cm^2 and were installed inside opaque tubes in order to avoid light penetration that could promote algae growth and at 1.2 m above soil. Bp collectors were installed in open areas (no trees were within 20 m of

the sampling point), located between a distance of 100 – 500 m and at the same altitude as those in 1-E. globulus and 1-Evergreen catchments. Bulk and throughfall collectors had an outer ring in order to exclude bird droppings (Kleemola and Soderman, 1993) and a thin mesh in the neck of the funnel, in order to prevent the entrance of solid particles or leaf litter to the collection bottles.

Cloud or fog water inputs were not sampled in open areas. Therefore, nutrient inputs from bulk precipitation might be underestimated. Nevertheless, in the eventuality of a fog event, throughfall collectors included the fog drip, especially in 1-Evergreen and 1-E. globulus catchments. However, since throughfall water fluxes were estimated from canopy interception literature (Huber and Oyarzún, 1992; Huber *et al.*, 1998; Huber and Iroumé, 2001; Soto-Schönherr and Iroumé, 2016). Throughfall water flux is underestimated, as these catchments are close to the shore (2 and 2.6 km, respectively) and received frequent fog events, especially at night due to the dominating winds going inland from the Pacific Ocean.

Other studies have shown that N deposition via clouds and fog can be important at coastal sites (Weathers *et al.*, 2000) and at high elevation sites at the Cordillera de los Andes (Oyarzún *et al.*, 2004) in south central Chile. Dry deposition was not included either. Staelens *et al.* (2005) reported 8.6 kg $N \cdot ha^{-1} \cdot yr^{-1}$ of dry DIN inputs for an agricultural site in the intermediate depression, between coastal and Andean mountain ranges. In a regional review of nitrogen deposition in south-central Chile, Godoy *et al.* (2003) reported wet DIN inputs were less than 1 kg $N \cdot ha^{-1} \cdot yr^{-1}$ at a site near the one used in the present study (less than 20 km away). However, this value could be underestimated since fog DIN inputs were not considered. Weathers *et al.* (2000) estimated fog DIN annual inputs to be around 2 kg $N \cdot ha^{-1} \cdot yr^{-1}$ for coastal sites at Chiloé national park, 300 km S from our study site.

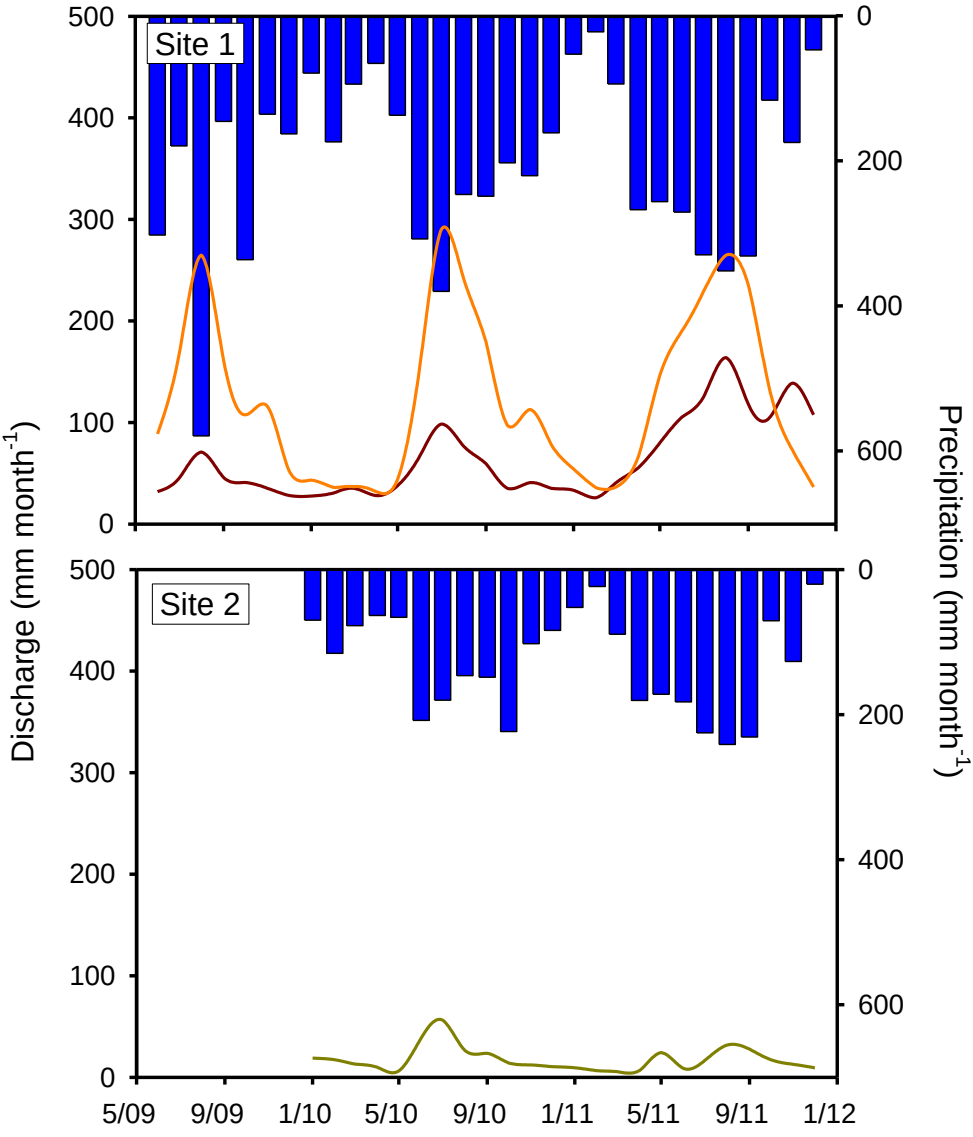

Figure 2.4: Precipitation (in mm·month^{-1}, blue bars) and discharge (in mm·month^{-1}, at site 1: dark red and orange solid lines represent 1-Evergreen and 1-E. globulus catchments, respectively. While at site 2, the dark yellow solid line stands for 2-Deciduous) at each studied site.

The estimation of canopy enrichment factors is calculated as the ratio between throughfall and bulk precipitation from different forest covers as follows:

$$Er_x = \frac{TF_x}{Bp_x} \quad (2.1)$$

where Er, TF and Bp stand for enrichment ratio, throughfall and bulk precipitation concentration, respectively. The subscript x stands for a specific nutrient. In this way, Er values lower than 1 indicate nutrient retention by the canopy, Er values higher than 1 indicate nutrient enrichment by the canopy, and Er values equals to 1 mean that there was no retention or enrichment of a specific nutrient species by the canopy.

2.3.5. Catchment nutrient fluxes and retention

Nutrient fluxes were estimated for the period January-December 2010 by multiplying the rainfall (1-Bulk and 2-Bulk, for bulk precipitation for site
s 1 and 2 respectively), throughfall or catchment discharge amounts with volume-weighted averages of element concentrations. Note that the throughfall precipitation volumes were estimated using interception values from literature (Oyarzún and Huber, 1999; Huber and Iroumé, 2001). Catchment balance for the different nitrogen fractions (NO_3^--N, NH_4^+-N, DIN, Org-N and TN) and phosphorus (soluble reactive phosphorus and total phosphorus, SRP and TP, respectively) was estimated as follows (Lovett *et al.*, 2000):

$$B_x = \frac{In_x\text{-}Out_x}{In_x} \quad (2.2)$$

where, In, Out and B (all in, $kg \cdot ha^{-1} \cdot yr^{-1}$) stands for a specific nutrient (subscript x) input, output and balance, respectively. In this way, B values lower than 0 indicate nutrient losses. B values higher than 0 indicate nutrient retention, and values equal to 0 mean nutrient equilibrium. However, since there are many studies in which the catchment nutrient balance has been calculated using either bulk precipitation or throughfall concentrations as inputs, in this study nutrient balances were estimated

using bulk precipitation at the specific site (site-Bulk), throughfall of dominant vegetation (DV) and throughfall weighted by vegetation cover (WVC) area of a specific cover within a catchment as nutrient inputs. Seasons were defined as follows: winter (JAS), spring (OND), summer (JFM), and autumn (AMJ). Only volume-weighted nutrient amounts were used for the estimation of nutrient balance.

2.3.6. Soil analyzes

Two pits were dug under each land cover, with two replicates each. For each soil sample we determined: bulk density and porosity using the core method (Salazar et al.,) stainless steel rings of 250 cm^3 volume and the gravimetric soil core method, soil pH in water (1: 2.5 v.v.) with a standard pH electrode, organic matter with the Walkley-Black method, P with Olsen method (i.e. available P), Soil N (NH_4^+-N + Org-N) by Kjeldahl method (seeTable 2.1).

2.3.7. Bulk, throughfall and stream water sampling and laboratory analyzes

Bulk precipitation, throughfall and stream water samples were collected in high-density polyethylene 1L bottles previously washed using HCl 0.5N and rinsed three times with distilled water prior sampling. Collectors were inspected for bird droppings to decide whether or not to discard the sample. The sampling bottle was rinsed three times again with small aliquots of water that was going to be sampled. Once the sample was collected, bulk and throughfall collectors were brushed and rinsed thoroughly with distilled water. Samples were stored at -5°C, and analyzed within 24 days after collection.

Prior to the analysis of NO_3^--N and NH_4^+-N, water samples were filtered through a borosilicate glass filter (Whatman) of 0.45 µm. NO_3^--N (as NO_3^--N + NO_2^--N) was determined by the cadmium reduction method, where NO_2^--N was always below detection limit (DL < 2 µg $N \cdot L^{-1}$ for NO_3^--N and NO_2^--N). NH_4^+-N was determined by the phenate method (blue indophenol) (DL < 2 µg $N \cdot L^{-1}$). Total-N was determined by the sodium hydroxide and persulfate digestion method (DL <15 µg $N \cdot L^{-1}$) (Eaton *et al*.,

2005). Org-N was estimated by subtracting DIN = (NH_4^+-N + NO_3^--N + NO_2^--N) concentration from TN. Total phosphorus (TP) was measured by the sodium hydroxide and persulfate digestion method (DL < 3 µg $N \cdot L^{-1}$), while soluble reactive phosphorus (SRP) was measured using molybdenum blue method (DL < 2 µg $P \cdot L^{-1}$).

2.3.8. Statistical analyses

Since our dataset was non-normally distributed and non-homoscedastic, all statistic tests were non-parametrical. Nutrient concentrations in bulk precipitation from both study sites were compared using a non-parametric Wilcoxon signed-rank test. Throughfall nutrient concentrations within sites (1-Evergreen with 1-E. globulus; and 2-Deciduous with 2-E. globulus, for sites 1 and 2 respectively) were compared using a non-parametric Wilcoxon matched pair test. All significant differences were at $p < 0.05$.

2.4. Results

2.4.1. Bulk precipitation and throughfall chemical composition

Bulk precipitation comparison showed that only Org-N and TN were significantly different ($p < 0.05$ and $p < 0.001$, respectively). The highest variability for all measured nutrients was observed in bulk precipitation of site 2. Only NO_3^--N showed a higher mean value at site 1 although this was not statistically significant (Table 2.2). Bulk precipitation from site-1, showed the lowest nutrient NO_3^--N, NH_4^+-N and SRP concentrations. The concentrations were lower than the detection limit in all cases, while bulk precipitation of site-2, NH_4^+-N; Org-N and TN showed the highest concentrations.

Higher concentrations were measured in throughfall nutrient chemistry at 1-Evergreen and 2-Deciduous, when compared to both *E. globulus* covers of sites 1 and 2. Only NO_3^--N concentrations at 1-Evergeen were ($p < 0.05$) lower than that of 1-E. globulus (2.0 ± 1.6 and 10.4 ± 33.7 µg $N \cdot L^{-1}$, for 1-Evergreen and 1-E. globulus, respectively). All other nutrient species were statistically higher in throughfall of native

covers, when compared to that of *E. globulus* covers (see Table 2.2). In general, throughfall nutrient concentrations collected under native trees (1-Evergreen and 2-Deciduous), double nutrient concentrations were measured in throughfall collected under *E. globulus*at both sites. NO_3^--N, SRP and TP concentrations were 10, 6 and 4 times higher in 2-Deciduous compared to 2-E. globulus throughfall samples, respectively. Throughfall NO_3^--N concentrations on 1-E. globulus, was 5 times higher compared to that of 1-Evergreen, while all other nutrient concentrations measured in throughfall were between 2 and 3 times higher in 1-Evergreen, when compared to those measured in 1-E. globulus (Table 2.2).

Throughfall nutrient enrichment ratios are shown in Figure 2.5 and Table 2.3. 2-Deciduous throughfall showed the highest enrichment of all measured nutrients, while 1-E. globulus showed the lowest. Seasonal NO_3^--N retention in canopies showed a high variability, ranging from 0.2 for 1-Evergreen in winter, up to 14.2 for 2-Deciduous in summer (Table 2.3). The highest enriched nutrient was SRP (56.8 and 48.4, for 2-Deciduous in autumn and summer, respectively) (for details see Table 2.3). 2-Deciduous showed the highest TN enrichment throughout seasons (4.0; 3.9; 4.1 and 7.6 for autumn, winter, spring and summer seasons, respectively), while 2-Deciduous annual enrichment ratio of SRP (43.7) was the highestof all nutrients.

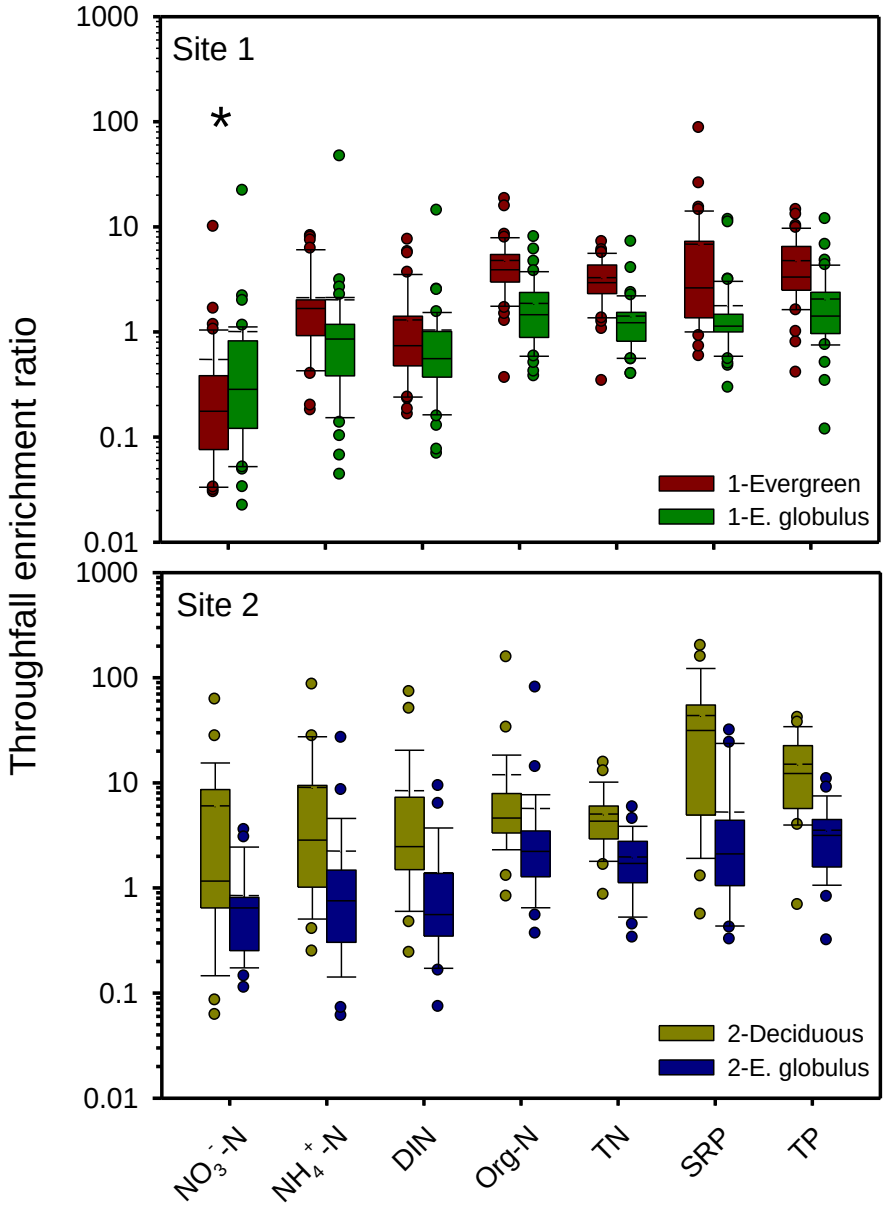

Figure 2.5: Throughfall enrichment ratios estimated for site 1 (upper panel): 1-Evergreen and 1-E. globulus. For site 2, (lower panel): 2-Deciduous and 2-E. globulus. Boxplots show average (dashed line), 25th, 50th (median) and 75th percentiles, whiskers represent 5- and 95-percentiles. Outliers are circles beyond the ends of the whiskers. Note: the asterisk marks the only nutrient where 1-E. globulus showed a higher enrichment than that of 1-Evergreen.

Table 2.2: Bulk and throughfall volume weighted nutrient concentrations (in μg $X \cdot L^{-1}$, Mean ± 1Sd, minima and maxima in parenthesis), where X stands for N or P species. Bulk precipitation (Bp-1 and Bp-2 for sites 1 (n = 41) and 2 (n = 28), respectively) and throughfall (1-Ev and 1-Eu, stand for 1-Evergreen and 1-E. globulus (n = 41 each), respectively on site-1; and 2-De and 2-Eu, stand for 2-Deciduous and 2-E. globulus (n = 27 each), respectively on site 2). Samples collected from individual rain events from June 2009 to March 2011. Statistical differences are indicated for the highest mean value as follows: *p < 0.05; † p < 0.01; ‡ p< 0.001.

	NO_3^--N	NH_4^+-N	Org-N	TN	SRP	TP
1-Bp	16.6 ± 18.5	21 ± 26	91.8 ± 86.1	129.4 ± 123.5	2.4 ± 2	10.4 ± 9.5
	(0.1 - 109.6)	(0.5 - 142.6)	(11.7 - 508.4)	(33.4 - 760.6)	(0.2 - 11.7)	(2.1 - 42.4)
2-Bp	15.8 ± 18.9	121.4 ± 322.3	225.1 ± 294.8*	362.3 ± 591.4†	9.3 ± 18.1	26.2 ± 44.6
	(2 - 90.6)	(2 - 1723)	(1.4 - 1449.4)	(35 - 3216.5)	(0.5 - 77.9)	(3 - 215.4)
1-Ev	2 ± 1.6	29.1 ± 60.6†	289.2 ± 154.4‡	320.3 ± 195.5‡	11.2 ± 26.5‡	35.5 ± 36.2‡
	(0 - 8.4)	(2 - 399.2)	(76 - 799)	(86.7 - 1200.3)	(1 - 173.3)	(6.6 - 241.5)
1-Eu	10.4 ± 33.7*	18.1 ± 29.9	129.5 ± 95.6	158 ± 142.7	4.6 ± 11.8	15.3 ± 16.4
	(0.3 - 216.3)	(0.5 - 172.8)	(14.7 - 486.3)	(24.3 - 875.4)	(0.5 - 78)	(3.2 - 107.2)
2-De	106.3 ± 414.5†	204.2 ± 304.3†	758.9 ± 522.9‡	1069.3 ± 974.8‡	116.3 ± 161‡	198.1 ± 229.9‡
	(0.5 - 2172.8)	(2 - 1267.9)	(218.3 - 2552.4)	(268.4 - 5193.3)	(2.9 - 741.2)	(27.5 - 1135.2)
2-Eu	10.4 ± 13.3	75.5 ± 164.6	372.6 ± 268.3	458.5 ± 407.4	19.9 ± 33.4	57.4 ± 74.4
	(1.3 - 47.4)	(2 - 770.5)	(104.9 - 1229)	(129.4 - 1764.4)	(0.5 - 119.9)	(8 - 341.1)

Table 2.3: Seasonal and annual throughfall enrichment ratios, from samples collected during June 2009 to March 2011.

	1-Evergreen					1-E. globulus				
	Autumn	Winter	Spring	Summer	**Annual**	Autumn	Winter	Spring	Summer	**Annual**
NO_3^--N	0.34	0.18	0.19	1.90	**0.55**	0.55	0.57	0.27	3.25	**1.01**
NH_4^+-N	2.61	1.54	1.36	4.00	**2.12**	0.81	3.55	0.59	1.47	**2.02**
Org-N	3.14	5.04	4.46	5.76	**4.79**	1.00	2.46	1.55	1.61	**1.87**
TN	2.81	2.63	3.18	5.06	**3.29**	0.91	1.69	1.16	1.51	**1.42**
SRP	6.98	2.80	4.12	18.50	**6.82**	0.75	1.25	1.20	4.32	**1.78**
TP	5.85	4.46	4.21	5.41	**4.76**	1.78	2.49	1.67	1.85	**2.06**
	2-Deciduous					2-E. globulus				
NO_3^--N	4.18	2.23	2.17	14.16	**6.03**	2.20	0.71	0.53	0.60	**0.84**
NH_4^+-N	4.99	9.11	4.28	16.36	**9.04**	1.98	1.52	0.65	4.59	**2.24**
Org-N	5.28	3.62	21.53	10.74	**11.95**	2.46	1.78	11.6	4.71	**5.69**
TN	3.98	3.87	4.09	7.57	**5.06**	1.92	1.46	1.67	2.73	**1.97**
SRP	56.77	25.56	45.94	48.36	**43.73**	1.92	2.27	6.14	8.72	**5.27**
TP	15.84	13.44	11.88	19.40	**15.04**	3.61	2.46	3.21	4.77	**3.54**

2.4.2. Nutrient concentrations in stream water

Figure 2.6 shows the stream N and P species concentrations. TN concentrations in 1-Evergreen catchment discharge showed lower concentrations than 1-E. globulus and 2-Deciduous catchments (see Figure 2.6).

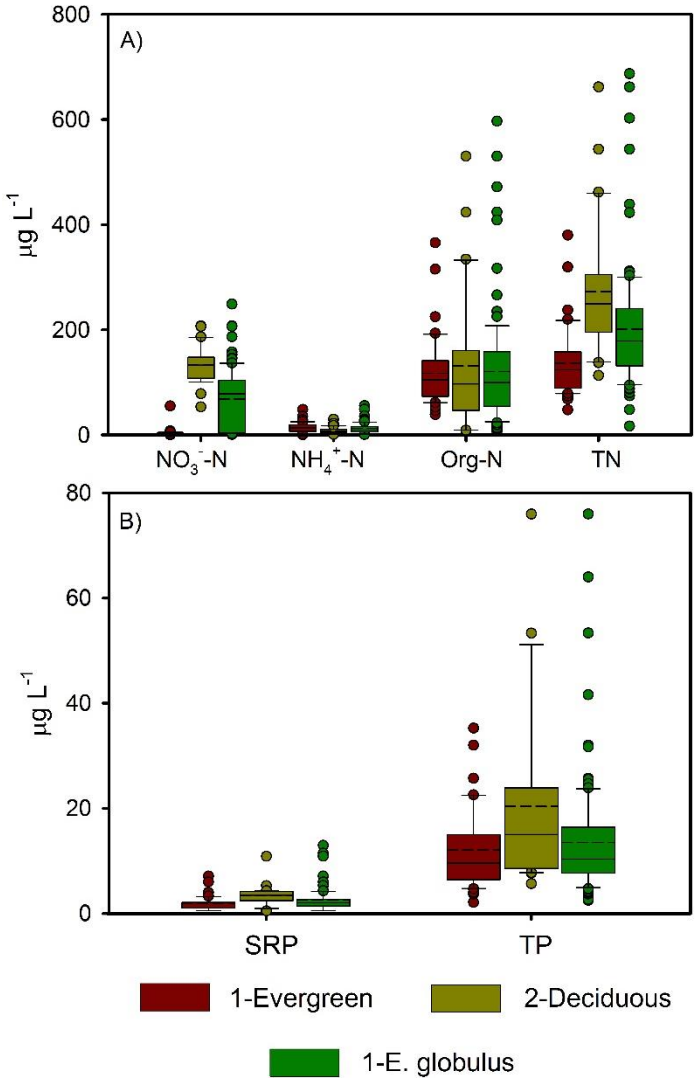

Figure 2.6: Nutrient stream concentrations of: A) Nitrogen species; and B) soluble reactive phosphorus (SRP) and TP. Boxplots show average (dashed line), 25th, 50th (median) and 75th percentiles, whiskers represent 5- and 95-percentiles. Outliers are circles beyond the ends of the whiskers.

2-Deciduous presented the highest annual mean for TN and NO_3^--N concentrations at discharge (316.6 ± 97.2 and 135.1 ± 37.4 µg $N \cdot L^{-1}$, respectively), while 1-Evergreen showed the lowest concentrations observed for TN and NO_3^--N (129.5 ± 65.2 and 3.4 ± 1.4 µg $N \cdot L^{-1}$, respectively). SRP showed the lowest concentrations at discharge in all catchments (1.7 ± 1.3; 5.0 ± 1.8 and 1.7 ± 0.8 µg $N \cdot L^{-1}$ for 1-Evergreen, 2-Deciduous and 1-E. globulus, respectively). Org-N was the dominant fraction of N in discharge of 1-Evergreen (111.8 ± 67.3 µg $N \cdot L^{-1}$), while at 2-Deciduous and 1-E. globulus DIN played a more important role (145.1 ± 36.6 and 93.8 ± 29.9 µg $N \cdot L^{-1}$, respectively).

Discharge DIN:Org-N ratios (Table 2.4) for 1-Evergreen resulted in values ranging from 5.5 ± 4.2 and 19.3 ± 21.3 for winter and autumn, respectively. 2-Deciduous showed the lowest values, ranging from 0.6 ± 0.6 to 1.2 ± 1.2 for autumn and winter, respectively (Table 2.4). The highest variability was observed in 1-Evergreen during autumn (minimum-maximum: 3.4 - 54.6), while the minimum variability was observed in 2-Deciduous during spring (ranging from 0.05 to 1.2).

2.4.3. Nutrient fluxes in bulk precipitation, throughfall and catchment discharge

The annual TN and TP fluxes are displayed in Table 2.4. Annual inputs of DIN, Org-N and TN via bulk precipitation were 0.2, 0.9 and 1.1 kg $N \cdot ha^{-1} \cdot yr^{-1}$, respectively at site 1; and 2.0, 2.4 and 4.4 kg $N \cdot ha^{-1} \cdot yr^{-1}$ for DIN, Org-N and TN at site 2. Throughfall DIN annual inputs ranged from 0.1 to 3.4 kg $N \cdot ha^{-1} \cdot yr^{-1}$ for 1-E. globulus and 2-Deciduous, respectively. Org-N showed throughfall input values going from 1.1 to 7.5 kg $N \cdot ha^{-1} \cdot yr^{-1}$, and TN from 1.3 to 11.0 kg $N \cdot ha^{-1} \cdot yr^{-1}$ for 1-E. globulus and 2-Deciduous, respectively. Catchment discharge fluxes for DIN ranged from 0.1 to 3.7 kg $N \cdot ha^{-1} \cdot yr^{-1}$ for 1-Evergreen and 1-E. globulus, respectively. Org-N fluxes ranged from 0.6 to 5.0 to kg $N \cdot ha^{-1} \cdot yr^{-1}$ for 2-Deciduous and 1-E. globulus, respectively. TN ranged from 1.0 to 8.6 kg $N \cdot ha^{-1} \cdot yr^{-1}$ for 2-Deciduous and 1-E. globulus, respectively (see Table 2.5).

Table 2.4: Volume weighted nutrient concentrations in $\mu g \cdot L^{-1}$ (mean ± 1SD, min - max values are shown below in between parenthesis) for each stream measured in this study. Samples collected from June 2009 to March 2011.

Catchment	NO_3^--N	NH_4^+-N	Org-N	TN	SRP	TP
1-E. globulus	84.9 ± 16.9	11 ± 7.4	106 ± 114	202 ± 116	2 ± 0.8	12 ± 10
	(51.2 - 126.0)	(0.5 - 29.5)	(11.4 - 596.8)	(96.2 - 687.3)	(0.5 - 3.8)	(2.7 - 64)
1-Evergreen	3.4 ± 1.4	14 ± 10	117 ± 67.4	135 ± 65.2	2 ± 1.3	12 ± 7.6
	(0.5 - 7.8)	(0.5 - 48.7)	(39.0 - 366.2)	(47.9 - 380.6)	(0.5 - 7.1)	(2.1 ± 35.3)
2-Deciduous	135 ± 37.4	8.1 ± 5.7	121 ± 101	264 ± 97.3	4 ± 1.9	19 ± 15
	(53.1 - 207.1)	(0.5 - 21.3)	(8.0 - 423.8)	(137.2 - 543.6)	(0.5 - 10.9)	(5.4 - 76)

Table 2.5: Annual nutrient bulk and throughfall inputs (Bulk and TF, respectively, in kg N or P·ha^{-1}·yr^{-1}) and catchment discharge exports (D, in kg N or P·ha^{-1}·yr^{-1}) estimated for the different studied catchments (1-Evergreen = second growth native evergreen; 1-E. globulus = *Eucalyptus globulus*, and 2-Deciduous = native deciduous).

	Site-1			Site-2				
		1-*E. globulus*		1-Evergreen		2-Deciduous		
Nutrient	Bulk	TF	D	TF	D	Bulk	TF	D
NO_3^--N	0.50	0.03	3.38	0.02	0.02	0.40	0.22	0.40
NH_4^+-N	0.62	0.11	0.30	0.14	0.08	2.01	3.21	0.03
DIN	1.12	0.13	3.67	0.16	0.10	2.41	3.43	0.43
Org-N	3.05	1.12	4.98	2.32	0.93	7.27	7.52	0.57
TN	4.17	1.25	8.63	2.46	1.03	9.68	10.9	1.00
SRP	0.08	0.05	0.08	0.09	0.01	0.34	1.27	0.02
TP	0.35	0.13	0.39	0.27	0.08	0.92	1.90	0.06

In this study, nutrient balances were estimated using bulk, throughfall and throughfall weighted by area of a specific cover within a catchment (Table 2.6). Results from this study suggest that even the slightest change in forest cover can have an effect on the nutrient balance (see Table 2.6). The only catchment which was fully covered by second growth native evergreen forest was 1-Evergreen. 1-E. globulus had 80% of *E. globulus* and 20% of second growth native evergreen forest as a buffer strip, while 2-Deciduous was covered by 85% and 15% of native deciduous forest and *E. globulus*, respectively.

The effect of vegetation over the nutrient balance is obvious (see Table 2.6). The biggest differences were observed for 1-E. globulus, ranging from -7.0 to -4.8 kg·ha^{-1}·yr^{-1} for TN, estimated using bulk concentrations and weighted vegetation cover, respectively (see Table 2.6). Overall, NO_3^--N was the least retained nutrient. Annual retention of TN was 0.6 and 0.9 kg·ha^{-1}·yr^{-1} for 1-Evergreen and 2-Deciduous, respectively. Only, 1-E. globulus showed a TN loss of 4.8 kg·ha^{-1}·yr^{-1}. The same pattern was observed for TP (0.7, 1.0 and -1.5 kg·ha^{-1}·yr^{-1} for 1-Evergreen, 2-Deciduous and 1-E. globulus catchments, respectively). In general, 1-E. globulus shows losses for all nutrients, while 1-Evergreen and 2-Deciduous only showed negative retention for NO_3^--N (Table 2.6).

Table 2.6: Land cover weighted nutrient balance (kg N or P·ha^{-1}·yr^{-1}) for 2010, for each studied catchment. Estimated for sites 1 and 2 with bulk precipitation (1-bulk and 2-bulk, respectively); and estimated for each catchment with throughfall from dominant vegetation (DV) and weighted vegetation cover (WVC, in bold) as nutrient inputs.

Nutrient	Site 1						Site 2		
	1-E. globulus			1-Evergreen			2-Deciduous		
	1-Bulk	DV	WVC	1-Bulk	DV	WVC	2-Bulk	DV	WVC
NO_3^--N	-56.3	-122.4	**-132.4**	0.61		**-0.34**	-0.3	-0.78	**-0.85**
NH_4^+-N	-2.2	-1.7	**-1.6**	0.12		**0.41**	0.98	0.99	**0.99**
DIN	-23.3	-26.3	**-25.5**	0.31		**0.33**	0.78	0.87	**0.86**
Org-N	-4.3	-3.4	**-2.66**	0		**0.6**	0.77	0.92	**0.92**
TN	-7	-5.9	**-4.79**	0.04		**0.58**	0.77	0.91	**0.9**
SRP	-0.8	-0.7	**-0.41**	0.67		**0.85**	0.89	0.98	**0.98**
TP	-3.1	-2	**-1.49**	0.17		**0.71**	0.77	0.97	**0.96**

2.5. Discussion

2.5.1. Bulk and throughfall fluxes and enrichment

Bulk deposition of DIN ranges from less than 1 kg N·ha^{-1}·yr^{-1} in the coastal mountain range to about 5 kg N·ha^{-1}·yr^{-1} for the Andean mountain range in south-central Chile (Godoy *et al*., 2003). Other studies conducted in south central Chile, close to an important agricultural productive zone, have reported higher values of DIN deposition (2.5 and 7.5 kg N·ha^{-1}·yr^{-1} for bulk and throughfall, respectively) (Oyarzún *et al.*, 2005). The values presented in this study confirm that both study sites were still exposed to a low nutrient input. However, in this study it cannot be disregarded that some anthropogenic influence or contamination at site 2, since it is close to a highway (1.5 km approximately). This could be the reason of the high TN inputs in bulk precipitation observed at site 2. Uyttendaele and Iroumé (2002) suggest that in areas near Valdivia city moderate pollution occurs, since biomass burning is a common activity used in agriculture and forestry during spring and autumn, in addition to heating from late autumn to early spring seasons.

Both native forests (deciduous and evergreen) showed the highest annual mean enrichment for all nutrients, especially Org-N (4.5 and 2.5 times, for 1-Evergreen and

2-Deciduous respectively), TN (2.9 and 5.1 times, for 1-Evergreen and 2-Deciduous respectively) and TP (4.7 and 18.1 times, for 1-Evergreen and 2-Deciduous respectively). Chiwa *et al*. (2010) found enriched N fluxes in throughfall of Moso-bamboo forest by 1.6 times, and attributed this behavior to the interception and retention of nitrogenous gases and particles. 2-Deciduous forest cover enriched throughfall by 5.8 times. The explanation given by Chiwa *et al*. (2010) seems plausible for our study, although it is a hypothesis and remains to be tested. Throughfall collectors at 2-Deciduous were under a thick layer of bamboo (*Chusquea* sp.), which covered the soil in some areas with a 2 to 3 m thick layer. We could also attribute this enrichment to atmospheric gas and particle capture, and to the retention of soil gases, therefore enriching throughfall precipitation (Staelens *et al*., 2008), in addition to poor ventilation (Chiwa *et al.,* 2010). It is necessary to mention that vegetation density was very high in both native forest covers (evergreen and deciduous), especially at 2-Deciduous with its *Chusquea quila* canopy (LAI of 6.5 and 5.0 $m^2 \cdot m^{-2}$ for 2-Deciduous and 1-Evergreen, respectively). These suggest that trees at 1-Evergreen and 2-Deciduous were under nutrient stress or in need for NO_3^--N and werefunctioning as a NO_3^--N sink. On the other hand, the very high LAI also explained the greater enrichment at 2-Deciduous during the summer months (see Table 2.3).

Canopy nutrient models suggest that forest canopies retain scarce or limiting nutrients such as N and P or base cations (Boy and Wilcke, 2008). Parron *et al.* (2010) found in a gallery forest in Brazil that canopies of three different kinds of vegetation retained TN. Also Parron *et al*. (2010) found NO_3^--N was enriched, but no enrichment was observed in NH_4^+-N. In this study, NH_4^+-N throughfall enrichment was observed under all canopies (2.3, 2.3, 10.1 and 2.5 times, for 1-Evergreen, 1-E. globulus, 2-Deciduous and 2-E. globulus respectively). The highest enrichment was observed during winter at 2-Deciduous (20.3 times), while the lowest was observed for 2-E. globulus in spring (0.8 times), suggesting a net retention of NH_4^+-N. In accordance with this study, the highest annual throughfall enrichments were observed at 2-Deciduous. The seasonal enrichment by the canopies was highly variable under all canopies.

Variability of the net enrichment could be the result of two processes: (i) washing off of the unquantified N input by dry deposition; and (ii) N uptake from wet, dry particulate and gaseous deposition by leaves, twigs, stem surfaces, and lichens. In the present study, the first process clearly occurred in native deciduous forest showing enrichments for NH_4^+-N and NO_3^--N in all seasons. The opposite was observed at site 1, where 1-Evergreen and 1-E. globulus were located, especially because the location of these catchments was far away from industrialized or intensive agricultural regions where the atmospheric inputs of N via dry deposition could have been an important factor. However, since bulk precipitation at Site 2 showed higher amounts of TN (nearly 4 times compared to Site 1), it is suggested that Site 2 should be considered a moderately contaminated site. Results from forested sites in North America and Europe indicate that the canopies are generally acting as sinks for DIN (Lovett, 1992). Edmonds *et al*. (1995) have reported that NO_3^--N concentrations decreased in stemflow and throughfall relative to precipitation in old-growth forest in North America. However, in a data compilation from 126 European sites under a high deposition regime in Scandinavia, Netherlands and Germany, Dise *et al*. (1998) reported enhanced inputs by up to 3-5 times in throughfall through addition of dry deposition.

2.5.2. Discharge nutrient concentrations and export

Stream concentrations of NO_3^--N in the 1-Evergreen catchment were low (3.4 ± 1.4 μg $N \cdot L^{-1}$). The opposite was found for 1-E. globulus and 2-Deciduous catchments discharge (82.8 ± 21.7 and 133.6 ± 45.4 μg $N \cdot L^{-1}$, respectively). Amishi *et al*. (2006) reported that the extremely low concentrations of N in broadleaf evergreen forests in southern Chile are due to high litter lignin content and associated low rate of N mineralization. Huygens *et al*. (2008) described for an evergreen *Nothofagus betuloides* forest in the Andean mountain range with soils developed from volcanic material that the parent material exerts a strong influence on anion sorption, charge development and micro aggregation associated with anaerobic microsite formation, potentially favoring dissimilatory nitrate reduction to ammonium (DNRA) and/or abiotic NO_3^--N immobilization in volcanic rainforest soils. If the latter applies to the present study sites, NH_4^+-N concentrations in stream water would have been higher than that

of NO_3^--N. The latter applies to 1-Evergreen, where NO_3^--N:NH_4^+-N ratio was on average 0.8 (0.07 and 39.8 for minimum and maximum, respectively). However, at 1-E. globulus the NO_3^--N:NH_4^+-N ratio was 12.1 (0.23 and 56.9 for minimum and maximum, respectively) and 28.6 (2.8 and 85.8 for minimum and maximum, respectively) for 2-Deciduous. On the other hand, Perakis and Hedin (2007) described that in small headwater catchments the NO_3^--N:NH_4^+-N ratio was always below 1, demonstrating that DIN retention was mostly due to non-biotic processes. All streams sampled by Perakis and Hedin (2007) were from catchments covered with pristine native forests in the south American cone (southern Chile and Argentina). In the present study, observed NO_3^--N:NH_4^+-N ratios suggest that retention at 1-Evergreen was more related to abiotic retention, while at 2-Deciduous and 1-E. globulus, nutrient retention was due to biotic activity. However, since all nutrients showed negative retention at 1-E. globulus, this suggests that *E. globulus* had inhibitory effect on soil biota involved in DIN retention. It is known that eucalypts release organic compounds through their roots in order to gain access to nutrients and to prevent competition (i.e. allelopathy) with other plants (Guerrero and Bustamante, 2007; Zhang and Fu, 2009). These compounds are also known to affect soil properties like water infiltration rates (Doerr *et al.*, 1996; Ferreira *et al.*, 2000).

Other authors have described that in southern South America, NO_3^--N retention is mostly due to abiotic factors (Huygens *et al*., 2008; Perakis and Hedin, 2007). In the present study, catchments have the same parent material (volcanic ashes over mica schist), however, nutrient retention was higher on both native covered catchments, suggesting that tree species composition (i.e. land cover) played an important role in nutrient retention. It has been described also that the dominant form of N leaching in unpolluted forests is DON (Perakis and Hedin, 2002), and those higher values of DON were attributed to watersheds with low anthropogenic influence and low inorganic nitrogen input. Presented results in this study, suggest otherwise. Since 1-Evergreen and 1-E. globulus received very low nutrient inputs (0.2 kg $N \cdot ha^{-1} \cdot yr^{-1}$ for bulk precipitation), both catchments should have had similar DON:DIN outputs. However, mean annual Org-N:DIN ratios were 9.9 ± 11.6; 1.4 ± 2.1 and 0.9 ± 0.9, for 1-Evergreen, 1-E. globulus and 2-Deciduous, respectively. Org-N:DIN ratios exhibited

high variability, nevertheless 1-Evergreen catchment showed the highest values, ranging from 5.5 ± 4.2 up to 19.3 ± 21.3 for winter and autumn, respectively.

It was hypothesized that the effect of previous soil history had affected soil nutrient retention capabilities, since both native covered catchments (1-Evergreen and 2-Deciduous) showed higher nutrient retention (0.6 and 0.9 kg $N \cdot ha^{-1} \cdot yr^{-1}$ for TN; and 0.7 and 1.0 kg $P \cdot ha^{-1} \cdot yr^{-1}$ for TP; for 1-Evergreen and 2-Deciduous, respectively). Studies in watersheds in the United States (Lajtha *et al*., 1995; Campbell *et al.,* 2004) reported that thin or porous soils with high infiltration rates have less capacity to retain N. However, in this study, catchments with high infiltration rates, such as 1-Evergreen and 2-Deciduous, showed greater N retention than soils with low infiltration rates, such as 1-E. globulus. Land disturbances, such as fires, agriculture and grazing, may strongly affect N retention (Campbell *et al*., 2004). The 1-E.globulus catchment was cleared (35 years ago) with fire to open areas for grazing animals, and in some areas for the extraction of wood. Recently (5 years ago) grassland cover was replaced by FGES (*E. globulus*). This soil alteration history is frequent along the south central coastal mountain range (Echeverría *et al.*, 2006; Locher-Krause *et al.*, 2017). Results in the current study, suggest that in native forests, rainfall water was infiltrating and percolating (subsurface flow) exporting less N, in contrast to 1-E. globulus, in which as soil has lower porosity and infiltration rates due to land use history (Oyarzún *et al*., 2011). This enhances the formation of surface runoff, allowing rainfall chemistry reaching the discharge flow chemically unaltered, therefore more concentrated in TN. However, NO_3^--N and TN concentrations in deciduous forest were higher, probably due to the influence of the area covered by the fast-growing *E. globulus* plantation. However, such an assumption requires further research.

Annual retention of DIN was 0.3 and 0.9 kg $N \cdot ha^{-1} \cdot yr^{-1}$ for 1-Evergreen and 2-Deciduous catchments, respectively. The 1-E. globulus catchment showed the highest net release of DIN (25.5 kg $N \cdot ha^{-1} \cdot yr^{-1}$); this was mostly due to the higher loss of NO_3^--N (132.4 kg $N \cdot ha^{-1} \cdot yr^{-1}$) relative to the throughfall flux as input (see Table 2.6). Campbell *et al*. (2004) evaluated the importance of forest cover with respect to NH_4^+-N and NO_3^--N outputs in 24 forest watersheds in the north-eastern United States, in a region with elevated atmospheric N deposition, but could not observe a clear

relationship. In our study, DIN retention differences were evident between both native forests (1-Evergreen and 2-Deciduous) and 1-E. globulus, as has been described previously by Oyarzún *et al*. (2007). Direct effects of past land use may occur via long-term (> 50 yr) physical alteration of the rhizosphere caused by historic practices (Huygens and Boeckx, 2009). Soil compaction is an enduring consequence of cultivation, grazing, and logging that can cause increased bulk density and reduce porosity. These changes may affect the abundance of aerobic and anaerobic microorganisms and subsequently affect the cycling of several elements, including N (Huygens and Boeckx, 2009). However, Cuevas *et al*. (2006) observed that land cover and watershed area explained nearly 90% of the variability in water quality (NO_3^--N, NH_4^+-N, DON, TP and electric conductivity) using local models in dry season. However, during the wet season, land cover and watershed area just explained 70%; and with the addition of geomorphology and precipitation, it explained 85% of the variability. On the other hand, Campbell *et al.* (2004) found that nutrient exports were highly related to the corresponding nutrient inputs. In our study, we found similar results for NH_4^+-N, TN and TP at 2-Deciduous; and NH_4^+-N and TP at 1-Evergreen, while 1-E. globulus showed no significant input/export relationship. This could be due to the observed low infiltration rates, which in turn could affect soil hydrological pathways.

2.6. Conclusions

In this study, we found that throughfall nutrient enrichment was higher under native deciduous forest cover, while the *Eucalyptus* plantations (at both study sites) showed the lowest throughfall nutrient enrichment. The highest annual nutrient enrichment was observed for SRP and TP under native deciduous forest cover. In general, differences in throughfall nutrient enrichment could be attributed to the very high LAI of both native forests and particularly to the presence of a thick layer of bamboo (*Chusquea quila*), which could be working as an extra layer and retain dry deposition coming from different anthropic activities, in addition to soil NO or NO_2 gas emission.

Annual retention of TN in native deciduous and second growth evergreen forests was 0.90 and 0.58 kg $N \cdot ha^{-1} \cdot yr^{-1}$, while TP retention was 0.96 and 0.71 kg $P \cdot ha^{-1} \cdot yr^{-1}$, respectively. In the *E. globulus* plantation covered catchment there was a net loss of TN and TP (-4.79 kg $N \cdot ha^{-1} \cdot yr^{-1}$ and -1.49 kg $P \cdot ha^{-1} \cdot yr^{-1}$, respectively). These results along with the NO_3^--N:NH_4^+-N values suggest that *E. globulus* might be affecting soil biota, hence, generating nutrient losses especially NO_3^--N.

The present study has shown that nutrient retention depends on biotic (i.e: vegetation), abiotic (soil parent material) and hydrological soil properties, such as porosity and infiltration rates. However, it is not possible to neglect that soil microorganisms and land use history could playa relevant role in nutrient retention. Therefore, before planting or any other forestry or agricultural activities, soil should be either: (i) treated in order to enhance nutrient retention capabilities; and/or (ii), since native forests showed the highest throughfall enrichment, maybe it could be possible to leave native patches within the catchment, other than the riparian buffer zone.

3. Chapter 3: Study sites

Since the following results chapters (i.e. chapters 4, 9 and 10) were conducted on the same study sites, a full description of both selected sites will be given in order to avoid repetition. However, different sampling protocols were used on the previously mentioned chapters. These sampling protocols are described on the respective chapter.

3.1. Study sites description

For this study, two nearby sites were selected 13 km apart from each other (NF and EP sites, see Figure 3.1).

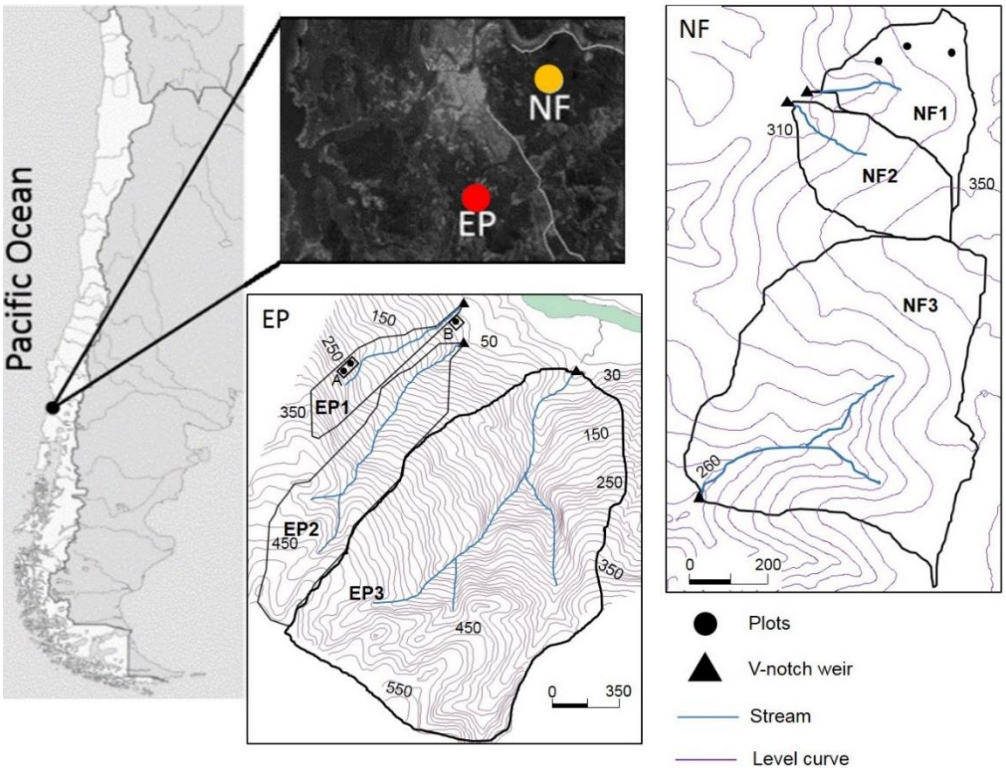

Figure 3.1: Old-growth native forest (NF, yellow circle) and Eucalyptus nitens plantation (EP, red circle) research sites near the city of Valdivia, South-Central Chile (40°S). Please note that these catchments are different from those used in Chapter 2.

Each site has 3 paired catchments, and are located in the coastal mountain range (40°S) near the city of Valdivia, Chile (-39.829 S; -73.236 W). The NF site catchments are covered by old-growth native evergreen rainforest. The drainage area of catchments in NF site: NF1, NF2 and NF3 were 12.5, 7.9 and 13.4 ha, respectively. The average altitude of NF site is 336 m a.s.l., while the average slope was 15.4%. The main canopy species in these catchments are *Aextoxicon punctatum, Laureliopsis philippiana* (Looser) R. Schodde and *Eucryphia cordifolia.* The understory was dominated by *Amormyrtus luma*, *Amomyrtus meli*, *Drimys winteri* and *Myrceugenia planipes*. Tree density in NF catchments ranged from 1747 to 4788 trees·ha^{-1}, while the basal area ranged from 78.2 to 315.1 m^2· ha^{-1} (Table 3.1).

Table 3.1: Area and land cover characteristics for each selected catchment.

	Site NF			Site EP		
Catchments	NF1	NF2	NF3	EP1	EP2	EP3
Area (ha)	12.5	7.9	13.4	11.7	40.3	281.7
Old-growth native evergreen forest land cover (%)	100	100	100	-	-	-
Managed area (%)	20	-	-	-	-	-
Riparian buffer and remaining native forest (%)	-	-	-	15	25	30
E. nitens land cover (%)	-	-	-	85	75	70
Tree density (trees·ha^{-1})	1747	4787	4055	2911	2733	2911
Basal area (m^2·ha^{-1})	78.2	133.8	315.1	131.9	139.1	144.7

In the EP site, catchments are covered with exotic fast growing *Eucalyptus nitens* and some remains of native evergreen forest (Table 3.1). Surface area of catchments at EP site are: 11.7, 40.3 and 281.7 ha for EP1, EP2 and EP3, respectively. This site had an average altitude of 35 m a.s.l. and an average slope of 34%. The EP catchment is covered with 16 and 4 years old *E. nitens* stands established on soils that already had five *E. nitens* rotations. Tree density ranged from 2733 to 2911 trees·ha^{-1}, while the basal area ranged from 131.9 to 144.7 m^2 ha^{-1} (Table 3.1). The riparian vegetation was dominated by native species such as *Aristotelia chilensis*, *Luma apiculata*, *Fuchsia magellanica*, *Podocarpus saligna* and

Embothrium coccineum covering up to 15% of the whole catchment area (Table 3.1 and Figure 3.1).

On chapters 4 and 9, research was conducted in NF1 and EP1 only. For a detail view of these catchments, see Figure 3.2.

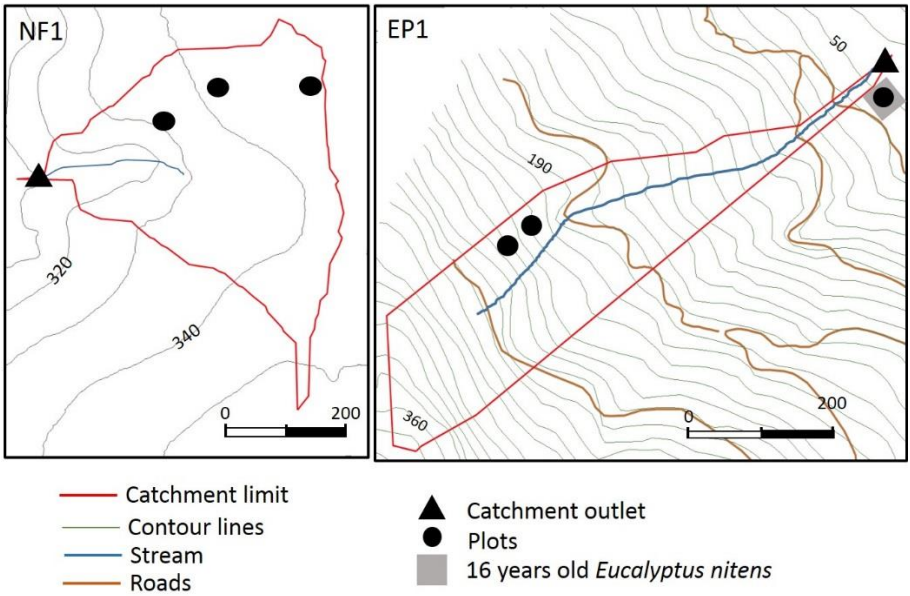

Figure 3.2: Old-growth native evergreen forest (NF1) and *Eucalyptus nitens* plantation (EP1) research catchments near the city of Valdivia, south-central Chile (40°S). In EP1, areas A and B stand for 4 and 16-year-old *E. nitens* stands. Please note that these catchments are different from those used in Chapter 2.

3.2 Precipitation and catchment discharge measurements

Bulk precipitation was measured using a calibrated tipping bucket type gauge connected to a HOBO data logger (Ben Meadows, USA) on each site. While throughfall precipitation (or precipitation under the canopy) was constantly monitored with two of the previously mentioned gauges installed nearby sampling plots on NF1 and EP1 catchments (see Figure 3.2). Unfortunately, these precipitation gauges stopped working after two months in the field. Therefore, all precipitation data given in chapters 4, 9 and 10 is from Miraflores meteorological station located (-39.833 S; -

73.251 W) at 10.5 km W from NF site and 14 km NW form EP site. This could result in an underestimation on precipitation inputs. This is due fog is common in the area and usually this input is only quantified as throughfall inputs. Catchment discharge was continuously measured only in NF1 and EP1 catchments using a pressure transducer paired with a baro diver (DIVER, Schulemberg Water Services, USA) on each site.

3.3 Plots and precipitation sampling

Four plots were installed in NF1 and EP1. One plot with no trees within a 50 m radius, was used for the collection of bulk precipitation. All three remaining plots were placed on the catchment hillslopes under tree cover and away from the riparian zone. On these plots, throughfall precipitation was collected using one collector per plot (Figures 3.2 and 3.3). Bulk and throughfall precipitation water was collected using passive sequential collectors modified from Vermette & Drake (1987).

Figure 3.3: Throughfall collectors installed under NF1 and EP1 land covers, A and B, respectively.

Each collector was designed to collect three 5 mm increments, two 10 mm increments and a 30 mm increment for each rainfall event. Bulk and throughfall collectors (surface area 254 cm^2) were installed 1.2 m above the forest floor, and positioned inside opaque tubes in order to avoid light penetration that could promote algae growth. In addition, all collectors had a thin mesh at the beginning of the neck of the funnel, in order to prevent insects and leaves entering the collection bottles, and designed with a plastic ring in order to exclude bird droppings (Kleemola and Soderman, 1998). Precipitation samples from bulk and throughfall were collected on a storm event basis, for nine individual storm events distributed over the study period. All precipitation samples (i.e. bulk and throughfall) were collected the day following a storm event.

3.4 Soils

Soil physical chemical and texture analysis for both sites were made in two soil pits in NF1 and EP1 catchments for the characterisation of soils in NF and EP sites, respectively (see Table 3.2).

Table 3.2: Soil characteristics for each sampled horizon at a specific depth (in cm). Soil pH, using 1:2,5 soil:H_2O and 1:2,5 $CaCl_2$ (0.01 M) methods; Cation Exchange Capacity ($cmol \cdot kg^{-1}$); Exchengeable aluminium (Ex. Al, in $cmol\ kg^{-1}$); Aluminium saturation (Al sat, in %); Soil texture (in %) and soil organic matter content (as OM, in %).

	Depth	pH		CEC	Ex. Al	Al sat	Soil texture (%)			
		H_2O	$CaCl_2$				Clay	Silt	Sand	OM
NF	0 – 14	5.5	4.8	3.52	1.03	29.1	31.1	58.1	10.8	17.8
	14 – 30	5.4	4.8	2.13	0.89	42.0	28	61.7	10.3	14.5
	30 – 65	5.4	4.8	0.57	0.07	12.4	36.3	55.1	8.6	15.9
	65 <	5.3	4.7	0.48	0.07	13.6	37.3	53	9.7	15.8
EP	0 – 15	5	4.3	1.66	1.14	68.3	45,1	45,1	9,8	17.1
	15 – 25	5.4	4.7	0.46	0.05	11.3	37,8	52,5	9,7	3.9
	25 – 60	5.3	4.6	0.47	0.04	7.9	36,9	53,6	9,5	2.5
	60 <	5.4	4.8	0.41	0.04	10.6	37.2	53.5	9.3	1.8

Soils in both catchments are classified as andic palehumult and typic paleudult for NF and EP sites, respectively (CIREN, 2003; Salazar *et al.*, 2005). However, in the world reference base for soil resources both soil types are classified as ultisols (FAO, 2015). Also known as red clayish soils, its main characteristic is that these soils were evolved from ancient volcanic ash deposited over a weathered metamorphic complex (Salazar et *al*., 2005). These soils are acidic, have a low CEC and a high Al^{3+} saturation, which reduces their fertility. Clay mineralogy is mainly formed of kaolin, which is a non-swelling type of soil. Soil texture analysis for the NF1 catchment showed a clay, silt and sand average content of 34 ± 3%, 58 ± 4% and 8 ± 1%, respectively. In EP1, showed clay, silt and sand average contents of 41 ± 4%, 49 ± 4% and 10%, respectively. Organic matter average content was 12 ± 6% and 9 ± 8% for NF and EP sites, respectively (see Table 3.2).

3.5 Climate

Climate in the studied area is rainy temperate, with a marked dry summer and a wet winter seasons. Mean annual precipitation is about 1871 mm. Rainfall concentrates in late autumn and winter (May-August, 62%) and decreases significantly in summer (January–March, 9%). The mean annual temperature is 12.0°C, January being the hottest month with average temperature of 17°C, and July being the coldest, with 7.6°C. These data represent 60-year averages, measured at Isla Teja meteorological station (25 m a.s.l.), and located at 12.6 and 9.8 km from NF and EP sites respectively. However, since Isla Teja meteorological station stopped its measurements on 2012, data presented in Table 3.3 shows air temperature, relative humidity and precipitation measured at Miraflores meteorological station (location mentioned in section 3) .

Table 3.3: Temperature (Temp, in °C) and relative humidity (RH, in %) average (± 1Sd) and range (min – max); and Precipitation amount (Pp, in mm) measured at Miraflores meteorological station measured during the study period (from autumn, 2013 until summer, 2014).

Seasons	Month	Temp (°C)		RH (%)		Pp (mm)
		Mean	Min - Max	Mean	Min - Max	
Autumn	Apr	12.8 ± 3.5	2.8 – 24.2	84.3 ± 9.1	46.0 – 93.0	130.4
	May	10.9 ± 2.9	0.5 – 17.1	88.0 ± 6.0	52.0 – 93.0	234.9
	Jun	8.4 ± 3.2	0.8 – 15.3	87.4 ± 5.4	61.0 – 93.0	177
Winter	Jul	7.9 ± 2.7	-0.7 – 14.1	84.3 ± 6.4	57.0 – 91.0	148.3
	Aug	7.7 ± 3.6	-1.4 – 15.1	82.0 ± 10.9	29.0 – 90.0	289.4
	Sept	9.3 ± 3.9	0.9 – 22.0	76.5 ± 14.8	27.0 – 90.0	198.9
Spring	Oct	11.9 ± 4.0	3.3 – 24.4	75.1 ± 11.1	38.0 – 88.0	83.1
	Nov	13.1 ± 3.8	5.2 – 23.1	73.0 ± 11.0	38.0 – 86.0	97.7
	Dec	17.5 ± 5.3	5.6 – 32.4	63.5 ± 14.1	27.0 – 83.0	24.1
Summer	Jan	18.9 ± 5.5	7.8 – 35.4	68.5 ± 14.8	34.0 – 92.0	43.2
	Feb	17.2 ± 4.5	7.1 – 32.1	74.6 ± 14.7	27.0 – 92.0	65.4
	Mar	15.0 ± 4.1	6.5 – 27.5	74.7 ± 13.9	29.0 – 92.0	45.9
Annual		12.5 ± 5.5	-1.4 – 35.4	77.7 ± 13.7	27.0 – 93.0	1538.2

4. Chapter 4: Hydrological controls on nutrient exportation

Adapted from Oyarzún, C., P. Hervé-Fernandez, D. Huygens, P. Boeckx and N. E. C. Verhoest. (2015). Hydrological Controls on Nutrient Exportation from Old-Growth Evergreen Rainforests and Eucalyptus nitens Plantation in Headwater Catchments at Southern Chile. Open Journal of Modern Hydrology, 5(2): 19-31.

4.1. Abstract

Soil cover disturbances have a direct effect on biogeochemistry, potentially enhancing nutrient loss, land degradation and associated changes in ecosystem services and livelihood support. The objective of this study was to assess how canopy affected throughfall chemistry; and how hydrology affected stream nutrient load responses in two watersheds dominated by native old-growth evergreen rainforest (NF1) and exotic plantation of *Eucalyptus nitens* (EP1), located at the Coastal mountain range of southern Chile (40° S). Nutrients such as nitrogen (NO_3^--N, NH_4^+-N, Organic nitrogen (Org-N) and Total nitrogen (TN)) and total phosphorus (TP) were measured at catchment discharge, and $\delta^{18}O$ in throughfall precipitation and stream discharge in both catchments, in order to separate throughfall (or new water) contributions from catchment discharge during storm events. It was hypothesized that all nutrients show an increase in concentration as discharge increases (or enhanced hydrological access) in EP1, but not in NF. In both catchments, Org-N, TN and TP concentrations showed a positive correlation to catchment discharge. However, NO_3^--N showed a negative correlation with catchment discharge. Org-N and TP showed a flush during storm events, contrary to NO_3^--N. This suggests that NO_3^--N is being retained by charged soil particles, micropores or microbiota, while Org-N is flushed as it is more concentrated in big pore water that is not tightly bound, in contrast to NO_3^--N.

4.2. Introduction

Human disturbances have a great impact on native forest communities. This may lead to land degradation, causing changes in ecosystem services and livelihood support (Zhao *et al.*, 2010). Stream nutrient loads are very sensitive to vegetation

changes and human disturbances (Cannell, 1999; Oyarzún et al. 2007; Uyttendaele & Iroumé, 2002), but also to variables related to ecosystem hydrology, including infiltration rates, rainfall, and surface runoff, referred to in this study as new water (Doerr *et al.*, 1996; Ferreira *et al.*, 2000; Huber *et al.*, 2010; Oyarzún *et al.*, 2011). Human-induced alterations of forest canopies and forest soils have a significant impact on the hydrological controls of the nutrients (nitrogen, phosphorus and base cations) that reach the stream water(Inamdar *et al.*, 2004; Jiang *et al.*, 2010; Oeurng *et al.*, 2010). In this sense, concentration of nutrients could exhibit one of three general trends with respect to stream discharge (Figure 4.1, after Salmon *et al.*, 2001):

(i) Dilution occurs whenever the net increase in water delivery to stream is greater than the increase in chemical delivery (Salmon *et al*., 2001). Chemicals are expected to follow this relationship when the source is internal watershed and does not increase in magnitude as a function of increased hydrologic throughput. Therefore, dilution of these elements is expected by enhanced throughput of water.

(ii) Hydrological constant controls are characterized by a balance between water discharge and chemical concentration. Chemicals expected to follow this relationship are entering the catchment as precipitation inputs, but lack significant internal production or consumption processes. In the strictest sense, such idealized hydrological constancy may be rare since evapotranspiration provides a mechanism for concentrating solutes in soil water pools (Allison and Hughes, 1978). Hence, it may impart differences in the delivery of chemicals and water depending on water flow paths in soils (Burns *et al.*, 2001). Some form of constancy may also be expected for elements that are chemically buffered within soils (e.g. via cation exchange reactions), but only if rates of hydrological throughput remain low enough to maintain some form of equilibrium between soils and soil solutions. This is not likely to occur in most natural soils that experience variable hydrologic inputs over time.

(iii) Enhanced hydrological access refers to controls that exhibit increasing chemical concentration with increasing discharge. The most common enhanced hydrological access is for chemicals found in areas of a watershed that are only active during periods of high flows, like macropores (Mcdonnell, 1990; Klaus *et al.*, 2013). For

example, in the case of elements produced in the surface soil horizons, as the region of subsurface flow deepens, i.e. as the saturated soil boundary approaches the soil surface, the flowing water increasingly accesses these elements. In recent years, this hydrological process is frequently referred to as 'piston flow' or 'translatory flow' (Hewlett and Hibbert, 1966).

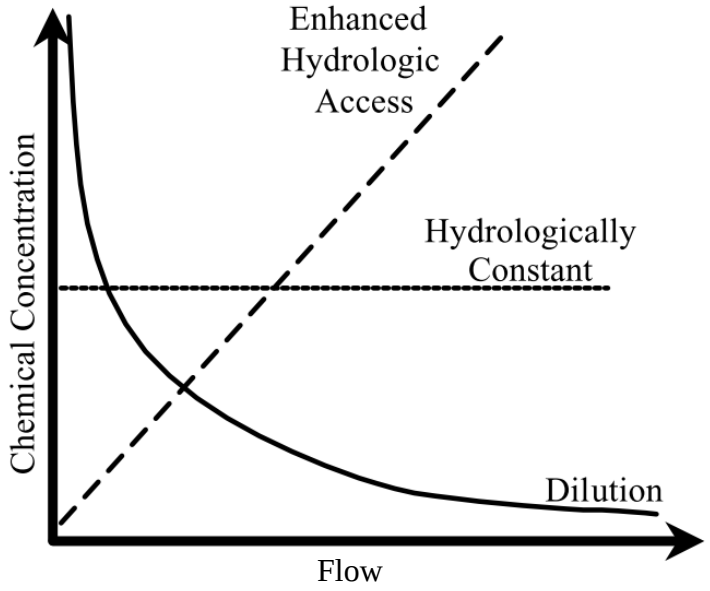

Figure 4.1: Schematic of the different hydrological responses, as catchment discharge or flow increases (from Salmon *et al*., 2001).

Native temperate rainforests of southern Chile, covering an area of 13.5 million ha, represent an important global reserve of temperate forests with an extraordinary genetic, phytogeographic and ecological significance (Armesto *et al.*, 2010). Native forests in the Valdivian eco-region (36° S through 48° S) have suffered anthropic disturbances due to fires, logging practices, or its conversion to agricultural land and exotic fast-growing plantations. Temperate rain forest ecosystems of southern Chile have efficient mechanisms of retention for essential nutrients, especially NO_3^- and NH_4^+ (Oyarzún *et al.*, 2004; Huygens *et al.*, 2007; Hervé-Fernández *et al.*, 2016a). Perakis and Hedin (2002) described that the dominant form of N leaching was dissolved organic nitrogen (DON) in unpolluted forests of southern Chile. Huygens *et al*. (2008) described that DIN inputs do not end up in the soil water compartment, and gave

evidence that DON losses originate from bio-unavailable compounds leaching from slow-turnover soil organic matter pools. Oyarzún *et al.* (2007) reported that conversion from native forests to exotic fast-growing plantations is likely to decrease catchment N retention.

The temperate climate region in southern Chile still reflects undisturbed, pre-industrial environmental conditions, with total nitrogen (TN) deposition (< 1 kg $N \cdot ha^{-1} \cdot yr^{-1}$) (Hedin *et al.*, 1995). This is in strong contrast with land use, which has been altered significantly over the last decades and centuries (Echeverría *et al.*, 2006; Zamorano-Elgueta *et al.*, 2015; Locher-Krause *et al.*, 2017). Only fragments of the original forest vegetation remain unaltered, and are located either in the coastal or in the Andean mountain ranges. Agricultural areas dominate the central valley of southern Chile; however, exotic tree plantations are spreading fast over the coastal mountain range (Oyarzún *et al.*, 2007; Huber *et al.*, 2010; Iroumé and Palacios, 2013). These observations make this region ideal to study land use change effects on biogeochemical nutrient cycling, without biases due to increased atmospheric nutrient depositions. In this study, the working hypothesis is that all nutrients, especially NO_3^--N would increase its concentrations as catchment discharge increases, hence, showing an enhanced hydrological access in EP1, but not in the catchment covered with old-growth native evegreen forest. Hence, the main objective of this study was to compare how hydrological variability (i.e. storm events) affects catchment nutrient load responses under different land covers of old growth native evergreen forest (NF1) and exotic plantation of *Eucalyptus nitens* (EP1), in order to evaluate possible effects of land cover. To find these differences, nutrients such as nitrogen species (NO_3^--N, NH_4^+-N, Org-N and TN) and total phosphorus (TP) were determined at catchment discharge, in addition to hydrograph separation analysis, in small headwater catchments located at the coastal mountain range in southern Chile (40° S).

4.3. Methods

4.3.1. Study sites

The description of study sites has been given previously in detail in chapter 3. However, in this study, studied catchments are shown on Figure 3.2.

4.3.2. Sampling and sample analysis

Five rainfall events were sampled during the period March – November 2013. However, in this work, only detailed data from the events of April 4th (3rd event) and August 2nd (5th event) will be presented. These correspond to events occurring at the end of dry season and to mid rainy season respectively. An automatic water sampler (ISCO-6712 Teledyne) was used to collect stream water samples in each catchment during selected storm events. Stream water samples were composed of two 250 mL aliquots taken each 30 minutes (1 h composed sample per bottle). Stream water samples taken three hours before the start of the storm event was considered as old water (i.e. groundwater) and throughfall water samples were considered as new water (or event water). Throughfall water was sampled as described in chapter 3, section 3.3, and the tracer average of all samples collected on a single event were used as the throughfall tracer signature. Stream water samples during the storm event, were considered as mixtures of old water and new water with different apportionments. These two different types of water were considered as the only contributing end members to stream water during a storm event (Petry *et al.*, 2002; Uhlenbrook *et al.*, 2002; Carey and Quinton, 2004; Laudon *et al.*, 2007; Chen *et al.*, 2012). If two end members have a difference in their tracer signature, i.e. $\delta^{18}O$ in this study, the stormflow hydrograph can be separated in its contributions based on a mass balance approach (Mcdonnell *et al.*, 1990; Klaus and McDonnell, 2013):

$$Q_t = Q_o + Q_n \tag{4.1}$$

$$C_t \cdot Q_t = C_o \cdot Q_o + C_n \cdot Q_n \tag{4.2}$$

$$F_n = \left(\frac{C_t - C_o}{C_n - C_o} \right) \tag{4.3}$$

Where Q_t is the streamflow, Q_o the contribution from old water, Q_n the contribution of new water, C_t, C_o and C_n is the tracer concentration or signature of streamflow, old water and new water, respectively. F_O is the fraction of pre-event water in the stream. The contributions of old water and new water can be determined using Eq.(4.3). The equation is constrained so that C_t falls between C_o and C_n and that Q_o

and Q_n are between zero and Q_t. The following assumptions underlie Eqs.(4.1) and (4.2) (Klaus and McDonnell, 2013):

i) The tracer signatures of event and pre-event water are significantly different;

ii) Event water maintains a constant tracer signature in space and time, or any variations can be accounted for;

iii) The tracer signature of the pre-event water is constant in space and time, or any variations can be accounted for;

iv) Contributions from the vadose zone must be negligible, or the isotopic signature of the soil water must be similar to that of groundwater;

v) Surface storage contributes minimally to the streamflow.

Abundance of stable water isotopologues is based on the isotopic ratios ($[^{18}O]/[^{16}O]$). The abundance is reported in the δ-notation and expressed as parts per thousand (‰, read as per mil). $\delta^{18}O$ values were determined on a Wavelength Scanned Cavity Ring-Down Spectrometer (WS-CRDS, L2120-*i* Picarro, USA). Standard deviations were equal to, or lower than, 0.03‰ for $\delta^{18}O$. All isotopic analyses were made at ISOFYS Laboratory, Ghent University, Belgium. Although, $\delta^{18}O$ has not yet been introduced, is just used as a hydrological tracer, as can be a cation (e.g. Ca^{2-}, Mg^{2-}, Na^{+} and/or K^{+}) or anion (e.g. Cl^{-} and/or SO_4^{2-}) concentration, electric conductivity, pH, temperature, etc.

Stream water samples were filtered through a borosilicate glass filter (Whatman) of 0.45 µm pore size. Nutrients were measured using the following methods: NH_4^+-N using the phenate method (blue indophenol), and NO_3^--N as (NO_3^--N + NO_2^--N) using the cadmium reduction method, NO_2^--N was always below detection limit (DL), which was 1.5 µg $N \cdot L^{-1}$, for nitrate, nitrite and ammonia. Dissolved inorganic nitrogen (DIN) was calculated as follows: DIN = NO_3^--N + NO_2^--N + NH_4^+-N. Total nitrogen (TN) was determined in unfiltered water samples by the sodium hydroxide and persulfate digestion method (DL < 15 µg $N \cdot L^{-1}$). Organic nitrogen (Org-N) was

calculated as follows Org-N = TN - DIN. Total phosphorus (TP) was measured in unfiltered water samples by the sodium hydroxide and persulfate digestion method (DL < 3 µg $P \cdot L^{-1}$) at LIMNOLAB (Limnology Laboratory, Universidad Austral de Chile).

4.3.3. Data analysis

Spearman correlations were used and best model fitting to determine whether catchment discharge or new water contributions had an influence on nutrient concentration. Then, catchment discharge and nutrient concentrations during the study period and each event were plotted in order to observe the behavior in the increase, decrease and peak flows. Statistical differences were considered if $p \leq 0.05$. Since TN concentration was almost 95% conformed by Org-N, only NO_3^--N, DIN, TN and TP are plotted.

4.4. Results and Discussion

4.4.1. Relationships between discharge and nutrient concentration

Figure 4.2 shows the hydrogram separation for the 3rd and 5th storm events (Figure 4.2 left and right side, respectively). Table 4.1 summarizes measured concentrations for stream discharge and nutrient concentrations for the different rainfall events. In both catchments, the highest values of discharge and nutrients concentrations were observed during the 5th event (August 2-4, 2013, Figure 4.2 right side). For this event, NF1 mean discharge was 17.8 ± 10.3 $L \cdot s^{-1}$. On average, Org-N amounted to 392.0 ± 315.6 µg $N \cdot L^{-1}$, whereas DIN was only 19.3 ± 3.8 µg $N \cdot L^{-1}$ resulting in a TN concentration of 411.4 ± 313.7 µg $N \cdot L^{-1}$, while TP was 37.0 ± 37.0 µg $P \cdot L^{-1}$ (Table 4.1). In EP1, mean discharge was 20.1 ± 15.5 $L \cdot s^{-1}$. DIN and Org-N concentrations were 28.7 ± 9.9 µg $N \cdot L^{-1}$ and 363.9 ± 560.7 µg $N \cdot L^{-1}$, respectively). TN and TP concentrations were 391.7 ± 567.9 µg $N \cdot L^{-1}$ and 63.2 ± 102.4 µg $P \cdot L^{-1}$ (Table 4.1). The 5th event was compared to the 3rd event (April 4-5, 2013) since both events showed the highest differences in precipitation and between Org-N and low DIN concentrations.

Figures 4.3 and 4.4 show the relationship between catchment discharge and nutrient concentration for the 3rd and 5th events. The correlations between nutrient fractions and catchments discharge were significant in both catchments for most of the nutrients (Table 4.3). In general, when discharge increases, TN and TP also does. This happened in all events, both sites (data not shown), for all N species, except for DIN in NF1. TN (and Org-N) and TP were best described by exponential and linear models for the 3rd and 5th event, respectively (Table 4.2 and Figures 4.3 and 4.4). Total discharge showed better correlation and r^2 values with measured nutrients, compared to those of new water (for details see Table 4.2). This suggests that TN and TP showed an enhanced hydrological access during the 3rd and 5th event (see Figures 4.3 and 4.4). It was hypothesized that these relations are due to the fact that these nutrients were more concentrated in mobile (or big pore) water in soil and not retained by soil particles or biologically transformed. Since TN (mostly conformed by Org-N, 95.6 ± 2.5% and 91.6 ± 3.8% for the 3rd event; and 97.0 ± 2.2% and 81.6 ± 10.7% for the 5th event for NF1 and EP1, respectively) increased as discharge increased, an enhanced hydrological access was found. Probably this behavior was observed because most of Org-N reaching the stream was present in pores that were easily accessed by water along its pathway, hence the mobile water compartment (or big pore water). The slope decrease from the 3rd to the 5th event could be the effect of several rainfall events prior to the 5th event (see Figures 4.3 and 4.4).

According to the 'translatory flow' theory (Hewlett and Hibbert, 1966), during storm events infiltrating water pushes soil water into the stream. However, water in soils is compounded of a mobile and a less mobile water compartment (McDonnell, 2014; Hervé-Fernández *et al.*, 2016a). This could explain the stronger relations that TN (and Org-N) and TP had with catchment discharge during the 3rd event in both catchments. Nevertheless, the 5th event revealed that TN (and Org-N) and TP concentrations were highly related to both catchment discharge ($r = 0.86$; $p < 0.001$ and $r = 0.93$; $p < 0.001$ for TN and TP, respectively) and new water contributions ($r = 0.92$; $p < 0.001$ and $r = 0.95$; $p < 0.001$ for TN and TP, respectively) in EP1. This was not observed in NF1, where TN and TP could be better explained by catchment discharge ($r = 0.60$; $p < 0.01$ and $r = 0.74$; $p < 0.001$ for TN and TP, respectively) than

new water ($r = 0.37$; ns and $r = 0.46$; $p < 0.05$ for TN and TP, respectively). Since TP is adsorpted to soil particles, the higher relation and slopes of the model, shown by catchment discharge vs TP and new water vs TP in EP1, could reflect higher erosion rates EP1, but not in NF1. Several studies have described high erosion rates in *Eucalyptus* spp. covered catchments (Oyarzún *et al.*, 2011). Schüller *et al*. (2013) described that 85% and 79% of exported sediment was coming from the stream bed in an *E. nitens* (100% coverage) and an *E. nitens* and *Pinus* spp. (66% and 33% of catchment cover, respectively) covered catchment in a nearby study site.

NO_3^--N and DIN, on the other hand, showed a different behavior and were best fitted with exponential decay models (see Table 4), showing a clear dilution behavior. During the 3rd event (Figures 4.2 right side, and 4.3), DIN concentrations were best explained by new water and by exponential decay models in both catchments. However, the model fitting was similar only for NO_3^--N (adjusted $r^2 = 0.59$; $p < 0.001$ and adjusted $r^2 = 0.57$; $p < 0.001$ for EP1 and NF1, respectively), but not for DIN (adjusted $r^2 = 0.43$; $p < 0.01$ and adjusted $r^2 = 0.08$; ns, for EP1 and NF1 catchments, respectively). During the 5th event (Figures 4.2 left side, and 4.4), for *E. nitens* NO_3^--N and DIN concentrations were more related with catchment discharge ($r = 0.51$; $p < 0.01$ and $r = 0.72$; $p < 0.001$, respectively) than with new water ($r = 0.14$; ns and $r = 0.43$; $p < 0.05$ for NO_3^--N and DIN, respectively). However, native evergreen forest showed the opposite behavior: NO_3^--N was closely related to new water ($r = 0.92$; $p < 0.001$) compared to catchment discharge ($r = 0.68$; $p < 0.001$). DIN concentrations showed the same behavior as NO_3^--N, being more related to new water than catchment discharge ($r = 0.92$; $p < 0.001$; $r = 0.67$; $p < 0.001$ for new water and discharge, respectively).

Recently, Hall *et al.* (2016) described that denitrification inside soil aggregates and microsites (where anaerobic conditions dominate) and transport of nitrogen in soil suction-lysimeter water (reflecting aerobic macropore water) showed different N and oxygen isotope ratios in the NO_3^- molecule. The authors go further in their analysis and suggest that their results imply that NO_3^- isotopic composition in streams, which are predominantly fed by mobile water, do not fully reflect terrestrial soil N cycling. In this study, the dilution observed for NO_3^--N and DIN, as catchment discharge and new

water increased suggests that these nutrients have a strong internal source, even though, throughfall was highly enriched in NO_3^--N and DIN. Several biological processes occurring at soil level use inorganic forms of nitrogen. Also Strahm and Harrison (2006) described that acid soils formed by volcanic ashes had the capability of retaining anions, like NO_3^- and PO_4^{-3}.

Table 4.1: Precipitation amount (Pp, in mm); Duration of the rain event (D, in hr); catchment discharge (Q, in L s^{-1}) and old water contribution (OWC, in %). Mean values ± 1 standard deviation for catchment discharge and concentrations (in µg $N \cdot L^{-1}$) of dissolved inorganic nitrogen (DIN), organic nitrogen (Org-N), total nitrogen (TN) and total phosphorus (TP, in µg $P \cdot L^{-1}$) for the rainfall events in old growth evergreen native forest (NF1) and *Eucalyptus nitens* plantation (EP1) covered catchments. nd stands for not determined.

Catchment	Events	Pp	D	Q	OWC (%)	DIN	Org-N	TN	TP
NF1	1st	10.7	3.5	3.8 ± 0.9	100	9.3 ± 2.2	220.8 ± 224.5	229.7 ± 223.0	27.4 ± 23.4
	2nd	nd	nd	4.6 ± 1.4	98	12.1 ± 5.9	161.3 ± 151	174.2 ± 150.5	19.3 ± 15.2
	3th	5.1	4	8.3 ± 2.7	99	7.4 ± 2.9	254.5 ± 215.9	262.0 ± 216.3	22.5 ± 26.0
	4th	30.2	20	13.8 ± 5.9	92.4	6.3 ± 1.2	246 ± 191.2	251 ± 19.5	28.9 ± 20.5
	5th	61.1	48	17.8 ± 10.3	92	19.3 ± 3.8	392 ± 315.6	411.4 ± 313.7	37 ± 37
EP1	1st	10.7	3.5	nd		nd	nd	nd	nd
	2nd	nd	nd	2 ± 0.4	93	14.7 ± 5.9	155.7 ± 224.3	170 ± 228.3	32 ± 30.5
	3th	5.1	4	3.4 ± 1.8	99	19.2 ± 2.0	138.5 ± 101.0	148.2 ± 100.3	44.9 ± 87.1
	4th	30.2	20	10.7 ± 9.1	96.8	26.3 ± 5.1	246.4 ± 374.2	271.0 ± 377.1	63.9 ± 108.1
	5th	61.1	48	20.1 ± 15.5	92	28.7 ± 9.9	363.9 ± 560.7	391.7 ± 567.9	63.2 ± 102.4

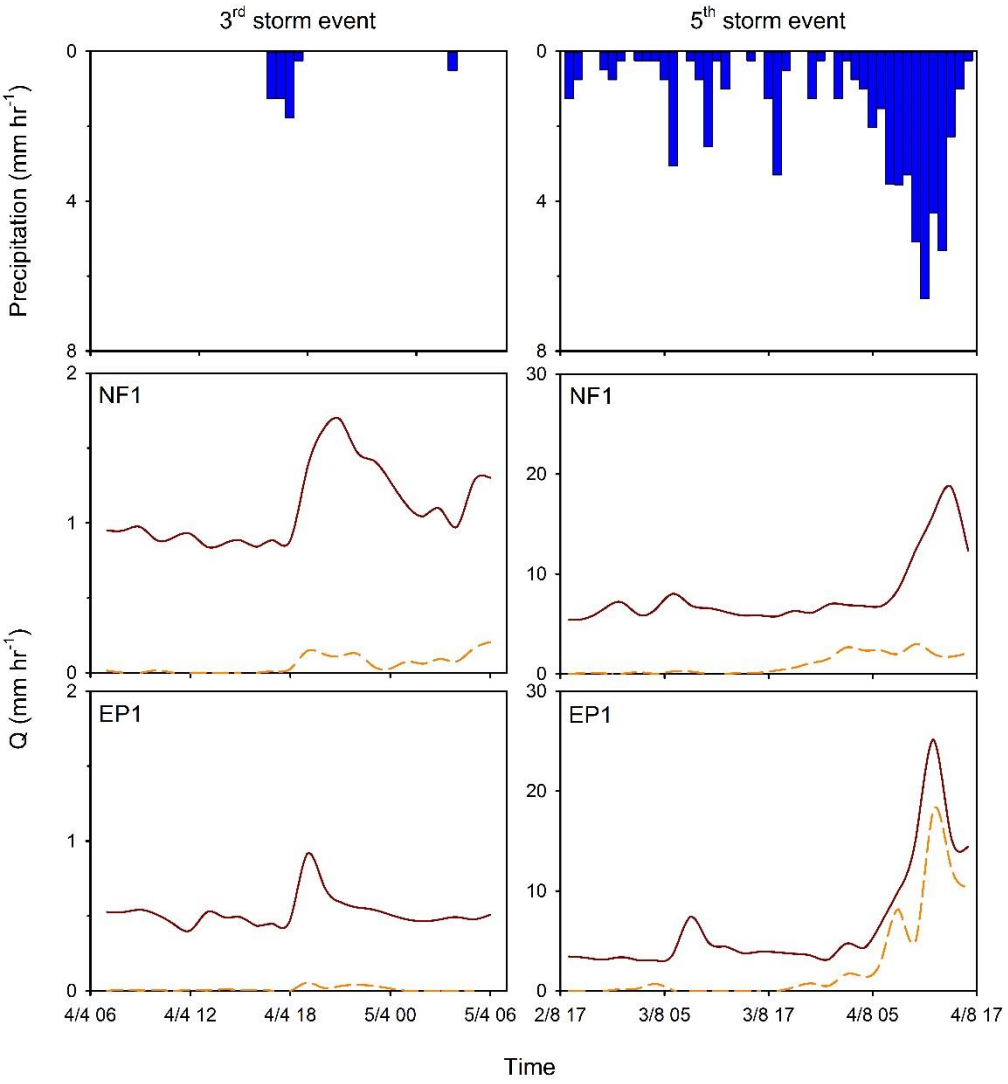

Figure 4.2: Precipitation (in mm hr-1) and new water hydrogram (dashed orange line) separation for the 3rd (left side) and 5th (right side) storm events, for NF1 and EP1 (mid and bottom plots, respectively). Please, note the different scales for the 3rd and 5th storm event hydrograms.

Table 4.2: Results of applied models (M), Spearman correlations (r); and best fitted models adjusted r^2 (Adj r^2): Linear models (L, $y = y0 + a \cdot x$); two parameter exponential decay (ED2, $y = a \cdot e^{(-b \cdot x)}$), and three parameter exponential decay (ED3, $y = y0 + a \cdot e^{(-b \cdot x)}$), for old growth native forest (NF1) and *E. nitens* plantation (EP1).

		Total discharge				New water			
Site	Nutrient	M	r	Adj r^2	P	M	r	Adj r^2	p
					3rd event				
EP1	NO_3^--N	ED2	0.66	0.41	p < 0.001	ED2	0.78	0.59	p < 0.001
	DIN	ED2	0.31	0.06	NS	ED3	0.69	0.43	p < 0.01
	TN	ED2	0.73	0.51	p < 0.001	L	0.52	0.23	p < 0.01
	TP	ED2	0.81	0.63	p < 0.001	ED3	0.67	0.42	p < 0.001
NF1	NO_3^--N	ED2	0.73	0.51	p < 0.001	ED2	0.77	0.57	p < 0.001
	DIN	L	0.22	0.01	NS	L	0.34	0.08	NS
	TN	ED3	0.58	0.31	p < 0.01	L	0.42	0.14	p < 0.05
	TP	ED3	0.60	0.34	p < 0.01	L	0.39	0.12	p < 0.06
					5th event				
EP1	NO_3^--N	ED2	0.51	0.23	p < 0.01	L	0.14	0.01	NS
	DIN	ED3	0.72	0.47	p < 0.001	L	0.43	0.14	p < 0.05
	TN	L	0.86	0.73	p < 0.001	L	0.92	0.84	p < 0.001
	TP	L	0.93	0.85	p < 0.001	L	0.95	0.9	p < 0.001
NF1	NO_3^--N	ED2	0.68	0.44	p < 0.001	ED2	0.92	0.84	p < 0.001
	DIN	ED2	0.67	0.43	p < 0.001	ED2	0.92	0.83	p < 0.001
	TN	L	0.60	0.33	p < 0.01	L	0.37	0.10	NS
	TP	L	0.74	0.52	p < 0.001	L	0.46	0.18	p < 0.05

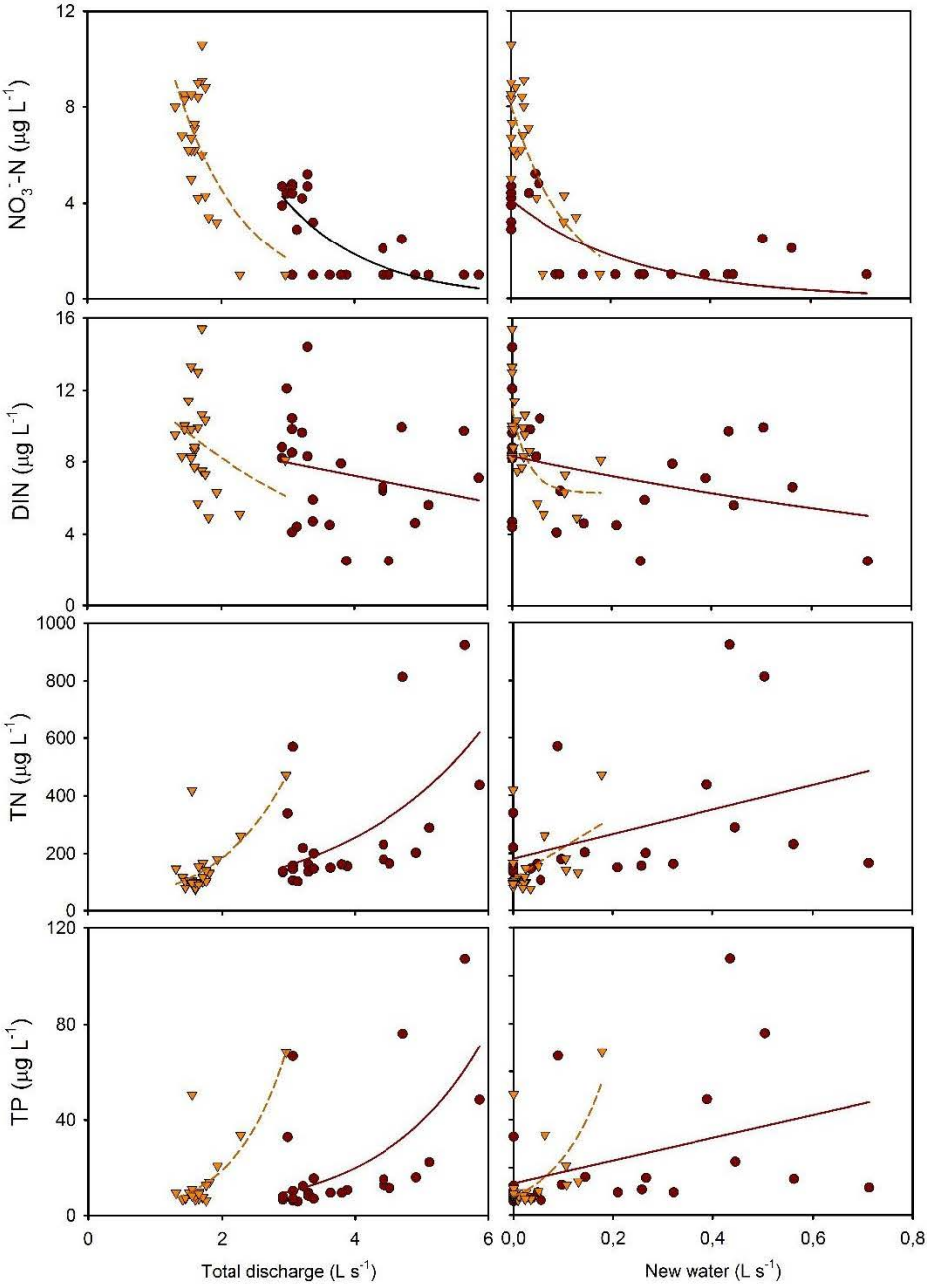

Figure 4.3: Nutrient concentrations (NO_3^--N, DIN, TN and TP) vs catchment dicharge (left side) and new water ($L \cdot s^{-1}$) (right side), for both studied catchments during the 3rd event: old growth native evergreen forest (NF1), in black circles and *Eucalyptus nitens* plantation (EP1) in white inverted triangles. Solid and dashed lines stand for the modeled regression for NF1 and EP1, respectively.

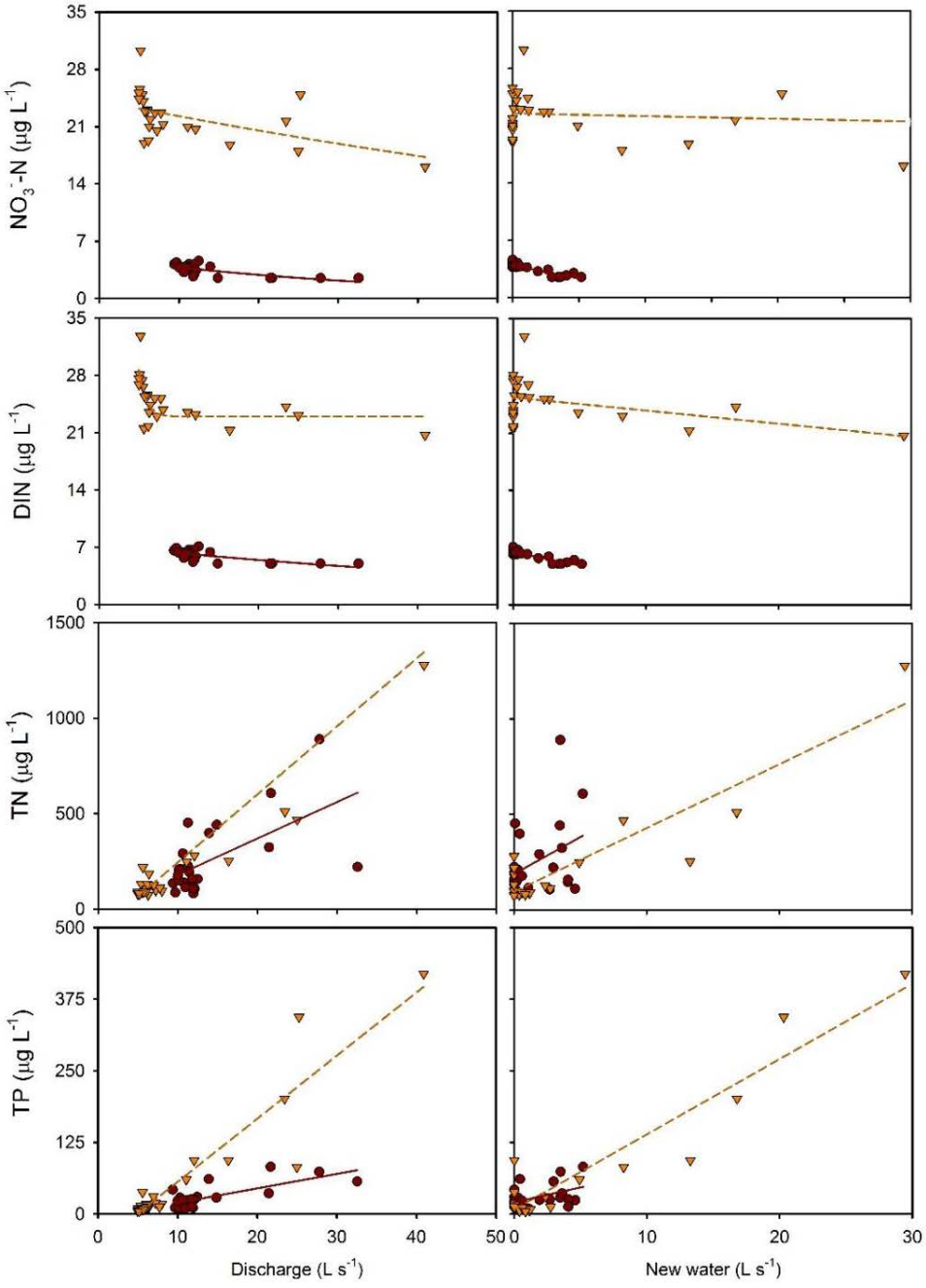

Figure 4.4: Nutrient concentrations (NO_3^--N, DIN, TN and TP) vs catchment dicharge (figures on the left side) and new water (figures on the right side), both in $L \cdot s^{-1}$ for the 5th event. Old growth native forest (NF1), in black circles and *Eucalyptus nitens* plantation (EP1) in white inverted triangles. Solid and dashed lines stand for the modeled regression for NF1 and EP1, respectively.

Huygens *et al*. (2008) described that DIN inputs do not end up in the soil water compartment (i.e. mobile water). If the rate of NO_3^--N and DIN supply remains relatively unchanged during precipitation events, it is expected that these compounds be diluted by the enhanced throughput of water. Hence, it could be hypothesized that NO_3^--N and DIN are either largely consumed by microorganisms or being retained by soil particles. The last suggests that NO_3^--N and DIN are mainly inaccessible for moving water, maybe due to the fact that they are strongly attached to soil particles or that they are simply not hydrologically accessible. This is in accordance with the 'two nitrate worlds' described for the first time by Hall *et al*. (2016). On the other hand, Lozanos (2011) observed both positive and negative correlations between stream discharge and NO_3^--N in an old-growth evergreen rainforest located in the Andean mountain range (40° S), which was attributed to differences in peak flow. NO_3^--N has a different behavior during storm events because the streamflow can dilute NO_3^--N at peak discharge, but when the streamflow increases slowly, usually NO_3^--N also increases (Lozanos, 2011). Results fromthis study show that when stream discharge increases, NO_3^--N concentrations decrease (Figures 4.3 and 4.4). This finding can have a small, but serious consequence, especially when modelling NO_3^--N exports based on monthly or bi-weekly stream water sampling. Hence, in order to understand NO_3^--N and other solutes are exported, sampling campaigns should also include sampling during storm or precipitation events. Org-N flushes, along with the dilution of NO_3^--N, has been previously described in literature (Cirmo and McDonnell, 1997; Inamdar and Mitchell, 2007). In this work, this was attributed to the fact that Org-N is present in the soil macropores, which are accessible to the water flux, hence easily flushed. However, Inamdar and Mitchell (2007) relate DON export to soil anaerobic conditions, in addition to the reductive dissolution of Fe and Al oxides under anaerobic conditions can lead to previously adsorbed dissolved organic matter (DOM) on the oxides. It is hypothesized that NO_3^--N is being reduced to NO_2^--N. The latter reacts with DOM, forming DON. The latter process has been known as the 'Ferrous wheel hypothesis' (Davidson *et al.*, 2003). However, this hypothesis should be tested thoroughly. Although, it is also supported by the TNW, previously described by Hall et al. (2016).

4.4.2. TN and TP concentrations in stream water for forest ecosystems of southern Chile

TN and TP concentrations in stream water are variable in forest ecosystems of southern Chile (see Table 4.3).

Table 4.3: Mean concentrations ($\mu g \cdot L^{-1}$) of total nitrogen (TN, in $\mu g\ N \cdot L^{-1}$) and total phosphorus (TP, in $\mu g\ P \cdot L^{-1}$) in stream water from different forest ecosystems under a low-deposition regime located in the Andean or Coastal mountain ranges (A and C, respectively), southern Chile.

Forest description	Location	TN	TP	References
N. pumilio	AMR	nd	67.3	(Godoy *et al.*, 2001)
N. betuloides	AMR	nd	9.2	(Godoy *et al.*, 2001)
N. betuloides	AMR	62.0	nd	(Oyarzún *et al.*, 2004)
Old-growth evergreen	AMR	157.1	18.0	(Oyarzún and Campos, 1997)
Old-growth evergreen	AMR	67.3	37.4	(Oyarzún and Hervé-Fernández, 2015)
N. nervosa-N. obliqua	AMR	73.3	44.0	(Oyarzún and Hervé-Fernández, 2015)
Old-growth deciduous	AMR	45.0	nd	(Little *et al.*, 2008)
S. conspicua-L. philippiana	AMR	108.6	4.9	(Lozano, 2011)
F. cuppressoides	CMR	176.5	4.6	(Oyarzún *et al.*, 1998)
Evergreen	CMR	36.8	24.1	(Oyarzún *et al.*, 2007)
N. dombeyi	CMR	153.0	nd	(Oyarzún and Huber, 2003)
Eucalyptus globulus	CMR	94.8	30.1	(Oyarzún *et al.*, 2007)
Second-growth evergreen	CMR	135	12	(Hervé-Fernández *et al.*, 2016a)
Eucalyptus globulus	CMR	202	12	(Hervé-Fernández *et al.*, 2016a)
Evergreen	CMR	127.2	11.1	(Oyarzún *et al.*, 2015)
Eucalyptus nitens	CMR	100.1	11.0	(Oyarzún *et al.*, 2015)

nd = not determined; *N.* = *Nothofagus*; *S.* = *Saxegothaea*; *L.* = *Laureliopsis*; *F.* = *Fitzroya*.

In general, the highest TN and TP concentrations were found in *Fitzroya cuppressoides* forest (176.5 µg $N \cdot L^{-1}$), located in the coastal mountain range (CMR) and in *Nothofagus pumilio* forest (67.3 µg $P \cdot L^{-1}$), and located in the Andean mountain range (AMR). The lowest values were found in evergreen forest (36.8 µg $N \cdot L^{-1}$) and in *Fitzroya cuppresoides* forest (4.6 µg $P \cdot L^{-1}$) both located in CMR. Concentrations of DIN were smaller than Org-N concentrations in NF1 (33.2 µg $N \cdot L^{-1}$ versus 94.4 µg $N \cdot L^{-1}$, respectively) and EP1 (33.6 µg $N \cdot L^{-1}$ versus 67.0 µg $N \cdot L^{-1}$, respectively) (see Table 4.3). These results are in agreement with previous research in southern Chile (Perakis and Hedin, 2002; Oyarzún *et al.*, 2004; Hervé-Fernández *et al.*, 2016a) demonstrating that organic nitrogen is responsible for the majority of nitrogen losses from these unpolluted forest ecosystems. According to Oyarzún *et al*. (2007), the DON:DIN ratio is smaller in evergreen native forests than that of *Eucalyptus* spp.

4.5. Conclusions

DIN and NO_3^--N showed a dilution during the 3rd event as discharge and/or new water apportionment increased. During the 5th event, DIN and NO_3^--N was slightly diluted as catchment discharge or new water apportionment increased. Since our study sites were in a region which is under chronic nutrient limitation due to low N inputs (1 to 2.5 kg $DIN \cdot ha^{-1} \cdot yr^{-1}$ and 4 to 10 kg $N \cdot ha^{-1} \cdot yr^{-1}$ for DIN and TN, respectively) forest ecosystems in this region have developed strategies of high nutrient retention. In this case NO_3^--N and DIN are rapidly retained (biotically or abiotically) by the soil ecosystem. Both catchments showed very similar behavior with respect to all measured nutrients. However, it was clear that during the 5th event DIN (therefore NO_3^--N) and TP showed higher concentrations in EP1, than NF1. Nevertheless, the 3rd event was associated with similar concentrations of catchment discharge of nutrients like TN, DIN and TP. These results support Huygens *et al.* (2008), who described NO_3^--N and DON losses in volcanic soil catchments. TN and TP concentrations showed positive correlations with catchment discharge. During the 5th event, this pattern was repeated only in NF1, while in EP1, TN and TP concentrations showed positive correlations with new water apportionment, rather than with catchment discharge. This was expected since *E. nitens* covered catchments are known to have low water infiltration rates (Huber *et al.*, 2010; Oyarzún *et al.*, 2011). In addition, P is attached to

soil particles. Soil erosion sustained this relation during the 5th event, which was evident from the amount of sediment in the sampling bottles.

The quantification of other inputs (i.e: bacterial atmospheric fixation) of nitrogen are taking place in the understory of native forest and FGES plantations are important to really have an idea on how different ecosystems are affected by land cover changes. Only then, it will be able to understand hydrological and biogeochemical processes in these forest ecosystems. So far, most of the differences between native forests and FGES are water infiltration rates (higher in native forests), soil erosion (lower in native forests) and nutrients (higher exportation in FGES, especially for NO_3^--N and TP than in native evergreen forest). Further studies needs to be conducted in order to unravel the different pathways and sources of N and P in complex ecosystems in which native forests are decreasing and FGES is growing each year.

Annu. Rev. Earth Planet. Sci. 1996. 24:225–62

OXYGEN AND HYDROGEN ISOTOPES IN THE HYDROLOGIC CYCLE

J. R. Gat

Department of Environmental Sciences and Energy Research, Weizmann Institute of Science, 76100 Rehovot, Israel

KEY WORDS: isotope fractionation, evapo-transpiration, precipitation, soilwaters, groundwaters

ABSTRACT

Changes of the isotopic composition of water within the water cycle provide a recognizable signature, relating such water to the different phases of the cycle. The isotope fractionations that accompany the evaporation from the ocean and er surface waters and the reverse process of rain formation account for the most le changes. As a result, meteoric waters are depleted in the heavy isotopic of H and O relative to ocean waters, whereas waters in evaporative systems akes, plants, and soilwaters are relatively enriched. During the passage aquifers, the isotope composition of water is essentially a conservative mbient temperatures, but at elevated temperatures, interaction with may perturb the isotope composition. These changes of the isotope mospheric waters, surface water, soil, and groundwaters, as well are applied in the characterization of hydrological system as aleo-climatological conditions in proxy materials in climatic ake sediments, or organic materials.

cycle as expounded by the preacher, that et the sea is never filled, and still to their ble, English translation, 1970), remains e concept of a steady-state one-cycle

0225$08.00

225

CESSES
1369 (2000)

ric water balance—the isotopic perspective

Joel R. Gat*

ual Sciences and Energy Research, Weizmann Institute of Science, 76100 Rehovot, Israel

Abstract:

spheric moisture is determined foremost by the isotope fractionation that ing over the oceans. This subsequently is modified by rainout on the one recycling of precipitation into the atmosphere as a result of evapo- om droplets beneath the cloud base. The marine part of the atmospheric Craig and Gordon, showing the *d*-excess value to reflect the humidity the sea (a function of both temperature and salinity) to the ambient to a value of $d = 10‰$. However, on the leeside of continents and udity deficit in the dry and cold air is large, higher values of up to found when the evaporated vapour from lakes and other open del enabling the quantitative evaluation of the contribution of exemplified by the case of the North American Great Lakes. ed on the isotopic composition of runoff and precipitation is 0 John Wiley & Sons, Ltd.

DUCTION

of the water in the hydrosphere, only 10^{-5} e continents. However, as the annual flux residence time of water in the atmosphere) xing times within the atmosphere, especially close to

Figure 1 (adapted from Chow (1964) water cycle, namely the return flux by the evaporation from the oceans. To a first ap can be ignored. As is evident from Figure 1, h the continent accounts for almost three times as mu by evapotranspiration. The continental atmosphere th budget. The return-flux into the atmosphere

5. Chapter 5: The water molecule, its phases and stable isotopes

5.1. The water molecule

The water molecule (i.e. H_2O) is composed of three atoms, two hydrogen atoms and a single oxygen atom (Figure 5.1). These atoms have specific characteristics that give the water molecule special characteristics such as (Mazor, 2004):

- A high heat capacity, meaning that in comparison with most other materials it takes much more energy input to cause a similar rise in temperature of water.

- Subtraction of energy does not cause water to cool as fast as other materials. This property makes water a good energy storer, and a conservative thermal influence.

- The hydrogen bond to oxygen, and to other water molecules through Van der Waals bonds, gives the water molecule a higher heat capacity, heat of melting and of vaporization, leading to relatively high melting and boiling points.

These qualities are essential for the comprehension of the movement of the water molecule throughout the hydrological cycle. The dipolar configuration of the water molecule is given by the fact that its hydrogen and oxygen atoms share two of the four tetrahedrally oriented electron orbits, which give rise to a dipolar configuration (Clark, 2015). Even though the water molecule is considered neutral, its charge is unevenly distributed, giving one side a negative charge, and the other positive charge (Figure 5.1):

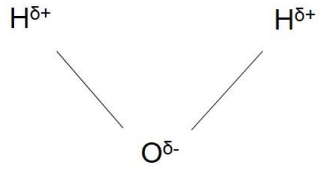

Figure 5.1: Water molecule and its asymmetrical charge distribution.

The positive and negative poles of neighbouring water molecules attract each other to form weak hydrogen bonds (i.e. Van der Waals interactions). These interactions are easily broken, although easily formed again.

5.2. Water phases

These interactions also allow the water molecule to adopt different phases according to temperature and relative humidity (Figure 5.2).

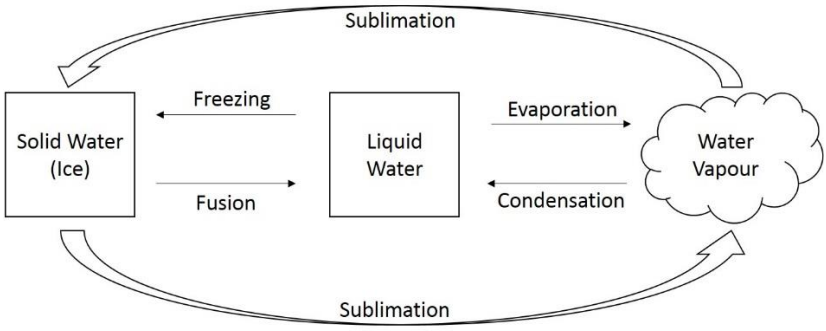

Figure 5.2: Physical states of water (i.e. solid, liquid and gaseous). Arrows show the direction of each process.

Usually, water phases change due to variations of available energy in the environment. Meteorological parameters such as temperature and air moisture content are the typical forms of measuring the energy available for phase changes. In general, air moisture content is expressed as relative humidity (RH, in %), defined as the ratio of actual vapor pressure in the air to the saturation vapor pressure at a certain temperature.

The opposite of evaporation (i.e. from liquid to gas), the process of condensation (i.e. gas to liquid) of water vapor from the atmosphere occurs at dew point temperature, which is the lowest temperature, at constant pressure and water content, to reach saturation. When humidity exceeds the dew point (i.e. RH > 100%), or temperature lowers enough such that capacity to hold water vapor in the air mass,

reduces to such extent that hydrogen bonds reform and water vapor condenses; while, other changes in temperature and relative humidity generate evaporation. These are key processes and characteristics of the water molecule that maintain the water cycle cycling.

5.3. Isotope basics

The main characteristic of isotopes of a specific chemical element is that they possess the same number of protons (i.e. particles with a positive charge), but different number of neutrons (i.e. non-charged particles). In isotope nomenclature, these are written as follows:

$$^{AMU}_{P^+}I_{N^0} \tag{5.1}$$

where I is the chemical element, the superscript AMU stands for atomic mass unit, or the atomic weight (i.e. sum of the number of protons and neutrons). P^+ stands for the atomic number (i.e. number of protons). This particle is positively charged, and N^0 stands for the number of neutrons, which have no charge. Isotopes are usually written with the element and the total weight (AMU), and even though there are many stable isotopes, this work refers only to some of them that form the water molecule, i.e. hydrogen (H) and oxygen (O) stable isotopes. In nature, the most common isotope of hydrogen is protium, formed by a single proton (^1_1H). However, H has other natural isotopes i.e. deuterium (^2_1H, a stable isotope) and tritium (^3_1H, a radioactive or unstable isotope) have one proton, but one and two neutrons, respectively. Molecules containing heavy stable isotopes are more stable, therefore, need more energy to break their bonds (i.e. have a higher dissociation energy) than molecules with lighter isotopes. Hence, differences between isotopologues (molecules with different isotopes) are explained by differences in their zero point energies (ZPE), which is the lowest possible energy in vacuum conditions (Figure 5.3). In this figure, is possible to observe that H-H (i.e. ^1H-^1H) bond approximately needs 2 kcal·mole^{-1} less energy than the bond of D-D (i.e. ^2H-^2H). Hence, ^1H-^1H bonds are broken more easily (i.e. less energy needed) than those of ^2H-^2H, which are stronger and harder to break. It is

expected that chemical reaction rates where these bonds are broken will show an isotope effect, depending on the energy input. These effects are more obvious at low temperatures (Kendall and McDonnell, 1998; Gat, 2005).

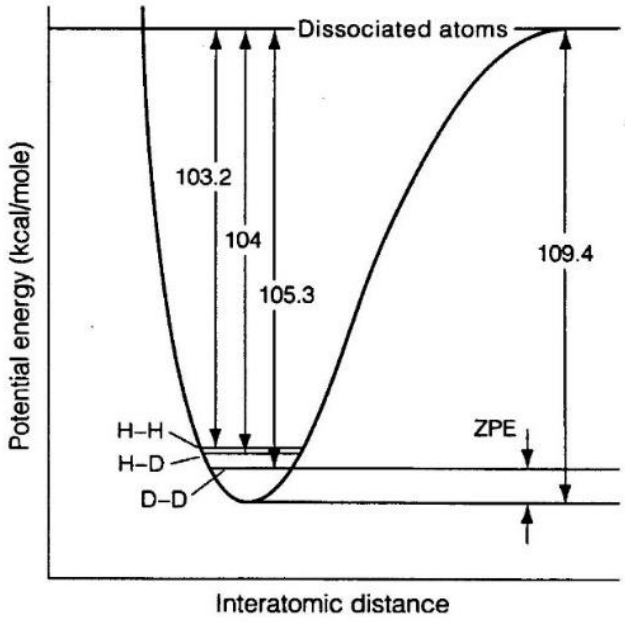

Figure 5.3: Interatomic distance and potential energy relationship for stable hydrogen isotopes (protium and deuterium; H and D, respectively) of a molecule. Higher zero point energies (ZPE) result in less stable molecules (from Kendall and McDonnell, 1998).

The energy differences associated with isotope effects are about 1000 times smaller than the available energy for chemical reactions, and hence cannot be the driving force for chemical equilibrium (Kendall and McDonnell, 1998). This is the main reason why stable isotopes are good tracers, used in several hydrological, biochemical and biogeochemical processes.

5.4. Stable isotope delta (δ) notation and per mil

Isotopic composition is expressed in terms of heavy/light isotopes ratios (e.g. $[^{2}H]/[^{1}H]$ and $[^{18}O]/[^{16}O]$). These ratios are represented in δ-notation, indicating the deviation from a designated reference, i.e. VSMOW (Vienna Standard Mean Ocean

Water) in the case of water, and stands for a particular ratio of $[^{2}H]/[^{1}H]$ and $[^{18}O]/[^{16}O]$, respectively, in distilled ocean waters. It is important to mention that the first reference water was known as Standard Mean Ocean Water (SMOW) and Harmond Craig and collegues made it, using distilled ocean waters from different places around the world (Figure 5.4).

Figure 5.4: Original container of Standard Mean Ocean Water (SMOW).

Later in 1968, SMOW water was running out and the International Atomic Energy Agency proposed a new reference called VSMOW. This is new reference material was calibrated against SMOW and prepared along with the European Institute for Reference Materials and Measurements and the American National Institute of standards and Technology. Since 2006, VSMOW2 is being used which is very similar to VSMOW, hence it is frequently refered to as VSMOW.

Their respective values are close to 0 for both isotopes ($[^{2}H]/[^{1}H] = 155.95 \cdot 10^{-6}$; and $[^{18}O]/[^{16}O] = 2005.2 \cdot 10^{-6}$, respectively (Leibundgut et al., 2009). Equation (5.2) shows how the δ-value is calculated for ^{18}O:

$$\delta^{18}O_{sample} = \frac{\left(\frac{[^{18}O]}{[^{16}O]}\right)_{sample} - \left(\frac{[^{18}O]}{[^{16}O]}\right)_{reference}}{\left(\frac{[^{18}O]}{[^{16}O]}\right)_{reference}} = \left(\frac{R_{sample}}{R_{VSMOW}} - 1\right) \quad (5.2)$$

This normalized difference between a sample and a reference, namely VSMOW, is a very small number. Hence, it is usually multiplied by 1000, and expressed in per mil (‰, Eq. (5.3)):

$$\delta^{18}O_{sample} = \left(\frac{\left(\frac{[^{18}O]}{[^{16}O]}\right)_{sample}}{\left(\frac{[^{18}O]}{[^{16}O]}\right)_{VSMOW}} - 1\right) \cdot 1000 = \left(\frac{R_{sample}}{R_{VSMOW}} - 1\right) \cdot 1000 \quad (5.3)$$

where R stands, in this example, for the $[^{18}O]/[^{16}O]$ ratio (Gat, 2005). Due to differences in the properties of the isotopic atoms and isotopologues (i.e. same molecule formed of different isotopes), be it rates of motion, frequencies of intermolecular vibrations, rotations or stability of chemical bonds, the relative abundance of the isotopes in the source material (i.e. reactant) and the product of a dynamic process is different (Kendall and McDonnell, 1998). This relative change in isotope abundance is due to a process known as fractionation.

5.5. Fractionation factor (α) and enrichment (ε)

Changes of the isotopic composition of water within the water cycle provide a recognizable signature, relating such water to the different phases of the cycle. The term “isotope fractionation” is used to denote any situation where the isotopic abundance changes (Kendall and McDonnell, 1998). For example, the isotope fractionation that accompanies the evaporation from the ocean and other water surfaces and the reverse process, that is, condensation of water vapor during rain

formation accounts for the most notable changes (Gat, 1996). These changes in the isotopic signature of water due to fractionation, which is principally controlled by temperature and relative humidity (RH, in %), within the hydrological cycle give us a recognizable tracer in all of its components (Leibundgut *et al.*, 2009). In this way, it is possible to distinguish the different components and pathways of water molecules in the hydrological cycle (Gat, 2005; Clark, 2015).

Chemical reactions involve the transfer or mass from reactants to products. Theoretically, at t = 0, the system has only reactants, and as reactions proceeds the reactants are transformed to products. The mass transfer, from reactants to products, and vice versa in a system, known as equilibrium reaction is referred to in this thesis as equilibrium process (i.e. Eq. (5.4)). Yet, the reaction transforms reactants to products and the velocities of chemical reaction (or physical process) and back reaction (or reverse process) are not equal. Hence, mass is accumulated in the product (Eq. (5.5)) it is known as a non-equilibrium reaction, and in the present document it will be referred as non-equilibrium process.

$$\text{reactant} \longleftrightarrow \text{product} \tag{5.4}$$

$$\text{reactant} \longrightarrow \text{product} \tag{5.5}$$

In general, the reactant and the product is written in chemistry in the following order: product – reactant (Clark, 2015). For example in an evaporating water body (w) that releases water vapor (v) into the atmosphere will be written as ‘v-w’; while the opposite reaction, which is condensation will be written as ‘w-v’.

Isotopes in the water molecule (i.e. ^{2}H and/or ^{18}O) from an evaporating water pool can follow equilibrium and non-equilibrium processes, which will generate different labelling processes (i.e. differences generated by changes in the isotopic signature). For the case of water, equilibrium processes are energy (i.e. temperature) driven; while non-equilibrium processes are diffusion driven. Each of these processes are explained in detail below.

5.5.1. Equilibrium process

Equilibrium as such refers to a thermodynamic state, in which there are no net flows of energy and matter, either within a system or between systems. Usually these systems have a tendency towards the state of minimum energy (Gat, 1996). Systems in mutual thermodynamic equilibrium are simultaneously in mutual thermal, mechanical, chemical, and radiative equilibria (Kendall and McDonnell, 1998). Isotope-exchange reactions in equilibrium conditions involve the redistribution of isotopes of a common element among various species or compounds (in a strict sense, this only occurs in a closed, well-mixed system at chemical equilibrium, such as boundary interfaces). At isotopic equilibrium, forward and backward reaction rates of a particular isotope are identical. Even in so-called equilibrium systems, where the amount and concentration of the chemical compounds involved do not change, one encounters differences in the abundance of the isotopic species in the various components of such a system (Clark, 2015). However, since bonds between lighter atoms are broken more easily than heavier atoms, this generates differences in the isotope ratios (R) are generated; R_w and R_v (isotope ratios for water and vapor, respectively) resulting from differences in bond strength of the different isotopic species.

5.5.1.1. Fractionation under equilibrium conditions

An isotopic fractionation factor, for example, for ^{18}O from vapor to liquid phase (i.e. condensation, $\alpha^{18}O_{w\text{-}v}$) is defined as follows:

$$\alpha^{18}O_{w\text{-}v} = \frac{\left(\frac{[^{18}O]}{[^{16}O]}\right)_w}{\left(\frac{[^{18}O]}{[^{16}O]}\right)_v} = \frac{R_w}{R_v} \tag{5.6}$$

where $\alpha^{18}O_{w\text{-}v}$ should be understood and read as the fractionation factor α of $^{18}O_{w\text{-}v}$ during the condensation process. Please note that for ^{2}H the example is exactly the same. While for evaporation, α is the inverse as shown below:

$$\alpha^{18}O_{v\text{-}w} = \frac{\left(\frac{[^{18}O]}{[^{16}O]}\right)_v}{\left(\frac{[^{18}O]}{[^{16}O]}\right)_w} = \frac{R_v}{R_w} \quad (5.7)$$

where R is the ratio of the abundance of the heavy isotope to the abundance of the lighter isotope (e.g. $[^{2}H]/[^{1}H]$ or $[^{18}O]/[^{16}O]$) in water and vapor (subscripts w and v, respectively). In analogy to the reversible chemical reactions at equilibrium (exchange reactions), one can define a thermodynamic constant of the isotopic exchange reaction (Clark, 2015):

$$\left[H_2\ ^{16}O\right]_w + \left[H_2\ ^{18}O\right]_v \leftrightarrow \left[H_2\ ^{18}O\right]_w + \left[H_2\ ^{16}O\right]_v \quad (5.8)$$

The thermodynamic reaction constant K for ^{18}O in vapor-water is estimated as follows (Clark, 2015):

$$K_{w\text{-}v} = \frac{\left[H_2\ ^{18}O\right]_w \cdot \left[H_2\ ^{16}O\right]_v}{\left[H_2\ ^{16}O\right]_w \cdot \left[H_2\ ^{18}O\right]_v} = \frac{\left(\frac{[^{18}O]}{[^{16}O]}\right)_w}{\left(\frac{[^{18}O]}{[^{16}O]}\right)_v} = \frac{R_w}{R_v} = \alpha^{18}O_{w\text{-}v} \quad (5.9)$$

The inverse is for the evaporation process, where $K_{w\text{-}v}$ is the thermodynamic reaction constant of vapor to water. This does not mean that the isotopic compositions of both compounds at equilibrium are identical, but only that the ratios of the different isotopes in each compound are constant for a particular temperature (figure 5.5, Kendall and McDonnell, 1998).

A typical example for an equilibrium process would be the condensation of water vapor in rain clouds (Gat, 2000; Gat and Airey, 2006). The heavier water isotopologues (containing ^{18}O and ^{2}H) become enriched in the liquid phase (i.e. heavier phase) while the lighter isotopes (containing ^{16}O and ^{1}H) remain in the vapor

phase (i.e. lighter phase). Atomic bonds zero point energies are responsible for the equilibrium fractionation effects (see Figure 5.3). This is more evident at lower temperatures and practically disappears at higher temperatures due to the amount of free energy. The latter is because at higher temperatures, higher rotational-vibrational energy states become more common. Hence, energy differences between the different isotopologues become smaller and smaller with increasing height of the corresponding energy levels. This can be observed in Figure 5.5, where the black and grey thick lines approach the dashed line (i.e. equal fractionation factor), as temperature increases. In general, the higher the temperature, the less the difference between the equilibrium isotopic compositions of any two species (this is due to the population size of higher energy levels that changes with temperature. Hence, the differences between these higher rotation/vibrational energy levels and the dissociation energy become smaller between the different isotopologues the differences in ZPE between the species become smaller). The value of such equilibrium fractionation factors can be estimated for ^{18}O and ^{2}H for the reaction water to vapor or vapor to water for the temperature range from 0 to 374° C (Horita and Wesolowski, 1994):

$$\ln\alpha_{18_O} = \frac{-7.685 + 6.7123\cdot\left(\frac{10^3}{T}\right) - 1666.4\cdot\left(\frac{10^6}{T^2}\right) + 0.35041\cdot\left(\frac{10^9}{T^3}\right)}{1000} \quad (5.10)$$

$$\ln\alpha_{2_H} = \frac{1158.8\cdot\left(\frac{T^3}{10^9}\right) - 1620.1\cdot\left(\frac{T^2}{10^6}\right) + 794.84\cdot\left(\frac{T^2}{10^3}\right) - 161.04 + 2.9992\cdot\left(\frac{10^9}{T^3}\right)}{1000} \quad (5.11)$$

where T stands for temperature in Kelvin. Please, note that the fractionation factor α is calculated the same way for evaporation (water to vapor) and condensation (vapor to liquid water). The fractionation factors (i.e. α) show small differences from the equal-energy value of 1 (Figure 5.5).

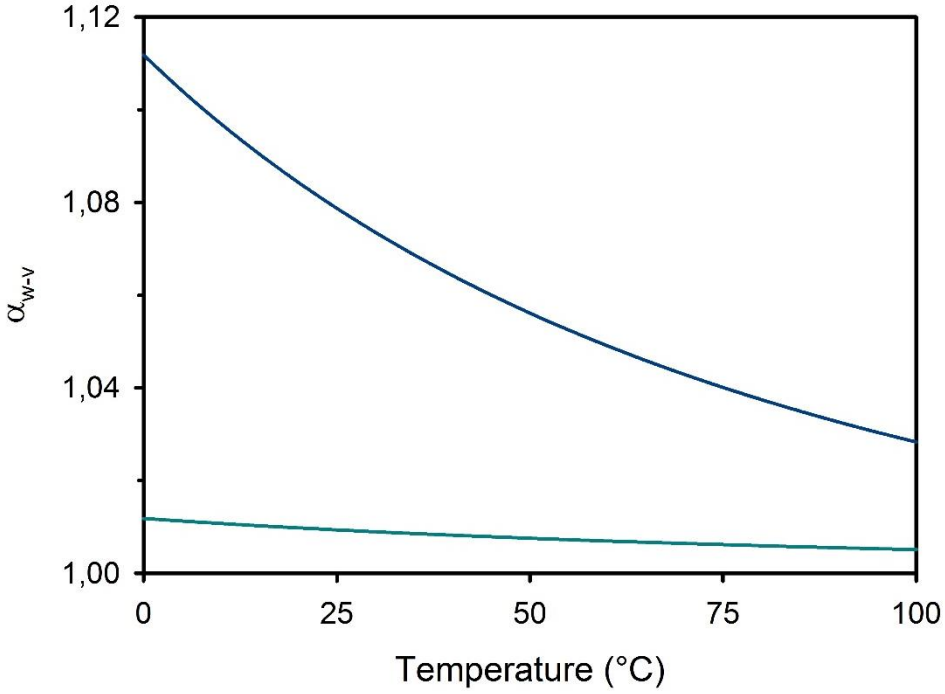

Figure 5.5: Equilibrium fractionation factor for the reaction vapor to water estimated according to Horita and Wesolowski (1994) for ^{18}O and ^{2}H (light and dark blue solid lines, respectively). Note that as temperature increases fractionation factor α reaches a constant value. In this case, this is beyond 340°C. Therefore, at lower temperatures we can expect the highest fractionation factors between water and vapor.

The sign and magnitude of α are dependent on many factors, of which temperature is the most important. Other factors may include chemical composition (e.g. salinity and dissolved cations and anions (for details see Craig and Gordon, 1965; Gonfiantini, 1986; Lerman *et al.*, 1995) and vapor pressure. However, these are only important when working with sea water and brines (Horita *et al.*, 1995; Kendall and McDonnell, 1998; Gat, 2005).

The fractionation factor (α) for forward (i.e. condensation, w-v) and reverse (i.e. evaporation, v-w) reactions is calculated using Eqs. (5.10) and (5.11) for ^{18}O and ^{2}H, respectively. However, they are written as follows:

$$\alpha^{+}_{\text{reactant-product}} = \frac{1}{\alpha^{+}_{\text{product-reactant}}} \tag{5.12}$$

The above equation shows the fractionation factor $\alpha^{+}_{w\text{-}v}$ (left side, i.e. from water vapor to liquid water) for a typical condensation process; while its inverse, $1/\alpha^{+}_{v\text{-}w}$ (right side, i.e. from liquid water to water vapor), is the fractionation factor used for the evaporation process. Craig and Gordon (1965) defined equilibrium fractionation factors as follows:

$$\alpha^{+}_{w\text{-}v} = \frac{R_w}{R_v} > 1 \tag{5.13}$$

and

$$\alpha^{*}_{v\text{-}w} = \frac{R_v}{R_w} < 1 \tag{5.14}$$

Eqs. (5.13) and (5.14), indicate that the vapor isotopic signature is depleted in relation to the water isotopic signature (Merlivat and Coantic, 1975). This usage has become traditional when discussing atmospheric processes. In general, $\alpha^{+}_{w\text{-}v}$ is used for condensation problems, whereas $\alpha^{*}_{v\text{-}w}$ (i.e. $1/\alpha^{+}_{v\text{-}w}$) is preferred for evaporation problems (Craig and Gordon, 1965; Gat, 2005). However, in this text $\alpha^{+}_{w\text{-}v}$ and $1/\alpha^{+}_{v\text{-}w}$ are used instead for condensation and evaporation processes, respectively. In literature, the fractionation factor is estimated in the same way for condensation and evaporation (i.e. $\alpha^{+}_{w\text{-}v}$ and $\alpha^{+}_{v\text{-}w}$, see Eqs. (5.10) and (5.11)) (Kendall and McDonnell, 1998). Usually it is either abbreviated as α or simply removed from equations, for an example see Gat (1996) and Gibson *et al.* (2008) and Appendix H, Eq. (H.16). This is because the number is very small and close to 1.

Fractionation factors (α) can be easily be related to the δ-notation as follows (Clark, 2015):

$$\alpha^{+}_{w\text{-}v} = \frac{R_w}{R_v} = \frac{\frac{R_w}{R_{VSMOW}}}{\frac{R_v}{R_{VSMOW}}} = \frac{\left[1+\left(\frac{R_w}{R_{VSMOW}}-1\right)\right]\cdot 1000}{\left[1+\left(\frac{R_v}{R_{VSMOW}}-1\right)\right]\cdot 1000} = \frac{(1000+\delta_w)}{(1000+\delta_v)} \quad (5.15)$$

The above case is for condensation (i.e. vapor to water). For evaporation (i.e. v-w) R_w and R_v are simply inverted, as in R_v/R_w. Where δ_w and δ_v are expressed in ‰.

5.5.1.2. Enrichment under equilibrium conditions

In order to compare isotope fractionations factors (α) with the δ-notation, the fractionation factor α can also be expressed in δ-notation, then it is referred to as enrichment factor (i.e. ε). Therefore, ε is calculated for the condensation process as follows:

$$\varepsilon^{+}_{w\text{-}v} = (\alpha^{+}_{w\text{-}v} - 1)\cdot 1000 \quad (5.16)$$

Eq. (5.16) represents the enrichment (i.e. gain in heavier isotopes) of the first condensate of water vapor. However, when water evaporates the exact opposite reaction occurs, hence:

$$\varepsilon^{*}_{v\text{-}w} = \left(\frac{1}{\alpha^{+}_{v\text{-}w}} - 1\right)\cdot 1000 \quad (5.17)$$

The enrichment (ε) is used to express fractionation factors in δ-notation for vapor-water enrichment, from an evaporating or condensing source (i.e. water body or cloud, respectively). This is the same expression as the δ-notation used to express isotope signatures, the equilibrium enrichment factor $\varepsilon^{+}_{w\text{-}v}$ (for condensation) and $\varepsilon^{*}_{v\text{-}w}$ (for evaporation) can be added and substracted with measured or estimated δ values. Hence, using the example of fractionation for condensation of water vapor into liquid water, as in Eq. (5.13), the enrichment is estimated as follows:

$$\varepsilon^{+}_{w\text{-}v} = \left(\frac{R_w}{R_v} - 1\right)\cdot 1000 \quad (5.18)$$

Note that Eq. (5.16) is similar to Eq. (5.18), only written differently. Therefore,

$$\varepsilon^{+}_{w\text{-}v} = \delta_w - \delta_v \tag{5.19}$$

This is only valid if the water vapor is small ($\delta_v \ll 1000$). In Appendix A is shown how Eq. (5.19) is derived and how it changes when the previously mentioned assumption is not met.

A brief example on how to use and interpret the fractionation factor (α) and the enrichment factor (ε) is the following: let us take the process of precipitation formation through the condensation of water vapor in a cloud (typical textbook example for equilibrium process). Imagine water vapor of a known isotopic signature (i.e. $\delta^{18}O_v$ = 0‰), and condensing at a temperature of 25°C. First, we need to estimate the fractionation factor. Hence, solving Eq. (5.10) yields a fractionation factor of 1.0093. Now, calculating the enrichment factor ($\varepsilon^{+}_{w\text{-}v}$), that is solving Eq. (5.16), yields a value for δ_w = 9.3‰. This value corresponds to the first condensation of the evaporate, at 25° C and tells us how enriched this condensed water is compared to its source vapor. Now, we simply replace our known values in Eq. (5.19), which yields a $\delta^{18}O$ $\varepsilon^{+}_{w\text{-}v}$ = 9.3‰, which is the theoretical isotopic signature of the first condensed water (i.e. liquid water). Further sequential condensation occurs, however, now the isotope signature changes to a lighter or depleted one, as the remaining vapor becomes depleted in heavy isotopes. This process also known as rainout effect is explained at the end of chapter 6, Figure 6.2.

5.5.2. Non-equilibrium process

A non-equilibrium process means that the transfer from reactants (e.g. water) to the products (e.g. water vapor) is faster than that of products to reactants. Hence, the product accumulates. While in equilibrium exchange processes, the reactant product-reaction and vice versa occurs at a constant rate. Therefore, there is no accumulation of products or reactants. In the early literature, observed fractionation effects under non-equilibrium conditions were attributed to differences in the

movement of the isotopologues. This process was termed “kinetic isotope fractionation” or “diffusion fractionation” (referred to as α_K, in this work (Eq.(5.20)) and is present when there is an outgoing flux with different isotopic ratios than that of the bulk of the material. Isotopic fractionation of H and O isotopes occurs during the transport of water molecules in the gas phase within the boundary layer. These differences in transport are due to the different velocities of the three most abundant isotopologues $^{1}H_2{}^{16}O$ (mass 18), $^{1}H^{2}H^{16}O$ and $^{2}H^{1}H^{16}O$ (mass 19) and $^{1}H_2{}^{18}O$ (mass 20) as they diffuse through the air column from the boundary layer of water-saturated air over the evaporating water surface. Please note that this layer is as thick as a single or a couple of molecules, hence very small.

5.5.2.1. Fractionation under non-equilibrium conditions

The enrichment of $\delta^{18}O$ over $\delta^{2}H$ occurs due to differences in diffusion rates of the water molecules in free air during evaporation in non-saturated environments (i.e. RH < 100%). Diffusion fractionation (α_K) is due to the differences in diffusion from the different molecular velocities “v” or diffusion of the common and heavy (subscript i) isotopologues, which can be calculated according to the kinetic theory of gases, also known as the Graham’s law of effusion, that comes from the ideal gas law:

$$\alpha_K = \alpha_{\text{diffusion in atmosphere}} = \frac{\bar{v}_i}{\bar{v}} = \frac{\sqrt{\frac{3\cdot k\cdot T}{(m_i)}}}{\sqrt{\frac{3\cdot k\cdot T}{m}}} = \sqrt{\left(\frac{m}{m_i}\right)} \qquad (5.20)$$

Thus, from the mean molecular velocity of isotopologues it can be shown that diffusion rates for an ideal gas in a *vacuum* are just inversely proportional to the square root of the mass of its particles (i.e. molecular weight), as shown in Eq. (5.20), commonly known as Graham’s law. However, with increasing pressure, molecular collisions and diffusion (referred to as D in equation (5.21)) between gases becomes more important and its effects need to be accounted for, as shown in the following simple gas theory equation (Stewart, 1975; Criss, 1999; Luz *et al.*, 2009):

$$\alpha_K = \frac{D}{D_i} = \left(\frac{\Gamma_i+\Gamma_G}{\Gamma+\Gamma_G}\right)^2 \cdot \sqrt{\left(\frac{m\cdot(m_i+m_G)}{m_i\cdot(m+m_G)}\right)} \quad (5.21)$$

where D is diffusion coefficient, the subscript G refers to a gas media (e.g. air, 28.8 $g\cdot mol^{-1}$) and Γ is the collision diameter of the heavy (subscript i) and light water isotopologue. Please note that Eq. (5.21) is different to that of Eq. 16 in Merlivat (1978). In the past, Γ was assumed to be equal for all isotopologues (Gat, 1996). Recently, Luz *et al.* (2009) showed that diffusion rates of ^{18}O and ^{2}H were similar to those of ^{16}O and ^{1}H. This was tested under an atmosphere saturated with helium (He = 4 $g\cdot mol^{-1}$), dry air (i.e. $O_2 + N_2$ = 28.8 $g\cdot mol^{-1}$) or argon (Ar = 39.9 $g\cdot mol^{-1}$). Therefore, it can be assumed that collision diameters are identical for different water isotopologues, $\Gamma_i = \Gamma$; then D/D_i = 0.9939 and 0.9687 for $^{1}H^{2}H^{16}O$ (and $^{1}H_2{}^{17}O$, both with a molecular weight of 19 $g\cdot mol^{-1}$) and $^{1}H_2{}^{18}O$ (20 $g\cdot mol^{-1}$), respectively. These values are different from those estimated by Merlivat (1978), i.e., 0.9723 and 0.9755 for masses of 19 and 20 $g\cdot mol^{-1}$, respectively. All given values, differ from simple kinetic gas theory, based on the molecular weights (i.e. Eq. (5.21)). These variations could be due to hydrogen bonding in the gas phase (Gat, 1996) or to temperature dependence (Luz *et al.*, 2009), neither of which is taken into account in the kinetic theory of gases (Eq. (5.21)) or the Chapman-Eskog kinetic theory, which assumes that diffusion occurs through monoatomic gases (Gat, 2005; Luz *et al.*, 2009). Despite these theoretical differences, measured values by Merlivat (1978) and by Luz *et al*. (2009) are very similar and in agreement. Hence, in this study values from Merlivat (1978) are used.

5.5.2.2. Enrichment under non-equilibrium conditions in a dry atmosphere and under variable moisture conditions

The diffusion enrichment ε_K, generated from evaporating water is estimated as follows:

$$\varepsilon_K = (\alpha_K - 1)\cdot 1000 \quad (5.22)$$

Using results from Luz *et al*. (2009), this results in enrichments of 31.3‰ for $^{1}H_2{}^{18}O/^{1}H_2{}^{16}O$ and 6.1‰ for $^{2}H_2{}^{16}O/^{1}H_2{}^{16}O$. These results clearly show that the fractionation by diffusion (α_K) is stronger for ^{18}O than for ^{2}H. The above equation holds true only for dry air (i.e. $O_2 + N_2 = 28.8\ g{\cdot}mol^{-1}$) with a relative humidity of 0%. However, in nature, a relative humidity of 0% is rare. During evaporation under non-equilibrium conditions, an enhanced ^{18}O enrichment occurs compared to ^{2}H, in the liquid phase. This is due to differences in diffusion rates of the water molecule in free air during evaporation in non-saturated environments (i.e. RH < 100%), the higher vapor pressure of $^{1}H^{2}HO$ (mass 19) and $^{1}H_2{}^{18}O$ (mass 20) and the resulting enrichment of ^{18}O compared to ^{2}H in the remaining water. This effect is much easier to follow in the $\delta^{18}O$ vs $\delta^{2}H$ space, and follows a so called evaporation line; lake evaporation line or soil evaporation lines (LEL and SEL, respectively). In general, EL's have a lower slope compared to the Local Meteoric Water Line (or LMWL) slope (Gat, 1996). These differences are due to the inverse relationship of the effect of equilibrium fractionation on the different water isotopologues (fractionation eight times stronger for $^{2}H^{1}H^{16}O$ than for $^{1}H_2{}^{18}O$) and the effect of kinetic fractionation on the two isotopologues (fractionation about five times stronger for $^{1}H_2{}^{18}O$ than for $^{2}H^{1}H^{16}O$). The slope of the LMWL is the result of the combined action of both kinds of fractionation. If kinetic fractionation is stronger (i.e., if RH is small), than the slope decreases. If kinetic fractionation is small (i.e., if RH is large), the slope is only slightly lower than 8. The meaning and interpretation of LMWL and EL will be given in detail in chapter 8.

In nature, evaporation under a dry atmosphere rarely occurs. Hence, the effect of moisture content in the atmosphere during the evaporation process will affect the enrichment of $\delta^{18}O$ and $\delta^{2}H$ distinctly. In this sense, in addition to ε_K, there is also non-equilibrium enrichment, referred as $\Delta\varepsilon$, which is used to describe the isotope enrichment of an evaporating water reservoir under non-equilibrium conditions relative to changes in relative humidity. $\Delta\varepsilon$ is defined following Craig and Gordon (1965) as:

$$\Delta\varepsilon = C_K{\cdot}\theta{\cdot}n{\cdot}(1 - h) \qquad (5.23)$$

C_K is a "kinetic" constant with values of 28.5‰ and 25.115‰ for $\delta^{18}O$ and $\delta^{2}H$, respectively (Merlivat, 1978). When evaporation occurs from within the soil column or

from leaves, C_K may then be double (or twice as high) compared to the case of evaporation occurring from a freely exposed water surface (Gat and Bowser, 1991). θ represents the ratio of transport resistances in the molecular diffusion layer. This term is generally assumed to be 1. However, Gat *et al.*, (1994) found that for the North American Great Lakes, θ was 0.88; and a value of about 0.5 was reported for evaporation in the eastern Mediterranean Sea (Gat *et al.*, 2003). The complete detailed derivation of Δε is given in Appendix C. The weighting term 'n' varies between $0.5 < n < 1$. n can be assumed equal to 1 for small water bodies whose evaporation flux does not perturb the ambient moisture significantly (Lerman *et al.*, 1995). For an open water body, a value of $n = 0.5$ seems appropriate (Gat, 1996). However, for evaporation of water through a stagnant air layer such as in soils (Barnes and Allison, 1988) or leaves (Allison *et al.*, 1985), a value of $n \sim 1$ fits the data reasonably well. However, it can also be derived in other ways for different soil and methodological conditions (see Braud *et al.*, 2005, and references therein). Derivation of 'n' is given for soils in Appendix D. h, corresponds to the relative humidity normalized to the evaporation surface temperature, and is calculated as shown on Eq. (F.2), in Appendix F.

6. Chapter 6: The Rayleigh model

6.1. The Rayleigh model

Isotopic signatures can be modelled for evaporation (Tsujimura and Tanaka, 1998; Clark, 2015) and condensation processes (Salati *et al.*, 1979; Gat and Matsui, 1991), under equilibrium and non-equilibrium conditions using the Rayleigh model (Rayleigh, 1895; Gat, 1996; Clark, 2015). This model was first described by Lord Rayleigh, about 120 years ago, which described the depletion of alcohol by distillation from an alcohol/water mixture (Gat, 2005). The Rayleigh equation depicts an exponential relation that describes the partitioning between two reservoirs as one reservoir decreases in size (e.g. water/alcohol mixture) while the other compartment increases (e.g. distilled alcohol). The same equation has been used to model isotopic signatures of the evaporating reservoir. The Rayleigh equation has been used to describe an isotope fractionation process under the following assumptions (Gat, 2005):

1) Material is removed continuously from a mixed system containing molecules of two or more isotopic species, such that equilibrium exists (or virtually exists!).

2) The fractionation accompanying the removal process (e.g. evaporation or condensation) at any instance is described by a known fractionation factor, α.

3) The fractionation factor, α, remains constant during the process.

When the isotopic species removed (i.e. condensed or evaporated) at every instant are in thermodynamic equilibrium with those remaining in the system, we have the circumstances of the so called Rayleigh distillation (Gat, 1996). Remember that from water vapor to liquid water, i.e. condensation, $\alpha^{+}_{w\text{-}v}$ is used, while from liquid water to water vapor, i.e. evaporation, $\alpha^{*}_{v\text{-}w} = 1/\alpha^{+}_{w\text{-}v}$ is used instead. Note that the fractionation factor α '*per se*' has the same value when used for evaporation or condensation processes. On Figure 6.1, $\delta^{18}O$ signatures of water and vapor enrichment (i.e. increasing the number of heavier atoms relative to the lighter ones)

are shown for a full water compartment ($f = 1$, abscissa on Figure 6.1), losing water through evaporation ($f \to 0$) when subjected to Rayleigh fractionation.

The Rayleigh equation can be used to describe how mass is removed constantly with a constant fractionation factor (i.e. temperature). These processes can occur under two different boundary conditions, even when fractionation factors are the same for open or closed systems.

6.2. Open and closed systems

Frequently in isotope hydrology literature, descriptions of evaporation or condensation processes under equilibrium conditions in open or closed systems. In open systems, instantaneous vapor is in equilibrium with the evaporating water. However, the vapor fraction is removed out of the contact of the evaporating water. In Figure 6.1, lines A, B and C show the instantaneous $\delta^{18}O$ isotopic signature of remaining or evaporating water (line A) as water evaporates and forms water vapor (line B), and the accumulated water vapor (line C). The distance between lines A and B represents the enrichment ε, with a constant fractionation factor (i.e. $\alpha = 1.01$), hence an $\varepsilon = 10‰$, as the fraction f diminishes (X-axis, Figure 6.1). As seen in Figure 5.5, the fractionation factor becomes smaller as temperature increases. The same effect is observed for the enrichment. Hence, at a higher temperature, the distance between lines A and B is reduced (Kendall and McDonnell, 1998).

In a closed system, water and vapor pools remain always in contact, hence the water and vapor δ-values differ only by the enrichment, that is, if temperature remains constant. In Figure 6.1, this is shown with lines D and E, which correspond to water and vapor, respectively. It is important to mention that in open and closed systems, if distillation is complete (i.e. $f = 0$), the accumulated vapor mass must have a δ-value equal to the initial water mass. This last is shown in the intercept of lines E and C, which corresponds to the lines A and D initial δ-value. Mathematically, the Rayleigh model used to describe the evaporation and condensation process in open and closed systems is equal (Kendall and McDonnell, 1998; Gat, 2005; Clark, 2015).

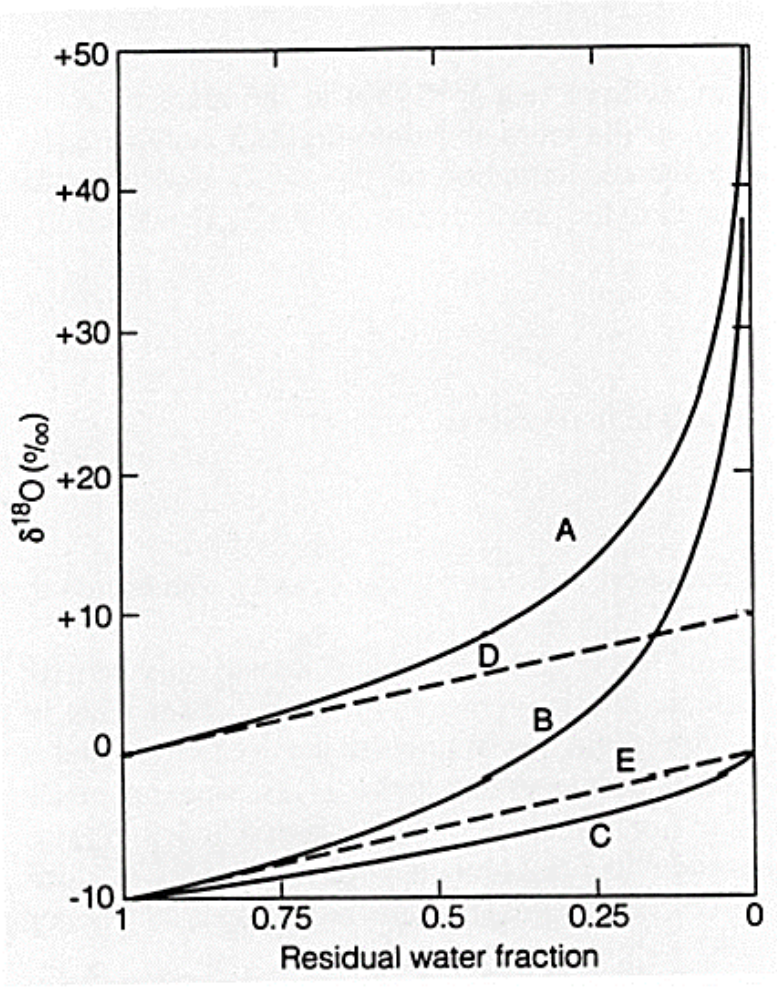

Figure 6.1: Isotopic change under open- and closed-system Rayleigh conditions for evaporation, with a fractionation factor α = 1.01 and an initial water composition of $\delta^{18}O$ = 0‰. **Open system**: curves A, B and C: under a Rayleigh regime, showing the residual water, the instantaneous vapor flux and the total removed vapor, respectively; and a **Closed system**: curves D and E: The liquid and vapor composition, respectively, for a closed system (from Gat, 2005).

As a rule, fractionations in a true “open-system” Rayleigh process create a much larger range in the isotopic compositions of the products and reactants than in a closed-system (see Figure 6.1, compare lines A and C, with D and E). This is due to the reverse reactions (e.g. condensation-evaporation) in the open system

(Dansgaard, 1964). Mass balance considerations require that the isotope content of the total accumulated amount of the removed material approaches R_0 as f approaches 0 (X-axis, Figure 6.1). In general, evaporation and condensation processes will produce fractionations between these two "ideal" cases (Kendall and McDonnell, 1998).

6.3. Uses of the Rayleigh equation

The Rayleigh equation is used to describe evaporation, condensation and rainout processes. Below, it is described how this can be done. According to Kubota & Tsuboyama (2003), isotopic fractionation between throughfall and stream flow is mainly caused by evaporation of water during the water infiltration process in soils. Therefore, in theory it is possible to estimate the evaporation rate from the forest floor by calculating the soil evaporation rate from the isotopic fractionation between throughfall and catchment discharge during non-storm periods. This process can be physically represented and estimated by a Rayleigh distillation process or evaporation under equilibrium conditions (Liu *et al.*, 2006). Under this condition, a difference in the isotopic ratio occurs between water vapor and liquid water.

In theory, the Rayleigh fractionation should be used only for open systems where the isotopic species removed at every instant are in thermodynamic and isotopic equilibrium with those remaining in the system at the moment of removal (e.g. Figure 6.2). Such an ideal Rayleigh distillation is one where the water (e.g. reactant) reservoir is finite and well mixed, and does not re-react with the vapor (e.g. product; Kendall and McDonnell, 1998). However, the term "Rayleigh fractionation" can also be used to describe other boundary conditions, closed equilibrium (or two phase equilibrium model). Kinetic fractionations can also be derived by this process as well, as they are mathematically identical (Kendall and McDonnell, 1998). The Rayleigh equation can be used with either enrichment or fractionation factors. The following example is given for $\delta^{18}O$:

$$\delta^{18}O_{wr} = \delta^{18}O_{wi} + \varepsilon^{*}_{v\text{-}w}{}^{18}O \cdot \ln f_{wr} \qquad (6.1)$$

or fractionation factor, α, using Eq. (5.16):

$$\delta^{18}O_{wr} = \delta^{18}O_{wi} + \left(\frac{1}{\alpha^{+}_{v\text{-}w}} - 1\right) \cdot 1000 \cdot \ln f_{wr} \qquad (6.2)$$

where $\varepsilon^{*}_{v\text{-}w}$ (for evaporation) stands for the enrichment factor under equilibrium conditions. Please note that for condensation $\varepsilon^{*}_{v\text{-}w}$ changes to $\varepsilon^{+}_{w\text{-}v}$ and $1/\alpha^{+}_{w\text{-}v}$ changes to $\alpha^{+}_{w\text{-}v}$. The full derivation of the Rayleigh model is given in appendix E. Rayleigh equation (Eqs. (6.1) or (6.2)) has been used to model the δ-values on the generation of vapor (through evaporation) or water (through condensation) and to model how this water vapor changes its isotopic signature as the air mass travels and condensation occurs and forms precipitation (Salati *et al.*, 1979). This process, known as "rainout effect" is a classic textbook example of an equilibrium process (Figure 6.2).

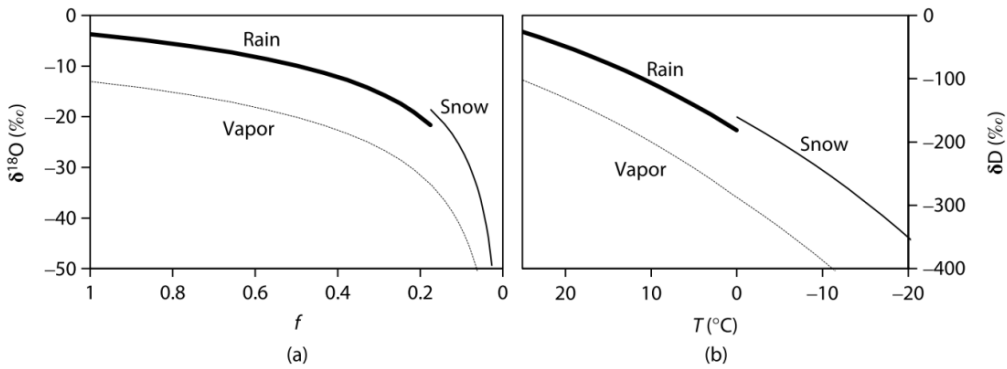

Figure 6.2: Empirical $\delta^{18}O$ and $\delta^{2}H$ values for the evolution of rain and snow during the rainout process. (a) Plot shows $\delta^{18}O$ and $\delta^{2}H$ values as the residual vapor fraction f diminishes towards 0. Both isotopes follow the same depletion (**note different scales for a and b plots**) with decreasing residual vapor fraction f. The distance between each line is known as the enrichment factor or $\varepsilon = 9.3‰$ and 76‰ for $\delta^{18}O$ and $\delta^{2}H$, respectively at 25° C (b) Plot shows the ideal evolution of $\delta^{18}O$ and $\delta^{2}H$ for a single vapor mass undergoing cooling, showing the depletion in $\delta^{18}O$ and $\delta^{2}H$ with decreasing temperature (in °C). Note the jump to higher $\delta^{18}O$ and $\delta^{2}H$ at the rain-snow transition due to the greater fractionation between vapor and ice versus vapor and water (from Clark, 2015).

The distance between the rain and vapor curves in Figure 6.2 (plots a and b) represents the isotopic enrichment $\varepsilon^{+}_{w\text{-}v}$ (i.e. condensation) or $\varepsilon^{*}_{v\text{-}w}$ (i.e. evaporation).

This value is always similar under equilibrium conditions, e.g. at 25° C, 9.3‰ and 76‰ for $\delta^{18}O$ and $\delta^{2}H$ (Figure 6.2 plots a and b, respectively). The rainout process follows a Rayleigh type equation that has been used for the estimation of evaporation contribution to oceanic moisture content when passing over large continental areas (Salati *et al.*, 1979; Gat and Matsui, 1991; Gat *et al.*, 2003). While Eq. (6.2) has been used by Tsujimura and Tanaka (1998) and Lee *et al.* (2010) for the estimation of water losses through soil evaporation at catchment scale.

In general, isotope signatures from precipitation are mainly governed by temperature and the rainout process. Hence, it is considered an equilibrium process and can be modelled using the Rayleigh equation. See Appendix A for exceptions of the assumption that δ_v is small ($\delta_v \ll 1000$) is not met.

7. Chapter 7: The Craig and Gordon model

7.1. The Craig and Gordon model application

The evaporation and condensation processes, govern the hydrological cycle and keep it cycling. In general, the condensation process is most of the time occurring under equilibrium conditions. However, the evaporation process frequently occurs under non-equilibrium conditions. Hence, if we know the water vapor isotopic signature we can understand the source and process of the water vapor condensing in clouds and forming precipitation. Craig and Gordon (1965) developed a model to describe the isotopic fractionation associated with evaporation under non-equilibrium conditions. Originally, it was thought as a way to study changes in ocean salinity. However, the Craig and Gordon model has been applied to several evaporating surfaces such as lakes (e.g. Skrzypek *et al.*, 2015), soils (e.g. Allison *et al.*, 1983), and leaves (e.g. Allison *et al.*, 1985; Dubbert *et al.*, 2013).

7.2. The Craig and Gordon model assumptions

In the Craig and Gordon model approach, the atmosphere above the water surface is divided into three discrete layers (as shown on Figure 7.1):

1) Equilibrium conditions at the air/water interphase, so that the relative humidity at the evaporating surface and above is 100% (i.e. $h = 1$). Hence,

$$R_v = \frac{1}{\alpha^{+}_{v\text{-}w}} \cdot R_S \qquad (7.1)$$

Where R_v and R_s stand for the isotopic ratios of water vapor and the evaporating surface. Please note that Eq. (7.1) is similar to Eq.(5.9).

2) A laminar layer above the water/air interphase, where molecular diffusion dominates.

3) A turbulent atmosphere where turbulent transport dominates and where no fractionation occurs.

Layer 1 is a saturated (i.e. RH = 100% or h = 1) sublayer, hence isotopic equilibrium is assumed (Equilibrium vapor in Figure 7.1). Layer 2 (Diffusive sub-layer in Figure 7.1) is dominated by the vertical transport of water molecules due to the molecular diffusion across the humidity gradient (RH < 100%). This results in isotopic fractionation due to their difference in molecular diffusivities. Once the vapor reaches layer 3 (Turbulent mixed sublayer in Figure 7.1), it is assumed that no isotopic fractionation occurs as this layer is characterized by turbulent transport (however, see Eriksson, 1965).

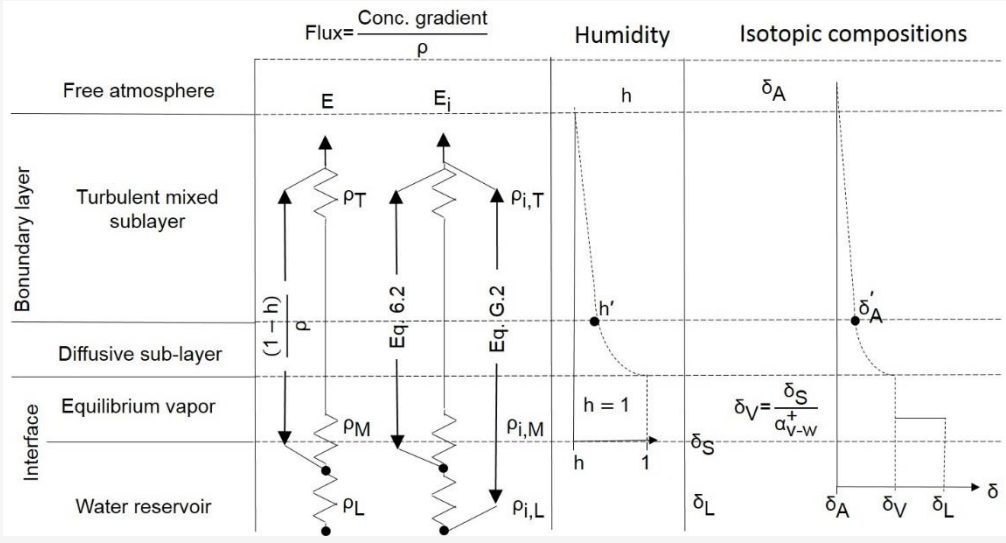

Figure 7.1: Craig and Gordon model as a resistance model scheme. Where ρ stands for resistance in the liquid, laminar or turbulent layers (subscripts L, M and T, respectively) and the subscript i indicates the heavy isotope species. Subscripts L, S, V, and A stand for liquid, surface, vapor and atmospheric δ-values, while δ'_A stands for atmospheric isotopic signature at a lower level than that of δ_A. Eq (6.2) is shown below, while Eq. (G.2) is shown on Appendix G.

The equation given below (Eq. (7.2)) is known as the Craig and Gordon model

$$\delta_E = \frac{1}{(1-h)+\Delta\varepsilon} \cdot \left(\frac{\delta_S}{\alpha^+_{v\text{-}w}} - (h \cdot \delta_A) - \left(\Delta\varepsilon + \frac{\varepsilon^*_{v\text{-}w}}{\alpha^+_{v\text{-}w}} \right) \right) \tag{7.2}$$

Since equilibrium and non-equilibrium enrichment during evaporation will be used in several coming equations, it is better to introduce a term for total enrichment, ε^T, calculated as follows:

$$\varepsilon^T = \Delta\varepsilon + \frac{\varepsilon^*_{v\text{-}w}}{\alpha^+_{v\text{-}w}} \tag{7.3}$$

Therefore inserting Eq. (7.3) in Eq. (7.2) yields:

$$\delta_E = \frac{1}{(1-h)+\Delta\varepsilon} \cdot \left(\frac{\delta_S}{\alpha^+_{v\text{-}w}} - (h \cdot \delta_A) - \varepsilon^T \right) \tag{7.4}$$

The full derivation of the Craig and Gordon model is given in Appendix F. In Chapter 8, a simple but effective example is given, relating $\delta^{18}O$, δ^2H, the Rayleigh model and the Craig and Gordon model in the $\delta^{18}O$ / δ^2H space.

8. Chapter 8: $\delta^{18}O/\delta^{2}H$ relations in meteoric and evaporated water

8.2. The Global Meteoric Water Line

In precipitation or meteoric waters (i.e. snow, hail, rain and fog), the rainout, evaporation and condensation processes occur under equilibrium conditions. Hence, all of them follow the same linear relation between $\delta^{18}O$ and $\delta^{2}H$, which is referred to as the meteoric water line (MWL). This line is the result of the linear regression of $\delta^{18}O$ vs $\delta^{2}H$ (Figure 8.1), which was first estimated using river, lake and precipitation water from around the world (Craig, 1961).

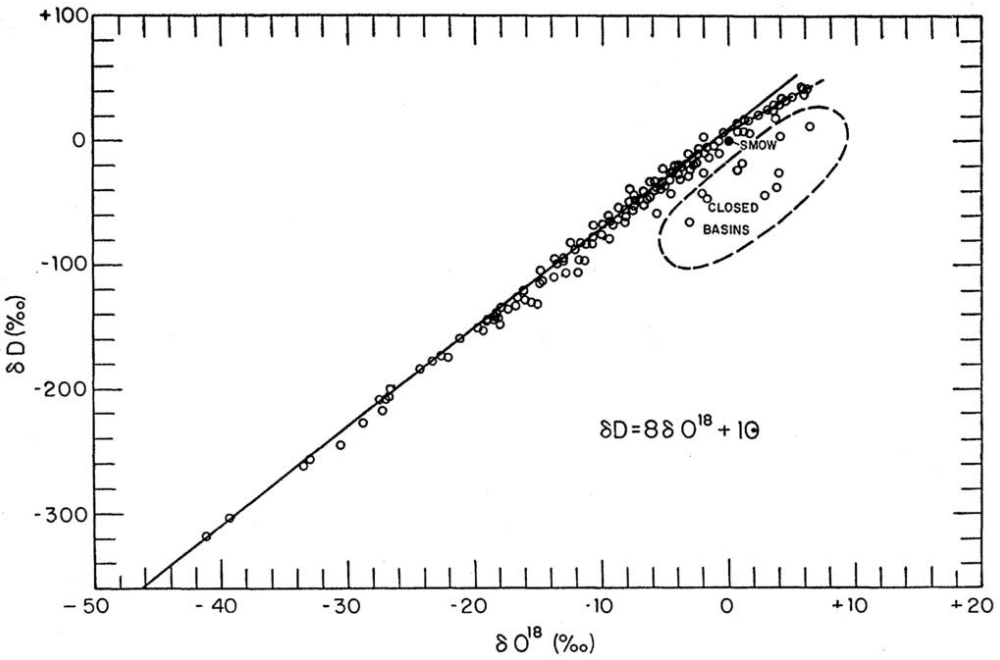

Figure 8.1: First described meteoric water line using $\delta^{2}H$ and $\delta^{18}O$ signatures from water sampled from rivers, lakes and precipitation. δ-values relative to "standard mean ocean water" (≈ 0‰, ≈ 0‰ for $\delta^{18}O$ and $\delta^{2}H$ SMOW, respectively). Points which fit the dashed line at upper end of the curve are rivers and lakes from East Africa. Please note the decrease in slope on the upper end of the regression line (from Craig, 1961). For more detailed explanation see 'Dole effect' on section 8.2.3.

The estimated regression model by Craig (1961) is referred to as the Global Meteoric Water Line (from now on referred to as GMWL) or the Craig line. The line (or equation) in Figure 8.1 results from the first study in which $\delta^{18}O$ and $\delta^{2}H$ were plotted together using water samples from different sources (Craig, 1961). The GMWL parameters have changed very little since. The importance of the GMWL proves that in general, meteoric water is formed under "ideal" or "close" to equilibrium conditions, therefore its vapor (i.e. source) signature can be estimated using the Rayleigh equation, if the temperature or fractionation factor is known (Dansgaard, 1964; Eriksson, 1965; Salati *et al.*, 1979; Gat *et al.*, 2003). Recent GMWL estimates show little deviation from the original line proposed by Craig, although there have been some changes in the methodologies for its estimation. Since Dansgaard (1964), MWL's are estimated using an ordinary linear regression (OLR) using monthly amount-weighted $\delta^{18}O$ and $\delta^{2}H$ meteoric water signatures. A recent study showed that the OLR in theory is not the appropriate method for its estimation. This is mostly due OLR only accounts for error on the dependent variable (i.e. $\delta^{2}H$), while Reduced Major Axis accounts for the error on the dependent and independent variable (i.e. $\delta^{18}O$). Hence, RMA linear regression is a more appropriate met (for details see Crawford *et al.*, 2014). In this chapter, the GMWL is calculated using OLR and RMA methods with data from the Global Network of Isotopes in Precipitation from the International Atomic Energy Agency (GNIP-IAEA, 2015; Figure 8.2 and Eqs. (8.1) and (8.2)). Eq. (8.1) is taken from Rozanski *et al.* (1993) and is used as the standard GMWL in *most, if not all* isotope hydrology studies. Eq. (8.2) represents the RMA linear regression with the most up to date isotope data (GNIP, 2015).

$$\delta^{2}H = 8.17\ (\pm\ 0.04)\cdot\delta^{18}O + 11.7\ (\pm\ 0.35) \tag{8.1}$$

$$\delta^{2}H = 8.25\ (\pm\ 0.04)\cdot\delta^{18}O + 12.15\ (\pm\ 0.01) \tag{8.2}$$

No statistical differences were found when slopes ($p > 0.4$; t-test) and intercepts ($p > 0.1$; t-test) were compared.

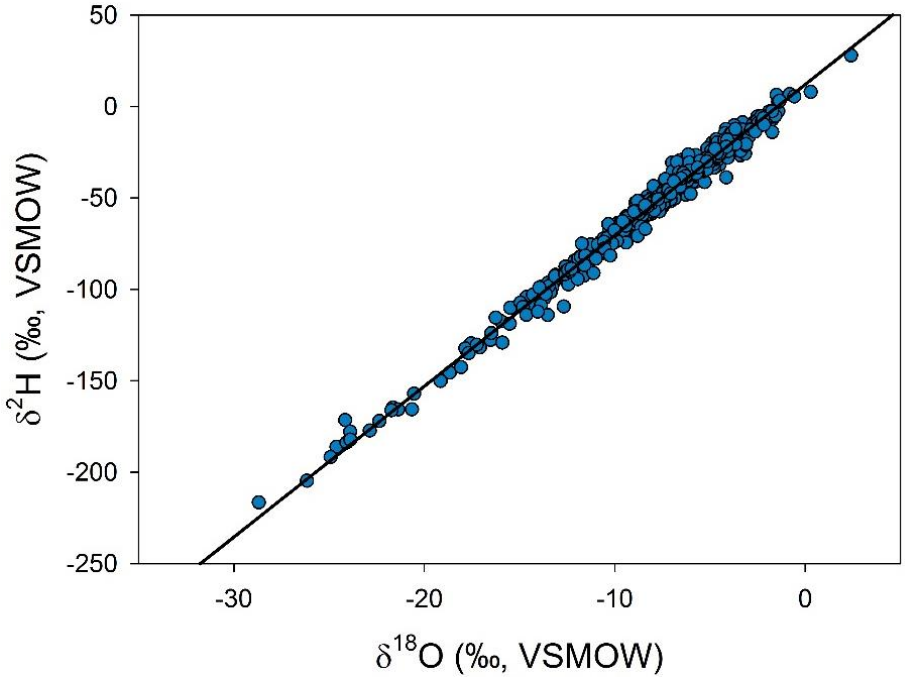

Figure 8.2: Global meteoric water line (GMWL) estimated using the yearly weighting method used in Rosanski *et al*. (1993) on accumulated GNIP data up to 2015. Ordinary and reduced major axis linear regressions (OLR (Eq. (8.1)) and RMA (Eq. (8.2)), respectively) method were used for the estimation of regression lines (source: this work).

When the newly formed vapor condenses in droplets of water, it does so in equilibrium for ^{18}O and ^{2}H, hence following the MWL slope. This is simply because each region and/or locality will have a characteristic evaporation conditions (i.e. temperature and RH) and a different and variable vapor source (evaporation from soil, canopy interception, transpiration and water bodies, including the ocean) that eventually will form rainfall, which will follow the rainout process when precipitating (as shown in Chapter 6, Figure 6.2). In general, the LMWL is calculated from precipitation $\delta^{18}O$ and $\delta^{2}H$ signatures, although there are some examples where stream water from small catchments (Kendall and Coplen, 2001) and/or groundwater (Evaristo *et al.*, 2015) has been used in addition to or instead of precipitation when no data was available. This is because streams in small catchments and groundwater are generally in equilibrium, hence plotted along the LMWL. In general, GMWL is used as a reference for other LMWLs. Hence, both MWL should be plotted on the same graph,

in addition to the studied water compartments (e.g. rainfall, surface waters and/or groundwater). When part of the rained-out moisture is returned to the atmosphere by means of evapotranspiration, then a simple Rayleigh law no longer applies. The downwind effect of the evapotranspiration flux on the isotopic composition of the atmospheric moisture and precipitation depends on the meteorological environment (i.e. temperature and relative humidity) in the evaporation and transpiration processes. This process has been already explained in detail in chapter 7.

8.3. Physical meaning of the GMWL

In general, MWL are plotted and compared to stream, groundwater and soil water isotope signatures. The position of the plotted isotope signatures relative to the MWL is of utmost importance. Therefore, the proper understanding and significance of the MWL is for the proper understanding of the current hydrological system under study. It is important to mention that each study site has different characteristics. Hence, a LMWL is calculated for the selected study site. The LMWL and GMWL interpretation is the same, however, the LMWL is used for local, while GMWL is used for the global understanding of the hydrological cycle.

8.3.1. GMWL slope meaning

The slope of the estimated GMWL shows the higher fractionation of $\delta^{2}H$, which is 8 times higher than that of $\delta^{18}O$, at 25° C (Dansgaard, 1964). The theoretical slope of the GMWL is also estimated using the ratio of the enrichment factors as follows:

$$\frac{\varepsilon^{2}H}{\varepsilon^{18}O} = \frac{76‰}{9.3‰} = 8.17 \text{ at } 25° \text{ C} \qquad (8.3)$$

As shown above, using the isotopic enrichment values (Figure 8.1 Figure 8.2), the $\delta^{18}O/\delta^{2}H$ slope for an ideal Rayleigh distillation (i.e. equilibrium process) is larger than the slope 8, as estimated before by Craig (1961) and Dansgaard (1964). However, it is very similar to the slope estimated by Rozanski *et al*. (1993, see Eq.(8.1)). However, the observed differences in Eqs. (8.1) and (8.2) slopes, could be

due to the rainout process being not “ideal” and to variable contributions of vapor coming from continental evapotranspiration (Aggarwal *et al.*, 2012). In addition to error estimates (Crawford *et al.*, 2014), kinetic effects, fractionation and/or ice formation in stratospheric processes (Dansgaard, 1964; Eriksson, 1965; Criss, 1999; Gat *et al.*, 2001), which have different fractionation factors than those of water to vapor or viceversa (Criss, 1999; Ellehoj *et al.*, 2013). It is important to mention that LMWL with slopes in the range of 5 to 9 are rare (see Crawford *et al*., 2014).

8.3.2. GMWL intercept meaning

A suggested meaning of the intercept of the GMWL was introduced by Dansgaard (1964) and referred to it as deuterium excess (or *d-excess*). The meaning of this parameter is related to the evaporation conditions in which the vapor source for precipitation is formed. This parameter was estimated using all isotope data gathered by the GNIP-IAEA up to year 1963. *d-excess* is used to indicate the $\delta^{2}H$ deviation of a specific sample from the GMWL (i.e. GMWL intercept). Even though now there are more data available and the intercept has changed (see Eqs. (8.1) and (8.2)), the *d-excess* parameter is still calculated using the same parameters estimated by Dansgaard (1964) as follows:

$$d\text{-}excess = \delta^{2}H - (8 \cdot \delta^{18}O) \tag{8.4}$$

On average d-excess has a value of 10‰ (since it’s the intercepts of the GMWL described by Dansgaard, 1964). However, *d-excess* varies regionally from less than 10‰ to well over 20‰, and it is linked to evaporation under non-equilibrium conditions (hence to h and $\Delta\varepsilon$ in equation (5.23) and the Craig and Gordon model (Chapter 7) of course). In general, *d-excess* increases when h is low, and decreses when h is higher (see section 5.5.2). *d-excess* is frequently used to trace the origin of water vapor and its evaporation conditions (Rozanski, 1985; Clark, 2015). The interpretation of *d-excess* is straightforward: *d-excess* ≈ 10‰ suggests that water vapor is coming from an oceanic source; while *d-excess* > 10‰ suggests that water is coming from re-evaporation or has been recycled. *d-excess* < 10‰ indicates that water vapor has been evaporated at low RH (Kurita, 2011) or it could also suggest that the water

sample has evaporated due to poor handling. Therefore, for the correct interpretation of *d-excess*, a good sampling device(s), methods (e.g. analytical and statistical) and careful individual sample validation are essential (Rozanski *et al.*, 1993).

Landwehr and Coplen (2004) introduced the land conditioned excess (or lc-excess), which is a term similar to *d-excess*. However, instead of using the GMWL as a reference, it uses the Local Meteoric Water Line (LMWL) instead. The LMWL is the same as the GMWL, but it is estimated using only local precipitation samples. lc-excess is calculated as follows:

$$\text{lc-excess} = \delta^2\text{H} - \left(\text{LMWL}_{\text{slope}} \cdot \delta^{18}\text{O}\right) - \text{LMWL}_{\text{intercept}} \quad (8.5)$$

Where $\text{LMWL}_{\text{slope}}$ and $\text{LMWL}_{\text{intercept}}$ stand for the slope and intercept of the LMWL. Usually, lc-excess is used as a measurement of a specific sample deviation from the LMWL. Note that Eqs. (8.4) and (8.5) are similar. However, in Eq. (8.5), since the $\text{LMWL}_{\text{intercept}}$ is subtracted, lc-excess starts from 0‰ and not 10‰ as for *d-excess* (i.e. Eq. (8.4)). Its interpretation is very similar to *d-excess*, although it has been used by some authors as a measure of evaporation (Sprenger *et al.*, 2016) and ecohydrological connectivity (Hervé-Fernández *et al.*, 2016b).

8.3.3. Isotope effects in precipitation

Isotopic signatures in precipitation are mostly dependent on the local evaporation conditions. However, there are other effects related to other variables such as temperature, altitude, precipitation amount and distance from the main vapor source (i.e. ocean, also known as continental effect) that also have an effect on isotopic precipitation signatures. Although, in this document these effects are not studied in detail. These are considered common knowledge and helps to understand how isotope signatures can vary. The first to describe these four effects was Dansgaard (1964), as follows:

- *Temperature effect*: Effects of temperature and fractionation under equilibrium conditions, have already been explained in section 5.5.1. This effect is why water stable isotopes ($\delta^{2}H$ and $\delta^{18}O$) are used as proxies for paleotemperatures or aspaleothermometer (Dansgaard, 1964; Gat, 1996). In general, colder regions will show depleted values, compared to temperate regions, which will show depleted values when compared to tropical regions (Figure 8.3).

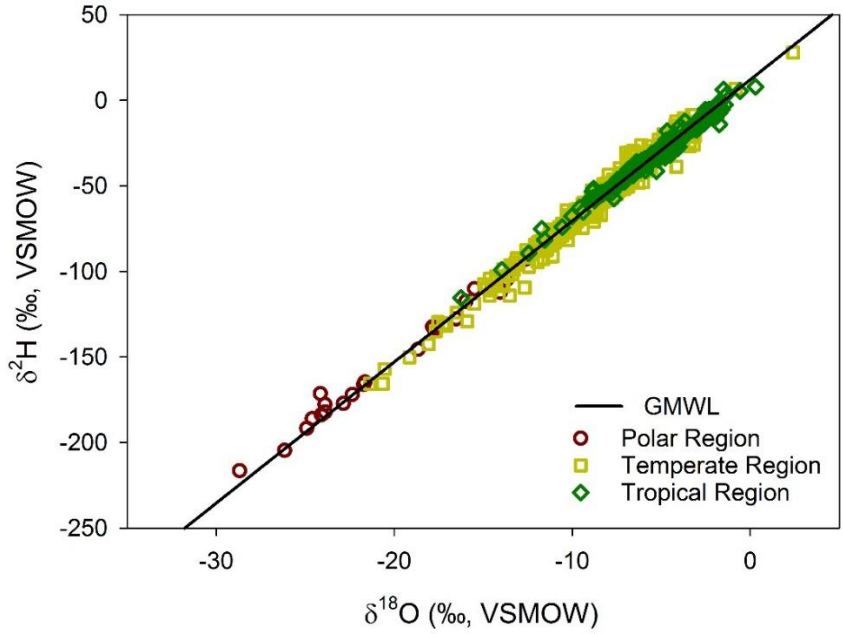

Figure 8.3: Meteoric isotope signature shown for Polar, Temperate and Tropical regions. Variations along the GMWL are due to seasonality (i.e. changes in temperature) and sites closer to other regions.

- *Altitude effect*: This effect is also partly due to temperature. As the cloud increases in altitude, water precipitates due to adiabatic cooling. First, rainfall isotopic signature will be enriched (i.e. closer to 0‰), however, as rain clouds gain altitude, due to the rainout and temperature effects rainfall becomes more depleted. This depletion, occurs along the MWL, hence it occurs under equilibrium conditions. Any deviation from the MWL will be due to the mixing with water vapor (above the MWL) or evaporation (below the MWL).

- *Amount effect*: is evidenced by a negative correlation between δ signature and the amount of monthly precipitation, i.e. low δ's (i.e., depleted signatures) in rainy months and high δ's (i.e., enriched signatures) in months with sparce rain. This "amount effect" is found all the year round at most tropical stations, and in the summer time at mid latitudes, but never at polar stations, where the temperature effect is the dominating factor (Dansgaard, 1964).

- *Continental effect*: This effect is observed for inland precipitation. The proximity of oceans exerts a control on the isotope composition of precipitation as vapor masses move inland, due the vapor source changes from an oceanic source to vapor coming from evapotranspiration (transpiration and evaporation from water bodies, soil and canopy intercepted rainfall) (Salati *et al.*, 1979; Gat and Matsui, 1991; Gat *et al.*, 2003). Therefore, this effect is expected to increase as the vapor masses move inland. Graphically, this effect will be evidenced as precipitation waters that plot above the MWL (Dansgaard, 1964; Gat *et al.*, 1996; Gat, 2005; Gat and Airey, 2006). A frequently used tracer or proxy for this is *d-excess*. Hervé-Fernández *et al.* (2015) found this effect near the coast, in an area of high confluence of estuaries, wetlands, rivers and forests, as shown in Figure 8.4.

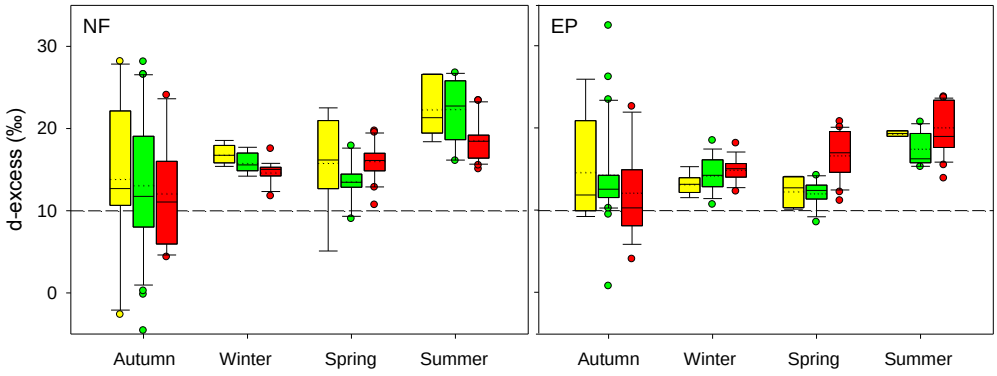

Figure 8.4: Seasonal *d-excess* values for bulk, throughfall and stream water (yellow, green and red, respectively) sampled on NF and EP sites (30 km from Pacific Ocean coast). Boxplots show average (dashed line), 25th, 50th (median) and 75th percentiles, whiskers represent 5- and 95-percentiles, while outliers are shown in by the respective symbol. Dashed line marks *d-excess* = 10.

Figure 8.4 suggests that for the two sites shown, water vapor forming precipitation is not only coming from the oceans as *d-excess* is higher than 10‰ (dashed line in Figure 8.4). It is shown that the NF site (Figure 8.4, left panel) has a higher effect of water vapor coming from either evaporation from nearby water bodies (i.e. rivers and wetlands) and/or transpiration compared to the EP site (Figure 8.4, right panel). These results have also been linked to a re-recycling of water, hence, an inner forest hydrological cycle (Gat and Matsui, 1991; Froehlich *et al.*, 2007; Scholl *et al.*, 2007; Lai and Ehleringer, 2011; Kong *et al.*, 2013).

- *Dole effect*: Although this effect is not considered in common literature as a precipitation effect *per se*, it is important to know it. Especially when working in the tropics or places were high vegetation, respiration rates are common (e.g. green house). This effect was first described by Dole (1935), who found differences in O isotope ratios from water and air. In a revision of this experimental work Lane and Dole (1956), described that this effect was due to the fractionation of 18O during respiration of living organisms. In this process, there is a greater preference to retain ^{16}O, hence ^{18}O enriched CO_2 is preferentially respired. This generates that atmospheric $\delta^{18}O$ from CO_2 is enriched. When raining, H_2O falling interacts and mixes with CO_2, therefore, oxygen atoms exchange generating that rainfall has an enrichment in $\delta^{18}O$. This is the reason why there is a decrease in the slope ($\delta^{18}O$ enrichment) of the GMWL estimated by Craig (1961; see Figure 8.1).

8.3.4. Evaporation slopes

Evaporating water under non-equilibrium conditions (i.e. $h < 1$, where h is the relative humidity normalised to the evaporating surface temperature, calculated as in Eq. (F.2), from Appendix F) will show a typical slope which is characterized by being less than that of the LMWL, hence (for an exception see Jasechko *et al.* (2013)). In some cases RH can be used instead of h, as an approximation. However, if precision is required then efforts to calculate h correctly, should be done. At low relative humidity, the kinetic fractionation during evaporation becomes even stronger. Therefore, water vapor is highly depleted in ^{18}O, compared to ^{2}H that shows a lower

depletion rate. As explained before in section 5.5.2.2. The influence of h is such that under drier conditions the slope of the evaporation line (i.e. EL) is lower than that of the MWL (see Figure 8.5; Gonfiantini, 1986).

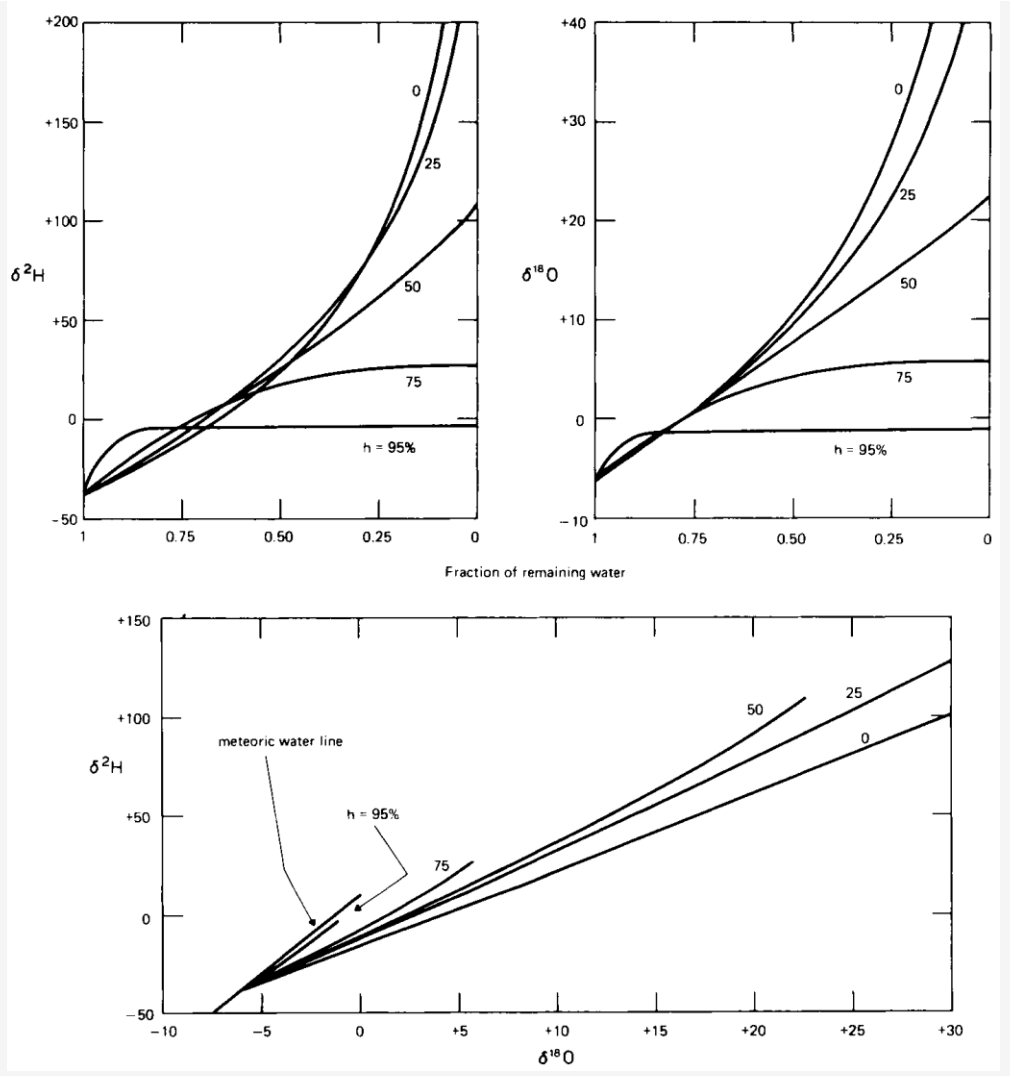

Figure 8.5: Stable isotope composition of an evaporating water body as a function of the fraction of remaining water, computed for 0; 25; 50; 75 and 95% h. At h = 0, the heavy isotope enrichment obeys a law similar to that of the Rayleigh distillation. The initial isotopic composition of water is assumed δ^2H = -38‰ and $\delta^{18}O$ = -6‰. The isotopic composition of the atmospheric vapor is assumed δ^2H = -86‰ and $\delta^{18}O$ = -12‰. The lower diagram shows the change of the slope of the δ^2H-$\delta^{18}O$ relationship for various relative humidities (from Gonfiantini, 1986).

Water vapor ($^{1}H_2{}^{16}O$) is a relatively light gas when compared to $^{14}N_2$ and $^{16}O_2$ (18, 28 and 32 g·mol^{-1}, respectively). Thus, when water vapor concentration increases, the amount of oxygen and nitrogen decrease per unit volume (Clark, 2015). Therefore, atmospheric density decreases because its mass is decreasing. Hence, diffusion of the heavier water molecules into the atmosphere is easier. The opposite can be expected in a dry atmosphere. Therefore, generating an accumulation or enrichment of ^{18}O in the evaporating water. This is why air relative humidity affects the evaporation line slope. On Figure 8.5, the effect of h is shown on the enrichment of $\delta^{2}H$, $\delta^{18}O$ and evaporation line slope.

The equation given below has been used for the estimation of evaporation line slopes (Gat, 1996):

$$EL_{Slope} = \frac{\left[h\cdot(\delta_A - \delta_P)+\varepsilon^T\right]_{2_H}}{\left[h\cdot(\delta_A - \delta_P)+\varepsilon^T\right]_{18_O}} \tag{8.6}$$

where δ_P and ε^T respectively stand for the precipitation isotopic signature and total enrichment factors. Recently, Gibson *et al.* (2008) presented another way to estimate the evaporation slope, derived from the Craig and Gordon model (Craig and Gordon, 1965), as follows:

$$EL_{Slope} = \frac{\left[\frac{h\cdot(\delta_A - \delta_P)+(1+\delta_P)\cdot\varepsilon^T}{h-\varepsilon^T}\right]_{2_H}}{\left[\frac{h\cdot(\delta_A - \delta_P)+(1+\delta_P)\cdot\varepsilon^T}{h-\varepsilon^T}\right]_{18_O}} \tag{8.7}$$

Full derivation of Eq. (8.7) is given in detail, in Appendix H. It is important to acknowledge that the Craig and Gordon model does not account for the case where evaporation of droplets and spray contribute to the evaporation flux (Gat, 1996). In addition, if surface water is not well mixed so that a concentration gradient can build up between the evaporating surface skin and the water column, this needs to be taken

into account by introducing a parameter to take into account the water column into the Craig and Gordon evaporation model (Gat, 1996; see Figure 7.1 and Eq. (G.2) in Appendix G).

The lower the slope of the evaporation line, the higher the deviation relative to its MWL. Hence, the water vapor coming from the evaporating surface will have a higher *d-excess* signature. This has been shown in several studies describing a negative correlation of *d-excess* versus relative humidity (Rozanski, 1985; Gibson *et al.*, 2008; Kurita, 2011). It is important to note that the evaporation lines of lakes and soils are slightly different. This is mostly due to the higher contribution of the kinetic diffusive process of water vapor in soils, hence soil evaporation lines have a lower slope compared to that of a lake (Gat, 1996, 2005).

The evaporation process is ubiquitous and occurs under equilibrium and non-equilibrium conditions. A special case is presented when δ_S (i.e. evaporating surface water) and δ_A (i.e. atmospheric water vapor) plot along the MWL, hence when both are in isotopic equilibrium (i.e. plots along the MWL) with each other for both isotopic species, in which case the evaporation slope under equilibrium conditions (EL^{+}_{Slope}) is estimated as follows (Gat, 1996):

$$EL^{+}_{Slope} = \frac{(\varepsilon^{+} + \theta \cdot n \cdot C_K)_{2_H}}{(\varepsilon^{+} + \theta \cdot n \cdot C_K)_{18_O}} \tag{8.8}$$

Eq. (8.8) is independent of the h parameter. In this case, EL^{+}_{Slope} is 3.54 when $\theta = 1$ and $n = 0.5$ and is lower for the case of the fully developed boundary layer, when $n = 1$ the calculated evaporation line slope would be 2.69. When $\theta < 1$, the slope of the relevant evaporation line will increase, as will be the case when $\delta_S - \delta_A > -\varepsilon^{*}_{v\text{-}w}$ (Gat, 1996).

So far, we have described mathematically how fractionation factors (α) and enrichment (ε) are calculated for equilibrium and non-equilibrium at dry conditions and at variable atmospheric moisture content. Also the meaning of the meteoric water line

and evaporation lines have been discussed. However, all these processes and terms are much easier to follow graphically. Hence, water that has undergone evaporation under equilibrium and non-equilibrium conditions (i.e. RH ≈ 100% and RH < 100%, respectively) will plot in the $\delta^{18}O$ / $\delta^{2}H$ space in a special and characteristic way (see Figure 8.6).

Knowing the fractionation factors α and enrichment ε of evaporating water or water vapor are necessary to properly "trace" back to the original source of that water or vapor. In Figure 8.6, or any $\delta^{18}O$ / $\delta^{2}H$ plot with a MWL, one can define two areas: a condensing region (above the MWL) and an evaporating region (below the MWL). Hence, samples that plot below the MWL, will be evaporated. While samples in the condensation region, will have undergone condensation (or originate from condensation). Figure 8.6 shows how a hypothetical atmospheric water vapor with δ_A, condenses at 25° C and forms precipitation with δ_P. A general assumption is that δ_A and δ_P are in equilibrium (Gat and Airey, 2006; Gibson and Reid, 2010), hence, plot along the MWL.

Water with a δ_P signature can evaporate under equilibrium or non-equilibrium conditions. Evaporation under equilibrium conditions will enrich δ_P (i.e. move it forward, along the MWL), while the vapor coming from that evaporation under equilibrium conditions will travel the opposite way in the $\delta^{18}O/\delta^{2}H$ space, therefore, will be depleted or lighter than its source water that is heavier or enriched. However, evaporation under non-equilibrium conditions, the water source (i.e. δ_P), will be enriched following the EL, δ_S (i.e. surface evaporating water). Hence, both will plot following the EL (see Figure 8.6). The water vapor isotopic signature coming from δ_S is written as δ_E, and plots on the opposite side of the MWL (i.e. condensation side). In order to close the hydrological water cycle, δ_E mixes with water vapor from δ_A, forming $\delta_A^{'}$, which eventually will condense again and form $\delta_P^{'}$. This process follows a trend, which in this text will be referred to as condensation line (or CL, in Figure 7.6). As it can be observed, δ_E, $\delta_A^{'}$ and $\delta_P^{'}$ are above the MWL, hence will have a higher intercept than that of the MWL shown in Figure 7.6. This increase in the intercept, is usually compared to the GMWL intercept, hence *d-excess* (see section 8.3.2). Although it is

also possible to use the LMWL as a reference, then lc-excess should be used instead. As for as the author knows, *d-excess* is preferred for precipitation, while lc-excess is used to further characterize water from soils, stream/river and xylem. (Landwehr *et al.*, 2014; Hervé-Fernández *et al.*, 2016b).

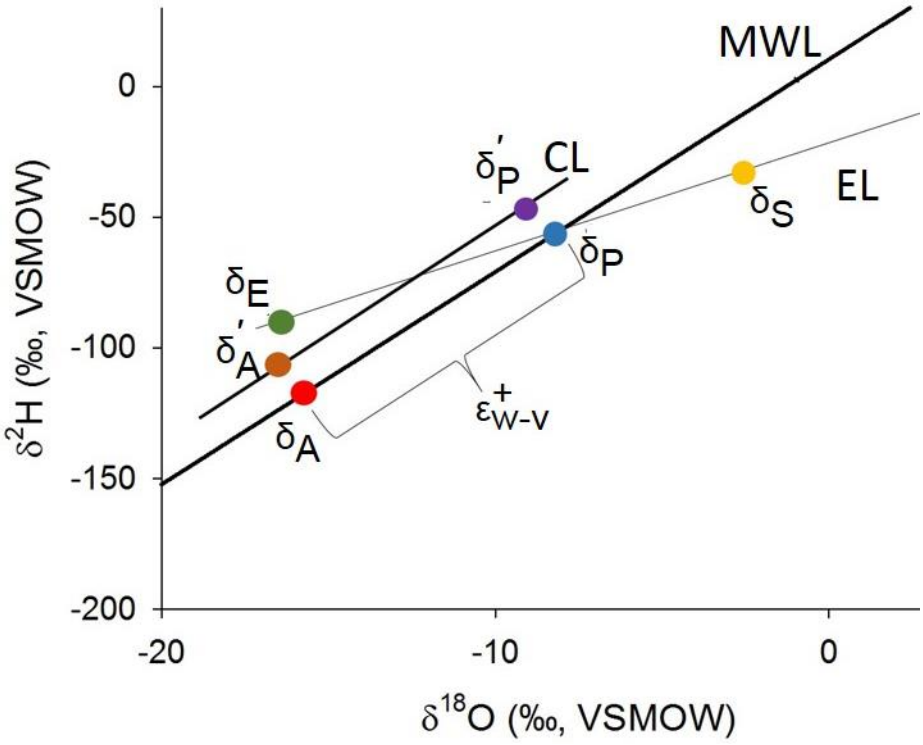

Figure 8.6: MWL, EL and CL stand for meteoric water line, evaporation line and condensation line. δ subscripts A, P, S and E stand for atmospheric, precipitation, evaporating surface and water vapor, respectively. ε^+_{W-V} isotpopic enrichment from vapor to water (i.e. condensation). δ' stands for the second formation of the respective subscript.

The increase in intercept shows that the atmospheric water vapor, the evaporated and newly formed precipitation water, it is above the MWL. Usually, also with a higher *d-excess,* this is interpreted as recycled water vapor (Figure 8.7).

It is important to mention that this example was made for a single atmospheric water vapor sample. Hence, it is possible to estimate the sources of water vapor,

falling as precipitation. In order to be accurate with the modelling of isotope signatures in water mixtures, only volume weighted sample isotopic signatures should be used for this pourpose (Gat and Issar, 1974; Gat and Carmi, 1987; Gat, 2000; Gibson *et al.*, 2008).

Figure 8.7: The condensation of water vapor coming from the ocean near tree canopies mixes with transpiration, canopy interception and water vapor from soil evaporation.

It is also possible to estimate how much of the input (i.e. precipitation) water has been lost through evaporation. The typical model for the estimation of water lost through evaporation under equilibrium conditions is the Rayleigh model (explained in detail in Chapter 6: The Rayleigh model). The Rayleigh model has been used for the estimation of evaporation amount or proportion under non-equilibrium conditions (Clark, 2015). However, in this thesis it is used only under equilibrium conditions (see Chapter 10).

9. Chapter 9: Ecohydrological connectivity

After Hervé-Fernández, P., C. Oyarzún, C. Brumbt, D. Huygens, S. Bodé, N.E.C. Verhoest and P. Boeckx. (2016). Assessing the 'two water worlds' hypothesis and water sources for native and exotic evergreen species in south-central Chile. Hydrological Processes, 30 (23): 4227-4241.

9.2. Abstract

Recent studies using water stable isotopes ($\delta^{18}O$ and $\delta^{2}H$) have suggested an ecohydrological separation of water flowing to streams or recharging groundwater (i.e. mobile water compartment) and water used by trees (i.e. static water compartment), known as the "two water worlds" (TWW) hypothesis. In this study, water isotopic composition was measured in precipitation (bulk and throughfall, i.e. LMWL), the mobile water compartment (i.e. stream and soil solution), bulk soil water (considered a mixture of mobile and static water) and xylem water over a period of 1.5 years in two headwater catchments: NF1, covered with old growth native evergreen forest (*Aetoxicon punctatum*, *Laureliopsis phillipiana* and *Eucriphya cordifolia*); and EP1, covered with 4- and 16-year-old *Eucalyptus nitens* stands. Our results show that precipitation, stream and soil solution plot approximately along the local meteorical water line (LMWL), while xylem waters from all studied tree species plot below the LMWL, supporting the TWW hypothesis. However, we also found evidence of ecohydrological connectivity during the wet season, likely controlled by the amount of antecedent precipitation. These observations hold true for all investigated tree species. At both sites, a different precipitation source for stream and xylem water was observed. However, EP1 bulk soil showed a similar precipitation source as xylem water from both *E. nitens* stands. This suggests that *E. nitens* may use water that is recharging the bulk soil compartment. We conclude that under a rainy temperate climate the TWW hypothesis is temporal and does not apply during wet seasons.

9.3. Introduction

The relationship between plants, soil and water has attracted the interest of scientists since the days of ancient Rome and Pliny "the Elder" (1st century AD)

(Andréassian, 2004). While thinking on the subject has clearly evolved over the centuries, the interactions between these fundamental environmental elements are no less important today. For many years, it has been assumed that water in soil matrix is completely mixed (Hewlett and Hibbert, 1966). This assumption is critical to the translatory flow concept or "piston flow" model, which states that water stored in hillslope soils is rapidly displaced by "new water" (i.e. rain) (Brooks *et al.*, 2010; McDonnell, 2014). These concepts influenced ecology and hydrology, leading to the idea that roots take up water from the same pool that is moving towards a stream. Furthermore, this implies that vegetation withdraws water from a completely mixed soil water pool for transpiration. These assumptions are usually accepted and treated as paradigms in most ecohydrological processes. However, all of these paradigms have been recently questioned using variation of natural abundance of water stable isotopes (Brooks *et al.*, 2010; Goldsmith *et al.*, 2011; McDonnell, 2014; Evaristo *et al.*, 2015). Isotopic composition, expressed in terms of $^{2}H/^{1}H$ and $^{18}O/^{16}O$ ratios, are represented by δ-values (5.3), which indicates the deviation from a designated standard (i.e. VSMOW, Vienna Standard Mean Ocean Water) in parts per thousand (‰). $\delta^{18}O$ or $\delta^{2}H$ have been used extensively to estimate plant water sources. This possibility arises from the fact that isotopic signature of xylem water does not change compared to its source. Therefore, it can be used as a tracer for plant water sources (Zimmermann *et al.*, 1967; Brooks *et al.*, 2010).

The $\delta^{18}O$ and $\delta^{2}H$ measured in precipitation around the world shows an empirical linear relationship, described by the Global Meteoric Water Line (GMWL): $\delta^{2}H = 8.2 \cdot \delta^{18}O + 11.3$ (Rozanski *et al.,* 1993). Local meteorological conditions (i.e. temperature and relative humidity (RH)) and other occurring processes (e.g. evaporation, condensation and mixing) can alter this relationship. Therefore, the relationship between $\delta^{18}O$ and $\delta^{2}H$ at a particular site is better described by a Local Meteoric Water Line (LMWL), which can differ from that of the GMWL (Gat, 2005). A well-known fractionation process is evaporation, which can occur under equilibrium or non-equilibrium conditions. Under equilibrium conditions, lighter isotopologues are preferentially evaporated, while the heavier ones are preferentially condensed (Clark, 2015). This type of fractionation is dependent on temperature and only occurs in saturated environmental conditions (RH ≈ 100%). Local equilibrium conditions are

characterized by a LMWL. In contrast, under non-equilibrium conditions heavier water isotopologues (i.e. $^{1}H_{2}^{18}O$, mass 20) in the liquid phase evaporate and diffuse at slower speeds to the gaseous phase, opposite to lighter water isotopologues (i.e. $^{1}H_{2}^{16}O$ and $^{2}H^{1}H_{16}O$, mass 18 and 19, respectively). This generates an enhanced loss of ^{16}O and ^{1}H resulting in accumulation of ^{18}O and ^{2}H in the residual water (Gat, 2005; Clark, 2015). This mass-dependent effect causes evaporating water in soils, in non-saturated environments (RH < 100%), to follow a characteristic Soil Evaporation Line (SEL). In nature, streams, groundwater and meteoric water (i.e. fog, rain, hail and snow) will usually plot along the LMWL, while water that has undergone evaporation in soils will plot along the SEL (Gat, 1996). The LMWL and SEL therefore represent two forms of evaporation processes, which label water isotopes differently. This *in situ* water labeling is used to demonstrate the TWW hypothesis (Brooks *et al.*, 2010; McDonnell, 2014).

The TWW hypothesis was first described by Brooks *et al.* (2010), who challenged the assumption of water being completely mixed in soils (Hewlett and Hibbert, 1966). Based on soil solution, bulk soil water and xylem water isotopic signatures, Brooks *et al.* (2010) and Goldsmith *et al.* (2011) found that xylem water plotted along the SEL, instead of along the LMWL. This suggested that trees were not using water from the “available”, “gravitational” or mobile water compartment, plotted along the LMWL. Using isotopic signatures, Brooks *et al.* (2010) hypothesized that trees were using water tightly bounded to soil particles. This static water compartment was recharged with the first rainfall events after dry summers; and its isotopic signature was not affected by following rainfall events (Brooks *et al.*, 2010). These results gave rise to the TWW hypothesis (McDonnell, 2014), which is defined as: “poor and incomplete mixing of subsurface water; with one water reservoir sustaining plant transpiration, and another contributing to groundwater recharge and stream flow” (Brooks *et al.*, 2010; Goldsmith *et al.*, 2011; McDonnell, 2014). Evaristo *et al.* (2015) revealed that the TWW was spread across different biomes, and was more common than previously thought. Good *et al.* (2015) needed a static water compartment to close the global water isotope budget. Even though ecohydrological connectivity (i.e. xylem water shows a similar isotopic signature to that of soil solution) appears to be a unifying concept and theoretical platform for moving hillslope biogeochemistry and

watershed hydrology forward (Kirchner, 2003; Hopp and McDonnell, 2009). There are also numerous studies suggesting that hillslope-stream connectivity is only sporadic (Tromp-van Meerveld and McDonnell, 2006a, 2006b; McGuire and McDonnell, 2010; Geris *et al.*, 2015c; van Meerveld *et al.*, 2015). Furthermore, Geris *et al.* (2015a) found that hillslope-stream connectivity occurred occasionally throughout the year in a humid shallow groundwater site. On the same study site, Geris *et al.* (2015b) showed that there was no evidence supporting the TWW hypothesis, hence ecohydrological separation.

Increased land conversion rates have led to the widespread and dramatic degradation of forest ecosystems worldwide (Gibbs and Salmon, 2015), including damage to ecosystem services (Huber *et al.*, 2010; Oyarzún *et al.*, 2012; van der Plas *et al.*, 2016), such as fresh water supply (Costanza et al., 1997; Strange et al., 1999; Ellison et al., 2012). Brown *et al.* (2005) reviewed paired catchment studies and concluded that coniferous and *Eucalyptus* spp. plantations trigger larger changes on catchment water discharge than those of deciduous hardwoods. Fresh water supply from catchments is important, due to the projected growth in water demand for human consumption, irrigation, tourism, fish farming and hydropower generation (Barbier, 2004; Little and Lara, 2010). Chile has developed an important economy based on ca. 2.6 million hectares of planted forests established with fast growing exotic species (FGES) (Iroumé and Palacios, 2013). FGES like *Pinus* spp. and *Eucalyptus* spp. have been planted at rates of 57000 and 40000 $ha \cdot yr^{-1}$ for the periods 1990-2000 and 2000-2010, respectively (Zamorano-Elgueta *et al.*, 2015). This has generated a large land cover conversion from native forest to FGES like *Eucalyptus* spp., which has been blamed for droughts and other social and economic water-related conflicts (Engel *et al.*, 2005; Forrester *et al.*, 2010; Huber *et al.*, 2010; Nahuelhual *et al.*, 2012; Iroumé and Palacios, 2013).

The study of plant-soil-water relations is of utmost concern, especially for future forest and agriculture expansion in areas where water resources are under pressure. In Chile, this is especially important due to persistent summer drought conditions and an estimated 40% reduction in precipitation for most of the country by 2050 (Magrin *et al.*, 2014). Hence, water resources are under pressure in Chile. In particular, land

cover changes alter catchment discharge, groundwater level and recharge rates (Huber *et al.*, 2010; Walden *et al.*, 2015), and thereby likely affect either the static or mobile water compartments in soil. In this study, the following was tested: (1) whether the TWW hypothesis holds true for our study sites and (2) whether there is a difference in ecohydrological connectivity or (3) water sources (i.e. mobile versus static compartments) between old native evergreen forest species (*Aetoxicon punctatum*, *Laureliopsis phillipiana* and *Eucriphya cordifolia*) and *Eucalyptus nitens* stands.

9.4. Study sites

The description of study sites has been given previously in detail in chapter 3. However, catchments used in this study are shown on Figure 3.2, while precipitation sampling details are given in chapter 3, section 3.2.

9.4.1. Soil water compartments

Water in soils consists of a mobile (in this study referred as soil solution) and an immobile or static water pool (i.e. water attached to soil particles or trapped in small pores due to capillary forces) in unknown proportions (Sprenger *et al.*, 2015). At each plot under the tree cover, the mobile water pool was sampled using a set of three suction lysimeters at 0.3 m, 0.6 m and 0.9 m depth per plot. A 60 kPa vacuum was applied to each suction lysimeter and water was collected the next day. Since the EP1 catchment was covered mainly by 4-year-old *E. nitens* stand, we decided to install two suction lysimeter sets under this cover, and only one set below the 16-year-old *E. nitens* stand. In the vadose zone, bulk soil water contains both mobile and static water pools in unknown proportions, but with static water as the larger fraction (Phillips, 2010; Brooks, 2015; Sprenger *et al.*, 2015). These samples were used to characterize the bulk soil water compartment and to estimate the SEL for each catchment. Bulk soil was sampled using a soil auger, at 0.05 m, 0.3 m, 0.6 m, 1 m, 1.5 m and 1.8 m soil depth, only on tree canopy covered plots. These sampling depths were selected to observe $\delta^{18}O$ and $\delta^{2}H$ variation with depth and time (Brooks *et al.*, 2010). Xylem water was also sampled, as this water represents the actual water that trees are withdrawing

from soil, which is assumed to be from the static water compartment (McDonnell, 2014). To do so, wood cores were sampled whenever possible using a 5 mm diameter increment borer. If the tree was too small (i.e. thin) twigs were sampled. Soil solution, bulk soil and xylem were sampled approximately twice per season. This low sampling frequency was enforced by economic constraints.

In order to prevent sample water loss and fractionation, bulk soil and xylem samples were sealed in glass vials that were kept inside a cooler box. Once in the laboratory, they were stored in the freezer until extraction. Water from bulk soil and xylem was extracted from their respective matrix using the cryogenic vacuum distillation method described by West *et al.* (2006) with an extraction time of 4-5 hours, as suggested by Araguás-Araguás *et al.* (1995) (Figure 9.1).

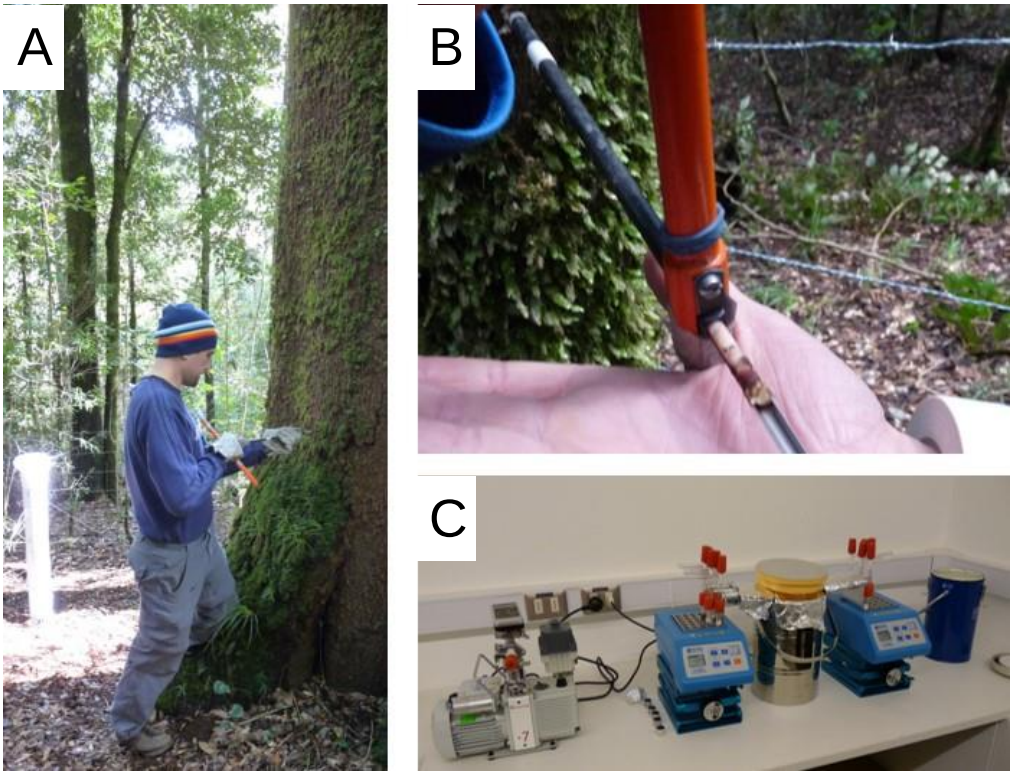

Figure 9.1: Sampling xylem (A and B). Cryogenic vacuum distillation extraction setup (C, for details on the setup see West *et al*., 2006).

All samples were weighted pre- and post-water extraction, as well as after an additional oven drying (48 h at 105°C), and were compared to determine water extraction efficiency. Only samples that reached a water recovery higher than 98% were used for further isotope analysis (Araguás-Araguás *et al.*, 1995; Orlowski *et al.*, 2016). All water samples were pre-filtered (0.45 µm) and stored in 2 mL or 0.4 µL glass vials covered by silicone/PTFE septa and kept inside a refrigerator to prevent evaporation, as recommended by International Atomic Energy Agency (IAEA) standards. Isotope analyses were carried out using a wavelength-scanned cavity ring-down spectrometer (WS-CRDS, L2120-*i,* Picarro, USA) coupled with a vaporizing module (A0211 high-precision vaporizer) and a micro-combustion module (MCM), which eliminates noise from organic compounds (Martín-Goméz *et al.*, 2015). Calibration of measured samples was achieved using internal laboratory references. Each sample was measured 10 times, of which only the last 5 were considered for the estimation of the final isotopic signature and standard deviation of the analyzed sample. The ± 1σ measurement uncertainty of the WS-CRDS was ± 0.1‰ and ± 0.3‰ for $\delta^{18}O$ and $\delta^{2}H$, respectively. All stable isotopic values are expressed relative to VSMOW.

9.4.2. Isotope sample characterization

All water isotopic signatures were characterized using $\delta^{2}H$ deviations from the LMWL, or line conditioned excess (referred as lc-excess, in ‰). Since plant water uptake does not affect the isotopic composition (Zimmermann *et al.*, 1967; Dawson and Ehleringer, 1991; Brooks *et al.*, 2010; Evaristo *et al.*, 2015), it also does not affect lc-excess values. In contrast, evaporation of meteoric water from soil under non-equilibrium conditions results in negative lc-excess values. Therefore, negative lc-excess is used to quantify the degree of “offset” of environmental waters from meteoric water inputs (i.e. LMWL), whereas positive lc-excess values indicate mixing of several sources, including relatively newly evaporated moisture (Landwehr and Coplen, 2004). By comparing meteoric water (LMWL) to xylem water lc-excess values, it is possible to assess the TWW hypothesis. lc-excess was calculated as previously described in chapter 8, Eq. (8.5) (Landwehr and Coplen, 2004). Please,.note that lc-excess is used and not lc-excess*, as done by Evaristo *et al.* (2015), as it expresses

the distance from the LMWL (in ‰), while lc-excess* confronts this distance to a measurement accuracy (unitless). Therefore, lc-excess* stands for a statistical test and not to a distance measurement *per se*. Since the LMWL represents meteoric water inputs to the catchment, δ^2H_{LMWL} intersection was calculated in order to trace the isotopic signature of the precipitation source for the various water compartments measured in this study (i.e. stream, soil solution, bulk soil and xylem water). This variable therefore represents the precipitation source for each of the measured water compartments (Evaristo *et al.*, 2015). The δ^2H_{LMWL} intersection (in ‰) with the LMWL was calculated for stream, soil solution, bulk soil and xylem water as follows:

$$\delta^2H_{LMWL}\text{intersection} = LMWL_{sl} \cdot \left(\frac{\delta^2H_s - LMWL_{int} - EL_{sl} \cdot \delta^{18}O_s}{LMWL_{sl} - EL_{sl}} \right) + LMWL_{int} \qquad (9.1)$$

where the subscripts “sl”, “s” and “int” stand for slope, sample and intercept, respectively, while EL stands for the respective evaporation line. In this way, the precipitation water source can be traced back and can be compared with those of other water compartments or other sites. The full derivation of Eq. (9.1) is given in Appendix J.

In general, slopes and intercepts for the LMWLs, SELs and xylem evaporation lines (XWL) can be estimated using the ordinary least square linear regression method, if it can be assumed that no errors are associated with the independent variable ($\delta^{18}O$), or, as done in this paper, through reduced major axis (RMA) linear regression, which is more appropriate when errors are associated with both variables ($\delta^{18}O$ and δ^2H) (see details for each estimation in Crawford *et al.*, 2014). In depth comparisons and differences between LMWLs, SELs and XWLs will not be addressed in this study. Given that the selected catchments have different heights (336 and 35 m a.s.l. for NF1 and EP1, respectively) and aspects (windward and leeward sides for NF1 and EP1, respectively), the LMWL and EL lines were calculated independently for the respective study site.

Since all data were not normally distributed, statistical analyses were made using non-parametric Mann-Whitney rank sum test (M-W) for comparisons of isotopic

signatures ($\delta^{18}O$ and $\delta^{2}H$) within and between sites for bulk and throughfall precipitation, stream, soil solution, and bulk soil samples. The Kruskall-Wallis test (K-W) with *a posteriori* multiple comparison using the Dunn method, was used to analyze isotopic signatures of xylem waters, lc-excess and the $\delta^{2}H_{LMWL}$ intersection of all samples. Slopes and intercepts of LMWL and SEL were compared using a Student's t-test . Statistical significance was set at $\alpha = 0.05$.

9.5. Results

9.5.1. Precipitation water

Figure 9.2. plots collected bulk (50 and 39 samples for NF1 and EP1, respectively) and throughfall precipitation (99 and 103 samples for NF1 and EP1, respectively) $\delta^{18}O$ and $\delta^{2}H$ signatures, which showed no differences in NF1 ($p > 0.05$ using M-W, for both $\delta^{18}O$ and $\delta^{2}H$) and EP1 ($p > 0.5$ using M-W, for both $\delta^{18}O$ and $\delta^{2}H$). Therefore, all bulk and throughfall precipitation samples were grouped as "precipitation". Precipitation $\delta^{18}O$ and $\delta^{2}H$ showed no differences ($p > 0.3$ and $p > 0.07$ using M-W for $\delta^{18}O$ and $\delta^{2}H$, respectively) when compared between sites. However, both isotopic signatures from autumn were found to be different from all other seasons ($p < 0.01$ and $p < 0.05$ for $\delta^{18}O$ and $\delta^{2}H$ using Dunn method, Figure 9.2).

All precipitation samples were used to estimate the local meteoric water lines for NF1 and EP1, respectively:

$$NF1_{LMWL},\ \delta^{2}H = 8.08 \cdot \delta^{18}O + 16.34 \quad (r^{2} = 0.85;\ p < 0.01) \tag{9.2}$$

$$EP1_{LMWL},\ \delta^{2}H = 8.37 \cdot \delta^{18}O + 17.01 \quad (r^{2} = 0.94;\ p < 0.01) \tag{9.3}$$

LMWL among sites showed no differences in slopes or intercepts ($p > 0.2$ using Student's t-test for both parameters) (Figure 9.2). Since lc-excess and $\delta^{2}H_{LMWL}$ intersection are highly dependent on the LMWL, each of these parameters were nonetheless calculated with their respective LMWL.

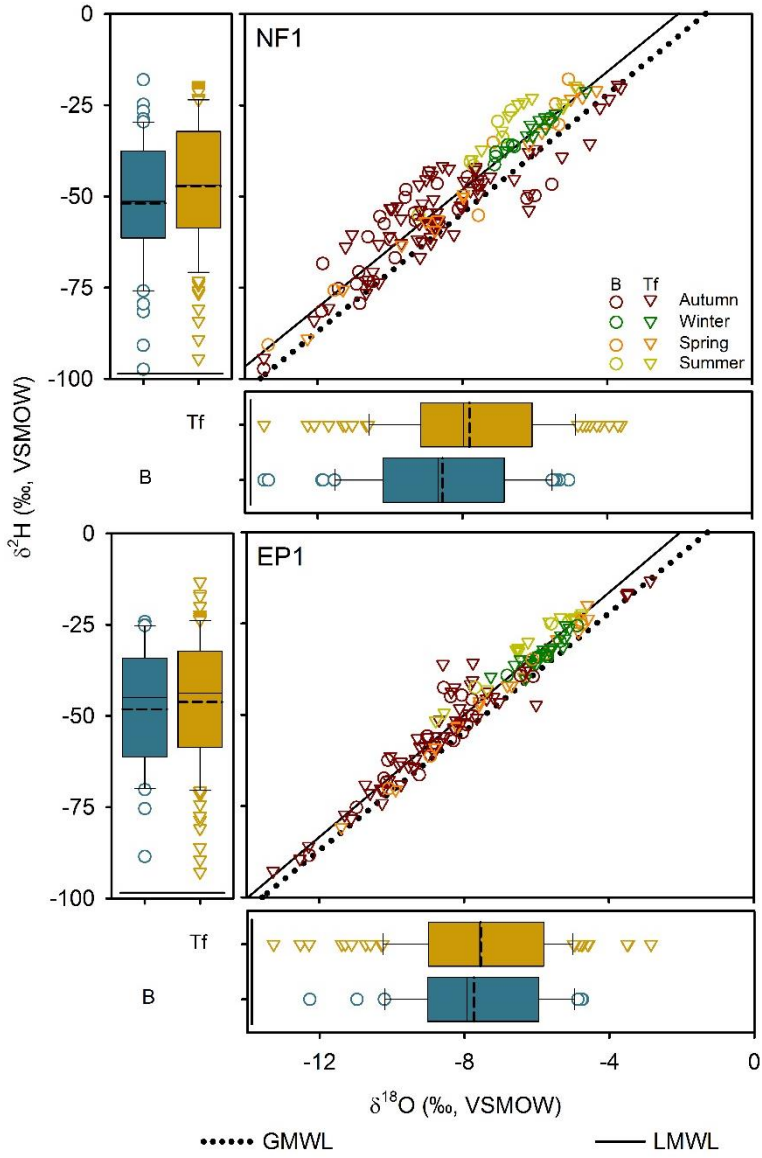

Figure 9.2: $\delta^{18}O$ and $\delta^{2}H$ signatures for bulk (B) and throughfall (Tf) precipitation collected in different seasons for NF1 and EP1 catchments (upper and lower plots, respectively). GMWL (Rozanski *et al*., 1993) and LMWL are shown in solid and dotted black lines, respectively. Bulk and throughfall precipitation isotopic signatures are summarized in boxplots (below and left of each main plot for $\delta^{18}O$ and $\delta^{2}H$, respectively). Boxplots show average (dashed line), 25th, 50th (median) and 75th percentiles, whiskers represent 5- and 95-percentiles, while outliers are shown in by the respective symbol. Statistical grouping ($\alpha = 0.05$) is indicated by a continuous line to the left or below for $\delta^{18}O$ and $\delta^{2}H$, respectively.

9.5.2. Stream and soil solution water: mobile water compartment

Stream water was collected fortnightly at NF1 and EP1 (Figure 9.3; n = 25 and 22, respectively). While δ^2H showed differences (median: -38.0‰ and -36.4‰ for NF1 and EP1, respectively; $p < 0.001$ using M-W), no differences were found for $\delta^{18}O$ (median: -6.8‰ and -6.8‰ for NF1 and EP1, respectively; $p > 0.1$ using M-W). Soil solution water samples collected using the suction lysimeters (n = 67 and 57 for NF1 and EP1, respectively) showed that δ^2H (median: -30.2‰ and -26.1‰ for NF1 and EP1, respectively) and $\delta^{18}O$ (median: -5.6‰ and -4.7‰ for NF1 and EP1, respectively) were different ($p < 0.001$ using M-W, for both analyses, Figure 9.3).

9.5.3. Bulk soil water: mixed mobile/static compartment

Bulk soil water sample isotopic signatures collected at NF1 and at EP1 (Figure 9.3 n = 120 and 179, respectively) showed differences in $\delta^{18}O$ between catchments (median: -6.3‰ and -6.0‰ for NF1 and EP1, respectively; $p < 0.05$ using M-W). However, δ^2H showed no differences between catchments (median: -42.2‰ and -41.2‰ for NF1 and EP1, respectively; $p > 0.1$ using M-W).

All bulk soil samples were used to estimate the SEL for NF1 and EP1, respectively:

$$NF1_{SEL},\ \delta^2H = 5.67 \cdot \delta^{18}O - 6.51\ (r^2 = 0.81;\ p < 0.01) \quad (9.4)$$

$$EP1_{SEL},\ \delta^2H = 5.51 \cdot \delta^{18}O - 8.19\ (r^2 = 0.78;\ p < 0.01) \quad (9.5)$$

Slopes and intercepts showed no differences among sites ($p > 0.3$ for both using t-student test). Both SEL suggest that water in soils is evaporating in non-equilibrium conditions (Figure 9.3).

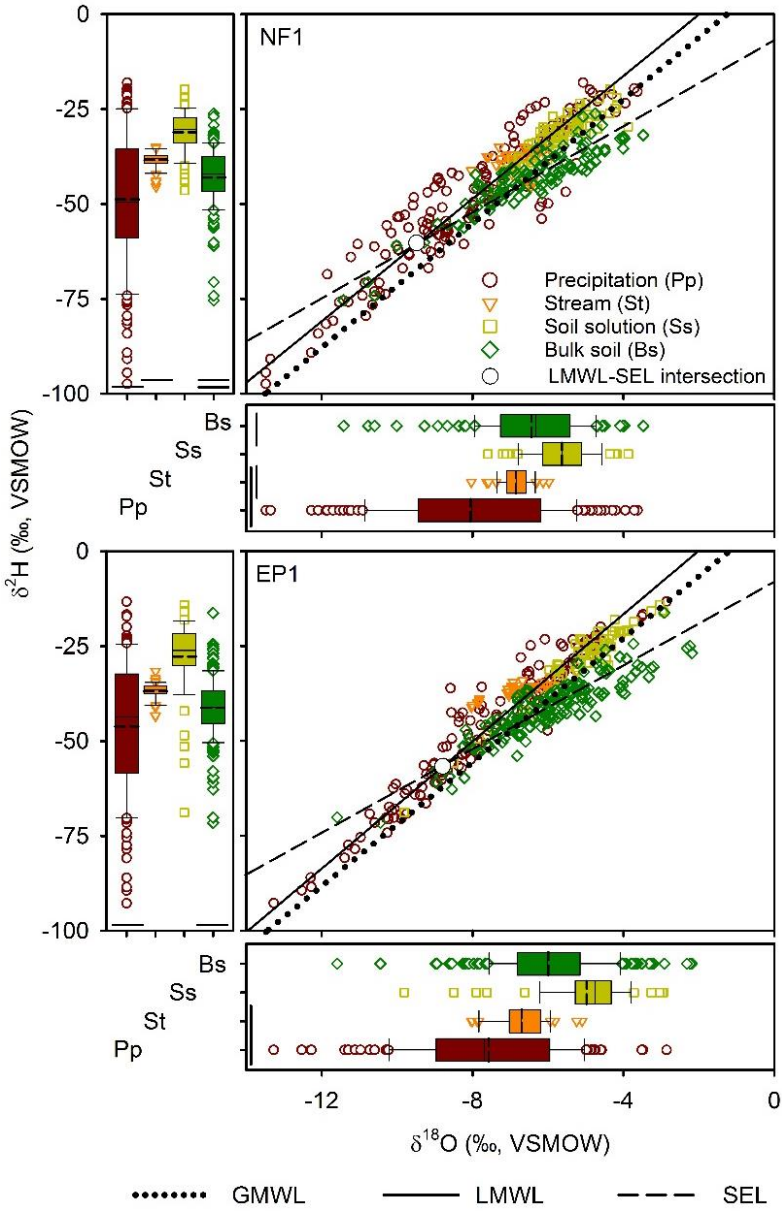

Figure 9.3: $\delta^{18}O$ and $\delta^{2}H$ plot for the different sampled water compartments in NF1 and EP1 (upper and lower plots, respectively). Each plot has the Global Meteoric Water Line (GMWL, Rozanski *et al.*, 1993), Local Meteoric Water Line (LMWL) and soil evaporation line (SEL) (dotted, solid and segmented lines, respectively) as references. Boxplots show average (dashed line), 25th, 50th (median) and 75th percentiles, whiskers represent 5- and 95-percentiles, while outliers are shown in by the respective symbol. Statistical grouping is indicated by a continuous line to the left or below for $\delta^{18}O$ and $\delta^{2}H$, respectively.

9.5.4. Xylem water

Figure 9.4 shows xylem water isotopic signatures for NF1 and EP1 (n = 136 and 121, respectively). $\delta^{18}O$ from xylem water among all sampled species showed that the 4-year-old *E. nitens* stand xylem water was significantly different from those of *L. philippiana* ($p < 0.01$ using Dunn method) and *E. cordifolia* ($p < 0.001$ using Dunn method). $\delta^{18}O$ signatures from the 16-year-old *E. nitens* stand xylem water were different only when compared to those of *E. cordifolia* ($p < 0.05$ using Dunn method, Figure 9.4). $\delta^{2}H$ from xylem water among all sampled species showed that the 4-year-old *E. nitens* stand was different from all native evergreen species ($p < 0.001$ using Dunn method, for all native species), while 16-years-old *E. nitens* stand xylem $\delta^{2}H$ showed differences when compared to those of *A. punctatum* ($p < 0.05$ using Dunn method) and *E. cordifolia* ($p < 0.001$ using Dunn method). Among native evergreen species, $\delta^{2}H$ from *E. cordifolia* xylem water showed differences when compared to those of *A. punctatumn* and *L. philippiana* ($p < 0.05$ using Dunn method, for both, Figure 9.4).

9.5.5. Two water worlds assessment and lc-excess

Ecohydrological separation or the TWW is supported by negative lc-excess from xylem water (Figure 9.5). If xylem water lc-excess is close to 0‰, this indicates that xylem water lies on the LMWL, indicating no ecohydrological separation. Under this scenario, water in soils is completely mixed (see Figure 9.5). In NF1, lc-excess from stream and soil solution showed no differences ($p > 0.5$ using non-parametric K-W test, Figure 9.5A). However, lc-excess from bulk soil showed differences when compared to lc-excess of soil solution and stream ($p < 0.001$ for all comparisons using Dunn method, Figure 9.5A). Bulk soil lc-excess showed differences compared to those of xylem water from *A. punctatum* and *E. cordifolia* ($p < 0.01$ and $p < 0.05$ respectively, using Dunn method), but not when compared to *L. philippiana* ($p > 0.2$ using Dunn method, Figure 9.5A). Native evergreen tree species showed no differences for lc-excess when compared to each other (Figure 9.5A).

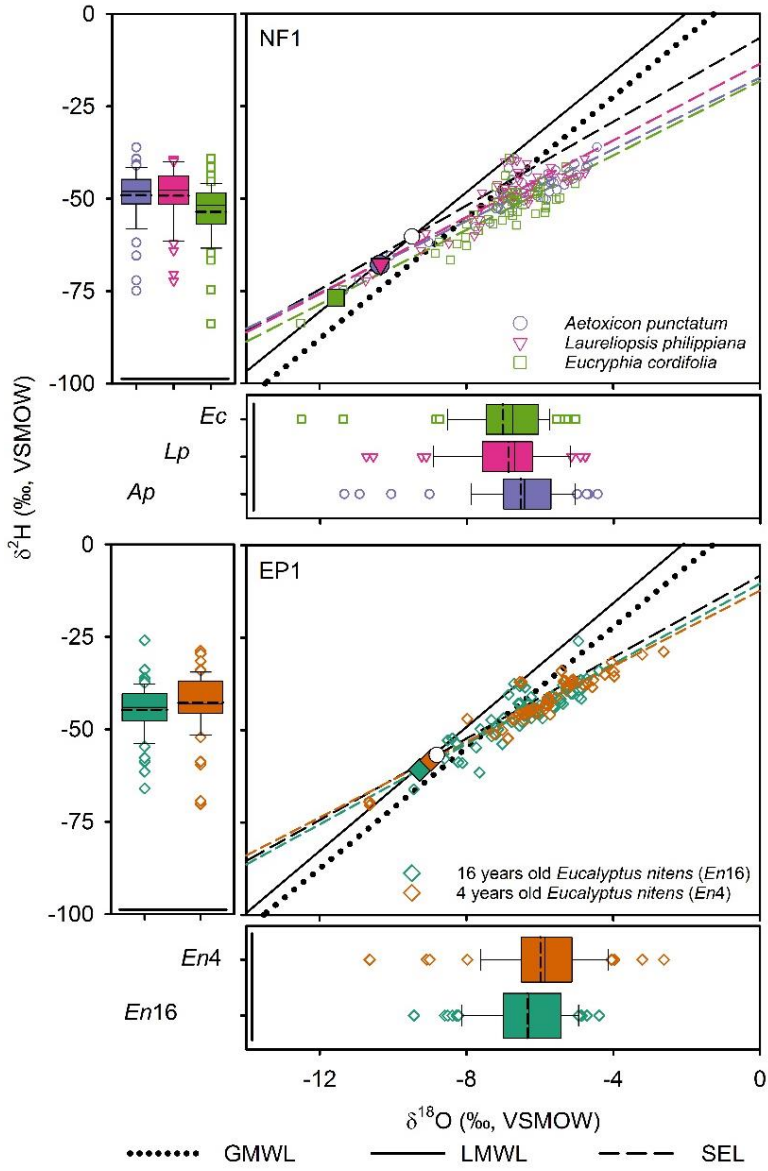

Figure 9.4: $\delta^{18}O$ and $\delta^{2}H$ plot for tree xylem water for NF1 and EP1 (upper and lower main plots, respectively). Xylem evaporation lines (XEL) are shown in the same color as the respective species. LMWL-XEL intersection is illustrated with the same symbol and color of respective species. Each plot has the Global Meteoric Water Line (GMWL, Rozanski *et al.*, 1993), Local Meteoric Water Line (LMWL) and soil evaporation line (SEL) (dotted, solid and segmented lines, respectively) as references. Boxplots show average (dashed line), 25th, 50th (median) and 75th percentiles, whiskers represent 5- and 95-percentiles, while outliers are shown in by the respective symbol. Statistical grouping is indicated by a continuous line to the left or below for $\delta^{18}O$ and $\delta^{2}H$, respectively.

In EP1, lc-excess from stream water showed differences when compared to soil solution lc-excess ($p < 0.05$ for all comparisons using Dunn method). Bulk soil lc-excess values also showed differences when compared to soil solution and stream ($p < 0.001$ for all comparisons using Dunn method). Xylem lc-excess from the 4- and 16-year-old *E. nitens* stands (Figure 9.5B) showed no differences when compared to each other. However, lc-excess from both *E. nitens* stands showed differences when compared to stream and soil solution ($p < 0.05$ for all comparisons using Dunn method), but not when compared to bulk soil ($p > 0.5$ using Dunn method, Figure 9.5B)

In NF1, bulk soil and xylem water from native evergreen tree species showed lc-excess values close to zero in the last sampling campaign in autumn 2013 (Figure 9.5A). In EP1, similar observations were made during the late autumn 2013 and winter 2013 sampling campaigns, i.e. lc-excess from bulk soil and xylem for both *E. nitens* stands were close to zero (i.e. closer to the LMWL, Figure 9.5A). These lc-excess values suggest a single water world or ecohydrological connection, and not two as had been previously hypothesized (see Figure 9.5).

9.5.6. δ^2H_{LMWL} intersection and precipitation sources of water

Figure 9.6 shows δ^2H_{LMWL} intersections for all measured water compartments and xylem water from NF1 and EP1 (Figure 9.6C and D, respectively). Within catchments, stream and soil solution δ^2H_{LMWL} intersection were different from those of bulk soil and xylem water ($p < 0.001$ for all comparisons using Dunn method, Figure 9.6). In NF1, bulk soil δ^2H_{LMWL} intersection was different from those of stream, soil solution and xylem water ($p < 0.001$ for all comparisons using Dunn method, Figure 9.5). However, in EP1 bulk soil δ^2H_{LMWL} intersection showed no differences when compared to that of both *E. nitens* xylem water ($p > 0.2$ using Dunn method). Yet, δ^2H_{LMWL} intersections from xylem water of the different sampled species and stands showed no differences within catchments ($p > 0.5$ and $p > 0.9$ using Dunn method for NF1 and EP1, respectively). However, when compared to each other, both *E. nitens* stands δ^2H_{LMWL} intersection were different from those of *A. punctatum*, *L. phillipiana* and *E. cordifolia* ($p < 0.05$ using Dunn method, Figure 9.6C).

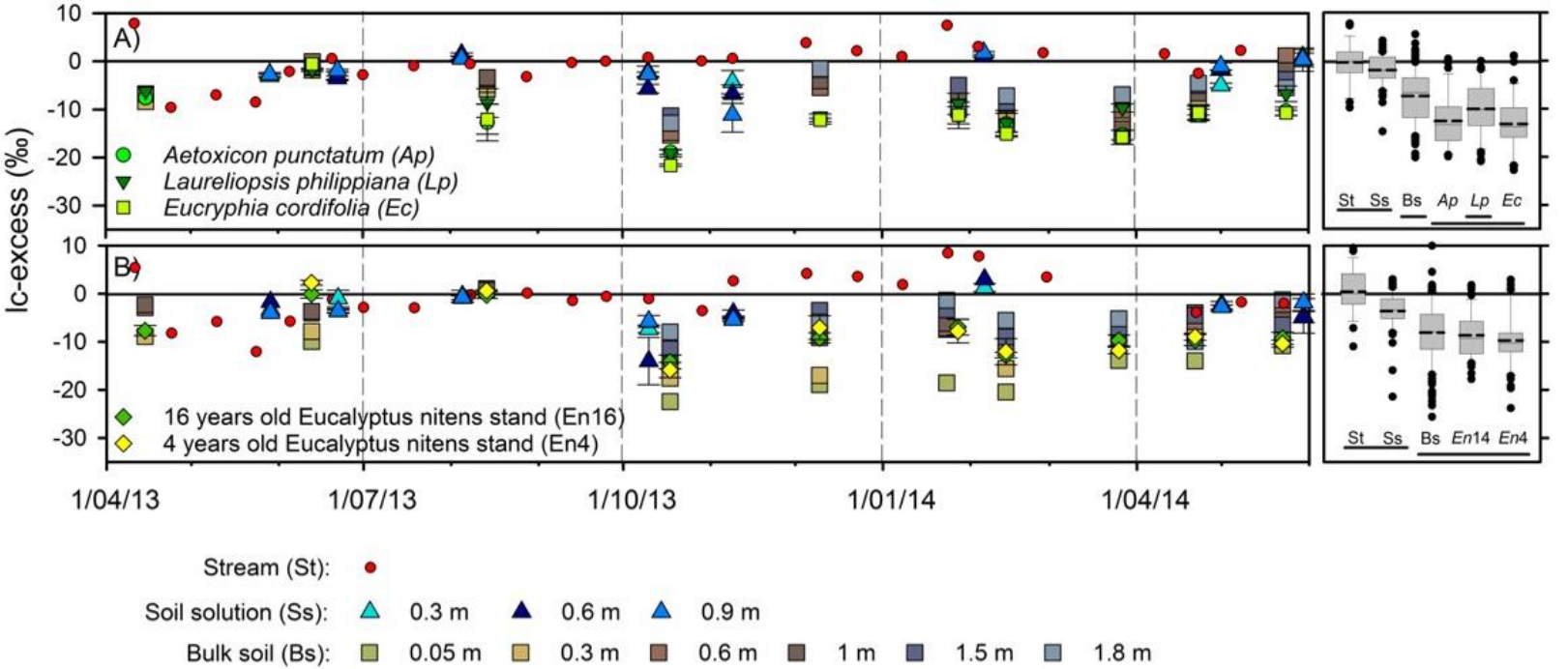

Figure 9.5: Two Water Worlds hypothesis assessment. lc-excess is shown for stream (St), soil solution (Ss, mean ± 1 SE), bulk soil (Bs, means) at sampled depths and xylem water (mean ± 1 SE) for NF1 and EP1 (higher and lower plots, respectively). A solid black line indicates 0‰ as a reference for the LMWL. Boxes on the right show 25th percentile, median (solid line), average (dashed line), 75th percentile, while whiskers represent 5- and 95-percentiles, while outliers are shown in black circles. Statistical grouping (α = 0.05) is shown by continuous line (modified from Hervé-Fernández *et al*., 2016b).

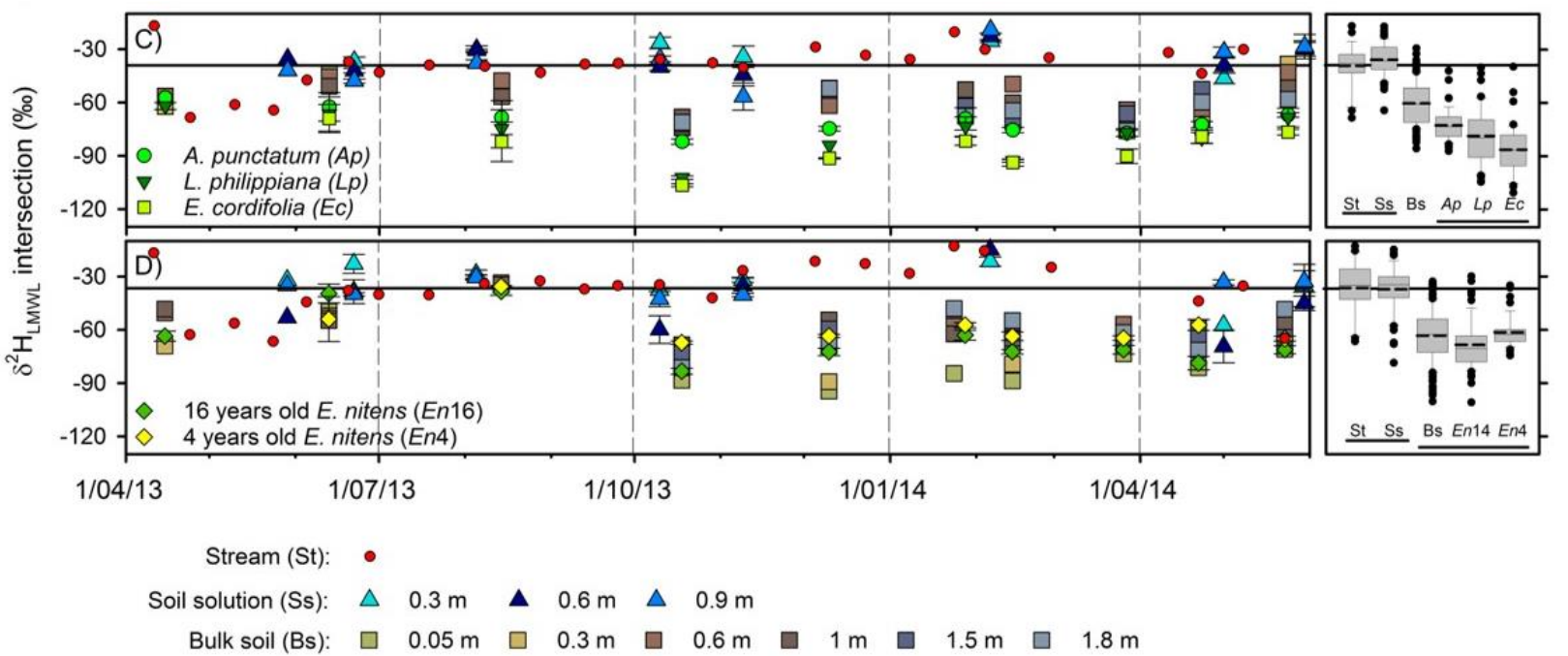

Figure 9.6: δ^2H_{LMWL} intersection estimated for stream (St), soil solution (Ss, mean ± 1 SE), bulk soil (Bs, means) at sampled depths and xylem water (mean ± 1 SE) for NF1 and EP1 (C and D, respectively). A solid black line indicates the average stream δ^2H_{LMWL} intersection value. Boxplots on the right side summarize the respective data. Boxes on the right show 25th percentile, median (solid line), average (dashed line), 75th percentile, while whiskers represent 5- and 95-percentiles, while outliers are shown in black circles. Statistical grouping ($\alpha = 0.05$) is shown by continuous line (modified from Hervé-Fernández *et al.*, 2016b).

9.6. Discussion

9.6.1. Precipitation: bulk and throughfall

In the present study, $\delta^{18}O$ and $\delta^{2}H$ of bulk and throughfall precipitation showed no differences within sites. This contradicts the common assumption that throughfall precipitation should be enriched, since water could have evaporated while passing through the canopy (Kubota and Tsuboyama, 2003; Allen *et al.*, 2014). However, this assumption does not always hold true (Scholl *et al.*, 2011). Studies comparing $\delta^{18}O$ and $\delta^{2}H$ of bulk and throughfall precipitation have described a high variability in throughfall signatures. For example, Scholl *et al.* (2011) and Allen *et al.* (2014) found that throughfall $\delta^{18}O$ and $\delta^{2}H$ had depleted signatures when compared to those of bulk precipitation, either due to mixing of water or to other processes that are not fully understood. Other variables that could help to explain differences in isotopic signatures include rainfall intensity and amount (Dansgaard, 1964), as well as canopy structure, which generates rainfall hot spots or “drip points” (Scholl *et al.*, 2011).

In general, precipitation is depleted in $\delta^{18}O$ and $\delta^{2}H$ during wet seasons and more enriched in dry seasons due to a known temperature and amount effect (Dansgaard, 1964). In this study however, only autumn was significantly different from all other seasons, showing more depleted values. Precipitation during the winter event showed a similar enrichment as was observed in spring and summer. A similar result was previously described by Scholl *et al*. (2007) for rainfall occurring during fog events on leeward and windward positioned sites. This could be relevant for this study, as fog events are frequent in the coastal mountain range along the pacific ocean coast, where the selected sites for this study are located (Aravena *et al.*, 1989; Dawson, 1998; Squeo *et al.*, 2006).

An analysis of the LMWLs estimated for each catchment shows that the slopes (+8.08 and +8.37 for $NF1_{LMWL}$ and $EP1_{LMWL}$, respectively) appear to be in line with that of the GMWL (Rozanski *et al.*, 1993). However, LMWL intercepts (+16.4‰ and +17.0‰ for NF1 and EP1, respectively) indicate an important contribution of re-evaporated waters from nearby water bodies, canopy interception, soil evaporation and/or transpiration of surrounding vegetation (Rozanski *et al.*, 1993; Gat, 1996).

9.6.2. Mobile and bulk soil water compartments

Our results showed that stream and soil solution samples plot along the LMWL. Typically, as precipitation infiltrates into the soil profile, soil macro and mesopores are filled, and soil micropores are recharged through adsorption or capillarity (Or and Tuller, 1999; Tuller *et al.*, 1999; Phillips, 2010; Brooks, 2015). Evaporation from the mobile water compartment occurs under equilibrium conditions, as demonstrated by shown data (i.e. it plots along the LMWL). However, once water has been adsorbed/absorbed by soil particles, it follows an evaporation line that plots away from the LMWL, indicating evaporation under non-equilibrium conditions. These two evaporation processes that are sometimes referred to as first and second-stage evaporation (Or *et al.*, 2013), fractionate isotopes differently and therefore result in different isotopic labels of the mobile and bulk soil water compartments (Phillips, 2010; Sprenger *et al.*, 2015), bearing in mind that bulk soil water contains both mobile and static water, with static water being the larger fraction. These differences have been used to hypothesize about the TWW, in which the mobile water compartment flows to streams, and the static water compartment is used by trees (McDonnell, 2014). In this study, xylem water plots to the right of the LMWL, supporting the TWW hypothesis.

9.6.3. lc-excess: Assessment of the “two water worlds” hypothesis

In the present study, lc-excess was used to evaluate the δ^2H distance that separates the TWW. Overall, xylem water from native evergreen species showed lower lc-excess (i.e. plotted further away from the LMWL) than both *E. nitens* stands suggesting that native evergreen species are withdrawing an even more evaporated water source than *E. nitens*. Results in this study also suggest that in both catchments, bulk soil water, a large fraction of which is static water, and the water source that trees are using (i.e. xylem water) have undergone evaporation under non-equilibrium conditions. It can therefore be deduced that xylem water comes from the static water compartment in the soil (Brooks *et al.*, 2010; McDonnell, 2014). This suggests an ecohydrological separation whereby mobile water drains into streams while static water is used by tree species. While lc-excess provides evidence to support the TWW hypothesis during dry periods (Brooks *et al.*, 2010; Goldsmith *et al.*, 2011; Penna *et*

al., 2013; McDonnell, 2014; Evaristo *et al.*, 2015), it does not support the same conclusion for wet periods. In wet periods (i.e. NF1: late autumn 2013; EP1: late autumn 2013 and winter 2013), lc-excess from stream, soil solution, bulk soil and xylem water were similar to each other and close to 0‰ (i.e. the LMWL). Therefore, during these periods, no clear ecohydrological separation (i.e. xylem water showing a similar isotopic signature as of soil solution) could be observed. To further examine the relationship between ecohydrological connectivity and precipitation, antecedent precipitation indexes (API, as in Kim *et al.*, 2005) for all sampling campaigns were estimated and are shown in Table 9.1. Sampling campaigns in which ecohydrological connectivity was observed have an API_{14} of 100 mm or higher (see Table 9.1), while API_7 appears to be unrelated to the ecohydrological connectivity observed in this study.

Table 9.1: Rainfall depth (in mm) accumulated in the 7 and 14 days prior to a sampling campaign. ● indicates ecohydrological connectivity between stream and xylem water.

	2013					2014				
API	Apr-15	Jun-13●	Aug-14●	Oct-09	Dec-05	Jan-24	Feb-14	Mar-26	Apr-22	May-23
API_7	20	27.1	51.2	42.8	0.3	34.7	0.5	nd	7.2	25.8
API_{14}	27.6	120.7	155.3	42.8	9.13	34.7	26.6	nd	20	72.2

Large amounts of rainfall in the 14 days prior to sampling may trigger lateral hydrological connectivity between hillslopes and streams, resulting in isotopic homogenization of soil water (Figure 9.5; 9.7 and 9.8). Recent advances in describing hillslope-stream connectivity (McGuire and McDonnell, 2010; van Meerveld *et al.*, 2015) have shown that hillslope-stream connectivity is only achieved during occasional wet periods, even in places where groundwater is shallow (Geris *et al.*, 2015c). This is consistent with our results.

The differences observed among study sites could be due to rainfall characteristics, canopy interception (30% and 5% for NF1 and EP1, respectively) (Oyarzún and Huber, 1999; Huber and Iroumé, 2001) and/or forest stratification, which

is high in NF1 but very low in EP1, since 90% of land cover in this catchment is by 4-year-old *E. nitens* stand. During frequent or long rainfall events, soils get sufficiently wet to replenish the static water to such an extent that isotopic signatures from the mobile and static water compartment mix eventually, it gets a similar isotope signature as the infiltrating water. This was clearly observed during the wet season in EP1 (late autumn 2013 and winter 2013 sampling campaigns) but not in NF1 (only late autumn campaign showed connectivity). Other studies have described either a complete separation between the TWW (Brooks *et al.*, 2010; Goldsmith *et al.*, 2011; Evaristo *et al.*, 2015) or a full connection (Geris *et al.*, 2015a). However, most of these studies result from sampling campaigns of 1 to 2 days (i.e. 10 to 15 xylem samples), causing that their conclusions may not be representative for all situations. In this sense and to the best of our knowledge, our study is the first that accounts for temporal variability and shows that the TWW hypothesis does not hold true, for all circumstances. Results from this study show evidence of ecohydrological connectivity at the studied site in periods characterized by high antecedent precipitation (see Table 9.1 and Figures 9.5; 9.7 and 9.8).

9.6.4. Precipitation sources of water, δ^2H_{LMWL} intersection

All water has its origin from meteoric sources, represented by the LMWL. Theoretically, the LMWL is a linear model for the isotopic signatures of meteoric water inputs. Therefore, it can be used to predict the precipitation source of a specific water sample. Essentially, the intersection between the LMWL and the $\delta^{18}O$ and δ^2H values of a water sample gives the original isotopic signature of that sample's precipitation source. In this way, it is possible to qualitatively assess whether or not any of the measured water compartments (e.g. xylem water, stream, bulk soil water, etc.) share a precipitation source.

In general, our data suggest that the sampled tree species do not exclusively use water from the mobile water compartment (i.e. stream/groundwater and soil solution). In NF1, δ^2H_{LMWL} intersections for stream, soil solution and bulk soil water were different from those of xylem water, indicating that native evergreen species rely on different precipitation sources than stream, soil solution and bulk soil. At EP1, the

xylem water δ^2H_{LMWL} intersection was different than those of stream and soil solution, however, bulk soil showed the same δ^2H_{LMWL} intersections as xylem water from both *E. nitens* stands. This suggests that *E. nitens* may use water from the bulk soil compartment, which consists of both static and mobile water.

Within catchments, all species/stands showed similar xylem δ^2H_{LMWL} intersections and therefore used a similar precipitation source of water. However, between sites, precipitation source of xylem water showed differences. During the sampling campaigns in which a single water world was observed, δ^2H_{LMWL} intersections showed similar stream and xylem water precipitation sources in EP1, but not in NF1. These campaigns have in common that they were performed during periods of high antecedent precipitation (see Table 9.1 and Figures 9.6, 9.7 and 9.8). The winter 2013 sampling campaign in EP1 showed similar δ^2H_{LMWL} intersections for stream, bulk soil and xylem water for both *E. nitens* stands. This common precipitation source could have been caused by high levels of autumn and winter rainfall, which could have resulted in very moist (to saturated) conditions in the upper soil layer, thereby mixing all water compartments in the soils. $\delta^{18}O$ and δ^2H signatures for xylem and water compartments during the late autumn 2013 (Figures 9.5; 9.6 and 9.7) and winter 2013 (Figure 9.8) sampling campaigns. This further supports the analysis: $\delta^{18}O$ and δ^2H signatures from xylem water plotted close to the LMWL and in some cases even closer to stream water. These observations were similar for both studied catchments (see Figure 9.8).

Xylem water from native evergreen species showed similar δ^2H_{LMWL} intersections. For all species, xylem water shows a depleted isotopic signature, which is an observation that has been made in previous studies (Brooks *et al.*, 2010; Evaristo *et al.*, 2015) and suggests that water is being recharged during the rainy season. There is also evidence that soil particles, especially clays, are able to hold water with a different isotopic signature than that of mobile water (Ingraham and Shadel, 1992; Araguás-Araguás *et al.*, 1995; Kendall and McDonnell, 1998; Brooks *et al.*, 2010; McDonnell, 2014). In this sense, xylem water from native evergreen species agree with those that have been described previously by Brooks *et al.* (2010), Goldsmith *et*

al. (2012) and Evaristo *et al.* (2015), which suggest that trees use water that is depleted in heavy isotopes and recharged during rainy seasons.

Xylem water from both *E. nitens* stands shows a similar δ^2H_{LMWL} intersection to that of bulk soil in EP. In theory, this suggests that *E. nitens* stands are withdrawing from the same water mixture (i.e. mobile/static water compartments) present in bulk soil water, which is recharged throughout the year (Gat, 1996; Gibson *et al.*, 2008). This could be due to the low canopy interception by the younger *E. nitens* stand. However, further efforts should be made to address this issue. Many authors have shown evidence that FGES have negative impacts on the catchment water balance through their effects on evapotranspiration: altering either canopy interception, soil evaporation and transpiration (Oyarzún and Huber, 1999; Little *et al.*, 2009; Huber *et al.*, 2010; Iroumé and Palacios, 2013). On the other hand, Huber and Iroumé (2001) found that adult individuals of *Eucalyptus* species (*E. nitens* and *E. globulus*) showed similar canopy interception to that of native evergreen species.

Results in this study indeed show that all sampled tree species use water that does not easily drain to the streams. However, this does not necessarily mean that trees use the immobile water compartment exclusively. In fact, the similar isotopic signatures, evaporation lines and δ^2H_{LMWL} intersections between xylem water and bulk soil in EP1 could suggest that *E. nitens* stands rather use all water present in bulk soil (mobile/static mixture), rather than a completely immobile water compartment. *Eucalyptus* spp. have been described that use lateral and/or tap roots to withdraw water (Dawson and Pate, 1996; Whitehead and Beadle, 2004; Fritzsche *et al.*, 2006), which may help to explain this observed difference between species. However, since current methods are not able to separate or define proper mobile and static end members in bulk soil samples, differentiating between water withdrawn from these two compartments by vegetation is currently not possible. However, further efforts should be made to distinguish and separate the static and mobile water compartments in bulk soil as independent end members.

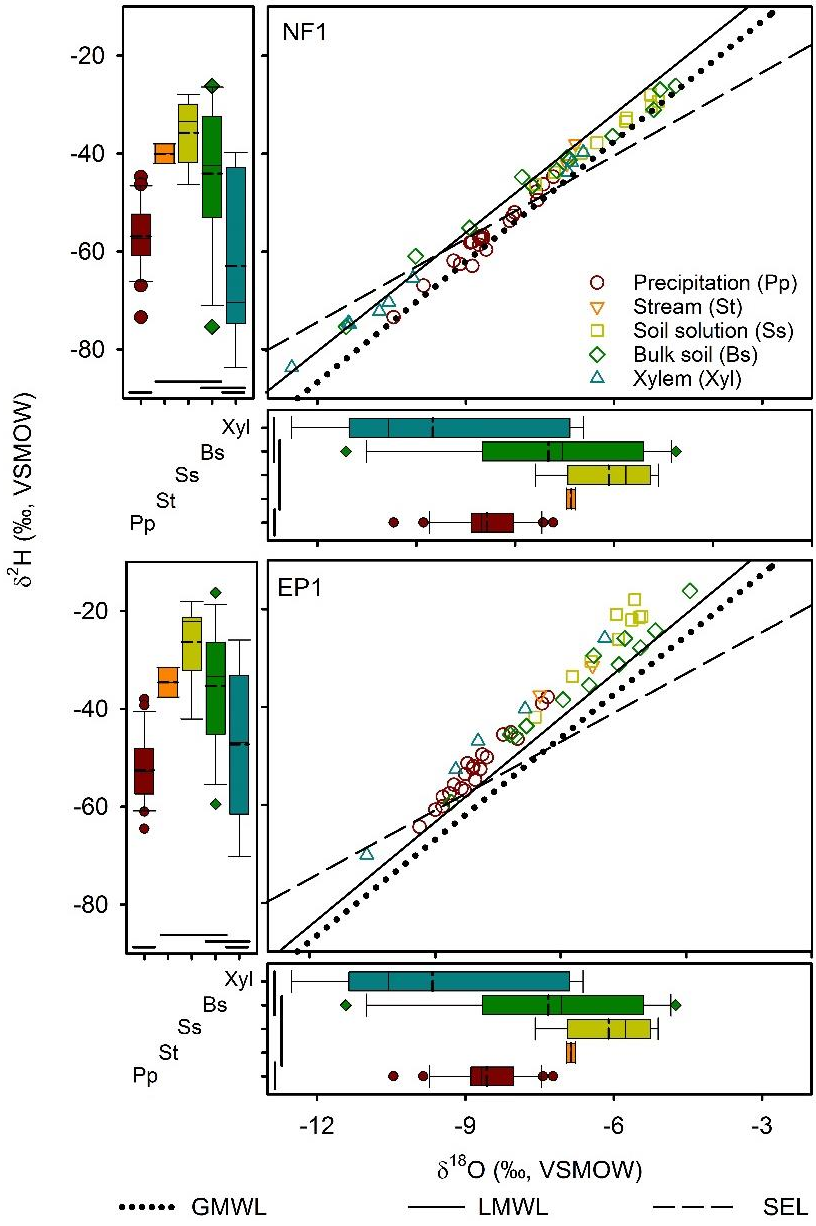

Figure 9.7: $\delta^{18}O$ and $\delta^{2}H$ plots for precipitation (Pp), stream (St), soil solution (Ss), bulk soil (Bs) and tree xylem (Xyl) water collected on NF1 and EP1 (upper and lower main plots, respectively) for late autumn 2013 sampling campaign during the first observed hydrological connectivity period. GMWL, LMWL and SEL are also plotted (dotted, solid and dashed lines, respectively) as references. Boxplots show average (dashed line), 25th, 50th (median) and 75th percentiles, whiskers represent 5- and 95-percentiles, while outliers are shown by the respective symbol. Statistical grouping is indicated by a continuous line to the left or below for $\delta^{18}O$ and $\delta^{2}H$, respectively.

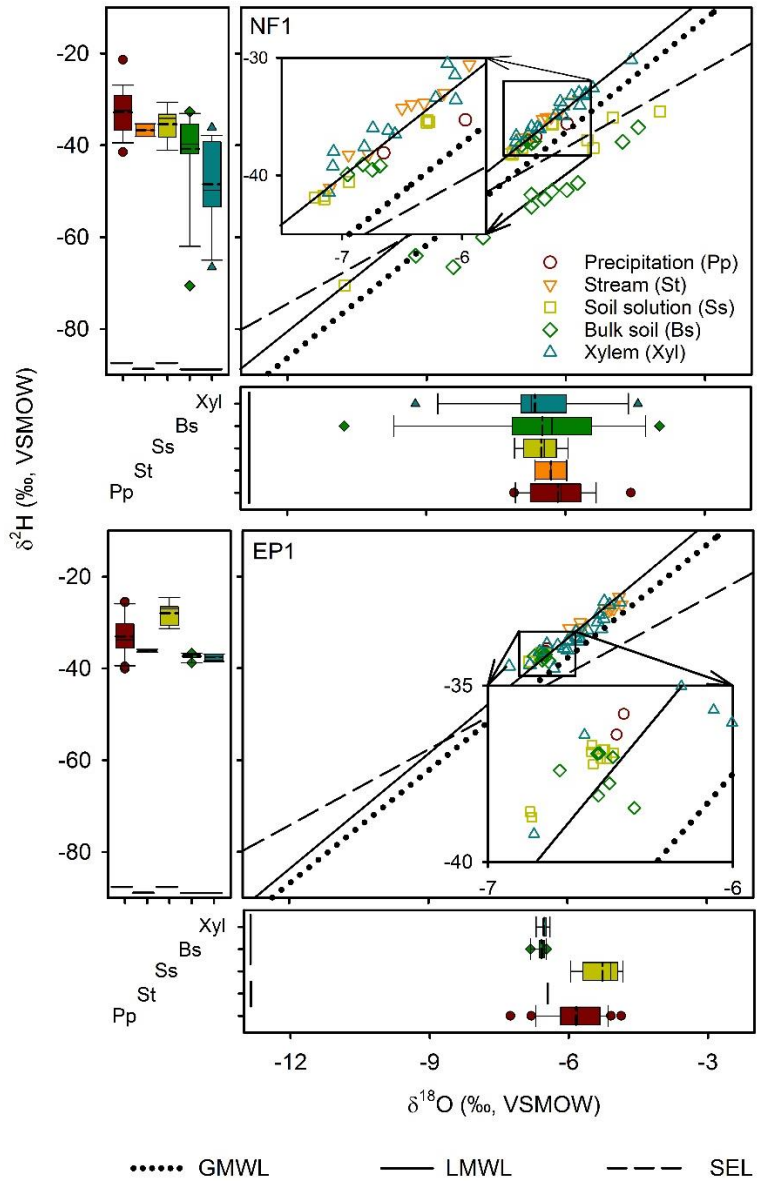

Figure 9.8: $\delta^{18}O$ and $\delta^{2}H$ plots for precipitation (Pp), stream (St), soil solution (Ss), bulk soil (Bs) and tree xylem (Xyl) water collected on NF1 and EP1 (upper and lower main plots) for the winter 2013 sampling campaign, during the observed hydrological connectivity period. GMWL, LMWL and SEL are also plotted (dotted, solid and dashed lines, respectively) as references. Zoom panels on plots show more detail where data is clustered. Boxplots show average (dashed line), 25th, 50th (median) and 75th percentiles, whiskers represent 5- and 95-percentiles, while outliers are shown by the respective symbol. Statistical grouping is indicated by a continuous line to the left or below for $\delta^{18}O$ and $\delta^{2}H$, respectively.

9.6.5. Current limitations

9.6.5.1. Sampling limitations

Sampling frequency remains one of the most important limitations on ecohydrological studies, since it is time consuming and expensive. Past studies relied on single or a couple (i.e. dry-wet season) of sampling campaigns (Brooks *et al.*, 2010; Goldsmith *et al.*, 2011; Geris *et al.*, 2015a; Evaristo *et al.*, 2016) or a compilation of isotopic studies made so far (Evaristo *et al.*, 2015). Regardless of sampling frequency and intensity used in a specific study, the TWW hypothesis should be tested for longer periods. Some groups have been able to deploy isotope ratio infrared spectrometry (IRIS) equipment in the field for automatic isotope measurements in stream and rainfall (Berman *et al.*, 2009) and soil water (Soderberg *et al.*, 2012; Wang *et al.*, 2013). However, sampling of xylem water, needed to test the TWW hypothesis, presents its own complications and challenges, which remain to be addressed (e.g. dealing with resins, and other organic compounds present in xylem water). However, so far field sampling campaigns remain the most common (if not the only) method available to have xylem water isotopic measurements.

9.6.5.2. Water extraction limitations

In order to understand from which soil water compartment trees withdraw water, we need to have a solid understanding of water soil interactions, and more specifically on the close interrelations between water, nutrients and carbon (Kirchner, 2003). Our current methodology on water extraction techniques, especially of soil bound water, remains one of the biggest challenges in achieving this goal. In this work, cryogenic vacuum extraction was used to extract water from bulk soil and xylem samples (Tang and Feng, 2001; Brooks *et al.*, 2010; Goldsmith *et al.*, 2011; Evaristo *et al.*, 2016). However, Orlowski *et al*. (2016), in a recent inter-comparison study of soil pore water extraction methods for stable isotope analysis, found that for clay and sandy soil samples, cryogenic vacuum extraction was outperformed by all other methods used (i.e. centrifugation, mechanical squeezing, direct vapor equilibration and microwave extraction). Furthermore, even though there are known artifacts which can alter isotopic signatures, especially for $\delta^{18}O$, which is strongly dependent on soil type

(Araguás-Araguás *et al.*, 1995), carbonate and water content (Meißner *et al.*, 2013; Oerter *et al.*, 2014), cation exchange capacity (Oerter *et al.*, 2014) and organic carbon (Orlowski *et al.*, 2015), we still lack a study in which all end members are measured (i.e. mobile and static water). This is particularly important because oxygen is a highly reactive element that interacts and exchanges with other oxygen atoms in the surroundings, whether solid (e.g. clays), liquid (e.g. water) or gaseous (e.g. CO_2).

Another limitation to this method results from freezing the soil sample, which is the first stage of the cryogenic vacuum extraction. Freezing causes water molecules to organize in such a way that the specific volume increases. This usually breaks most of the structures in which water is contained. This could generate a serious artifact, since this could cause oxygen from water to be mixed/exchanged with other sources (e.g. clay minerals). In spite of these limitations, cryogenic vacuum extraction remains an effective method for plant (i.e. xylem and leaves) water extractions (Peters and Yakir, 2008; Orlowski *et al.*, 2016).

9.7. Conclusion

The TWW hypothesis was assessed in south central Chile, considering two catchments, NF1 covered by native evergreen species (*A. punctatum*, *L. phillipiana* and *E. cordifolia*) and EP1 covered by *Eucalyptus nitens*. Our study is the first (to our knowledge) to be conducted seasonally, over a long period, testing the TWW hypothesis under a temperate climate.

Xylem water isotopic signatures ($\delta^{18}O$ and $\delta^{2}H$) from both *Eucalyptus nitens* stands plotted on, while the trees in the NF1 plot below their respective SEL. These results indicate that both forest types make use of water being recharged in the rainy season and throughout the year for NF1 and EP1, respectively. At both sites, it is not possible to discard that these forest types make, to an unknown proportion, use of both mobile and static water within the soil. Nevertheless, its major proportion seems to be water from the static water compartment. From the $\delta^{2}H_{LMWL}$ intersection points, it could be demonstrated that at both sites none of the species shared a common

water source with those of stream and soil solution, and only *E. nitens* stands showed no differences to that of bulk soil in EP1.

This study provided evidence that supports the TWW hypothesis in both studied catchments during dry periods, based on observed differences in plots of $\delta^{18}O/\delta^{2}H$, as well as differences in lc-excess values from soil solution, stream and xylem water samples. However, the TWW hypothesis did not hold true in periods characterized by high antecedent rainfall amounts. To explain the findings on the present study findings, it is hypothesized that the trees always extract water from the small pores where capillary water resides, even during wet periods. During dry periods, mobile water is hardly present in soils while the trees still take up capillary water. Because of evaporation within the soil, the capillary water is enriched under non-equilibrium conditions causing xylem samples to deviate far from the LMWL. Once the soil gets wetted again, this capillary water is replenished with the infiltrating precipitation water, causing a $\delta^{18}O$ depletion (as measured in xylem water). We thus hypothesize that there is not a true and continuous separation between two water worlds, but rather that plants are continuously taking water from the smaller pores that are occasionally replenished.

10. Chapter 10: Evaporation losses from soil at catchment level

After Hervé-Fernández, P., Oyarzún C., Brumbt, C., Boeckx, P. and N.E.C Verhoest. Evaporation losses from soil at catchment level, using $\delta^{18}O$ from old-growth native evergreen forest and Eucalyptus nitens covered catchments, in south-central Chile (40°S), to be submitted to Journal of Hydrology.

10.2. Abstract

Water losses through soil evaporation are still poorly quantified and hard to assess. The aim of this study was to estimate soil evaporation from catchments covered with old growth native forests (NF, n = 3) and *Eucalyptus nitens* (EP, n = 3) using $\delta^{18}O$ from stream and throughfall precipitation; and to compare water losses through soil evaporation as a proportion of precipitation water inputs. Observed results show that soil evaporation at both sites was similar (10.8 ± 0.6% and 8.4 ± 1.2% for NF and EP sites, respectively). The use of the Rayleigh equation is a simple and an informative method and it can be used as a benchmark for comparison with other methodologies used for soil evaporation estimation studies at catchment level is suggested.

10.3. Introduction

Evaporation from soils accounts for approximately 6% of continental water fluxes to the atmosphere (Good *et al.*, 2015). It constitutes a fundamental and fast ecosystem feedback at regional and global scales when compared to transpiration (Gat, 2000; Gat & Airey, 2006; Gibson & Reid, 2010; Jasechko *et al.*, 2013). In dense forests, evaporation from the forest floor is often considered to be minor when compared to other hydrological compartments, such as canopy interception (Williams *et al.*, 2004). However, it can be an important component of the catchment water budget (Gibson and Edwards, 2002); especially for the estimation of transpiration at catchment level (Ferguson and Veizer, 2007; Freitag *et al.*, 2008; Lee *et al.*, 2010).

Naturally, occurring stable isotopes (^{18}O and ^{2}H) in water have been highly instructive as tracers in the field of hydrology. Isotopic composition is expressed in terms of $[^{2}H]/[^{1}H]$ and $[^{18}O]/[^{16}O]$ ratios, represented by δ-values indicating the

deviation in parts per thousand (‰) from a designated standard (VSMOW, Vienna Standard Mean Ocean Water) as shown in Eq. (5.3).

Studies trying to separate evapotranspiration in to its components (i.e. transpiration, canopy interception and soil evaporation) are few. There is an obvious lack of studies regarding actual measurements or estimations of soil evaporation, independently from transpiration and canopy interception. In this study, we tested the following hypothesis; *Eucalyptus nitens* covered catchments have a higher soil evaporation than catchments covered with old-growth native evergreen forest, due lower tree density and higher bare soil exposure.

10.4. Material and Methods

10.4.1. Study sites

The description of study sites has been given previously in detail in chapter 3. However, for this study all catchments were sampled (Figure 3.1).

10.4.2. Sample collection and analysis

Precipitation samples were collected as already mentioned in chapter 3, section 3.2. Stream samples were collected regularly each 15 days on all studied catchments outlets at NF (i.e. NF1, NF2 and NF3) and EP (i.e. EP1, EP2 and EP3) sites.

Soil samples were collected and its water was cryogenically extracted as described previously in chapter 9, subsection 9.3.1. Stable isotope analysis was conducted in the same way as previously described in chapter 9, subsection 9.3.1.

10.4.3. Stable isotopes for the estimation of water evaporation losses from soil

For the estimation of evaporation from soil at catchment level, equations (5.10) and (6.2), from section 5.5.1 from chapters 5 and 6, respectively, were used. Hence, with a known fractionation factor, $\alpha^{+}_{v\text{-}w}$, and the δ-values of initial and remaining water, then the remaining water proportion (i.e. f in Eq. (6.2)) can be determined. In order to

reduce error in the estimation, $\delta^{18}O$ is used instead of $\delta^{2}H$ (Gat, 1996). This is because ^{18}O is less sensitive to temperature changes, than ^{2}H (see Figure 5.5). Hence, the $\alpha^{+}_{v\text{-}w}$ value for ^{18}O is given by equation (5.10), from section 5.5.1.

In this study, air temperatures for the estimation of $\alpha^{+}_{v\text{-}w}$ were obtained from baro diver (Schlumberger water services), every 30 min, with an accuracy of ± 0.1°C, at the catchment discharge of NF1 and EP1. These temperatures were assumed similar as those of the other catchments on their respective sites. The instrument was fixed next to the V-notch weir in NF1 and EP1 catchments. Mean annual temperatures measured during year 2013, were 10.1 ± 3.3°C, and 12.8 ± 5.5°C for NF1 and EP1, respectively. Solving Eq. (5.10), for the estimation of the fractionation factor, $\alpha^{+}_{v\text{-}w}$, and then Eq. (6.2), used to calculate the proportion of water remaining in a specific compartment (i.e. catchment). Hence, water lost through soil evaporation equals to the difference between 100% and the calculated proportion of water remaining.

LMWL and SEL were estimated using the Reduced Major Axis or Orthogonal Linear Regression method (Crawford *et al.*, 2014). Comparisons between the LMWL's and SEL's slopes and intercepts and estimated proportional evaporation results were compared using a t-student statistical test. Independent tests for $\delta^{18}O$ and $\delta^{2}H$ in precipitation and stream among sites were performed using a Mann-Whitney (M-W) test. Significance level was set to 0.05.

10.5. Results

10.5.1. Precipitation, stream and bulk soil water isotopic signatures

Results of precipitation stable isotope signatures have been already given in chapter 9, in the results section. Hence, it will not be repeated here. LMWLs where already given in Chapter 9, Eqs (9.2) and (9.3) for NF and EP, respectively.

10.5.2. Stream water

Stream water was collected once a fortnight approximately, in all studied catchments at NF and EP sites (n = 82 and 79, respectively). $\delta^{2}H$ showed differences

(-39.3 ± 2.7‰ and -37.3 ± 3.0‰ for NF and EP sites, respectively; $p < 0.001$ using M-W), but no differences were found for $\delta^{18}O$ (-6.9 ± 0.5‰ and -6.7 ± 1.0‰ for NF and EP, respectively; $p > 0.1$ using M-W). Please, note that in Figure 10.1, stream data for all catchments are plotted.

10.5.3. Bulk soil water and the soil evaporation line

Bulk soil water isotopic values for NF1 and EP1 have already been given in section 9.4.3 from chapter 9 (see precipitation details in Figure 9.2). SELs where already given in chapter 9, Eqs. (9.4) and (9.5) for NF and EP sites, respectively. In order to have a comparison between precipitation, stream from all catchments and bulk soil water isotopic signatures, all these are plotted on Figure 10.1.

10.5.4. Catchment evaporation loss estimation through Rayleigh equation

Using Eq. (6.2), and replacing δ_{wi} and δ_{wr}, with the average $\delta^{18}O$ from precipitation and stream, for each catchment on their respective site it is possible to estimate the amount or proportion of evaporated water losses. Using mean annual temperature of 10.1 ± 3.3 °C and 12.8 ± 5.5 °C for NF1 and EP1, respectively ($p < 0.01$), in Eq. (5.10) yields an equilibrium fractionation factor α^+ value of 1.0107 ± 0.0011 and 1.0105 ± 0.0021 for NF1 and EP1, respectively. These fractionation factors measured in NF1 and EP1 were used for all catchment from their respective sites. Replacing the above values on Eq. (6.2) yields an average f value (or remaining fraction of water from the total assumed to be 1) of 0.892 ± 0.006 and 0.917 ± 0.012 for catchments at NF and EP sites, respectively. Hence, based on these results, catchments at NF and EP sites, show on average 10.8 ± 0.6% and 8.4 ± 1.2% ($p > 0.4$; t-test) of precipitation water inputs being lost to evaporation from soil and stream surface in catchments at the NF and EP sites, respectively (see details in Table 10.1).

10.6. Discussion

In this study, $\delta^{18}O$ from precipitation and stream water was determined with the aim to test whether old-growth native evergreen forest or *Eucalyptus nitens* covered

catchments showed differences in soil and open channel evaporation losses using the Rayleigh distillation method, assuming equilibrium conditions. Results from this study showed that both study sites have similar evaporation losses at catchment scale. Other studies have estimated soil evaporation proportion using different methods under a temperate regime as the used study sites, with evaporation estimations ranging from 20% to 2% (see Table 9.4).

Since the underlying assumptions of the Rayleigh method are met (mobile water is evaporating under equilibrium conditions), obtained results should be approximate. Water in soils of NF1 and EP1 is not a mixture, accordingly to the "two water worlds" hypothesis described by recently published studies (Brooks *et al.*, 2009; Goldsmith *et al.*, 2011; McDonnell, 2014; Evaristo *et al.*, 2015; Brooks, 2015; Good *et al.*, 2015; Hervé-Fernández *et al.*, 2016b). Therefore, it is expected that all studied catchments behave similarly. Since evaporation of mobile water (e.g. stream) occurs along the LMWL, this is also an indication that evaporation is occurring under saturated conditions (i.e., RH = 100%). As such it can be stated that evaporation is occurring under equilibrium conditions, and thus, the assumptions for the use of the Rayleigh distillation method are met. Bulk soil samples clearly show that the water retained by soils is evaporating under non-equilibrium conditions. In general, SEL slopes are good indicators of the evaporation conditions and evaporation rates. In this study, SEL slopes were not statistically different, suggesting that at least NF1 and EP1 (where bulk soil samples were collected) were subject to similar evaporating conditions and also that both catchments had similar evaporation rates from their respective soils (Allison *et al.*, 1983).

Table 10.1: Annual evaporation loss estimations (in %) of total precipitation inputs, estimated using the Rayleigh distillation method for catchments 1, 2 and 3 for sites NF and EP.

	Catchment											
Site	1			2			3			Average		SD
NF	10.7	±	0.3	11.6	±	0.7	10.2	±	1.8	10.8	±	0.6
EP	6.7	±	3.2	9.4	±	0.8	9.0	±	3.2	8.4	±	1.2

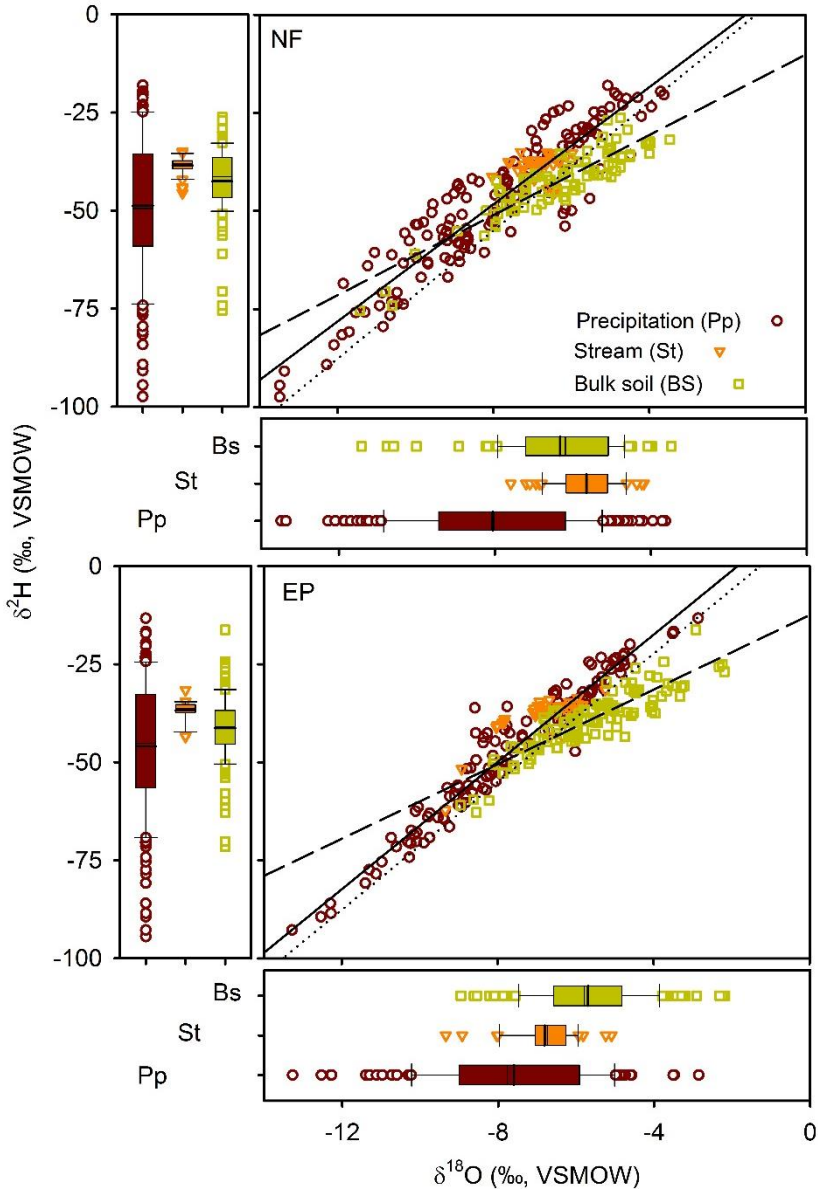

Figure 10.1: Global meteoric water line (GMWL, black dotted line); Local meteoric water line (solid black line); Local evaporation line (long dashed line) for NF and EP (top and bottom main panels, respectively). Precipitation, stream,soil solution and bulk soil data distribution is represented by boxplots that show average (dashed line), 25th, 50th (median) and 75th percentiles, whiskers represent 5- and 95-percentiles, while outliers are shown by the respective symbol. Please note that all stream samples are plotted in the above Figure.

Several methods have been used across the globe to quantify evaporation losses using water stable isotopes (either $\delta^{2}H$ or $\delta^{18}O$) by several authors (Tsujimura & Tanaka, 1998; Liu *et al.*, 2006; Wenninger *et al.*, 2010; Sutanto *et al.*, 2012; Good *et al.*, 2015). Estimations of evaporation using stable isotopes under experimental conditions and at catchment level have reported values of less than 10% of total water inputs. Tsujimura & Tanaka (1998) estimated evaporation of 2% of annual precipitation inputs, while Liu *et al*. (2006) described that soil evaporation varied from one year to the next from 2.8% to 3.4% of total throughfall inputs, in which fog drip was also included. There is an obvious lack of studies comparing results estimated with different methods (i.e., hydrological models, scintillation method and/or stable isotope analysis, Sutanto *et al.*, 2012).

Sutanto *et al*. (2012) estimated evaporation using $\delta^{18}O$ isotope mass balance (IMB) and Penmann-Monteith (PM, in HYDRUS-1D) to model soil evaporation from prepared soil cores covered with grass and compared these methods with gravimetric measurements (Sutanto *et al.*, 2012). They showed showed that soil evaporation was 12.1% and 26.9% of total water inputs, using $\delta^{18}O$ IMB and PM, respectively. The IMB method was closer to reality and showed a 2.4% lowersoil evaporation compared to that derived from gravimetric measurements. Soil evaporation estimations were 5.4% higher using the PM routine in HYDRUS-1 compared to the gravimetric method (Sutanto *et al.*, 2012). Williams *et al.* (2004) compared evapotranspiration (ET) measured during 15 days using eddy covariance and sap flux measurements in order to split ET into soil evaporation and transpiration; and $\delta^{2}H$ measurements for partitioning ET in soil evaporation and transpiration. Their soil evaporation estimates using eddy covariance and sap flux were similar to $\delta^{2}H$ results during midday, when ecosystem gas exchange was at maximum. However, it compared less favourably during late afternoon periods. This could be due to the use of $\delta^{2}H$ instead of $\delta^{18}O$. It is known that temperature changes affect fractionation factors ($\alpha^{+}_{v\text{-}w}$) of ^{2}H more than those of ^{18}O (Gat, 2005). This difference is reduced when temperatures are higher than 50° C, and diminishes above 340° C.

Table 10.2: Soil evaporation (in % of total precipitation water inputs) estimation using different isotope and physical modelling approaches.

Source	Method	E (%)	Dominant species
Stälfelt (1963)	P-M	20	Young Picea *albis*
Baumgartner (1967)	P-M	10	Young Pine
Tajchman (1972)	P-M	5	Young Pine
Hattori (1983)	Rayleigh $\delta^{18}O$ (Pp-St)	8.9	*Chamaecyparis obtuse* (Cypress)
Tsujimura & Tanaka (1998)	$\delta^{18}O$ (Pp-Ml)	2	Oak deciduous forest
Sutanto *et al*. (2012)	$\delta^{18}O$ (IMB)	12.1	Grass
	HYDRUS-1D	26.9	
Liu *et al.* (2006)	Rayleigh $\delta^{18}O$ (Pp-St)	3.1 ± 0.3	*Pometia tomentosa* and *Terminalia myriocarpa*
Good *et al*. (2015)	$\delta^{2}H$ (satellite based)	4.4 ± 3.3	Global estimation
Martens *et al*. (2016)	GLEAM v3	18.9 ± 26.9	Global estimation (including Antartica)
This study	Rayleigh $\delta^{18}O$ (Pp-St)	9.0 ± 0.6	Old growth native evergreen forest
This study	Rayleigh $\delta^{18}O$ (Pp-St)	8.6 ± 1.2	*Eucalyptus nitens* plantation

P-M, Penmann-Monteith; Pp-St, using precipitation and stream water $\delta^{18}O$; Pp-Ml, using precipitation and soil water $\delta^{18}O$. Note that soil water was sampled using microlysimeters; IMB, Isotopic mass balance, using $\delta^{18}O$.

Global-scale evaporation studies have been conducted using modelling approaches based on meteorological (Miralles *et al.*, 2015; Martens *et al.*, 2016) and stable isotope data (Jasechko *et al.*, 2013; Good *et al.*, 2015). Without doubt, modelling approaches feature the advantage of quantifying differences across biomes and ecosystems. However, the assumptions underlying some of these methodologies may not be realistic(see Miralles *et al.*, 2015). The potential use of stable isotopes in global datasets (e.g. GNIP and GNIR) in addition to satellite isotope measurements (Good *et al.*, 2015) could provide a powerful way to support and add robustness to meteorologically based modelling approaches.

The slight observed variability on evaporation within sites could be due to a range of different factors. Although catchment size ranged from 7.9 to 281.7 ha, results were consistent within sites. Hence, the slight differences might be attributable to grasses covering soils at EP, while a 5 cm layer of leaf litter covered soils at NF. Indeed, having a layer of leaf litter could induce higher soil evaporation rates as shown by Allison et al. (1983). Their experiment was carried out under laboratory conditions and at constant environmental conditions of 33°C and 30% RH using a plate filled with water. It showed lower evaporation rates (SEL slope of 4.3), when compared to a water surface covered by a perforated steel sheet and a layer of 15 mm of mulch on top of that (SEL slope of 2.66, for details see Allison *et al.*, 1983). A higher difference between evaporation losses between sites was expected. In addition, catchments covered with eucalyptus showed a very similar evaporation loss, despite EP1 was covered 90% by 4-year-old eucalypts, while EP2 and EP3 were covered by adult eucalypt individuals and some remnants of second growth native evergreen forest. In addition, in this study water inputs to native evergreen forest could have been underestimated since fog interception was not included in this study.

Fog is isotopically the most isotopically enriched meteoric water (Gat *et al.*, 1996; Scholl *et al.*, 2002; Gat, 2005). Fog events have been described to play an important role in catchment water balance, especially in areas were the canopy interception is high (i.e., native forests and mountainous forests), showing values of positive interception (Oyarzún *et al.*, 2004). Other studies have described that fog can account for up to 50% of throughfall inputs (Cavelier *et al.*, 1996). This could in fact

have a negative effect on the volumetric water losses to evaporation in catchments under native forests that are more efficient in fog capture. Probably, including fog inputs with its enriched isotope signature, would have an effect on the precipitation inputs – stream water distance in the δ^2H/ $\delta^{18}O$ plot, i.e., reducing it. Theoretically, this could lower the estimation of soil evaporation, although a high canopy interception may also mean that less water is entering the forest floor because of the high interception losses of native forest during small (i.e. < 10 mm) rain events. In a study conducted near our study area, Huber and Oyarzún (1992) described that canopy interception accounted for 30% of water inputs (not including fog), but also 8.3% was retained by the leaf litter. Huber and Iroumé (2001) observed that almost 30% of precipitation was intercepted in native evergreen forests, while 4-year-old *E. globulus* intercepted only 5% of rainfall in south central Chile (Huber and Iroumé, 2001; Soto-Schönherr and Iroumé, 2016). Essential in this type of studies is to have constant measurements of rainfall inputs. In this study, all systems to measure precipitation (bulk and throughfall) failed. This indeed is a caveat in this study. Hence, this study is to be a soil evaporation approximation. In order to improve our current knowledge on catchment evaporation losses from soil, further studies should be conducted using additional methodologies.

Catchment water balance studies in the area have reported the *Eucalyptus spp.* covered catchments show higher amounts of evapotranspiration (Huber *et al.*, 2010; Oyarzún & Huber, 1999), while other studies have reported that eucalypts and other exotic species have a great impact on water resources (Little *et al.*, 2009; Oyarzún *et al.*, 2011; Iroumé and Palacios, 2013). Other studies comparing tree water fluxes have shown that *E. globulus* and native Chilean trees are not that different (Jiménez-Castillo *et al.*, 2011; Hervé-Fernández *et al.*, 2016b). Results from this study suggest that catchments covered with old-growth native forest and *E. nitens* show similar evaporation losses. This result suggests that the differences in evapotranspiration estimated in previous studies could be due to transpiration rates of planted species and canopy interception, rather than soil evaporation, which plays a minor role in water losses at catchment level. Recently, Hervé Fernández *et al*. (2016) showed for the same study area, that *E. nitens* withdrew water with a similar isotopic signature as

stream water, thus, eventually *E. nitens* uses groundwater, while native evergreen trees withdraw water from a soil reservoir recharged during the rainy season.

10.7. Conclusions

Evaporation from soil was estimated from old growth native evergreen (*A. punctatum*, *L. phillipiana* and *E. cordifolia*) forest and *Eucalyptys nitens* plantation in southern Chile. In this study it was shown that evaporation from soil at catchment level was similar under both land cover types. The Rayleigh method used for the evaporation estimation at catchment level showed no effect with catchment size (7.9 to 281.7 ha).

Although these data should be supplemented with a more regular and sistematic sampling (e.g. monthly or daily rainfall samples), using flux weighted isotope samples in addition to micrometeorological data (i.e. relative humidity and air temperature). This will enable to get more details on the evaporation processes under both land cover types. The method outlined in this study still presents the advantage that is easy to implement, estimate and interpret. Hence, in order to provide a reference and robustness in other soil evaporation studies at catchment level, it is suggested to use it as a reference for future evaporation studies at catchment level, using other approaches (i.e. modelling, scintillation (i.e. sensible and latent heat fluxes), stable isotope analysis, etc…). This study showed a simple method on how to estimate evaporation losses from soils at catchment scale. Hence, it is suggested to use this simple and informative method in order to have a simple reference in future catchment evaporation studies.

11. Chapter 11: General conclusions and outlook

Since the results of this work have already been discussed in previous chapters, the aim of this section section is to provide a more general conclusion on the findings and implications of this thesis.

11.1. Contribution of the thesis

Land cover changes pose a great threat to water quality and quantity. Although these effects are clear, there is still a lot to conceptualize, understand and discuss. The effects on water quality usually relate to a decrease of nutrient retention by soils. Hence, an increase in nutrient inputs to downstream ecosystems is expected. The alteration on water quantity is already affecting rural, urban and ecological communities worldwide. Therefore, the main driver of this work has been the above-mentioned differences found described on nutrient inputs and exportation; tree water sources and the estimation of evaporation in old growth native evergreen forests and *Eucalyptus nitens* covered catchments.

11.2. Answer to research questions

11.2.1 What is the effect of land cover on nutrient inputs and nutrient exportation?

In chapter 2, the effect of land cover on nutrient concentration and fluxes was assessed along with stream nutrient export, on a rainfall event basis. My study is the first to show frequent nutrient sampling in the studied area. In general, my research showed that *Eucalyptus globulus* land cover had a lower throughfall nutrient enrichment, while second growth evergreen and deciduous showed a higher throughfall nutrient enrichment for all measured N and P species. Stream water nutrient chemistry showed that the only difference among studied catchments was in NO_3^--N concentrations, all other measured N species showed no statistical differences.

The effect of using nutrient input fluxes from bulk (i.e. bulk), throughfall of dominant vegetation (i.e. DV) or throughfall weighted by vegetation cover (i.e. WVC)

showed to be an important factor when estimating wet nutrient inputs through precipitation. In chapter 2, it was shown the effects of using each of the before mentioned methods. The WVC nutrient balance method offers a better approach for the estimation of wet deposition nutrient inputs compared to those of bulk and dominant species.

11.2.2. What is the relation of N and P species, total catchment discharge and new water discharge?

Unfortunately, due to problems with the property owner, these results are from different catchments than those used in the study presented in chapter 2. In Chapter 3, similar effects as those described in chapter 2 were observed for NO_3^--N concentrations in catchment discharge. During storm events, NO_3^--N showed a negative relation with discharge, hence, a dilution. Usually, chemical compounds showing this behavior are not hydrologically accessible, meaning that they are not freely accessible for water transport. Opposite to NO_3^--N, Org-N increased in concentration as catchment discharge increased, showing an enhanced hydrological access, i.e. freely accessible for water transport. These attributed differences could be due to nutrient adsorption to soil particles, or to the simple fact that NO_3^--N is preferentially located in small pores, while Org-N is in bigger pores. This could explain the observed behavior during storm events. NO_3^--N is less concentrated in bigger pores, compared to Org-N, hence when both are flushed, NO_3^--N shows a rapid dilution, while Org-N increases in concentration in stream water. TN and TP concentrations were more related to catchment discharge and not to new water. During the 5th event the pattern was repeated only in NF1. Whether in EP1, TN and TP concentrations are more related to new water rather than catchment discharge. This was expected since *Eucalyptus* covered catchments known to have low water infiltration rates in soil. In addition, P is attached to soil particles. This relation is sustained by higher soil erosion rates observed during the 5th event, and frequently described in literature (Oyarzún *et al.*, 2011; Mohr *et al.*, 2013; Schuller *et al.*, 2013).

11.2.3 From which compartment are trees withdrawing water?

In chapter 8, the two water worlds hypothesis and the precipitation source of trees was assessed. In this study, the two water worlds hypothesis was refuted, as postulated initially by McDonnell (2014), this is: “different subsurface compartmentalized pools of water supply either plant transpiration fluxes or the combined fluxes of groundwater and streamflow”. In this study, hydrological connectivity was found after a 14 days antecedent precipitation higher than 120 mm, this sole finding is enough to refute a hypothesis. However, during the 7 remaining sampling campaigns, the ecohydrological separation was clear and evident. The obtained results also showed that both *E. nitens* stands relied on a more mobile source of water than that of native evergreen species. This was evidenced by the seasonality of the water recharge, where *E. nitens* withdrew water from the yearly averaged water recharge, while native evergreen forests relied on a rainy season recharge. This can be interpreted as a less mobile water source for native evergreen trees, when compared to *E. nitens* stands. Even though results from this study are conclusive for the two water worlds hypothesis, further research is needed in order to understand these occasional ecohydrological connectivities/discontinuities.

11.2.4 What is the importance of water evaporation from soils for the water budget of catchments with different land cover?

Soil evaporation at catchment level was estimated using unweighted $\delta^{18}O$ water signatures from stream and precipitation inputs. Results from the present study show that catchments with old-growth native evergreen forest and *E. nitens* land cover display a similar proportion of water inputs lost through evaporation. Total precipitation input lost through soil evaporation was 10.8 ± 0.6% and 8.4 ± 1.2% for NF and EP sites, respectively. These results show that water losses through soil evaporation are playing a minor role compared to that of transpiration and canopy interception. However, the latter is affected by stand age, hence soil water losses through evaporation could be playing a major role in early stages of forest or plantations. Even though in our study, hydrological data from catchments is missing, these values should be considered as an approximation and not as “true” soil evaporation. Further studies

should be conducted using flux weighted $\delta^{18}O$ signatures from stream and precipitation inputs and compared with other methodologies (i.e. modelling, scintillation, etc…). It is suggested that the Rayleigh method for the estimation soil evaporation could be useful for comparison with other studies that estimate evaporation using different methodologies.

11.3 General conclusion and final remarks

The main question and driver of this thesis was to try to understand how vegetation and stream water are connected. In chapter 2, it is shown that land cover changes affect nutrient inputs and hence affect the nutrient fluxes reaching the catchment soil. Stream water chemistry showed that only NO_3^--N is the main difference between native evergreen forest and *Eucalyptus globulus* land covered catchments. It was hypothesized that in native evergreen covered catchments, soil microorganisms or soil particles retained NO_3^--N. However, in this study it is not possible to assure that soil microorganisms retained NO_3^--N. In chapter 4, it is shown that the NO_3^--N source is in the smaller pores in soil. This was evidenced by NO_3^--N dilution during storm events. The opposite behavior was observed for TP and Org-N, where the first is known to be attached to soil particles, while it was hypothesized that the second is found within larger pores. So far, this study has not been able to show hydrological or ecohydrological connectivity, which is clearly described in chapter 9. In it, stable isotope signatures clearly showed that ecohydrological and hydrological connectivity occur sporadically throughout the year, and only after more than 100 mm of accumulated rainfall in the previous 14 days. It also shown that sporadically *Euclayptus nitens* shared a common source of water with that of the stream. This connectivity was also observed in native trees. In addition, native trees withdrew water that revealed beingmore evaporated (highly attached to soil particles) than that of *E. nitens* which withdrew less static water. The separation between mobile and less mobile water is also influencing biogeochemical conceptualization where recent work suggests “two nitrate worlds” (Hall *et al.*, 2016), where denitrification inside soil aggregates (where anaerobic microsites dominate) and transport of nitrogen in soil suction lysimeter water (reflecting aerobic macropore water) (Zhang *et al.*, 2017). All this information leaves us with even more questions than answers.

All these processes (nutrient uptake and tree water use) are obviously linked somehow in the transpiration and photosynthetic process. As such, the measurement of transpiration is a titanic challenge. In chapter 9, an estimation of soil evaporation showed surprising results, displaying no differences in the proportion of water lost through soil evaporation under both studied land covers. Hence, observed differences found on catchment water balance are due to not only the magnitude of tree transpiration; then, the study and understanding on how vegetation uses different water sources. Although there are several methods for the estimation of evaporation from soils (scintillation, modelling, mass balance, etc…), none of them are properly (i.e. really) mass calibrated, despite what experts of their own areas might say! During this time, I have only found two publications comparing hydrological modelling and/or scintillation and/or mass balance methods (Williams *et al.*, 2004; Sutanto *et al.*, 2012). This is, in my opinion, is the next step in measuring hydro and ecohydrological linkages.

11.4 Future perspectives

Although this study has shown, the effects of land cover changes on nutrient inputs and exports. This study does not include other important biogeochemical processes, like N fixation or emissions. This, in my opinion, leaves plenty of room for improvement, and future research topics should focus on the understanding of biogeochemical processes linked to hydrological processes. Each one independently are important, but do not provide an explanation of how the biogeochemical cycles are really affected by changes in hydrological processes.

The initial intention at the start of this project was to describe hydrological pathways and processes, and relate them to nutrient exportation and tree water sources. However, working with storm events was not feasible from a financial point of view. Carefull planning, good logistics and instruments (i.e. loggers, tipping buckets, computers) are very important in this or any study. Future studies related to hydrological pathways should be addressed with all the above mentioned suggestions in mind. This will give a good and reliable base on which future research could be conducted in a more effective and efficient manner.

Frequent sampling in defined catchments is also very important to improve the work/results effort. Most of the studies in the area (or those where I have actively participated) have been made in different catchments. This, I think, is a huge drawback, since all equipment has to be taken from one place and to be installed or built, calibrated at another place. This takes a lot of time, effort and economic expenditure, which can be used for other analyses or invested in other material, implementing a good and reliable monitoring network such as meteorological stations, pluviometers, laboratory equipment. Recently, the NF study site became part of the Long Term Ecological Research (LTER) sites in Chile. This has a great potential for future research comparisons among other LTER sites in Chile and the world.

A good idea is to estimate the components of the catchment water balance, especially those of evapotranspiration, which indeed could be used to couple the hydrological cycle with nutrient cycle. This has been tried in the past, with several degrees of success for the estimation of carbon allocation at catchment scale. However, in this study the lack of hydrometric data resulted in the estimation of the proportion of water lost on both studied sites. Obtained results, however, prove that it is possible to estimate evaporation losses from soils. Although the comparison of old-growth native evergreen forest and *Eucalyptus nitens* plantation covered catchments gave similar values, these values should be considered just as a reference and not as the exact amount of soil evaporation losses.

In this thesis, it has been shown that the two water worlds hypothesis does not holds true, as previously hypothesized by McDonnell (2014). More interesting, it also showed that most of the time (i.e. sampling campaigns), sampled trees are disconnected from the mobile water compartment. This, of course, contradicts some well established hydrological, biogeochemical and plant physiological sciences. Furthermore, it suggests that either there is still lacking a complete picture. So far, it has not been tested wether ecohydrological connectivity/separation is just an artefact of sampling or extraction methodologies or simply some stable isotope hidden processes that is not fully understood. However, hydrological separation between hillslopes and catchment discharge has been described in other studies (Ocampo *et al.*, 2006; McGuire and McDonnell, 2010; Birkel *et al.*, 2014; van Meerveld *et al.*,

2015). It is my personal opinion, that even though there are still problems with cryogenic extraction protocols, there is some knowledge on stable isotope behavior during evaporation and other processes, although there is plenty of room for improvement. Current knowledge of the behavior of water in soils is still poor. Another caveat of this and other works related to water stable isotopes in vegetation is the flux or amount-wieghted isotopic signatures, although a first intention to weight xylem isotopic signatures by flux was made by Evaristo *et al.* (2015). This is also a key issue in order to have the weighted isotopic signatures and try closing the hydrological cycle as done by Jasechko *et al.* (2013), using water vapor coming from lakes around the world; or Good *et al.* (2015) using water vapor from spectrometric satellite data. In this sense, the use of stable isotope analysis provide an efficient way to calibrate and test hydrological models.

Recently, Hall *et al.* (2016) showed in a completely independent study indications of two nitrate worlds in soils. These were evidenced by differences in nitrate dual $\delta^{15}N$ and $\delta^{18}O$ isotopic signatures in microsites or anaerobic sites and in big pores or aerobic sites. Zhang *et al.* (2016), using tritium (^{3}H), described recently that apples from apple trees were 50 years old. Zhang *et al.* (2016) suggested that water, was either retained or in a *very* slow moving, almost static water compartment in soil. Recently, Berry *et al*. (2017) published a review on the two water worlds, which showed that there are more points in common than against it. However, it is my personal opinion that this experiments or sampling campaigns should be using several tracers and indicators, and not just one as they do now. Multitracer experiments along a multidisciplinary team of researchers are needed in order to clarify, or at least illuminate, a bit the missing pieces of the hydro-bio/eco-geochemical connection puzzle.

Without a doubt, something strange going on. The two water worlds hypothesis should be tested thoroughly in the most meticulous and multidisciplinary way under different conditions and environments.

Appendix A : Enrichment under equilibrium conditions

Eq. (5.19) is true only if $\delta_v << 1000$. Therefore, for the observed enrichment during condensation we have that:

$$\varepsilon^{+}_{w\text{-}v} = (\alpha^{+}_{w\text{-}v} - 1)\cdot 1000 = \left(\frac{R_w}{R_v} - 1\right)\cdot 1000 \tag{A.1}$$

Hence,

$$\varepsilon^{+}_{w\text{-}v} = \left(\frac{R_w - R_v}{R_v}\right)\cdot 1000 = \frac{\left(\frac{R_w}{R_{VSMOW}} - \frac{R_v}{R_{VSMOW}}\right)}{\frac{R_v}{R_{VSMOW}}}\cdot 1000 \tag{A.2}$$

Applying a mathematical null-operation by adding $+1-1$ in both numerator and denominator, and multiplying by $\frac{1000}{1000}$, results in:

$$\varepsilon^{+}_{w\text{-}v} = \frac{\left(\frac{R_w}{R_{VSMOW}} - 1\right)\cdot 1000 - \left(\frac{R_v}{R_{VSMOW}} - 1\right)\cdot 1000}{\frac{R_v}{R_{VSMOW}} - 1 + 1}\cdot\frac{1000}{1000} \tag{A.3}$$

Hence,

$$\varepsilon^{+}_{w\text{-}v} = \frac{\left[\left(\frac{R_w}{R_{VSMOW}} - 1\right)\cdot 1000 - \left(\frac{R_v}{R_{VSMOW}} - 1\right)\cdot 1000\right]\cdot 1000}{1000\cdot\left(\frac{R_v}{R_{VSMOW}} - 1\right) + 1000} = \frac{(\delta_w - \delta_v)\cdot 1000}{\delta_v + 1000} \tag{A.4}$$

If the assumption that water vapor amount is minimal (i.e. $\delta_v << 1000$), then Eq. (A.4) in the text, reduces to the familiarly known

$$\varepsilon^{+}_{w\text{-}v} = \frac{(\delta_w - \delta_v)\cdot 1000}{\delta_v + 1000} \approx \delta_w - \delta_v \tag{A.5}$$

In case δ_v is not much smaller than 1000, the $\varepsilon^+_{w\text{-}v}$ needs to be re-evaluated. In order to proof Eq. (A.5) or Eq. (5.19), we will use our previous example on the condensation of water vapor into liquid water. However, we will show the calculation step by step, just to improve understanding and leave no place to doubts or hesitation. Hence, if we already know that: $\delta^{18}O_w = 0‰$; $\varepsilon^+_{w\text{-}v} = 9{,}3‰$, then how can we obtain δ_v ?, therefore using Eq. (A.5) or Eq. (5.19), replacing our known values, leads to:

$$9.3 = \frac{(0 - \delta_v)\cdot 1000}{\delta_v + 1000} \tag{A.6}$$

$$\rightarrow 9.3\cdot(\delta_v + 1000) = -\delta_v \cdot 1000 \tag{A.7}$$

$$\rightarrow 9.3\cdot\delta_v + 9300 = -1000\cdot\delta_v \tag{A.8}$$

$$\rightarrow 1009.3\cdot\delta_v = -9300 \tag{A.9}$$

$$\delta_v = \frac{-9300}{1009.3} = -9.214‰ \tag{A.10}$$

This result is 0.086‰ smaller than the expected $\varepsilon^+_{w\text{-}v}$ of 9.3‰ when following the assumption that amount of water vapor is minimal, compared to that of liquid water. If we calculate δ_w from a known $\delta_v = 0‰$ at 25° C (i.e. $\varepsilon^+_{w\text{-}v} = 9{,}3‰$). Hence, Eq (A.5) is adjusted to:

$$\varepsilon^+_{v\text{-}w} = \frac{(\delta_w - \delta_v)\cdot 1000}{\delta_w + 1000} \tag{A.12}$$

Replacing the values, leads to:

$$9.3 = \frac{(\delta_w - 0)\cdot 1000}{\delta_w + 1000} \tag{A.13}$$

$$\rightarrow 9.3\cdot(\delta_w + 1000) = 1000\cdot\delta_w \tag{A.14}$$

$$\rightarrow 9.3\cdot\delta_w + 9300 = 1000\cdot\delta_w \tag{A.15}$$

$$\rightarrow 9300 = 1000\cdot\delta_w - 9.3\cdot\delta_w \tag{A.16}$$

$$\delta_w = \frac{9300}{990.7} = 9.387‰ \tag{A.17}$$

Not surprisingly, the value is 0.087‰ higher than the expected enrichment at 25° C (i.e. $\varepsilon^{+}_{w\text{-}v} = 9.3‰$). Please, note that the enrichment for condensation (i.e. $\varepsilon^{+}_{w\text{-}v}$, in Eq.(5.17)) and evaporation (i.e. $\varepsilon^{*}_{v\text{-}w}$, in Eq. (5.18)) are related as follows:

$$\varepsilon^{+}_{w\text{-}v} = (\alpha^{+}_{w\text{-}v} - 1)\cdot 1000 \tag{A.18}$$

$$\varepsilon^{*}_{v\text{-}w} = \left(\frac{1}{\alpha^{+}_{w\text{-}v}} - 1\right)\cdot 1000 = \frac{\alpha^{+}_{w\text{-}v} - 1}{\alpha^{+}_{w\text{-}v}}\cdot 1000 = \frac{\varepsilon^{+}_{w\text{-}v}}{\alpha^{+}_{w\text{-}v}}\cdot 1000 \tag{A.19}$$

$$\varepsilon^{*}_{v\text{-}w} = \frac{\varepsilon^{+}_{w\text{-}v}}{\alpha^{+}_{w\text{-}v}} = \frac{\varepsilon^{+}_{w\text{-}v}}{\frac{R_w}{R_v}} \tag{A.20}$$

Reworking the denominator of Eq. (A.20), adding +1-1 in both, numerator and denominator and multiplying both by 1000 leads to:

$$\frac{R_w}{R_v} = \frac{1000\cdot\left(\frac{R_w}{R_{VSMOW}}\right) - 1000 + 1000}{1000\cdot\left(\frac{R_v}{R_{VSMOW}}\right) - 1000 + 1000} = \frac{\delta_w + 1000}{\delta_v + 1000} \tag{A.21}$$

Hence, replacing Eq. (A.21) in Eq. (A.20) we get the following:

$$\varepsilon^{*}_{v\text{-}w} = \frac{\varepsilon^{+}_{w\text{-}v}}{\frac{\delta_w + 1000}{\delta_v + 1000}} = \varepsilon^{+}_{w\text{-}v}\cdot\frac{\delta_v + 1000}{\delta_w + 1000} = \varepsilon^{+}_{w\text{-}v}\cdot\alpha^{+}_{w\text{-}v} \tag{A.22}$$

written alternatively, Eq. (A.22) reads as:

$$\varepsilon^{*}_{v\text{-}w} \cdot (\delta_w + 1000) = \varepsilon^{+}_{w\text{-}v} \cdot (\delta_v + 1000) \quad \text{(A.23)}$$

or

$$\frac{\varepsilon^{*}_{v\text{-}w}}{\alpha^{+}_{v\text{-}w}} = \varepsilon^{+}_{w\text{-}v} \quad \text{(A.24)}$$

Eq. (A.24) proofs that both enrichments are not the same number, and that enrichment for evaporation needs a correction by the corresponding fractionation factor, that is under the assumption of δ_v is minimal. The linear distance on the $\delta^{18}O/\delta^{2}H$ space separating liquid water from water vapor, or *vice versa* will be very similar, probably within the errors given by the mass spectrometer used for the measuremen of water and vapor samples.

Using Eq. (A.23), we can calculate the isotopic signatures of either δ_w or δ_v, knowing the enrichment, hence fractionation under the assumption that both δ_w or δ_v are not minimal.

Appendix B : Derivation of Kinetic fractionation factor (α_K)

Kinetic fractionation (or α_K) under a dry atmosphere, hence under non-equilibirum conditions can be calculated using Eq. (5.20), which is derived from the known ideal gas law equation is given by ():

$$P \cdot V = n \cdot R \cdot T \tag{B.1}$$

Where P stands for pressure and V for volume. While n, R and T stand for number of moles, gas constant and temperature. The gas pressure calculated for the kinetic theory for an ideal gas:

$$P \cdot V = \frac{2N}{3} \cdot \left(\frac{1}{2} \cdot m \cdot \bar{v}^2 \right) \tag{B.2}$$

Where N, m and $\bar{v}$ stand for number of gas molecules, molecular weight and average velocity of a gas molecule. Using the right side of Eq. (B.1), Eq. (B.2) is re-written as:

$$n \cdot R \cdot T = \frac{2N}{3} \cdot \left(\frac{1}{2} \cdot m \cdot \bar{v}^2 \right) \tag{B.3}$$

hence,

$$n \cdot R \cdot T = \frac{N}{3} \cdot \left(m \cdot \bar{v}^2 \right) \tag{B.4}$$

Therefore,

$$\bar{v}^2 = \frac{3 \cdot n \cdot R \cdot T}{N \cdot m} \tag{B.5}$$

Where N/n is the Avogadro number ($N_A = 6.022 \cdot 10^{23}$)

$$\bar{v}^2 = \frac{3 \cdot R}{N_A} \cdot \frac{T}{m} \tag{B.6}$$

And $R/N_A = k$, which is the Boltzmann constant (i.e. $1.3806504 \cdot 10^{-23}$ $J \cdot K^{-1}$),

$$\bar{v}^2 = 3 \cdot k \cdot \frac{T}{m} \tag{B.7}$$

or

$$\bar{v} = \sqrt{3 \cdot k \cdot \frac{T}{m}} \tag{B.8}$$

hence,

$$\alpha_K = \alpha_{\text{diffusion in atmosphere}} = \frac{\bar{v}_i}{\bar{v}} = \frac{\sqrt{\frac{3 \cdot k \cdot T}{(m_i)}}}{\sqrt{\frac{3 \cdot k \cdot T}{m}}} = \sqrt{\frac{m}{m_i}} \tag{B.9}$$

Appendix C : Derivation of kinetic enrichment (Δε) during under variable atmospheric moisture conditions

During evaporation, water stable isotopes enrich. This is mostly due to diffusion of heavy isotopes in the atmosphere. Having this in mind, Craig and Gordon (1965) introduced an enrichment (i.e. Δε) that varies not only with atmospheric moisture content, but also with height and turbulence. The enrichment under variable atmospheric moisture conditions for non-equilibrium systems is derivated as follows (Gat, 1996):

$$\Delta\varepsilon = (1 - h)\cdot\left(\frac{\rho_i}{\rho} - 1\right) \quad \text{(C.1)}$$

Where h stands for the relative humidity normalized to the evaporation surface temperature. The second term on the right side of Eq. (C.1) can be worked out as follows (Craig and Gordon, 1965; Gat *et al.*, 1981; Gonfiantini, 1986; Gat, 1996):

$$\left(\frac{\rho_i}{\rho}\right) = \left(\frac{\rho_{i,M}+\rho_{i,T}}{\rho_M+\rho_T}\right) = \left(\frac{\rho_M}{\rho}\right)\cdot\left(\frac{\rho_{i,M}}{\rho_M}\right) + \left(\frac{\rho_T}{\rho}\right)\cdot\left(\frac{\rho_{i,T}}{\rho_T}\right) \quad \text{(C.2)}$$

Where ρ and ρ_i respectively stand for the resistances for the common and rare isotopologues; and subscripts M and T stand for the laminar, turbulent resistances. This model, however, has the following assumptions (Craig and Gordon, 1965; Gat, 1996):

- The interface layer above the water-air interface is saturated (i.e. RH = 100%) with respect to the surface water.

- Overall mass-transfer and associated isotope effects at the water-air interface region are dominated by molecular diffusion as follows:

$$\frac{\rho_{i,M}}{\rho_M} > 1 \qquad \text{(C.3)}$$

- To a large extent the turbulent region does not fractionate isotopic species, this is:

$$\frac{\rho_{i,T}}{\rho_T} \cong 1 \qquad \text{(C.4)}$$

Where the subscript ρ_L stands for liquid resistance (see Figure 4.5). Hence, making use of Eq. (C.2):

$$\left(\frac{\rho_i}{\rho} - 1\right) = \frac{\rho_{i,M}}{\rho} + \frac{\rho_{i,T}}{\rho} - 1 \qquad \text{(C.5)}$$

$$\left(\frac{\rho_i}{\rho} - 1\right) = \left(\frac{\rho_{i,M}}{\rho_M} \cdot \frac{\rho_M}{\rho}\right) + \left(\frac{\rho_{i,T}}{\rho_T} \cdot \frac{\rho_T}{\rho}\right) - \frac{\rho_M + \rho_T}{\rho} \qquad \text{(C.6)}$$

$$\left(\frac{\rho_i}{\rho} - 1\right) = \left[\left(\frac{\rho_M}{\rho}\right) \cdot \left(\frac{\rho_{i,M}}{\rho_M} - 1\right)\right] + \left[\left(\frac{\rho_T}{\rho}\right) \cdot \left(\frac{\rho_{i,T}}{\rho_T} - 1\right)\right] \qquad \text{(C.7)}$$

And after following the above mentioned assumptions, Eq. (C.7) yields:

$$\left(\frac{\rho_i}{\rho} - 1\right) = \left[\left(\frac{\rho_M}{\rho}\right) \cdot \left(\frac{\rho_{i,M}}{\rho_M} - 1\right)\right] \qquad \text{(C.8)}$$

In case of a fully developed diffusion layer, $\rho_M = D^{-1}$, where D is the molecular diffusivity of water in air. Similar, for the rare isotope specie $\rho_{M,i} = D_i^{-1}$. In natural conditions however is not fully developed, causing:

$$\rho_M = D^{-n} \qquad \text{(C.9)}$$

and

$$\rho_{M,i} = D_i^{-n} \quad \text{(C.10)}$$

where n stands for the turbulent resistance parameter, which varies from $0.5 < n < 1$, where n = 0.5 corresponds to highly turbulent conditions and n = 1 for static conditions (see appendix D), where only diffusion occurs (Stewart, 1975; Luz *et al.*, 2009). Using Eqs. (C.9) and (C.10) in Eq. (C.8), and since diffusion flux in the laminar layer is largely proportional to (Gat, 2005):

$$\left(\frac{\rho_{i,M}}{\rho_M} - 1\right) = \alpha_K^{\,n} \quad \text{(C.11)}$$

where α_K is the diffusion coefficient of isotopic water species in air (same as Eq. (5.20), derived on Appendix B, and Eq. (5.21). After all these transformations, Eq. (C.1) can be rewritten as:

$$\Delta\varepsilon = (1-h)\cdot\left[\frac{\rho_{i,M}}{\rho}\cdot\left(\left(\frac{D_i}{D}\right)^n - 1\right)\right] \quad \text{(C.12)}$$

However, if

$$\frac{\rho_{i,M}}{\rho} = \theta = \frac{(1-h')}{(1-h)} \quad \text{(C.13)}$$

Where, θ is the ratio of the transport resistance in the molecular diffusion layer to the overall resistance (Gat *et al.*, 1994). In principle, this factor can be evaluated by comparing the upwind water content of the airmasses (expressed in terms of a humidity normalized with respect to the saturated vapor at the temperature of the evaporating surface (h) and that of air above the evaporating surface (h') (see Figure 5.3) Then,

$$\Delta\varepsilon = (1-h)\cdot\theta\cdot\left(\left(\frac{D_i}{D}\right)^n - 1\right) \quad \text{(C.14)}$$

In general, θ is assumed to be 1 (Gat, 1996; Horita *et al.*, 2008), suggesting that h and h' (in Eq. (C.13)) are equal. However, if

$$C_K = \left(\left(\frac{D_i}{D} \right)^n - 1 \right) \tag{C.15}$$

Then,

$$\Delta\varepsilon = (1 - h) \cdot \theta \cdot C_K \tag{C.16}$$

In the case of a fully developed diffusion layer (stagnant layer), $\rho_{i,M}$ is also proportional to α_K^{-1}, where α_K, is the molecular diffusivity of water in air (Eqs. (5.21) and (C.12)) (Gat, 1996). Under strong turbulent wind conditions and a rough water surface, the transient-eddy model of Brutsaert (1965) can be applied where ρ_M is proportional to $\sqrt{1/\alpha_K}$, as suggested by Eriksson, (1965). For moderate interface conditions (i.e. moderate wind speeds) a transition from the proportionality of $\sqrt[3]{1/\alpha_K^2}$ to $\sqrt{1/\alpha_K}$ can be expected (Gat, 1996). Defining the ratio of the molecular diffusivities of the heavy and light water molecules, respectively, as C_K then, the expression for $\Delta\varepsilon$ is re written in the form of (Craig and Gordon, 1965):

$$\Delta\varepsilon = (1 - h) \cdot \theta \cdot n \cdot C_K \tag{C.17}$$

Appendix D : Turbulence resistance parameter n

The turbulent resistance parameter n is generally assumed as either 1 or 0.5 as mentioned in the text and in appendix C. However, we know that evaporation occurs under several intermediate conditions. Here, we show another way to estimate the turbulent resistance parameter n in soils with variable soil moisture content.The exponent n in Eq. (D.1) (also known as nk, Stewart, 1975; Mathieu and Bariac, 1996; Dubbert *et al.*, 2014), which relates soil water content (β) to the contribution of turbulent resistance to total transport resistances in an unsaturated soil:

$$\alpha_K = \left(\frac{D}{D_i}\right)^n \tag{D.1}$$

The exponent n can be empirically estimated as:

$$n = \frac{(\beta_{SURF} - \beta_R)\cdot n_A + (\beta_{SAT} - \beta_{SURF})\cdot n_S}{(\beta_{SAT} - \beta_R)} \tag{D.2}$$

Where β_{SURF}, β_{SAT} and β_R stands for surface, saturated and residual volumetric soil water content, respectively. While, n_A (= 0.5) and n_S (= 1) are related to water vapor diffusivities in the atmosphere and soil, respectively.

Appendix E : The Rayleigh model

The Rayleigh model is simple and useful to characterise evaporation and condensation under closed and open equilibiurm conditions. It has been used not only with water stable isotopes but also with nitrogen, carbon and sulphur isotopes. Its derivation is easy to follow and the outcomes are easy to understand.

If material is removed from a mixed system containing I_i and I molecules of a rare and abundant isotopic species, respectively. The isotope ratio is:

$$R_w = \frac{I_i}{I} \tag{E.1}$$

Where R_w stands for water isotope ratio. Then, the isotope ratio of the removed product is at a certain instant,

$$R_E = \frac{dI_i}{dI} \tag{E.2}$$

Where R_E stands for the isotope ratio of the evaporate, considering equilibrium conditions with the fractionation accompanying the removal process at any instance is described by the unit fractionation factor $\alpha^{+}_{w\text{-}v}$,

$$\frac{\left(\frac{dI_i}{dI}\right)}{\left(\frac{I_i}{I}\right)} = \alpha^{+}_{w\text{-}v} \tag{E.3}$$

Then the evolution of the isotopic composition in the remaining material is described by the following equations, assuming $I \gg I_i$, where $I + I_i \approx I$, which holds for the natural isotope abundance of light element isotopes (e.g. H and O; Gat, 1996):

$$\frac{dR_w}{dI} = \frac{d\left(\frac{I_i}{I}\right)}{dI} = \frac{1}{I} \cdot \left(\frac{dI_i}{dI} - \frac{I_i}{I}\right) = \frac{R_w}{I}(\alpha^+_{w\text{-}v} - 1) \quad \text{(E.4)}$$

And thus:

$$\frac{dR_w}{R_w} = \frac{dI}{I} \cdot (\alpha^+_{w\text{-}v} - 1) \quad \text{(E.5)}$$

or

$$\frac{d(\ln R_w)}{d(\ln I)} = (\alpha^+_{w\text{-}v} - 1) \quad \text{(E.6)}$$

Eq. (E.4) can be immediately integrated from an initial condition ($R_{W,0}$, I_0) to any given stage, for a constant $\alpha^+_{w\text{-}v}$ value, as follows (Salati *et al.*, 1979):

$$\int_{R_{v,0}}^{R_v} d(\ln R_v) = (\alpha^+_{w\text{-}v} - 1) \cdot \int_{I_0}^{I} d(\ln I) \quad \text{(E.7)}$$

$$\ln\left(\frac{R_v}{R_{v,0}}\right) = (\alpha^+_{w\text{-}v} - 1) \cdot \ln\left(\frac{I}{I_0}\right) \quad \text{(E.8)}$$

$$\frac{R_v}{R_{v,0}} = \left(\frac{I}{I_0}\right)^{(\alpha^+_{w\text{-}v}-1)} \quad \text{(E.9)}$$

Now, if

$$\frac{I+I_i}{I_0+I_{i,0}} \approx \frac{I}{I_0} = f \quad \text{(E.10)}$$

where, f is the fraction of the material remaining in the system after part of it has been removed (where I_0, is the number of molecules at the beginning of the process). Hence, replacing Eq. (E.10) on Eq. (E.9), becomes:

$$R_v = R_{v,0} \cdot f^{(\alpha^{+}_{w\text{-}v}-1)} \tag{E.11}$$

where R_v is the isotope ratio of the reactant reservoir, which in this case is water vapor (v) at any given time t after some reaction (i.e. condensation) to some residual fraction; $f = I/I_0$. $R_{v,0}$ is the initial isotopic ratio of the reactant reservoir when $f = 1$, and $\alpha^{+}_{w\text{-}v}$ is the fractionation factor for the reaction, in this case condensation, at a given temperature (Gat, 2005). Please note that $\alpha^{+}_{w\text{-}v}$ was used, hence we are mathematically describing the condensation, and not the evaporation process. In order to describe the evaporation process, the fractionation factor needs to be adjusted from $\alpha^{+}_{w\text{-}v}$ to $1/\alpha^{+}_{w\text{-}v}$ also found as $\alpha^{*}_{v\text{-}w}$ in literature (Craig and Gordon, 1965; Gibson and Edwards, 2002).

For the condensation process, the relationship between the isotopic ratio of the initial vapor, R_{vi} and the instantaneous isotopic ratio of the remaining vapor, R_{vr} is given by the following:

$$\frac{R_{vr}}{R_{vi}} = f_{vr}^{(\alpha^{+}_{w\text{-}v}-1)} \tag{E.12}$$

where f_{vr}, is the fraction of the residual vapor. However, for water, the distillation process, hence, evaporation, and the isotopic ratios of initial water and remaining water are given by:

$$\frac{R_{wr}}{R_{wi}} = f_{wr}^{\left(\frac{1}{\alpha^{+}_{v\text{-}w}}-1\right)} \tag{E.13}$$

where f_{wr} is the fraction of the remaining water, while the subscripts wr and wi, stand for remaining and initial water, respectively. Please, note that $\alpha^{+}_{w\text{-}v}$, used in Eq. (E.12) (i.e. condensation) changed to $1/\alpha^{+}_{v\text{-}w}$ in Eq. (E.13) (i.e. evaporation), this is simply because we are referring to evaporation, and not condensation. Using the δ-values as shown in Eq. (5.3), Eq. (E.13) is rewritten as follows:

$$\frac{(\delta_{wr}+1000)}{(\delta_{wi}+1000)} = f_{wr}^{\left(\frac{1}{\alpha^{+}_{v\text{-}w}}-1\right)} \tag{E.14}$$

Rewriting in natural logarithmic from, Eq. E.14 becomes:

$$\ln\left(\frac{\delta_{wr}}{1000}+1\right) - \ln\left(\frac{\delta_{wi}}{1000}+1\right) = \left(\frac{1}{\alpha^{+}_{v\text{-}w}} - 1\right)\cdot \ln f_{wr} \tag{E.15}$$

A mathematical approximation, based on a McLaurin expansion (Criss, 1999):

$$\ln(x + 1) \cong x \qquad (x \ll 1) \tag{E.16}$$

allows to reduce Eq. (E.15) to:

$$\delta_{wr} - \delta_{wi} = 1000\cdot\left(\frac{1}{\alpha^{+}_{v\text{-}w}} - 1\right)\cdot \ln f_{wr} \tag{E.17}$$

or

$$\delta_{wr} - \delta_{wi} = \varepsilon^{*}_{v\text{-}w}\cdot \ln f_{wr} \tag{E.18}$$

Eqs. (E.17) and (E.18) can be used for the estimation of evaporation from a given water reservoir.

Appendix F : Craig and Gordon model for well mixed water reservoirs

The Craig and Gordon model is used to calculate isotopic signature of the net water flux across the molecular diffusion layer, corresponding to the evaporation flux "E", coming from a well-mixed water reservoir. This is proportional to the vapor concentration difference at the boundaries (Craig and Gordon, 1965; Gonfiantini, 1986):

$$E = -\frac{dN}{dt} = \frac{(C_S - C_A)}{\rho} = \frac{C_S \cdot (1-h)}{\rho} = \frac{C_S \cdot (1-h)}{\rho_M + \rho_T} \quad \text{(F.1)}$$

where ρ is the atmospheric resistance coefficient, which is compounded of laminar, turbulent and water resistances (ρ_M, ρ_T and ρ_L, respectively; see Figure 4.5). For the common and rare isotope specie the following nomenclature is used instead, e.g. ρ_M and $\rho_{M,i}$, for the common and rare isotope specie, respectively. C_S is the saturation concentration of vapor at the water-atmosphere interface, C_A is the vapor concentration in the turbulent atmospheric region, and

$$h = \frac{C_A}{C_S} \quad \text{(F.2)}$$

where h is the relative humidity of the latter normalized to the evaporating surface temperature, i.e. $0 \le h \le 1$. For the rare isotope specie ^{2}H or ^{18}O (denoted by the subscript i) the evaporation flux is given by:

$$E_i = -\frac{dN_i}{dt} = \frac{(C_S \cdot R_S - C_A \cdot R_A)}{\rho_i} = \frac{C_S \cdot \left(\frac{R_S}{\alpha^+_{v\text{-}w}} - h \cdot R_A\right)}{\rho_i} = \frac{C_S \cdot \left(\frac{R_S}{\alpha^+_{v\text{-}w}} - h \cdot R_A\right)}{\rho_{i,M} + \rho_{i,T}} \quad \text{(F.3)}$$

where $\alpha^+_{v\text{-}w}$, stands for the equilibrium fractionation factor; R_S and R_A correspond to the isotope ratios of the evaporating water mixed in the water surface and atmospheric vapor at the boundary layer, respectively. It should be noted that R_S sometimes is found as R_L which corresponds to the isotopic ratio of the whole water column, only if this is well mixed (Craig and Gordon, 1965; Gonfiantini, 1986; Lerman *et al.*, 1995). In

Eq. (F.3), water surface and water column isotope ratios are assumed to be well-mixed (i.e. $R_S = R_L$). Eqs. (F.1) and (F.3) give the net removal rates of $^1H_2{}^{16}O$ and their heavy isotopologues (i.e. $^1H^2H^{16}O$ and $^1H_2{}^{18}O$, respectively) from water, in terms of the transport resistances and the humidity and isotopic composition of the "free air" layer (Craig and Gordon, 1965).

Let us consider a completely mixed evaporating water body ($R_S = R_L$) with no inflow or outflow (Gonfiantini, 1986). In this case,

$$E = -\frac{dI}{dt} = \frac{C_S \cdot (1-h)}{\rho_M + \rho_T} \tag{F.4}$$

Therefore,

$$R_E = -\frac{dI_i}{dt} = \frac{C_S \cdot \left(\frac{R_S}{\alpha^+_{v\text{-}w}} - h \cdot R_A\right)}{\rho_{i,M} + \rho_{i,T}} \tag{F.5}$$

where I and I_i are the common and rare isotope specie present in water (i.e. the liquid phase); and R_E is the isotope ratio of the evaporation flux. Dividing Eq. (F.3) by Eq.(F.1), results in:

$$R_E = \frac{dI_i}{dI} = \frac{\left(\frac{R_S}{\alpha^+_{v\text{-}w}}\right) - (h \cdot R_A)}{(1-h) \cdot \left(\frac{\rho_i}{\rho}\right)} = \frac{\frac{R_S}{\alpha^+_{v\text{-}w}} - h \cdot R_A}{(1-h) \cdot \frac{\rho_{i,M} + \rho_{i,T}}{\rho_M + \rho_T}} \tag{F.6}$$

However, if

$$\frac{\rho_M + \rho_T}{\rho_{i,M} + \rho_{i,T}} = \frac{\rho}{\rho_i} = \alpha_K \tag{F.8}$$

Eq. (F.6), leads to:

$$E_i = \alpha_K \cdot \frac{\frac{R_S}{\alpha^+_{v\text{-}w}} - h \cdot R_A}{(1-h)} \quad \text{(F.9)}$$

where α_K stands for the kinetic fractionation. Re-writing Eq. (F.6) in δ-notation, we obtain:

$$1+\delta_E = \frac{\frac{(1+\delta_S)}{\alpha^+_{v\text{-}w}} - h \cdot (1+\delta_A)}{(1-h) \cdot \left(\frac{\rho_{i,M}+\rho_{i,T}}{\rho_M+\rho_T}\right)} \quad \text{(F.10)}$$

where, δ_S stands for surface isotopic signature and α^+_{v-w}, is the equilibrium fractionation factor. δ_A, corresponds to the atmospheric water isotopic signature, calculated as follows (Gat and Tzur, 1966; Gibson *et al.*, 2008):

$$\delta_A = \frac{\delta_P - \varepsilon^*_{v\text{-}w}}{\alpha^+_{v\text{-}w}} \quad \text{(F.11)}$$

where δ_P is the isotopic signature of precipitation. Introducing the enrichment factor for variable atmospheric water conditions, Δε, in Eq. (C.17), from appendix C. Δε is used for correcting isotopic enrichment occurring during evaporation under non-equilibrium conditions by the changes in h (Lerman *et al.*, 1995).

Rearranging Eq. (F.10) and introducing Δε from Eq. (C.17) from appendix C, we get:

$$\delta_E = \frac{\frac{\delta_S}{\alpha^+_{v\text{-}w}} - (h \cdot \delta_A)}{(1-h) \cdot \left(1+\frac{\Delta\varepsilon}{(1-h)}\right)} \quad \text{(F.12)}$$

Rearranging Eq. (F.9), and knowing that,

$$\varepsilon^{*}_{v\text{-}w} = \left(\frac{1}{\alpha^{+}_{v\text{-}w}} - 1\right)\cdot 1000 \qquad \text{(F.13)}$$

Then, Eq. (F.12) is substituted in Eq. (F.10) yielding:

$$\delta_E = \frac{\frac{\delta_S - \varepsilon^{*}_{v\text{-}w}}{\alpha^{+}_{v\text{-}w}} - (h\cdot\delta_A) + \Delta\varepsilon}{(1-h)\cdot\left(1+\frac{\Delta\varepsilon}{(1-h)}\right)} \qquad \text{(F.14)}$$

Note that Eqs. (F.8), (5.20) and (5.21) in chapter 4, are for calculating the kinetic fractionation of diffusion on air α_K.

Then, rearranging Eq. (F.14) by Eq. (F.13), leads to the known Craig and Gordon model (Craig and Gordon, 1965; Gonfiantini, 1986);

$$\delta_E = \frac{\frac{\left(\delta_S - \varepsilon^{*}_{v\text{-}w}\right)}{\alpha^{+}_{v\text{-}w}} - (h\cdot\delta_A) - \Delta\varepsilon}{(1-h)\cdot\left(1+\frac{\Delta\varepsilon}{(1-h)}\right)} = \frac{1}{1-h+\Delta\varepsilon}\cdot\left(\frac{\delta_S - \varepsilon^{*}_{v\text{-}w}}{\alpha^{+}_{v\text{-}w}} - h\cdot\delta_A - \Delta\varepsilon\right) \qquad \text{(F.15)}$$

Rearranging, leads to:

$$\delta_E = \frac{1}{(1-h)+\Delta\varepsilon}\cdot\left(\frac{\delta_S}{\alpha^{+}_{v\text{-}w}} - (h\cdot\delta_A) - \left(\Delta\varepsilon + \frac{\varepsilon^{*}_{v\text{-}w}}{\alpha^{+}_{v\text{-}w}}\right)\right) \qquad \text{(F.16)}$$

In order to have Eq. F.16 in permil (i.e. ‰), one should divide $\Delta\varepsilon$ and $\varepsilon^{*}_{v\text{-}w}$ by 1000.

Appendix G : Craig and Gordon model for poorly-mixed water reservoirs

In general, well-mixed water reservoirs are difficult to find. Hence, surface water is enriched in heavy isotopes as consequence of evaporation enrichment compared to deeper layers (i.e. $R_S \neq R_L$), then a term $\rho_{i,L}/\rho_L$ should be introduced to take into account the resistance of the vertical transport in the water column (Craig and Gordon, 1965). This assumption is not always justified while this term is usually neglected. $\rho_{i,L}/\rho_L$ values range from 0 to 0.2 for good mixing and extreme stratification, respectively (Gat *et al.*, 1981). As such, transport through the liquid layer or water column needs to be evaluated. This flux can be taken simply as E, water evaporation, the flux of the heavy isotopic species through this layer, due to molecular diffusion and mass flow is then given by (Craig and Gordon, 1965):

$$E_{i,L} = -\frac{dI_{i,L}}{dt} = \frac{\left[\left(1+E\cdot\rho_{i,L}\right)\cdot R_L - R_S\right]}{\rho_i} \qquad (G.1)$$

Eq. (F.16) is used for the calculation of the water vapor isotopic signature, coming from a completely mixed water reservoir. However, the water vapor isotopic signature, coming from a poorly mixed water reservoir is given by the following equation. Using Eqs. (G.1), (F.16) or (7.2) in δ-notation yields:

$$\delta_{E,L} = \frac{1}{(1-h) + \Delta\varepsilon + \left(\frac{E\cdot\rho_{i,L}}{\alpha^{+}_{v\text{-}w}}\right)} \cdot \left[\frac{\delta_L\cdot\left(1+E\cdot\rho_{i,L}\right)}{\alpha^{+}_{v\text{-}w}}\right] - (h\cdot\delta_A) - \varepsilon^T \qquad (G.2)$$

Remark that in order to have Eq. G.2, in permil (i.e. ‰), one should divide Δε and $\varepsilon^{*}_{v\text{-}w}$ by 1000.

Appendix H : Maximum possible enrichment, δ*

The Craig and Gordon model can be used for the estimation of the maximum possible enrichment (i.e. δ*) or when the last drop of water leaves the water reservoir in study, given specific local meteorological conditions. This will affect of course the vapor isotopic signature coming from that reservoir. Hence, the derivation of δ*, we will start from the general water balance of a reservoir:

Water and isotope mass balance on a well-mixed water reservoir undergoing evaporation while maintaining long term constant volume, and constant density of water are:

$$I_L = Q_L + E_L \tag{H.1}$$

$$I_L \cdot \delta_L = Q_L \cdot \delta_Q + E_L \cdot \delta_E \tag{H.2}$$

where I_L, Q_L and E_L stands for water inflow, water outflow and evaporation from the water reservoir, respectively; and δ_L, δ_Q and δ_E stand for the weighted isotopic compositions of inflow, outflow and evaporative flux, respectively. Assuming that $\delta_L = \delta_Q$, which is a fairly reasonable assumption since it means that water inputs weighted isotopic signature is similar to that of weighted isotopic outputs from a water reservoir. Eqs. H.1 and H.2 can be rearranged to

$$\frac{I_L}{E_L} = \frac{\delta_E - \delta_L}{\delta_I - \delta_L} \tag{H.3}$$

where I_L/E_L stands for $1/x$, were x is the fraction of water lost through evaporation. Eq. H.3 assumes no long-term storage changes in the reservoir. As noted earlier, δ_E is calculated using the Craig and Gordon model equation given in Appendix F.

$$\delta_E = \frac{1}{(1-h)+\Delta\varepsilon} \cdot \left(\frac{\delta_L}{\alpha^+_{v\text{-}w}} - (h \cdot \delta_A) - \left(\Delta\varepsilon + \frac{\varepsilon^*_{v\text{-}w}}{\alpha^+_{v\text{-}w}} \right) \right) \quad \text{(H.4)}$$

Hence, replacing Eq. H.4 in Eq.H.3 yields a denominator as follows:

$$\delta_E - \delta_L = \frac{1}{(1-h)+\Delta\varepsilon} \cdot \left(\frac{\delta_L}{\alpha^+_{v\text{-}w}} - (h \cdot \delta_A) - \left(\Delta\varepsilon + \frac{\varepsilon^*_{v\text{-}w}}{\alpha^+_{v\text{-}w}} \right) \right) - \delta_L \quad \text{(H.5)}$$

Introducing,

$$\varepsilon^T = \Delta\varepsilon + \frac{\varepsilon^*_{v\text{-}w}}{\alpha^+_{v\text{-}w}}, \text{(in ‰)} \quad \text{(H.6)}$$

or when

$$\varepsilon^T = \frac{\Delta\varepsilon}{1000} + \frac{\left(\varepsilon^*_{v\text{-}w} / 1000 \right)}{\alpha^+_{v\text{-}w}}, \text{(in δ-notation, i.e. decimal notation)} \quad \text{(H.7)}$$

Therefore, using Eq. (H.6), Eq. 5 yields to

$$\delta_E - \delta_L = \frac{\left(\frac{\delta_L}{\alpha^+_{v\text{-}w}} - (h \cdot \delta_A) - \varepsilon^T \right)}{(1-h)+\Delta\varepsilon} - \delta_L \quad \text{(H.8)}$$

First we need to multiply by the common denominator. This leads to the following:

$$\delta_E - \delta_L = \frac{\left(\frac{\delta_L}{\alpha^+_{v\text{-}w}} - (h \cdot \delta_A) - \varepsilon^T - \delta_S + (h \cdot \delta_L) - \Delta\varepsilon \cdot \delta_L \right)}{(1-h)+\Delta\varepsilon} = \frac{\text{Nom}}{\text{Den}} \quad \text{(H.9)}$$

where Nom and Den stands for nominator and denominator. Knowing that the isotopic enrichment for evaporation under equilibrium conditions is given by:

$$\varepsilon^{*}_{v\text{-}w} = \left(\frac{1}{\alpha^{+}_{v\text{-}w}} - 1\right) \cdot 1000 \qquad \text{(H.10)}$$

Hence,

$$\frac{1}{\alpha^{+}_{v\text{-}w}} = \left(1000 - \varepsilon^{*}_{v\text{-}w}\right) \qquad \text{(H.11)}$$

Please, note that in order to reduce the size of the equations, all equations will be given in decimal notation, rather than ‰.

Working with the nominator (i.e. Nom) from Eq (H.8), and adding Eq. H.9, yields to

$$\text{Nom} = \delta_L - \left(\varepsilon^{*}_{v\text{-}w} \cdot \delta_L\right) - (h \cdot \delta_A) - \varepsilon^{T} - \delta_L + (h \cdot \delta_L) - \Delta\varepsilon \cdot \delta_L \qquad \text{(H.12)}$$

$$\text{Nom} = (h \cdot \delta_L) - \Delta\varepsilon \cdot \delta_L - \left(\varepsilon^{*}_{v\text{-}w} \cdot \delta_L\right) - (h \cdot \delta_A) - \varepsilon^{T} - \delta_L \qquad \text{(H.13)}$$

Since

$$\varepsilon^{T} = \Delta\varepsilon + \frac{\varepsilon^{*}_{v\text{-}w}}{\alpha^{+}_{v\text{-}w}}, \text{(in ‰)} \qquad \text{(H.14)}$$

Eq. (H.13) is rewritten as

$$\text{Nom} = (h \cdot \delta_L) - \Delta\varepsilon \cdot \delta_L - \left(\varepsilon^{*}_{v\text{-}w} \cdot \delta_L\right) - (h \cdot \delta_A) - \left(\Delta\varepsilon + \frac{\varepsilon^{*}_{v\text{-}w}}{\alpha^{+}_{v\text{-}w}}\right) - \delta_L \qquad \text{(H.14)}$$

$$Nom = (h \cdot \delta_L) - \Delta\varepsilon \cdot \delta_L - \left(\varepsilon^*_{v\text{-}w} \cdot \delta_L\right) - (h \cdot \delta_A) - \Delta\varepsilon - \frac{\varepsilon^*_{v\text{-}w}}{\alpha^+_{v\text{-}w}} - \delta_L \tag{H.15}$$

Or

$$Nom = (h \cdot \delta_L) - (h \cdot \delta_A) - \Delta\varepsilon \cdot (1 + \delta_L) - \varepsilon^*_{v\text{-}w} \cdot \left(\frac{1}{\alpha^+_{v\text{-}w}} + \delta_L\right) \tag{H.16}$$

Assumming that $\alpha^+_{v\text{-}w} = 1$, hence, Eq. (H.16) can be simplified to:

$$Nom = (h \cdot \delta_L) - (h \cdot \delta_A) - \varepsilon^T \cdot (1 + \delta_L) \tag{H.17}$$

$$Nom = (h \cdot \delta_L) - (h \cdot \delta_A) - \varepsilon^T - \varepsilon^T \cdot \delta_L \tag{H.18}$$

or

$$Nom = \delta_L \cdot \left(h - \varepsilon^T\right) - (h \cdot \delta_A) - \varepsilon^T \tag{H.19}$$

Multiplying Eq. (H.19) by $\left(h - \varepsilon^T\right)$ yields in

$$Nom = -\left(h - \varepsilon^T\right) \cdot \left(\frac{(h \cdot \delta_A) - \varepsilon^T}{(h - \varepsilon^T)} - \delta_L\right) \tag{H.20}$$

And this results in Eq. (H.8) yields:

$$\delta_E - \delta_L = -\frac{\left(h - \varepsilon^T\right)}{(1 - h) + \Delta\varepsilon} \cdot \left(\frac{(h \cdot \delta_A) - \varepsilon^T}{(h - \varepsilon^T)} - \delta_L\right) \tag{H.21}$$

where the first term is known as the enrichment slope m as in Gibson and Edwards (2002) or B in Gonfiantini (1986); while the last term is known as the limiting isotopic composition under local climatological conditions, δ* or A in Gonfiantini (1986).

$$m = \frac{\left(h - \varepsilon^{T}\right)}{(1 - h) + \Delta\varepsilon} \tag{H.22}$$

$$\delta^{*} = \frac{(h \cdot \delta_{A}) - \varepsilon^{T}}{(h - \varepsilon^{T})} \tag{H.23}$$

Appendix I : Derivation of Gibson *et al*. (2008) evaporation slope equation

The importance of the evaporation line slope on the evaporation of water from a reservoir is very important to understand, not only evaporation losses, but also to understand the sources of water vapor that in time will contribute to atmospheric water vapor from other soircces and eventually precipitate as snow, hail, rain or fog. Derivation of the evaporation line (i.e. EL) slope equation given by Gibson *et al*., (2008):

$$EL_{Slope} = \frac{\text{rise}_{\,^2H}}{\text{run}_{^{18}O}} = \frac{\left[\delta^* - \delta_P\right]_{^2H}}{\left[\delta^* - \delta_P\right]_{^{18}O}} \qquad \text{I.1}$$

Where δ_P stands for precipitation, and using Eq. (H.24)

$$\delta^* = \frac{(h\cdot\delta_A) - \varepsilon^T}{(h - \varepsilon^T)} \qquad \text{I.2}$$

In order to simplify the enrichment terms, we introduce,

$$\varepsilon^T = \Delta\varepsilon + \frac{\varepsilon^+}{\alpha^+} \qquad \text{I.3}$$

Hence,

$$EL_{Slope} = \frac{\left[\delta^* - \delta_P\right]_{^2H}}{\left[\delta^* - \delta_P\right]_{^{18}O}} = \frac{\left[\frac{h\cdot\delta_A + \varepsilon^T}{h - \varepsilon^T} - \delta_P\right]_{^2H}}{\left[\frac{h\cdot\delta_A + \varepsilon^T}{h - \varepsilon^T} - \delta_P\right]_{^{18}O}} \qquad \text{I.4}$$

$$EL_{Slope} = \frac{\left[\frac{h\cdot\delta_A + \varepsilon^T}{h - \varepsilon^T} - \delta_P\right]_{^2H}}{\left[\frac{h\cdot\delta_A + \varepsilon^T}{h - \varepsilon^T} - \delta_P\right]_{^{18}O}} = \frac{\left[\frac{h\cdot\delta_A + \varepsilon^T - \delta_P(h - \varepsilon^T)}{h - \varepsilon^T}\right]_{^2H}}{\left[\frac{h\cdot\delta_A + \varepsilon^T - \delta_P(h - \varepsilon^T)}{h - \varepsilon^T}\right]_{^{18}O}} \qquad \text{I.5}$$

Hence,

$$EL_{Slope} = \frac{\left[\frac{h\cdot\delta_A+\varepsilon^T-\delta_P(h-\varepsilon^T)}{h-\varepsilon^T}\right]_{^2H}}{\left[\frac{h\cdot\delta_A+\varepsilon^T-\delta_P(h-\varepsilon^T)}{h-\varepsilon^T}\right]_{^{18}O}} = \frac{\left[\frac{h\cdot\delta_A+\varepsilon^T-h\cdot\delta_P+\delta_P\cdot\varepsilon^T}{h-\varepsilon^T}\right]_{^2H}}{\left[\frac{h\cdot\delta_A+\varepsilon^T-h\cdot\delta_P+\delta_P\cdot\varepsilon^T}{h-\varepsilon^T}\right]_{^{18}O}} \quad \text{I.6}$$

or

$$EL_{Slope} = \frac{\left[\frac{h\cdot(\delta_A-\delta_P)+(1+\delta_P)\cdot\varepsilon^T}{h-\varepsilon^T}\right]_{^2H}}{\left[\frac{h\cdot(\delta_A-\delta_P)+(1+\delta_P)\cdot\varepsilon^T}{h-\varepsilon^T}\right]_{^{18}O}} \quad \text{I.7}$$

The last section on the above equation is the evaporation slope equation. Replacing ε^T by its original values leads to the full evaporation slope as sown below:

$$EL_{Slope} = \frac{\left[\frac{h\cdot(\delta_A-\delta_P)+(1+\delta_P)\cdot\left(\Delta\varepsilon+\frac{\varepsilon^+}{\alpha^+}\right)}{h-\Delta\varepsilon-\frac{\varepsilon^+}{\alpha^+}}\right]_{^2H}}{\left[\frac{h\cdot(\delta_A-\delta_P)+(1+\delta_P)\cdot\left(\Delta\varepsilon+\frac{\varepsilon^+}{\alpha^+}\right)}{h-\Delta\varepsilon-\frac{\varepsilon^+}{\alpha^+}}\right]_{^{18}O}} \quad \text{I.8}$$

Appendix J : Derivation of the MWL intersection of a given sample

The following shows how the intersection of any sample with a given MWL is derived

Having defined the any (Global or Local) meteoric water line (MWL) and an evaporation line (EL), we can calculate the coordinates of the intersection of a line parallel to the EL (referred to as PEL) of any “evaporated sample” with the MWL (see black triangle on Figure J.1).

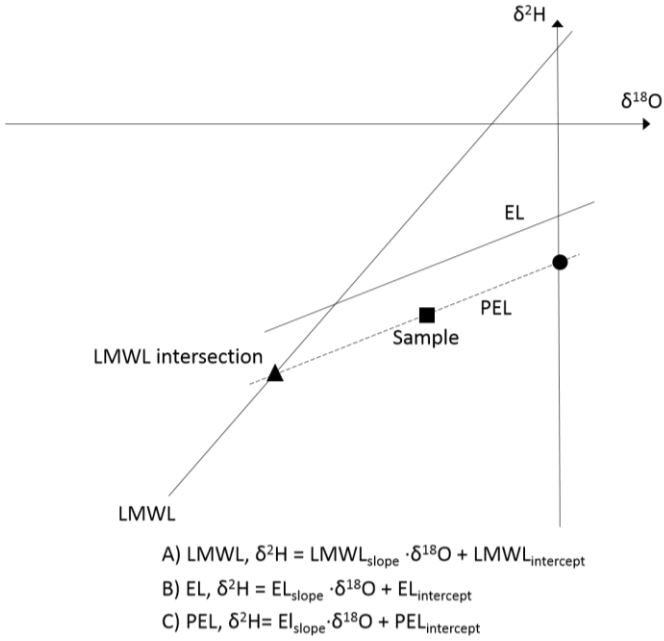

Figure J.1: Hypothetical local meteoric water line (MWL, A), evaporation line (EL, B) and a parallel line to the EL (PEL, C), which goes through the sample (black square) and the estimated Intercept (black circle). The black triangle shows the intersection between the MWL and PEL.

The equation of PEL is given by:

$$\delta^2H = PEL_{sl} \cdot \delta^{18}O + PEL_{int} \quad (J.1)$$

Where subscripts sl and int stand for slope and intercept, respectively. $PEL_{sl} = EL_{sl}$ as they are parallel. The intercept of PEL (i.e: the crossing of PEL with the δ^2H axis, black dot on Figure J.1) is given by:

$$PEL_{int} = EL_{int} - \left(EL_{sl} \cdot \delta^{18}O_s + EL_{int}\right) + \delta^2H_s \quad (J.2)$$

or

$$PEL_{int} = \delta^2H_s - EL_{sl} \cdot \delta^{18}O_s \quad (J.3)$$

Where the subscripts “sl”, “s” and “int” stand for slope, sample and intercept, respectively, and EL stands for evaporation line. The equation of this parallel line (PEL, dashed line on Figure J.1) is thus:

$$\delta^2H = EL_{sl} \cdot \delta^{18}O + (\delta^2H_s - EL_{sl} \cdot \delta^{18}O_s) \quad (J.4)$$

or

$$\delta^2H = EL_{sl} \cdot (\delta^{18}O - \delta^{18}O_s) + \delta^2H_s \quad (J.5)$$

Based on the equation of the parallel line (using Eqs. (J.4) and (J.5)), we can derive the values of $\delta^{18}O$ and δ^2H at the intersection ($\delta^{18}O_{MWL\text{-}intersection}$ and $\delta^2H_{MWL\text{-}intersection}$, respectively) of our sample with the MWL (black triangle on Figure J.1). Since we do not know either $\delta^{18}O_{MWL\text{-}intersection}$ or $\delta^2H_{MWL\text{-}intersection}$ values, we use a system of two equations to calculate both values:

$$\delta^2H_{MWL\text{-}intersection} = (MWL_{sl} \cdot \delta^{18}O_{MWL\text{-}intersection}) + MWL_{int} \quad (J.6)$$

$$\delta^2H_{MWL\text{-}intersection} = EL_{sl} \cdot \left(\delta^{18}O_{MWL\text{-}intersection} - \delta^{18}O_s\right) + \delta^2H_s \quad (J.7)$$

We can solve this set of equations for $\delta^{18}O_{LMWL\text{-}intersection}$ and $\delta^{2}H_{LMWL\text{-}intersection}$ as follows:

$$MWL_{sl}\cdot\delta^{18}O + MWL_{int} = EL_{sl}\cdot(\delta^{18}O_{MWL\text{-}intersection} - \delta^{18}O_{s}) + \delta^{2}H_{s} \quad (J.8)$$

or

$$MWL_{sl}\cdot\delta^{18}O + MWL_{int} = EL_{sl}\cdot\delta^{18}O_{MWL\text{-}intersection} - EL_{sl}\cdot\delta^{18}O_{s} + \delta^{2}H_{s} \quad (J.9)$$

or

$$MWL_{sl}\cdot\delta^{18}O = EL_{sl}\cdot\delta^{18}O_{MWL\text{-}intersection} - EL_{sl}\cdot\delta^{18}O_{s} + \delta^{2}H_{s} - MWL_{int} \quad (J.10)$$

and thus

$$\delta^{18}O_{MWL\text{-}intersection} = \frac{\delta^{2}H_{s} - MWL_{int} - EL_{sl}\cdot\delta^{18}O_{s}}{MWL_{sl} - EL_{sl}} \quad (J.11)$$

Then $\delta^{2}H_{MWL\text{-}intersection}$ is found by replacing $\delta^{18}O_{MWL\text{-}intersection}$ in Eqs. (J.6) or (J.7) with its solution given in above equation yielding:

$$\delta^{2}H_{MWL\text{-}intersection} = \left(\frac{\delta^{2}H_{s} - MWL_{sl} - EL_{sl}\cdot(MWL_{int} + MWL_{sl}\cdot\delta^{18}O_{s})}{MWL_{sl} - EL_{sl}}\right) \quad (J.12)$$

However, Evaristo *et al*., (2015) calculated their $\delta^{18}O_{MWL\ intersection}$ and $\delta^{2}H_{MWL\ intersection}$ as follows:

$$\delta^{2}H_{MWL\text{-}intersection} = \delta^{2}H_{s} + EL_{sl}\cdot\delta^{18}O_{s} \quad (J.13)$$

$$\delta^{18}O_{MWL\text{-}intersection} = \frac{\delta^{2}H_{MWL\text{-}intersection} - MWL_{int}}{MWL_{sl}} \quad (J.14)$$

In order to show graphical proof (Figure J.2) and show that the derived equations are correct, we compare our results with those as estimated by Evaristo *et al*. (2015). We calculated the $\delta^{18}O_{MWL\ intersection}$ and $\delta^{2}H_{MWL\ intersection}$ according to Eqs. (J.11) and (J.12) (i.e: orange inverted triangle, Figure J.2) and Evaristo *et al*. (2015) (i.e: using Eqs. (J.13) and (J.14), yellow square in Figure J.2) of a random sample (-5.0‰ and -75.0‰ for $\delta^{18}O$ and $\delta^{2}H$, respectively) using a MWL, $\delta^{2}H = 8.17 \cdot \delta^{18}O$ and an EL, $\delta^{2}H = 5.1 \cdot \delta^{18}O - 12$ (Figure J.2).

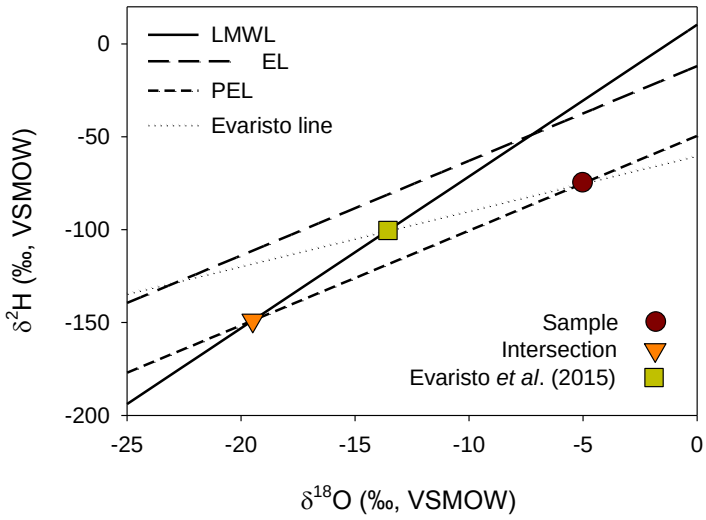

Figure J.2: Results of the calculated $\delta^{18}O_{MWL\ intersection}$ and $\delta^{2}H_{MWL\ intersection}$ of a reference sample (dark red dot) using the method explained here (inverted orange triangle) and the method used by Evaristo *et al*., (2015) (yellow square). MWL, EL and PEL and Evaristo line are in solid, segmented, dashed and point black lines.

In Figure J.2, it can be observed that EL and PEL are indeed parallel lines. This is not the case for Evaristo *et al*. (2015) line, which eventually intersects the EL. Using Eqs. (J.13) and (J.14) leads to an overestimation of both $\delta^{18}O_{MWL\ intersection}$ (≈ 5.9‰) and $\delta^{2}H_{MWL\ intersection}$ (≈ 48.4‰). on this example. When using the line proposed by Evaristo *et al*. (2015).

References

Aemisegger F, Pfahl S, Sodemann H, Lehner I, Seneviratne S, Wernli H. 2013. Deuterium excess as a proxy for continental moisture recycling and plant transpiration. *Atmospheric Chemistry and Physics* **13** (11): 29721–29784.

Aggarwal P, Alduchov O, Froehlich K, Araguás-Araguás L, Sturchio N, Kurita N. 2012. Stable isotopes in global precipitation: A unified interpretation based on atmospheric moisture residence time. *Geophysical Research Letters* **39** (11): 1–6.

Alexander R, Johnes P, Boyer E, Smith R. 2002. A comparison of models for estimating the riverine export of nitrogen from large watersheds. *Biogeochemistry* **57/58**: 295–339.

Allen S, Brooks J, Keim R, Bond B, Mcdonnell J. 2014. The role of pre-event canopy storage in throughfall and stemflow by using isotopic tracers. *Ecohydrology* **7** (2): 858–868.

Allison G, Hughes M. 1978. The use of environmental chloride and tritium to estimate total recharge to an unconfined aquifer. *Australian Journal of Soil Research* **16** (2): 181–195.

Allison G, Barnes C, Hughes M. 1983. The distribution of deuerium and 18O in dry soils 2. Experimental. *Journal of Hydrology* **64**: 377–397.

Allison G, Gat J, Leaney F. 1985. The relationship between deuterium and oxygen-18 delta values in leaf water. *Chemical Geology: Isotope Geoscience section* **58** (1–2): 145–156.

Almeida AC, Soares J V., Landsberg JJ, Rezende GD. 2007. Growth and water balance of Eucalyptus grandis hybrid plantations in Brazil during a rotation for pulp production. *Forest Ecology and Management* **251** (1–2): 10–21.

Anderson S, Dietrich W, Torres R, Montgomery D, Loague K. 1997. Concentration-discharge relationships in runoff from a steep, unchanneled catchment. *Water Resources Research* **33** (1): 211–225.

Andréassian V. 2004. Waters and forests: from historical controversy to scientific debate. *Journal of Hydrology* **291** (1–2): 1–27.

Araguás-Araguás L, Rozanski K, Gonfiantini R, Louvat D. 1995. Isotope effects accompanying vacuum extraction of soil water for stable isotope analyses. *Journal of Hydrology* **168**: 159–171.

Aravena R, Suzuki O, Pollastri A. 1989. Coastal fog and its relation to groundwater IV region of northern Chile. *Chemical Geology: Isotope Geoscience section* **79**: 83–91.

Armesto J, Rozzi R, Smith-Ramirez C, Arroyo M. 1998. Conservation Targets in South american Temperate Forests. *Science* **282** (November): 1271–1272.

Armesto J, Manuschevich D, Mora A, Smith-Ramirez C, Rozzi R, Abarzúa A, Marquet P. 2010. From the Holocene to the Anthropocene: A historical framework for land cover change in southwestern South America in the past 15,000 years. *Land Use Policy* **27** (2): 148–160.

Barbeta A, Mejía-Chang M, Ogaya R, Voltas J, Dawson T, Peñuelas J. 2014. The combined effects of a long-term experimental drought and an extreme drought on the use of plant-water sources in a Mediterranean forest. *Global change biology* **21**: 1213–1225.

Barbier E. 2004. Water and Economic Growth. *Economic Record* **80** (248): 1–16.

Barnes C, Allison G. 1988. Tracing of water movement in the unsaturated zone using stable isotopes of hydrogen and oxygen. *Journal of Hydrology* **100** (1–3): 143–176.

Belmar A, Carvajal L, Cortez M, Castro H, Silva S, Ferreiro K, Godoy J, Lama R, Larrain S, McRostie V, et al. 2010. *Conflicts over Water in Chile: Between human rights and market rules* (S Larrain and C Scheffer, eds). Santiago.

Berman E, Gupta M, Gabrielli C, Garland T, Mcdonnell J. 2009. High-frequency field-deployable isotope analyzer for hydrological applications. *Water Resources Research* **45**: 1–7.

Berry Z, Evaristo J, Moore G, Poca M, Steppe K, Verrot L, Asbjornsen H, Borma L, Bretfeld M, Hervé-Fernández P, Seyfried M, Schwendemann L, Sinacore K, De Wispelaere L, McDonnell, J. 2017. The two water worlds hypothesis: Addressing multiple working hypotheses and proposing a way forward. *Ecohydrology* DOI: 10.1002/eco.1843

Billy C, Birgand F, Ansart P, Peschard J, Sebilo M, Tournebize J. 2013. Factors controlling nitrate concentrations in surface waters of an artificially drained agricultural watershed. *Landscape Ecology* **28** (4): 665–684.

Birkel C, Soulsby C, Birkel C, Soulsby C, Tetzlaff D. 2014. Conceptual modelling to investigate the interplay of hydrological connectivity, catchment storage and tracer dynamics on non-stationary water ages. *Hydrological processes* 29 (13): 2956-2969.

Boeckx P, Paulino L, Oyarzún C, van Cleemput O, Godoy R. 2005. Soil delta15N patterns in old-growth forests of southern Chile as integrator for N-cycling. *Isotopes in Environmental and Health Studies* **41** (3): 249–259.

Bosch J, Hewlett J. 1982. A review of catachment experiments to determine the effect of vegetation changes on water yield and evapotranspiration. *Journal of Hydrology* **55**: 3–23.

Boy J, Wilcke W. 2008. Tropical Andean forest derives calcium and magnesium from Saharan dust. *Global Biogeochemical Cycles* **22** (1): 1–11.

Braud I, Bariac T, Gaudet J, Vauclin M. 2005. SiSPAT-Isotope, a coupled heat, water and stable isotope (HDO and $H_2{}^{18}O$) transport model for bare soil. Part I. Model

description and first verifications. *Journal of Hydrology* **309** (1–4): 277–300.

Brooks J. 2015. Water, bound and mobile. *Science* **349** (6244): 138–139.

Brooks J, Barnard H, Coulombe R, McDonnell J. 2010. Ecohydrologic separation of water between trees and streams in a Mediterranean climate. *Nature Geoscience* **3** (2): 100–104.

Bruijnzeel L. 2004. Hydrological functions of tropical forests: Not seeing the soil for the trees?. *Agriculture, Ecosystems & Environment* **104** (1): 185-228.

Brutsaert W. 1965. A model for evaporation as a molecular diffusion process into a turbulent atmosphere. *Journal of Geophysical Research* **70** (20): 5017–5024.

Buckley T, Miller J, Farquhar G. 2002. The Mathematics of Linked Optimisation for Water and Nitrogen Use in a Canopy. *Silva Fennica* **36** (July): 639–669.

Burns D, Mcdonnell J, Hooper R, Peters N, Freer J, Kendall C, Beven K. 2001. Quantifying contributions to storm runoff through end-member mixing analysis and hydrologic measurements at the Panola Mountain Research Watershed (Georgia , USA). *Hydrological Processes* **1924** (15): 1903–1924

Caldwell M, Dawson T, Richards J. 1998. Hydraulic lift: Consequences of water efflux from the roots of plants. *Oecologia* **113** (2): 151–161.

Campbell J, Hornbeck J, Mitchell M, Adams M, Castro M, Driscoll C, Kahl J, Kochenderfer J, Likens G, Lynch J, et al. 2004. Input-Output budgets of inorganic nitrogen for 24 forest watersheds in the northeastern United States: A review. *Water Air & Soil pollution* **151**: 373–396.

Cannell M. 1999. Environmental impacts of forest monocultures: water use, acidification, wildlife conservation, and carbon storage. *Water* **17**: 239–262.

Cao S, Zhang J. 2014. Political risks arising from the impacts of large-scale afforestation on water resources of the Tibetan Plateau. *Gondwana Research* DOI: 10.1016/j.gr.2014.07.002

Carey SK, Quinton WL. 2004. Evaluating snowmelt runoff generation in a discontinuous permafrost catchment using stable isotope, hydrochemical and hydrometric data. *Nordic Hydrology* **35** (4–5): 309–324.

Cavelier J, Solis D, Jaramillo M. 1996. Fog interception in montane forests across the Central Cordillera of Panamá. *Journal of Tropical Ecology* **12** (3): 349-357.

Cernusak L, Arthur D, Pate J, Farquhar G. 2003. Water relations link carbon and oxygen isotope discrimination to phloem sap sugar concentration in Eucalyptus globulus. *Plant physiology* **131** (4): 1544–1554.

Cernusak L, Winter K, Aranda J, Turner B. 2008. Conifers , Angiosperm trees, and Lianas: growth, whole-plant water and nitrogen use efficiency, and stable isotope composition ($\delta^{13}C$ and $\delta^{18}O$) of seedlings grown in a tropical environment. *Plant physiology* **148**(1): 642–659.

Chen N, Wu J, Hong H. 2012. Effect of storm events on riverine nitrogen dynamics in a subtropical watershed, southeastern China. *Science of the Total Environment* **431**: 357–365.

Chiwa M, Onozawa Y, Otsuki K. 2010. Hydrochemical characteristics of throughfall and stemflow in a Moso-bamboo (Phyllostachys pubescens) forest. *Hydrological Processes* **24** (20): 2924–2933.

CIREN. 2003. Estudio Agrologico: descripciones de suelos, materiales y simbolos, X región. 70 p.

Cirmo C, McDonnell J. 1997. Linking the hydrologic and biogeochemical controls of nitrogen transport in near-stream zones of temperate-forested catchments: a review. *Journal of Hydrology* **199** (1–2): 88–120.

Clark I. 2015. Groundwater Geochemistry and Isotopes (I Clark, ed.). CRC Press, Taylor and Francis Group: Boca Ratón, FL. 456 p.

Costanza R, D'Arge R, de Groot R, Farber S, Grasso M, Hannon B, Limburg K, Naeem S, O'Neill R, Paruelo J, et al. 1997. The value of the world's ecosystem services and natural capital. *Nature* **387** (6630): 253–260.

Craig H. 1961. Isotopic variations in meteoric waters. *Science* **133** (2): 1719–1723.

Craig H, Gordon L. 1965. Deuterium and oxygen 18 variations in the ocean and the marine atmosphere. In *Stable Isotopes in Oceanographic Studies and Paleotemperatures*, Tongiorgi E. (ed.). Spoleto; 9–130.

Crawford J, Hughes C, Lykoudis S. 2014. Alternative least squares methods for determining the meteoric water line, demonstrated using GNIP data. *Journal of Hydrology* **519** (PB): 2331–2340.

Criss R. 1999. Principles of stable isotope distribution (R Criss, ed.). Oxford University Press: New York. 264 p.

Cuevas J, Soto D, Arismendi I, Pino M, Lara A, Oyarzún C. 2006. Relating land cover to stream properties in southern Chilean watersheds: trade-off between geographic scale, sample size, and explicative power. *Biogeochemistry* **81** (3): 313–329.

Dansgaard W. 1964. Stable isotopes in precipitation. *Tellus* **16**: 438–468.

David T, Pinto C, Nadezhdina N, Kurz-Besson C, Henriques M, Quilhó T, Cermak J, Chaves M, Pereira J, David J. 2013. Root functioning, tree water use and hydraulic redistribution in Quercus suber trees: A modeling approach based on root sap flow. *Forest Ecology and Management* **307**: 136–146.

Davidson E, Chorover J, Dail D. 2003. A mechanism of abiotic immobilization of nitrate in forest ecosystems: the ferrous wheel hypothesis. *Global Change Biology* **9** (2): 228–236.

Dawson T, Ehleringer J. 1991. Streamside trees that do not use stream water. *Nature* **350** (6316): 335–337.

Dawson T, Pate J. 1996. Seasonal water uptake and movement in root systems of Australian phraeatophyUc plants of dimorphic root morphology: a stable isotope investigation. *Oecologia* **107**: 13–20.

Dawson T. 1998. Fog in the California redwood forest: ecosystem inputs and use by plants. *Oecologia* **117** (4): 476–485.

Doerr S, Shakesby R, Walsh R. 1996. Soil hydrophobicity variations with depth and particle size fraction in burned and unburned Eucalyptus globulus and Pinus pinaster forest terrain in the Agueda Basin, Portugal. *Catena* **27** (1): 25–47.

Dole M. 1935. the Relative Atomic Weight of Oxygen in Water and in Air. *Journal of the American Chemical Society* **57** (12): 2731–2731.

Dubbert M, Cuntz M, Piayda A, Maguás C, Werner C. 2013. Partitioning evapotranspiration – Testing the Craig and Gordon model with field measurements of oxygen isotope ratios of evaporative fluxes. *Journal of Hydrology* **496**: 142–153.

Dubbert M, Piayda A, Cuntz M, Correia A, Costa e Silva F, Pereira J, Werner C. 2014. Stable oxygen isotope and flux partitioning demonstrates understory of an oak savanna contributes up to half of ecosystem carbon and water exchange. *Frontiers in Plant Science* **5** (October): 1–16.

Echeverría C, Coomes D, Salas J, Rey-Benayas J, Lara A, Newton A. 2006. Rapid deforestation and fragmentation of Chilean Temperate Forests. *Biological Conservation* **130** (4): 481–494.

Echeverría C, Huber A, Taberlet F. 2007. Comparative study of water balance components in a native forest and a meadow in southern Chile. *Bosque* **28** (3): 271–280.

Ellehoj M, Steen-Larsen H, Johnsen S, Madsen M. 2013. Ice-vapor equilibrium fractionation factor of hydrogen and oxygen isotopes: Experimental investigations and implications for stable water isotope studies. *Rapid Communications in Mass Spectrometry* **27** (19): 2149–2158.

Ellison D, N. Futter M, Bishop K. 2012. On the forest cover-water yield debate: from demand- to supply-side thinking. *Global Change Biology* **18** (3): 806–820.

Engel V, Jobbágy E, Stieglitz M, Williams M, Jackson R. 2005. Hydrological consequences of Eucalyptus afforestation in the Argentine Pampas. *Water Resources Research* **41** (10): 1–14.

Eriksson E. 1965. Deuterium and oxygen-18 in precipitation and other natural waters Some theoretical considerations. *Tellus* **17** (4): 498–512.

Evaristo J, Jasechko S, McDonnell J. 2015. Global separation of plant transpiration from groundwater and streamflow. *Nature* **525** (7567): 91–94.

Evaristo J, McDonnell J, Scholl M, Bruijnzeel L, Chun K. 2016. Insights on plant water uptake from xylem-water isotope measurements in two tropical catchments with contrasting moisture conditions. *Hydrological Processes*: **19** (5): 1196-1201.

FAO. 2015. *World Reference Base for Soil Resources* (IW Group, ed.). FAO.: Roma.

Farley K, Jobbagy E, Jackson R. 2005. Effects of afforestation on water yield: a global synthesis with implications for policy. *Global Change Biology* **11** (10): 1565–1576.

Farquhar G, Cernusak L, Barnes B. 2007. Heavy water fractionation during transpiration. *Plant physiology* **143** (1): 11–18.

Feddema J, Oleson K, Bonan G, Mearns L, Buja L, Meehl G, Washington W. 2005. The importance of land-cover change in simulating future climates. *Science* **310** (5754): 1674–1678.

Ferguson P, Veizer J. 2007. Coupling of water and carbon fluxes via the terrestrial biosphere and its significance to the Earth's climate system. *Journal of Geophysical Research Atmospheres* **112** (24): 1–17.

Ferreira A, Coelho C, Walsh R, Shakesby R, Ceballos A, Doerr S. 2000. Hydrological implications of soil water-repellency in Eucalyptus globulus forests, north-central Portugal. *Journal of Hydrology* **231–232**: 165–177.

Forrester D, Theiveyanathan S, Collopy J, Marcar N. 2010. Enhanced water use efficiency in a mixed *Eucalyptus globulus* and *Acacia mearnsii* plantation. *Forest Ecology and Management* **259** (9): 1761–1770.

Freitag H, Ferguson P, Dubois K, Hayford E, von Vordzogbe V, Veizer J. 2008. Water and carbon fluxes from savanna ecosystems of the Volta River watershed, West Africa. *Global and Planetary Change* **61** (1–2): 3–14.

Frêne C, Ojeda G, Santibañez J, Donoso C, Sanzana J, Molina C, Andrade P, Nuñez-Ávila M. 2014. Agua en Chile, Diagnósticos territoriales y propuestas para enfrentar la crisis hídrica (C Frêne, P Andrade, and M Nuñez-Ávila, eds). America Ltda. 60 p.

Fritzsche F, Abate A, Fetene M, Beck E, Weise S, Guggenberger G. 2006. Soil-plant hydrology of indigenous and exotic trees in an Ethiopian montane forest. *Tree physiology* **26** (8): 1043–1054.

Froehlich K, Martin K, Papesch W, Rank D, Scheifinger H, Stichler W. 2007. Deuterium excess in precipitation of Alpine regions - moisture recycling. *Isotopes in Environmental and Health Studies* **44** (0): 1–14.

Galloway J, Dentener F, Capone D, Boyer E, Howarth R, Seitzinger S, Asner G, Cleveland C, Green P, Holland E, et al. 2004. Nitrogen cycles: past, present, and future. *Biogochemistry* **70**: 153–226.

Gat J, Tzur Y. 1966. Modification of the isotopic composition of rainwater by processes which occur before groundwater recharge (SM-83/4). In *Isotope Hydrology* Vienna; 49–60.

Gat J, Issar A. 1974. Desert isotope hydrology: water sources of the Sinai Desert. *Geochimica et Cosmochimica Acta* **38**: 1117–1131.

Gat J, Gonfiantini R, Magaritz M, Yurtsever Y, Árnason B, Fritz P, Panichi C, Fontes J, Payne B. 1981. Technical reports series No. 210 Stable Isotope Hydrology: Deuterium and Oxygen-18 in the water cycle. Vienna.

Gat J, Carmi I. 1987. Effect of climate changes on the precipitation patterns and isotopic composition of water in a climate transition zone : Case of the Eastern Mediterranean Sea area. *The Influence of Climate Chnage and Climatic Variability on the Hydrolic Regime and Water Resources* (168): 513–524.

Gat J, Matsui E. 1991. Atmospheric water balance in the amazon basin: an isotopic evapotranspiration model. *Journal of Geophysical Research* **96** (91): 13179–13188.

Gat J, Bowser C. 1991. The heavy isotope enrichment of water in coupled evaporative systems. *Stable Isotope Geochemistry: A Tribute to Samuel Epstein* **3** (3): 159–168.

Gat J, Bowser C, Kendall C. 1994. The contribution of evaporation from the Great Lakes to the continental atmosphere: estimate based on stable isotope data. *Geophysical Research Letters* **21** (7): 557–560.

Gat J. 1996. Oxygen and Hydrogen isotopes in the hydrologic cycle. *Annual Review of Earth and Planetary Sciences* **24**: 225–262.

Gat J, Shemesh A, Tziperman E, Hecht A, Georgopoulos D, Basturk O. 1996. The stable isotope composition of waters of the eastern Mediterranean Sea. *Journal of Geophysical Research* **101** (C3): 6441–6451.

Gat J. 2000. Atmospheric water balance — the isotopic perspective. *Hydrological Processes* **14**: 1357–1369.

Gat J, Mook W, Meijer A. 2001. *Environmental isotopes in the hydrological cycle, principles and applications. Volume II: Atmospheric water*.

Gat J, Klein B, Kushnir Y, Roether W, Wernli H, Yam R, Shemesh A. 2003. Isotope composition of air moisture over the Mediterranean Sea: An index of the air-sea interaction pattern. *Tellus, Series B: Chemical and Physical Meteorology* **55** (5): 953–965.

Gat J. 2005. Isotope Hydrology: A Study of the Water Cycle (J Gat, ed.). Imperial College Press: 57 Shelton Street, Covent Garden, London. 200 p.

Gat J, Airey P. 2006. Stable water isotopes in the atmosphere / biosphere / lithosphere interface : Scaling-up from the local to continental scale , under humid and dry conditions. *Global and Planetary Change* **51**: 25–33.

Gazis C, Feng X. 2004. A stable isotope study of soil water: evidence for mixing and preferential flow paths. *Geoderma* **119** (1–2): 97–111.

Geris J, Tetzlaff D, McDonnell J, Anderson J, Paton G, Soulsby C. 2015a. Ecohydrological separation in wet, low energy northern environments? A preliminary assessment using different soil water extraction techniques. *Hydrological Processes* **29** (25): 5139–5152.

Geris J, Tetzlaff D, Mcdonnell J, Soulsby C. 2015b. The relative role of soil type and tree cover on water storage and transmission in northern headwater catchments. *Hydrological Processes* **29** (7): 1844–1860.

Geris J, Tetzlaff D, Soulsby C. 2015c. Resistance and resilience to droughts: hydropedological controls on catchment storage and run-off response. *Hydrological Processes* **29** (21): 4579–4593.

Gibbs HK, Salmon JM. 2015. Mapping the world's degraded lands. *Applied Geography* **57**: 12–21.4

Gibson J, Edwards T. 2002. Regional water balance trends and evaporation-transpiration partitioning from a stable isotope survey of lakes in northern Canada. *Global Biogeochemical Cycles* **16** (2): 1–11.

Gibson J, Birks S, Edwards T. 2008. Global prediction of δA and δ2H- δ18O evaporation slopes for lakes and soil water accounting for seasonality. *Global Biogeochemical Cycles* **22** (2): 1–12.

Gibson J, Reid R. 2010. Stable isotope fingerprint of open-water evaporation losses and effective drainage area fluctuations in a subarctic shield watershed. *Journal of Hydrology* **381** (1–2): 142–150.

Godoy R, Oyarzún C, Gerding V. 2001. Precipitation chemistry in deciduous and evergreen Nothofagus forests of southern Chile under a low-deposition climate. *Basic and Applied Ecology* **72** (April 1999): 65–72.

Godoy R, Paulino L, Oyarzún C, Boeckx P. 2003. Atmospheric N Deposition in Central and Southern Chile: an Overview. *Gayana. Botánica* **60** (1): 47–53.

Goldsmith G, Matzke N, Dawson T. 2012. The incidence and implications of clouds for cloud forest plant water relations. *Ecology Letters* **16**: 307–314.

Goldsmith G, Muñoz-Villers L, Holwerda F, McDonnell J, Asbjornsen H, Dawson T. 2011. Stable isotopes reveal linkages among ecohydrological processes in a seasonally dry tropical montane cloud forest. *Ecohydrology* **5** (6): 779–790.

Gonfiantini R. 1986. Environmental Isotopes in Lake Studies. In *The Terrestrial Environment, B.* Elsevier B.V.; 113–168.

Good S, Noone D, Bowen G. 2015a. Hydrologic connectivity constrains partitioning of global terrestrial water fluxes. *Science* **349** (6244): 175–177.

Good S, Noone D, Kurita N, Benetti M, Bowen G. 2015b. D/H isotope ratios in the global hydrologic cycle. *Geophysical Research Letters* **42** (12): 5042–5050.

Goodale C, Thomas S, Fredriksen G, Elliott E, Flinn K, Butler T, Walter M. 2009. Unusual seasonal patterns and inferred processes of nitrogen retention in forested headwaters of the Upper Susquehanna River. *Biogeochemistry* **93** (3): 197–218.

Guarnaschelli A, Prystupa P, Lemcoff J. 2006. Drought conditioning improves water status, stomatal conductance and survival of *Eucalyptus globulus* subsp.

bicostata seedlings. *Annals of Forest Science* **63** (8): 941–950.

Guerrero P, Bustamante R. 2007. Can native tree species regenerate in Pinus radiata plantations in Chile? *Forest Ecology and Management* **253** (1–3): 97–102.

Hall S, Weintraub S, Bowling D. 2016. Scale-dependent linkages between nitrate isotopes and denitrification in surface soils: implications for isotope measurements and models. *Oecologia* **181** (4): 1221–1231.

Hedin L, Armesto J, Johnson A. 1995. Patterns of Nutrient Loss from Unpolluted , Old-Growth Temperate Forests : Evaluation of Biogeochemical Theory. *Ecology* **76** (2): 493–509.

Van Herpe Y, Troch P, Quinn P, Anthony S. 2002. Modelling Hydrological Mobilization of Nutrient Pollutants at the Catchment Scale. In *Agriculture, Hydrology and Water Quality*, Haygarth P, Jarvis S (eds).243–264.

Hervé-Fernández P. 2011. Controles hidrológicos y exportación de nutrientes en dos microcuencas con distinta cobertura vegetacional. MSc Thesis. Universidad austral de Chile. 74 p.

Hervé-Fernández P, Oyarzún C, Huygens D, Boeckx P, Verhoest N. 2015. Evaporation losses and sources of water vapour in old-growth native evergreen forest and Eucalyptus nitens covered catchments in South-Central, Chile (40 °S). *Boussinesq Meeting, 2015*: 1.

Hervé-Fernández P, Oyarzún C, Woelfl S. 2016a. Throughfall Enrichment and Stream Nutrient Chemistry in Small Headwater Catchments With Different Land Cover in Southern Chile. *Hydrological Processes* **30**: 4944–4955.

Hervé-Fernández P, Oyarzún C, Brumbt C, Huygens D, Bodé S, Verhoest N, Boeckx P. 2016b. Assessing the 'two water worlds' hypothesis and water sources for native and exotic evergreen species in south-central Chile. *Hydrological Processes* **30** (23): 4227–4241.

Hewlett J, Hibbert A. 1966. Factors affecting the response of small watershed to precipitation in humid areas. In *International Symposium on Forest Hidrology*Pergamon Press: Oxford & New York; 275–279.

Hopp L, McDonnell J. 2009. Connectivity at the hillslope scale: Identifying interactions between storm size, bedrock permeability, slope angle and soil depth. *Journal of Hydrology* **376** (3–4): 378–391.

Horita J, Wesolowski D. 1994. Liquid-vapor fractionation of oxygen and hydrogen isotopes of water from the freezing to the critical temperature. *Geochimica et Cosmochimica Acta* **58** (16): 3425–3437.

Horita J, Cole D, Wesolowski D. 1995. The activity-composition relationship of oxygen and hydrogen isotopes in aqueous salt solutions: III. Vapor-liquid water equilibration of NaCl solutions to 350°C. *Geochimica et Cosmochimica Acta* **59** (6): 1139–1151.

Horita J, Rozanski K, Cohen S. 2008. Isotope effects in the evaporation of water: a

status report of the Craig-Gordon model. *Isotopes in environmental and health studies* **44** (1): 23–49.

Horton J, Hawkins R. 1965. Flow path of rain from the soil surface to the water table. *Soil Science* **100** (6): 377–383.

Huber A, Oyarzún C. 1992. Redistribución de las Precipitaciones en un Bosque Siempreverde del Sur de Chile. *Turrialba* **42** (2): 192–199.

Huber A, Barriga P, Trecaman R. 1998. Efecto de la densidad de plantaciones de Eucalyptus nitens sobre el balance hídrico en la zona de Collipulli , IX Región (Chile)*. *Bosque* **19** (1): 61–69.

Huber A, Iroumé A. 2001. Variability of annual rainfall partitioning for different sites and forest covers in Chile. *Journal of Hydrology* **248** (1–4): 78–92.

Huber A, Trecaman R. 2004. Water-use efficiency for Pinus radiata stands in Chile. *Bosque* **25** (3): 33–43.

Huber A, Iroumé A, Mohr C, Frêne C. 2010. Effect of Pinus radiata and Eucalyptus globulus plantations on water resource in the Coastal Range of Biobío region, Chile. *Bosque* **31** (3): 219–230.

Huygens D, Rütting T, Boeckx P, Van Cleemput O, Godoy R, Müller C. 2007. Soil nitrogen conservation mechanisms in a pristine south Chilean Nothofagus forest ecosystem. *Soil Biology and Biochemistry* **39** (10): 2448–2458.

Huygens D, Boeckx P, Templer P, Paulino L, Van Cleemput O, Oyarzún C, Müller C, Godoy R. 2008. Mechanisms for retention of bioavailable nitrogen in volcanic rainforest soils. *Nature Geoscience* **1** (8): 543–548.

Inamdar SP, Christopher SF, Mitchell MJ. 2004. Export mechanisms for dissolved organic carbon and nitrate during summer storm events in a glaciated forested catchment in New York, USA. *Hydrological Processes* **18** (14): 2651–2661.

Inamdar S, Mitchell M. 2007. Storm event exports of dissolved organic nitrogen (DON) across multiple catchments in a glaciated forested watershed. *Journal of Geophysical Research* **112** (G2): 1–18.

Ingraham N, Shadel C. 1992. A comparison of the toluene distillation and vacuum/heat methods for extracting soil water for stable isotopic analysis. *Journal of Hydrology* **140** (1–4): 371–387.

Iroumé A, Huber A. 2000. Intercepción de las lluvias por la cubierta de bosques y efecto en los caudales de crecida en una cuenca experimental en Malalcahuello , IX Región , Chile *. *Bosque* **21** (1): 45–56.

Iroumé A, Palacios H. 2013. Afforestation and changes in forest composition affect runoff in large river basins with pluvial regime and Mediterranean climate, Chile. *Journal of Hydrology* **505**: 113–125.

Jansson Å, Folke C, Rockstro J, Gordon L. 1999. Linking freshwater Flows and Ecosystem Services Appropriated by People: The Case of the Baltic Sea

Drainage Basin. *Ecosystems* **2**: 351–366.

Jasechko S, Sharp Z, Gibson J, Birks S, Yi Y, Fawcett P. 2013. Terrestrial water fluxes dominated by transpiration. *Nature* **496** (7445): 347–350.

Jeddi K, Cortina J, Chaieb M. 2009. Acacia salicina, Pinus halepensis and Eucalyptus occidentalis improve soil surface conditions in arid southern Tunisia. *Journal of Arid Environments* **73** (11): 1005–1013.

Jiang R, Woli K, Kuramochi K, Hayakawa A, Shimizu M, Hatano R. 2010. Hydrological process controls on nitrogen export during storm events in an agricultural watershed. *Soil Science and Plant Nutrition* **56** (1): 72–85.

Jiménez-Castillo M, Lobos-Catalán P, Aguilera-Betti I, Rivera R. 2011. Daily transpiration rates and hydraulic relationships in tree species with different shade tolerance level in a Chilean temperate forest. *Gayana Botánica* **68** (2): 155–162.

Kendall C, Coplen T. 2001. Distribution of oxygen-18 and deuterium in river waters across the United States. *Hydrological Processes* **15** (7): 1363–1393.

Kendall C, McDonnell J. 1998. Isotope tracers in catchment hydrology. (C Kendall and J Mcdonnell, eds). Elsevier B.V.: Amsterdam. 839 p.

Kim H, Sidle RC, Moore RD, Jeong H. 2005. Shallow lateral flow from a forested hillslope: Influence of antecedent wetness. *Catena* **60** (3): 293–306.

Kirchner J. 2003. A double paradox in catchment hydrology and geochemistry. *Hydrological Processes* **17** (4): 871–874.

Klaus J, McDonnell J. 2013. Hydrograph separation using stable isotopes: Review and evaluation. *Journal of Hydrology* **505**: 47–64.

Klaus J, Zehe E, Elsner M, Külls C, McDonnell J. 2013. Macropore flow of old water revisited: experimental insights from a tile-drained hillslope. *Hydrology and Earth System Sciences* **17**: 103–118.

Kong Y, Pang Z, Froehlich K. 2013. Quantifying recycled moisture fraction in precipitation of an arid region using deuterium excess. *Tellus, Series B: Chemical and Physical Meteorology* **65**: 1–8.

Kubota T, Tsuboyama Y. 2003. Intra- and inter-storm oxygen-18 and deuterium variations of rain, throughfall, and stemflow, and two-component hydrograph separation in a small forested catchment in Japan. *Journal of Forest Research* **8** (3): 179–190.

Kurita N. 2011. Origin of Arctic water vapor during the ice-growth season. *Geophysical Research Letters* **38** (2): 1–5.

de la Crétaz A, Barten P. 2007. Land use effects on streamflow and water quality in the northeastern United States. CRC Press: Boca Ratón, London, New York. 344 p.

Lai C, Ehleringer J. 2011. Deuterium excess reveals diurnal sources of water vapor in

forest air. *Oecologia* **165**: 213–223.

Landwehr J, Coplen T. 2004. Line-conditioned excess: a new method for characterizing stable hydrogen and oxygen isotope ratios in hydrologic systems. In *Aquatic Forum 2004: International Conference on Isotopes in Environmental Studies*International Atomic Energy Agency: Monaco; 132–134.

Landwehr J, Coplen T, Stewart D. 2014. Spatial, seasonal, and source variability in the stable oxygen and hydrogen isotopic composition of tap waters throughout the USA. *Hydrological Processes* **28** (21): 5382–5422.

Lane G, Dole M. 1956. Fractionation of Oxygen Isotopes during Respiration. *Science* **123** (3197): 574–576.

Lara A, Soto D, Armesto J, Donoso P, Wernli C, Nahuelhual L, Squeo F. 2003. Componentes Científicos Clave Para Una Política Nacional Sobre Usos, Servicios Y Conservación De Los Bosques Nativos Chilenos (A Lara, D Soto, J Armesto, P Donoso, C Wernli, L Nahuelhual, and F Squeo, eds). 111 p.

Lara A, Little C, Nahuelhual L, Urrutia R, Díaz I. 2015. Lecciones, desafíos y recomendaciones de política para el manejo, conservación y restautración de los bosques nativos en Chile. 281 - 327. In *Conservacion de La Biodiversidad En La Americas*.

Laudon H, Sjöblom V, Buffam I, Seibert J, Mörth M. 2007. The role of catchment scale and landscape characteristics for runoff generation of boreal streams. *Journal of Hydrology* **344** (3–4): 198–209.

Lee D, Kim J, Lee K, Kim S. 2010. Partitioning of catchment water budget and its implications for ecosystem carbon exchange. *Biogeosciences* **7** (7): 1903–1914.

Leibundgut C, Maloszewski P, Kulls C. 2009. *Tracers in Hydrology*. Wiley-Blackwell.

Leiva D, Carlyle-Moses D, Tanaka T. 2011. *Forest Hydrology and Biogeochemistry, Synthesis of past research and future directions* (D Levia, D Carlyle-Moses, and T Tanaka, eds). Springer-Verlag.

Lerman A, Imboden D, Gat J. 1995. *Physics and Chemistry of LAKES* (A Lerman, D Imboden, and J Gat, eds). Springer-Verlag: Berlin Heidelberg.

Little C, Soto D, Lara A, Cuevas J. 2008. Nitrogen exports at multiple-scales in a southern Chilean watershed (Patagonian Lakes district). *Biogeochemistry* **87** (3): 297–309.

Little C, Lara A, McPhee J, Urrutia R. 2009. Revealing the impact of forest exotic plantations on water yield in large scale watersheds in South-Central Chile. *Journal of Hydrology* **374** (1–2): 162–170.

Little C, Lara A. 2010. Ecological restoration for water yield increase as an ecosystem service in forested watersheds of south-central Chile. *Bosque* **31** (3): 175–178.

Little C, Cuevas J, Lara A, Pino M, Schoenholtz S. 2015. Buffer effects of streamside native forests on water provision in watersheds dominated by exotic forest

plantations. *Ecohydrology* **8** (7): 1205–1217.

Liu W, Li P, Li H, Duan W. 2006. Estimation of evaporation rate from soil surface using stable isotopic composition of throughfall and stream water in a tropical seasonal rain forest of Xishuangbanna, Southwest China. *Acta Ecologica Sinica* **26** (5): 1303–1310.

Locher-Krause K, Volk M, Waske B, Thonfeld F, Lautenbach S. 2017. Expanding temporakl resolution in landscape transformations: Insights from a landsat-based case study in Southern Chile. *Ecological Indicators* **75**: 132–144.

Lovett G, Weathers K, Sobczak W. 2000. Nitrogen Saturation and Retention in Forested Watersheds of the Catskill Mountains, New York. *Ecological Applications* **10** (1): 73–84.

Lozanos A. 2011. Relación entre el Caudal y la Exportación durante otoño en un bosque templado lluvioso en la cordillera de los andes, sur de Chile. MSc Thesis. Universidad Austral de Chile. 61 p.

Luz B, Barkan E, Yam R, Shemesh A. 2009. Fractionation of oxygen and hydrogen isotopes in evaporating water. *Geochimica et Cosmochimica Acta* **73** (22): 6697–6703.

Rivera, R. 2010. Patrones de transpiración y ajustes hidraulicos en plantaciones de Eucalyptus nitens durante su desarrollo. MSc. Thesis. Universidad Austral de Chile. 70 p.

Magrin G, Marengo J, Boulanger J, Buckeridge M, Castellanos E, Poveda G, Scarano F, Vicuña S, Alfaro E, Anthelme F, et al. 2014. IPCC, Climate Change 2014: Impacts, Adaptation, and Vulnerability. Chapter 27.

Manzoni S, Vico G, Porporato A, Katul G. 2013. Biological constraints on water transport in the soil-plant-atmosphere system. *Advances in Water Resources* **51**: 292–304.

Martens B, Miralles D, Lievens H, van der Schalie R, de Jeu R, Férnandez-Prieto D, Beck H, Dorigo W, Verhoest N. 2016. GLEAM v3: satellite-based land evaporation and root-zone soil moisture. *Geoscientific Model Development Discussions* 10, 1903-1925.

Martín-Goméz P, Barbeta A, Voltas J, Penuelas J, Dennis K, Palacio S, Dawson T, Ferrio J. 2015. Methods Isotope-ratio infrared spectroscopy: a reliable tool for the investigation of plant-water sources? *New Phytologist* **207**: 914–927.

Mathieu R, Bariac T. 1996. A numerical model for the simulation of stable isotope profiles in drying soils. *Journal of Geophysical Research* **101** (D7): 12685–12696.

Mazor E. 2004. Global Water Dynamics: Shallow and Deep Groundwater, Petroleum Hydrology, Hydrothermal Fluids, and Landscaping. Marcel Dekker, Inc.: New York. 416 p.

McDonnell J. 1990. A rationale for old water discharge through macropores in a steep,

humid catchment. *Water Resources Research* **26** (11): 2821–2832.

McDonnell J, Bonell M, Stewart M, Pearce A. 1990. Deuterium variations in storm rainfall: Implications for stream hydrograph separation. *Water Resources Research* **26** (3): 455–458.

McDonnell J. 2014. The two water worlds hypothesis: ecohydrological separation of water between streams and trees? *Wiley Interdisciplinary Reviews: Water* **1** (4): 323–329.

McGuire K, McDonnell J. 2010. Hydrological connectivity of hillslopes and streams: Characteristic time scales and nonlinearities. *Water Resources Research* **46** (10): 1–17.

van Meerveld H, Seibert J, Peters N. 2015. Hillslope-riparian-stream connectivity and flow directions at the Panola Mountain Research Watershed. *Hydrological Processes* **3574** (May): 3556–3574.

Meißner M, Köhler M, Schwendenmann L, Hölscher D, Dyckmans J. 2013. Soil water uptake by trees using water stable isotopes (δ2H and δ18O) a method test regarding soil moisture, texture and carbonate. *Plant and Soil* **376**: 1–9.

Merino A, Balboa M, Rodríguez-Soalleiro R, González J. 2005. Nutrient exports under different harvesting regimes in fast-growing forest plantations in southern Europe. *Forest Ecology and Management* **207** (3): 325–339.

Merlivat L, Coantic M. 1975. Study of Mass Transfer at the Air-Water Interference by an Isotopic Method. *Journal of Geophysical Research* **80** (20): 3455–3464.

Merlivat L. 1978. Molecular diffusivities of $H_2{}^{16}O$, $HD^{16}O$, and $H_2{}^{18}O$ in gases. *The Journal of Chemical Physics* **69** (6): 2864–2871.

Mickler R, Earnhardt T, Moore J. 2002. Regional estimation of current and future forest biomass. *Environmental pollution* **116 Suppl**: S7-16.

Miralles D, Jiménez C, Jung M, Michel D, Ershadi A, McCabe M, Hirschi M, Martens B, Dolman A, Fisher J, et al. 2015. The WACMOS-ET project – Part 2: Evaluation of global terrestrial evaporation data sets. *Hydrology and Earth System Sciences Discussions* **12** (10): 10651–10700.

Mohr C, Coppus R, Iroumé A, Huber A, Bronstert A. 2013. Runoff generation and soil erosion processes after clear cutting. *Journal of Geophysical Research* **118** (February): 814–831.

Nahuelhual L, Donoso P, Lara A, Núñez D, Oyarzún C, Neira E. 2006. Valuing Ecosystem Services of Chilean Temperate Rainforests. *Environment, Development and Sustainability* **9** (4): 481–499.

Nahuelhual L, Carmona A, Lara A, Echeverría C, González M. 2012. Land-cover change to forest plantations: Proximate causes and implications for the landscape in south-central Chile. *Landscape and Urban Planning* **107** (1): 12–20.

Van Noordwijk M, Namirembe S, Catacutan D, Williamson D, Gebrekirstos A. 2014. Pricing rainbow, green, blue and grey water: Tree cover and geopolitics of climatic teleconnections. *Current Opinion in Environmental Sustainability* **6** (1): 41–47.

Ocampo C, Sivapalan M, Oldham C. 2006. Hydrological connectivity of upland-riparian zones in agricultural catchments: Implications for runoff generation and nitrate transport. *Journal of Hydrology* **331** (3–4): 643–658.

Oerter E, Finstad K, Schaefer J, Goldsmith G, Dawson T, Amundson R. 2014. Oxygen isotope fractionation effects in soil water via interaction with cations (Mg, Ca, K, Na) adsorbed to phyllosilicate clay minerals. *Journal of Hydrology* **515**: 1–9.

Oeurng C, Sauvage S, Sánchez-Pérez J-M. 2010. Temporal variability of nitrate transport through hydrological response during flood events within a large agricultural catchment in south-west France. *The Science of the total environment* **409** (1): 140–149.

Or D, Tuller M. 1999. Liquid retention and interfacial area in variably staurated porous media: Upscaling from single- pore to sample scale model. *Water Resources Research* **35** (12): 3591–3605.

Or D, Lehmann P, Shahraeeni E, Shokri N. 2013. Advances in Soil Evaporation Physics—A Review. *Vadose Zone Journal* **12** (4): 1-16.

Orlowski N, Breuer L, McDonnell J. 2015. Critical issues with cryogenic extraction of soil water for stable isotope analysis. *Ecohydrology* **9**(1): 3-10.

Orlowski N, Pratt D, Mcdonnell J. 2016. Intercomparison of soil pore water extraction methods for stable isotope analysis. *Hydrological Processes* 30 (19): 3434-3449.

Ostrom E. 2009. A General Framework for Analyzing Sustainability of Socio-Ecological Systems. *Science* **325** (1900): 419–421.

Oyarzún C, Campos H. 1997. Exportación de nutrientes en microcuencas con distinto uso del suelo en el sur de Chile (Lago Rupanco, X Región). *Revista Chilena de Historia Natural* **70**: 507–519.

Oyarzún C, Godoy R, Sepulveda A. 1998. Water and nutrient fluxes in a cool temperate rainforest at the Cordillera de la Costa in southern Chile. *Hydrological Processes* **12** (7): 1067–1077.

Oyarzún C, Huber A. 1999. Water Balance in Young Plantations of Eucalyptus globulus and Pinus radiata in Southern Chile. *TERRA Latinoamericana* **17**: 35–44.

Oyarzún C, Huber A. 2003. Nitrogen export from forested and agricultural watersheds. *Bosque* **60** (1): 63–68.

Oyarzún C, Godoy R, Schrijver A, Staelens J, Lust N. 2004. Water chemistry and nutrient budgets in an undisturbed evergreen rainforest of southern chile. *Biogeochemistry* **71**: 107–123.

Oyarzún C, Godoy R, Staelens J, Aracena C, Proschle J. 2005. Nitrogen fluxes in a Nothofagus obliqua forest and a Pinus radiata plantationin the central valley of southern Chile. *Gayana Botanica* **62** (2): 86–95.

Oyarzún C, Aracena C, Rutherford P, Godoy R, Deschrijver A. 2007. Effects of Land Use Conversion from Native Forests to Exotic Plantations on Nitrogen and Phosphorus Retention in Catchments of Southern Chile. *Water Air & Soil pollution* **179**: 341–350.

Oyarzún C, Frêne C, Lacrampe G, Huber A, Hervé P. 2011. Propiedades hidrológicas del suelo y exportación de sedimentos en dos microcuencas de la Cordillera de la Costa en el sur de Chile con diferente cobertura vegetal Soil hydrological properties and sediment transport in two headwater catchments with differe. *Bosque* **32** (1): 10–19.

Oyarzún C, Hervé-Fernández P, Frêne C. 2012. Effects of Land use changes and management practices on water yield in native forests and exotic plantations in Southern Chile. In *Forest Management: Technology, Practices and Impact.*, Bonilla A, , Guzman R (eds).NOVA Publishers, Inc.: New York; 79–101.

Oyarzún C, Hervé-Fernández P. 2015. Ecohidrology and Nutrient Fluxes in Forest Ecosystems of Southern Chile. In *Biodiversity in Ecosystems - Linking Structure and Function* 353–370.

Oyarzún C, Hervé-Fernández P, Huygens D, Boeckx P, Verhoest N. 2015. Hydrological Controls on Nutrient Exportation from Old-Growth Evergreen Rainforests and Eucalyptus nitens Plantation in Headwater Catchments at Southern Chile. *Open Journal of Modern Hydrology* **5** (3): 19–31.

Di Paolo E, Mammarella A, Ercole M, Piacente E, Pisante M. 2001. Yield, water use efficiency, soil water depletion of relay intercropping corn in response to tillage techniques and irrigation regime. In *1st World Congress on Conservation Agriculture*1–5.

Parron LM, Bustamante MMC, Markewitz D. 2010. Fluxes of nitrogen and phosphorus in a gallery forest in the Cerrado of central Brazil. *Biogeochemistry* **105** (1–3): 89–104.

Penna D, Oliviero O, Assendelft R, Zuecco G, van Meerveld H, Anfodillo T, Carraro V, Borga M, DallaFontana G. 2013. Tracing the Water Sources of Trees and Streams: Isotopic Analysis in a Small Pre-Alpine Catchment. *Procedia Environmental Sciences* **19**: 106–112.

Perakis S, Hedin L. 2002. Nitrogen loss from unpolluted South American forests mainly via dissolved organic compounds. *Nature* **415** (6870): 416–419.

Perakis S, Hedin L. 2007. State factor relationships of dissolved organic carbon and nitrogen losses from unpolluted temperate forest watersheds. *Journal of Geophysical Research* **112**: 1-7.

Peters L, Yakir D. 2008. A direct and rapid leaf water extraction method for isotopic analysis. *Rapid Communications in Mass Spectrometry* **22**: 2929–2936.

Peterson B, Wollheim W, Mulholland P, Webster J, Meyer J, Tank J, Marti E, Bowden W, Valett H, Hershey A, et al. 2001. Control of nitrogen export from watersheds by headwater streams. *Science (New York, N.Y.)* **292** (5514): 86–90.

Petry J, Soulsby C, Malcolm I a., Youngson a. F. 2002. Hydrological controls on nutrient concentrations and fluxes in agricultural catchments. *Science of the Total Environment* **294** (1–3): 95–110.

Phillips F. 2010. Soil-water bypass. *Nature Geoscience* **178** (3–4): 162–175.

van der Plas F, Manning P, Soliveresa S, Allana E, Scherer-Lorenzen M, Verheyen K, Wirthe C, Zavalag M, Ampoorter E, Baeten L, Barbaro L, Bauhus J, Benavides R, Benneter A, Bonall D, Bouriaud O, Bruelheide H, Bussotti F, Carnol M, Castagneyrol B, Charbonnier Y, Coomes D, Coppi A, Bastias C, Dawuds, S, De Wandeler H, Domisch T, Finér L, Gessler A, Granier A, Grossiord C, Guyot V, Hättenschwiler S, Jactel H, Jaroszewicz B, Joly F, Jucker T, Koricheva J, Milligana H, Mueller S, Muys B, Nguyenb D, Pollastrini M, Ratcliff S, Raulund-Rasmussens K, Selvi F, Stenlid J, Valladares F, Vesterdal L, Zielínski D, Fischer M. 2016. Biotic homogenization can decrease landscape-scale forest multifunctionality. *Proceedings of the National Academy of Sciences* **113** (13): 3557–3562.

Ponette-González A, Weathers K, Curran L. 2010. Tropical land-cover change alters biogeochemical inputs to ecosystems in a Mexican montane landscape. *Ecological applications* **20** (7): 1820–1837.

Poor C, McDonnell J. 2007. The effects of land use on stream nitrate dynamics. *Journal of Hydrology* **332** (1–2): 54–68.

Prentice I, Farquhar G, Fasham M. 2001. The carbon cycle and atmospheric carbon dioxide DOI: 10.1256/004316502320517344

Puckett L. 1991. Spatial variability and collector requirements for sampling throughfall volume and chemistry under a mixed-hardwood canopy. *Canadian Journal of Forest Research* **21**: 1581–1588.

Le Quéré C, Andres R, Boden T, Conway T, Houghton R, House J, Marland G, Peters G, Van Der Werf G, Ahlström A, et al. 2013. The global carbon budget 1959-2011. *Earth System Science Data* **5** (1): 165–185.

Rayleigh J. 1895. Theoretical considerations respecting the separation of Gases by diffusion and similar processes. *Philosophical Magazine Series 5* **42** (259): 493–498.

Rinaldo A, Benettin P, Harman C, Hrachowitz M, McGuire K, van der Velde Y, Bertuzzo E, Botter G. 2015. Storage selection functions: A coherent framework for quantifying how catchments store and release water and solutes. *Water Resources Research* **51** (6): 4840–4847.

Rothe A, Huber C, Kreutzer K, Weis W. 2002. Deposition and soil leaching in stands of Norway spruce and European Beech: Results from the Hoglwald research in

comparison with other European case studies. *Plant and Soil* **240** (1): 33–45.

Rozanski K. 1985. Deuterium and oxygen-18 in European groundwaters — Links to atmospheric circulation in the past. *Chemical Geology: Isotope Geoscience section* **52** (3–4): 349–363.

Rozanski K, Araguás-Araguás L, Gonfiantini R. 1993. Isotopic Pattern in Modern Global Precipitations. In *Climate Change in Continental Isotopic Records, Geophysical Monograph* 1–36.

Sala O, Chapin S, Armesto J, Berlow E, Bloomfield J, Dirzo R, Huber-sanwald E, Huenneke L, Jackson R, Kinzig A, Leemans R Lodge D, Mooney H, Oesterheld M, LeRoy Poff N, Sykes M, Walker B, Walker M, Wall D. 2000. Global Biodiversity Scenarios for the Year 2100. *Science* **287**: 1770–1774.

Salati E, Dall'Olio A, Matsui E, Gat J. 1979. Recycling of water in the Amazon basin: an isotopic study. *Water Resources Research* **15** (5): 1250–1258.

Salazar O, Casanova M, Luzio W. 2005. Correlation between world reference base and soil taxonomy for the soils from the Xth region, Chile. *Revista de la ciencia del suelo y nutrición vegetal* **5** (2): 35–45.

Salmon C, Walter M, Hedin L, Brown M. 2001. Hydrological controls on chemical export from an undisturbed old-growth Chilean forest. *Journal of Hydrology* **253** (1–4): 69–80.

San Martín C, Ramirez C, Figueroa H, Ojeda N. 1991. Estudio sinecológico del bosque de roble-laurel-lingue del centro-sur de Chile. *Bosque* **12** (2): 11–27.

Schlesinger W, Jasechko S. 2014. Transpiration in the global water cycle. *Agricultural and Forest Meteorology* **189**–**190**: 115–117.

Scholl M, Gingerich S, Tribble G. 2002. The influence of microclimates and fog on stable isotope signatures used in interpretation of regional hydrology : East Maui , Hawaii. *Journal of Hydrology* **264**: 170–184.

Scholl M, Giambelluca T, Gingerich S, Nullet M, Loope L. 2007. Cloud water in windward and leeward mountain forests: The stable isotope signature of orographic cloud water. *Water Resources Research* **43** (12): 1–13.

Scholl M, Eugster W, Burkard R. 2011. Understanding the role of fog in forest hydrology: stable isotopes as tools for determining input and partitioning of cloud water in montane forests. *Hydrological Processes* **25** (3): 353–366.

de Schrijver A, Geudens G, Augusto L, Staelens J, Mertens J, Wuyts K, Gielis L, Verheyen K. 2007. The effect of forest type on throughfall deposition and seepage flux: a review. *Oecologia* **153** (3): 663–674.

Schuller P, Walling D, Iroumé A, Quilodrán C, Castillo A, Navas A. 2013. Using 137Cs and 210Pbex and other sediment source fingerprints to document suspended sediment sources in small forested catchments in south-central Chile. *Journal of Environmental Radioactivity* **124**: 147–159.

Schwartz MW, Brigham C a., Hoeksema JD, Lyons KG, Mills MH, van Mantgem PJ. 2000. Linking biodiversity to ecosystem function: implications for conservation ecology. *Oecologia* **122** (3): 297–305.

Seibt U, Rajabi A, Griffiths H, Berry J a. 2008. Carbon isotopes and water use efficiency: Sense and sensitivity. *Oecologia* **155** (3): 441–454.

Skrzypek G, Mydłowski A, Dogramaci S, Hedley P, Gibson J, Grierson P. 2015. Estimation of evaporative loss based on the stable isotope composition of water using 'Hydrocalculator'. *Journal of Hydrology* **523**: 781–789.

Soderberg K, Good S, Wang L, Caylor K. 2012. Stable Isotopes of Water Vapor in the Vadose Zone: A Review of Measurement and Modeling Techniques. *Vadose Zone Journal* **11** (3): 1-14.

Solan M, Batty P, Bulling M, Godbold J. 2010. How biodiversity affects ecosystem processes: implications for ecological revolutions and benthic ecosystem function. *Aquatic Biology* **2** (3): 289–301.

Soto-Schönherr S, Iroumé A. 2016. How much water do Chilean forests use? A review of interception losses in forest plot studies. *Hydrological Processes* **30** (25): 4674–4686.

Soulsby C, Petry J, Brewer MJ, Dunn SM, Ott B, Malcolm I a. 2003. Identifying and assessing uncertainty in hydrological pathways: A novel approach to end member mixing in a Scottish agricultural catchment. *Journal of Hydrology* **274** (1–4): 109–128.

Sprenger M, Herbstritt B, Weiler M. 2015. Established methods and new opportunities for pore water stable isotope analysis. *Hydrological Processes* **29** (25): 5174–5192.

Sprenger M, Leisert H, Gimbel K, Weiler M. 2016. Illuminating hydrological processes at the soil-vegetation-atmosphere interfase with water stable isotopes. *Reviews of Geophysics* **54** (3): 674–704.

Squeo F, Aravena R, Aguirre E, Pollastri A, Jorquera C, Ehleringer J. 2006. Groundwater dynamics in a coastal aquifer in north-central Chile : Implications for groundwater recharge in an arid ecosystem. *Journal of Arid Environments* **67** (2): 240–254.

Staelens J, Godoy R, Oyarzún C, Thibo K, Verheyen K. 2005. Nitrogen Fluxes in Throughfall and Litterfall in Two Nothofagus Forests in Southern Chile. *Gayana. Botánica* **62** (2): 63–71.

Steppe K, De Pauw D, Doody T, Teskey R. 2010. A comparison of sap flux density using thermal dissipation, heat pulse velocity and heat field deformation methods. *Agricultural and Forest Meteorology* **150** (7–8): 1046–1056.

Stewart M. 1975. Stable isotope fractionation due to evaporation and isotopic exchange of falling water drops: Applications to atmospheric processes and evaporation of lakes. *Journal of Geophysical Research* **80** (9): 1133–1146.

Strahm BD, Harrison RB. 2006. Nitrate Sorption in a Variable-Charge Forest Soil of the Pacific Northwest. *Soil Science* **171** (4): 313–321.

Strange E, Fausch K, Covich A. 1999. Sustaining Ecosystem Services in Human-Dominated Watersheds: Biohydrology and Ecosystem Processes in the South Platte River Basin. *Environmental management* **24** (1): 39–54.1

Sutanto S, Wenninger J, Coenders-Gerrits A, Uhlenbrook S. 2012. Partitioning of evaporation into transpiration, soil evaporation and interception: a comparison between isotope measurements and a HYDRUS-1D model. *Hydrology and Earth System Sciences* **16** (8): 2605–2616.

Taiz L, Zeiger E. 2010. Plant Physiology, Fifth Edition. Sinauer Associates. Sunderland, MA.

Tang K, Feng X. 2001. The effect of soil hydrology on the oxygen and hydrogen isotopic compositions of plants' source water. *Earth and Planetary Science Letters* **185** (3–4): 355–367.

Taylor PJ, Nuberg IK, Hatton TJ. 2001. Enhanced transpiration in response to wind effects at the edge of a blue gum (Eucalyptus globulus) plantation. *Tree physiology* **21** (6): 403–408.

Thomas Q, Canham C, Weathers K, Goodale C. 2009. Increased tree carbon storage in response to nitrogen deposition in the US. *Nature Geoscience* **3** (1): 13–17.

Thorntwaite C. 1948. An Approach toward a Rational Classification of Climate. *American Geographical Society* **38** (1): 55–94.

Tromp-van Meerveld H, McDonnell J. 2006a. Threshold relations in subsurface stormflow: 1. A 147-storm analysis of the Panola hillslope. *Water Resources Research* **42** (2): 1–11.

Tromp-van Meerveld H, McDonnell J. 2006b. Threshold relations in subsurface stormflow: 2. The fill and spill hypothesis. *Water Resources Research* **42** (2): 1–11.

Tsujimura M, Tanaka T. 1998. Evaluation of evaporation rate from forested soil surface using stable isotopic composition of soil water in a headwater basin. *Hydrological Processes* **12** (13–14): 2093–2103.

Tuller M, Or D, Dudley L. 1999. Adsorption and capillary condensation in porous media: Liquid retention and interfacial configurations in angular pores. *Water Resources Research* **35** (7): 1949–1964.

Uhlenbrook S, Frey M, Leibundgut C, Maloszewski P. 2002. Hydrograph separations in a mesoscale mountainous basin at event and seasonal timescales. *Water Resources Research* **38** (6): 1-14.

Uyttendaele G, Iroumé A. 2002. The solute budget of a forest catchment and solute fluxes within a Pinus radiata and a secondary native forest site, southern Chile. *Hydrological Processes* **16** (13): 2521–2536.

Vermette S, Drake J. 1987. Simplified wet-only and sequential fraction rain collector. *Atmospheric Environment* **21** (3): 715–716.

Vitousek P, Mooney H, Lubchenco J, Melillo J. 1997. Human Domination of Earth's Ecosystems. *Science* **277** (5325): 494–499.

Vitousek P, Porder S, Houlton B, Chadwick O. 2010. Terrestrial phosphorus limitation: mechanisms, implications, and nitrogen-phosphorus interactions. *Ecological applications: a publication of the Ecological Society of America* **20** (1): 5–15.

Walden L, Harper R, Mendham D, Henry D, Fontaine J. 2015. Eucalyptus reforestation induces soil water repellency. *Soil Research* **53**: 168–177.

Wang L, Niu S, Good S, Soderberg K, McCabe M, Sherry R, Luo Y, Zhou X, Xia J, Caylor K. 2013. The effect of warming on grassland evapotranspiration partitioning using laser-based isotope monitoring techniques. *Geochimica et Cosmochimica Acta* **111**: 28–38.

Warren J, Meinzer F, Brooks J, Domec J. 2005. Vertical stratification of soil water storage and release dynamics in Pacific Northwest coniferous forests. *Agricultural and Forest Meteorology* **130** (1–2): 39–58.

Weathers K, Lovett G, Likens G, Caraco N. 2000. Cloudwater Inputs of Nitrogen to Forest Ecosystems in Southern Chile: Forms, Fluxes, and Sources. *Ecosystems* **3** (6): 590–595.

Wenninger J, Beza D, Uhlenbrook S. 2010. Experimental investigations of water fluxes within the soil-vegetation-atmosphere system: Stable isotope mass-balance approach to partition evaporation and transpiration. *Physics and Chemistry of the Earth* **35** (13–14): 565–570.

West A, Patrickson S, Ehleringer J. 2006. Water extraction times for plant and soil materials used in stable isotope analisys. *Rapid Communications in Mass Spectrometry* **20**: 1317–1321.

Whitehead D, Beadle C. 2004. Physiological regulation of productivity and water use in *Eucalyptus*: a review. *Forest Ecology and Management* **193**: 113–140.

Williams D, Cable W, Hultine K, Hoedjes J, Yepez E, Simonneaux V, Er-Raki S, Boulet G, de Bruin H, Chehbouni A, et al. 2004. Evapotranspiration components determined by stable isotope, sap flow and eddy covariance techniques. *Agricultural and Forest Meteorology* **125** (3–4): 241–258.

De Wispelaere L, Bodé S, Hervé-Fernández P, Hemp A, Verschuren D, Boeckx P. 2017. Plant water resource partitioning and xylem-leaf deuterium enrichment in a seasonally dry tropical climate. *Biogeosciences* **14**: 73–88.

Xu C-Y, Singh VP. 1998. A Review on Monthly Water Balance Models for Water Resources Investigations. *Water Resources Management* **12** (1): 20–50.

Zamorano-Elgueta C, Rey Benayas J, Cayuela L, Hantson S, Armenteras D. 2015. Native forest replacement by exotic plantations in southern Chile (1985-2011) and partial compensation by natural regeneration. *Forest Ecology and*

Management **345**: 10–20.

Zhang C, Fu S. 2009. Allelopathic effects of eucalyptus and the establishment of mixed stands of eucalyptus and native species. *Forest Ecology and Management* **258** (7): 1391–1396.

Zhang W. 2012. Did Eucalyptus contribute to environment degradation? Implications from a dispute on causes of severe drought in Yunnan and Guizhou, China. *Environmental Skeptics and Critics* **1** (2): 34–38.

Zhang Z, Chen X, Shi P, Ou G. 2013. Study of canopy transpiration based on a distributed hydrology model in a small karst watershed of southwest China. *Carbonates and Evaporites* **28** (1–2): 111–117.

Zhang Z, Evaristo J, Si B, Li Z, McDonnell J. 2017. Tritium analysis shows apple trees may be transpiring water several decades old. *Hydrological Processes* **31** (5): 1196–1201.

Zhao M, Zeng C, Liu Z, Wang S. 2010. Effect of different land use/land cover on karst hydrogeochemistry: A paired catchment study of Chenqi and Dengzhanhe, Puding, Guizhou, SW China. *Journal of Hydrology* **388**: 121–130.

Zimmermann U, Ehhalt D, Münnich K. 1967. Soil-Water movement and evapotranspration: changes in the isotopic composition of the water. In *Conference on Isotopes in Hydrology*Vienna; 567–585.

Personal Information

Full Name: Pedro Alejandro Hervé (24/08/1981, Valdivia, Chile).
Nationality: Chilean / French
Email: pedroherve@gmail.com

Education: 2012-2017, PhD, Applied Biological Sciences, Ghent University, Ghent, Belgium.
Thesis Supervisors: Prof. ir. Niko Verhoest and Prof. ir. Pascal Boeckx. Thesis: "Ecohydrological assessment of catchments covered with old-growth native evergreen forest and eucalyptus plantations, in south-central Chile".

2009-2011, MSc, in Hydrological Resources, Universidad Austral de Chile (UACh), Chile.
Thesis supervisor: Prof. dr. Carlos Oyarzún. Thesis: "Hydrological controls over nutrient exports in catchments with different land cover in southern Chile".

2006-2007, Environmental Biologist, UACh, Chile.
Profesional practice: Laboratory quality analyst, Waste water treatment plant, AGUAS DECIMA, Valdivia, Chile.

2001-2007, Licentiate in Biological Sciences, UACh, Chile.
Thesis supervisor: Prof. dr. Sandor Mulsow. Thesis: "Effect of β radiation on the behavior of the terrestrial isopod *Porcellio scaber* (Latreille, 1804)"

Web: https://www.researchgate.net/profile/Pedro_Herve-Fernandez

Working Experience

2012 (April) – 2015 (April), Researcher. Project: "Ecohydrological controls on nutrient export from forested headwater catchments in southern Chile". PI: Prof. dr. Carlos Oyarzún. Institute of Earth Sciences, UACh, Chile.

2011 (October) – 2012 (March), Gamma spectrometry laboratory and field technician. Project: "Sediment fingerprinting and sources in catchments covered with *Eucalyptus* sp. and *Pinus* sp". PI: Prof. dr. Paulina Schüller Radioecology laboratory, Institute of Chemical sciences, UACh, Chile.

2011 (March) – 2011 (July). Environmental sciences course lecturer. Department of History and Geography, Universidad San Sebastián, Chile. (40 students).

2009 (January) – 2011 (October), Researcher. Project: "Water yield, seasonal growth, vegetation and transpiration rate of small headwater catchments in southern Chile". PI: Prof. dr. Carlos Oyarzún. Institute of Earth Sciences, UACh, Chile.

2008 (April – July), Isotopes and radiotracers in ecotoxicology and pollution studies. Researcher. Project: IAEA CHI07-11, “Use of radioactive tracers (^{109}Cd) to study accumulation and depuration kinetics of cadmium, absorbed through dissolved and particulated pathways in *Mytilus chilensis* (Hupe, 1854)”. Marine Environmental Laboratory (MEL), International Atomic Energy agency (IAEA), Monaco, Monaco.

Other professional activities

2016, JOINT EUROPEAN STABLE ISOTOPES USER group MEETING (JESIUM). Ghent University. Belgium. 4–9 September. Geosciences and Hydrology chairman.

2016, Tracer hydrology consultancy, Mina Invierno (Coal Mine). Punta Arenas, Chile.

2016, Peer-reviewer for: Hydrological Processes (2016); Journal of Hydrology (2017); European Journal of Soil Science (2017); Biogeosciences (2017); and Catena (2017).

2015, Isotopes in Hydrology course colaborator. Principal lecturers: Prof. dr. Andrés Iroumé, Prof. dr. Paulina Schüller (UACh) and Prof. dr. Jeff McDonnell (Saskatoon University, Canada). January 5 – 9, UACh, Chile.

2015, Isotope hydrology consultancy, BIOFOREST S.A., Concepción, Chile.

2015, Thesis guidance during stable isotope experiments and evaluation in MSc. in Bioscience engineering: Forest and Nature Management. Student: Jeroen Schreel, Ghent University, Belgium.

2014, Thesis guidance during stable isotope experiments in MSc. in Bioscience engineering: Forest and Nature Management. Student: Shihab Uddin. Ghent University, Belgium.

Publications

Peer-reviewed indexed articles:

Berry, Z.; J. Evaristo; G. Moore; M. Poca; K. Steppe; L. Verrot; H. Asbjornsen; L. Borma; M. Bretfeld; **P. Hervé-Fernández**; M. Seyfried; L. Schwendenmann; K. Sinacore and L. De Wispelaere and J. McDonnell. The two water worlds hypothesis: Addressing alternative hypotheses and proposing a way forward. *Ecohydrology,* doi: 10.1002/eco.1843.

De Wispelaere, L., Bodé, S., **Hervé-Fernández, P.**, Hemp, A., Verschuren, D. and P. Boeckx. (2017). Plant water resource partitioning and isotopic

fractionation during transpiration in a seasonally dry tropical climate. *Biogeosciences*, 14: 73–88.

Hervé-Fernández P., Oyarzún C., Huyghens D., Verhoest N.E.C. and P. Boeckx. (2016). Assessing the “two water worlds hypothesis” for native and exotic evergreen species in south-central Chile, *Hydrological processes*, 30(23): 4225-4445.

Hervé-Fernández P., Oyarzún C. and S. Woelfl. (2016). Throughfall enrichment and stream nutrient chemistry in small headwater catchments with different land cover in southern Chile. *Hydrological Processes*, 30(26): 4944-4955.

Oyarzún, C.; C. Frêne; G. Lacrampe; A. Huber & **P. Hervé**. (2011). Land use, sediments transport and soil hydrological properties in two headwater catchments at the Coastal Mountain Range in southern Chile. *Bosque*. 32(1): 10-19.

Houlbrèque, F.; **P. Hervé-Fernández**, J. Teyssié; F. Oberhaënsli; S. Mulsow; F. Boisson and R. Jeffree. (2011). Cadmium bioaccessibility from Chilean mussels to humans using simulated digestion method. *Food Chemistry*. 126(3): 917 - 921.

Hervé-Fernández, P.; F. Houlbrèque, F. Boisson, S. Mulsow; J. Teyssié; F. Oberhaënsli; S. Azemard and R. Jeffree. (2010). Cadmium bioaccumulation and retention kinetics in the Chilean blue mussel *Mytilus chilensi*s: seawater and food exposure pathways. *Aquatic Toxicology*. 99(4): 448 - 456.

Peer-reviewed non-indexed articles

Oyarzún, C.; **Hervé-Fernández, P.**; Huyghens, D.; Boeckx, P. and N. E. C. Verhoest. (2015). Hydrological controls on nutrient exportation from Old-growth evergreen rainforests and *Eucalyptus nitens* plantation in headwater catchments at Southern Chile (40°S). *Open Journal of Modern Hydrology*. 5(2): 19 - 31.

Published book Chapters:

Oyarzún, C. & **P. Hervé-Fernández** (2014). Ecohydrology and nutrient fluxes in forest ecosystems of southern Chile. In "Biodiversity in Ecosystems - Linking Structure and Function". InTechOpen publishers. Editors: Juan A. Blanco and Yueh-Hsin Lo.

Oyarzún, C.; **P. Hervé-Fernández** and C. Frêne. (2012). Effects of Land Use Changes and Management Practices on Water Yield in Native Forests and Exotic Plantations in Southern Chile. In Forest Management: Technology, Practices and Impact. Nova publishers. Editors: Armando C. Bonilla Cruz and Ramona E. Guzmán Correa.

Workshops and Trainings

2015, Aberdeen Catchment Summer Science School, August 20 – 25, University of Aberdeen, Scotland. Course lecturers: D. Tetzlaff; J. McDonnell; C. Soulsby; R. Hopper and K. Beven.

2015, Isotopes in Hydrology, January 5 – 9, UACh, Chile. Course lecturers: A. Iroumé; J. McDonnell; P. Schüller

2009, Advanced biogeochemistry and aerosol transport modelling over long distances, September 8 – 14, UACh, Chile. Course lecturers: R. Godoy and J. Boy.

2008, Isotopes and Radiotracers in Ecotoxicology and Pollution studies, from April 1st until July 30, Marine Environmental Laboratory (MEL), International Atomic Energy agency (IAEA), Monaco. Monaco.

2008, Radiation protection course, June 19th, Marine Environmental Laboratory (MEL), IAEA. Monaco, Monaco.

Academic Awards and Fellowships

2017, M. G. Anderson Award Outstanding Paper of the Year, for: Assessing the “two water worlds hypothesis” for native and exotic evergreen species in south-central Chile, Hydrological processes, 30(23): 4225-4445.

2016, Bijzonder Onderzoeksfonds (BOF), finishing PhD scholarship (6 months).

2013, 2014, 2015 and 2016, Commissie Wetenschappelijk Onderzoek (CWO), Travel grants.

2010, Programa de Personal Avanzado, CONICYT, BECAS CHILE. PhD scholarship (4 years, from 2012 to 2016).

2009, 2010, Academic/Research assistance scholarship, UACh, Chile.

2008, Isotopes and radiotracers in ecotoxicology and pollution studies, from April 1st until July 30 MEL-IAEA. Monaco, Monaco.

2008, Solidarity Award, recognition to the undergraduate student that has excelled for their outstanding human qualities.

Memberships in scientific associations

European Geoscience Union (EGU, 2015).
Benelux Association for Stable Isotope Scientists (BASIS, 2014).
Soil Society of Belgium (SSSB, 2014).

Conference presentations (**presenter*)

Oral presentations:

De Wispelaere, L*; S. Bodé; **P. Hervé-Fernández**; A. Hemp; D. Verschuren and P. Boeckx. (2017). Plant phenological water cycle and implications for using δ²H-alkanes as paleo proxy in a semi-arid tropical climate. Benelux Association of Stable Isotope uSers (BASIS). Uthrecht, The Netherlands.

De Deurwaerder, H.*; **P. Hervé-Fernández**; C. Stahl; D. Bonal; B. Burbain; P. Boeckx and H. Verbeeck. (2017). A stable isotopic view on lianas' and trees' below ground competition for water. European Geoscience Union (EGU), Vienna, Austria.

Orlowski, N.*, L. Breuer, CIC team†, and J. McDonnell. (†CIC team: Angeli, N., Brumbt, C., Cook, C., Dubbert, M., Dyckmans, J., Gallagher, B., Gralher, B., Herbstritt, B., **Hervé-Fernández, P.**, Hissler, C., Koeniger, P., Legout, A., Macdonald, C., Oyarzún, C., Redelstein, R., Seidler, C., Siegwolf, R., Stumpp, C., Thomsen, S. and M. Weiler). (2016). Worldwide interlaboratory comparison of cryogenic water extraction systems for soil water stable isotope analysis. American Geoscience Union (AGU), San Francisco, USA.

De Deurwaerder, H.*; **P. Hervé-Fernández**; C. Stahl; D. Bonal; B. Burbain; P. Boeckx and H. Verbeeck. (2016). "A stable isotopic view on lianas' and trees' below ground competition for water". Joint European Stable Isotope User group Meeting (JESIUM). Ghent, Belgium.

Orlowski, N.*; Breuer, L.; CIC team (N. Angeli; C.; Boeckx, P.; Brumbt; C. Cook; M. Dubbert; J. Dyckmans; B. Gallagher; B. Gralher; B. Herbstritt; **P. Hervé-Fernández;** C. Hissler; P. Koeniger; A. Legout; C. Macdonald; C. Oyarzún; R. Redelstein; C. Seidler; R. Siegwolf; C. Stumpp; S. Thomsen; M. Weiler) & Jeffrey J. McDonnell. (2016). "Worldwide interlaboratory comparison of cryogenic water extraction systems for stable water isotope analysis". Joint European Stable Isotope User group Meeting (JESIUM). Ghent, Belgium.

De Deurwaerder, H.*; **P. Hervé-Fernández**; C. Stahl; D. Bonal; B. Burban; P. Boeckx and H. Verbeek. (2016). "Tapping another source: lianas' and trees' below ground competition for water". Association for Tropical Biology and Conservation (ATBC), Montpellier, France.

Hervé-Fernández, P.*; Oyarzún, C.; Huyghens, D.; Boeckx, P. and N.E.C. Verhoest. (2015). "The two water worlds, a stable isotope perspective on trees water sources in south central Chile (40°S)". Boussinesq lecture. Amsterdam, The Netherlands.

Hervé-Fernández, P.*; Oyarzún, C.; Boeckx, P. and N. E. C. Verhoest. (2015). "Water sources for native old growth and fast growing exotic plantation ecosystems in southern Chile". Benelux Association of Stable Isotope Scientists (BASIS). Utrecht, The Netherlands.

Hervé-Fernández, P.*; Oyarzún, C.; Huyghens, D.; Boeckx, P. and N. E. C. Verhoest. (2014). "Differential hydrological strategies: a stable isotope perspective on trees water sources". Soil Science Society Belgium. Brussels, Belgium (SSSB).

Oyarzún, C.*; **P. Hervé-Fernández**; Boeckx, P. and N. E. C. Verhoest. (2013). "Using stable isotopes to assess hydrological flow paths in small catchments with native evergreen forests and eucalyptus plantation in southern Chile". 17th International Soil Conservation Organization (ISCO). Medellín, Colombia.

Oyarzún, C.* and **P. Hervé-Fernández**. (2012). "Hydrologic controls over nutrient exportation in native and exotic plantation in southern Chile". International Congress on Ecosystem Services in the Neotropics: State of the art and future challenges. Asunción, Paraguay.

Oyarzún, C.; G. Lacrampe; Frêne, C.* and **P. Hervé-Fernández.** (2012). "Soil use, erosion rates in headwater catchments in the coastal mountain range, southern Chile". 16th Congress of the International Soil Conservation Organization (ISCO). Santiago, Chile.

Hervé-Fernández, P.* and C. Oyarzún. (2011). "Nitrogen and phosphorus fluxes in headwater catchments with different land cover in southern Chile". IX Congreso de la sociedad Chilena de Limnología. Valdivia, Chile.

Hervé-Fernández, P.* and C, Oyarzún. (2010). "Hydrological controls in soluble nitrogen exportation in two headwater catchments with different land cover in the coastal mountain range. Is there a loser?". VIII Congreso de la sociedad Chilena de Limnología. Villarrica, Chile.

Mulsow, S.*; F. Bravo; B. Cisternas; F. Docmac; M. T. Castro; B. García; **P. Hervé** and M. Manzano. (2008). Estimación de la tasa de bioperturbación en sedimentos mediante análisis fotografico pixel x pixel. XXVI Congreso de Ciencias del Mar. Iquique, Chile.

Hervé, P.*; S. Mulsow and M. Soto-Gamboa. (2006). Efecto de la radiación β en el comportamiento del isópodo terrestre *Porcellio scaber* (Latreille, 1804). !er Congreso de Biociencias. Valdivia, Chile.

Poster presentations:

De Wispelaere, L.*; S. Bodé; **P. Hervé-Fernández**; A. Hemp; D. Verschuren and P. Boeckx. (2017). “Plant phenological water cycle and implications for using δ²H-alkanes as paleo proxy in a semiarid tropical climate”. European Geoscience Union (EGU), Vienna, Austria.

De Wispelaere, L.*; S. Bodé; **P. Hervé-Fernández**; A. Hemp; D. Verschuren & P. Boeckx. (2016). “Partitioning of water resources and xylem-leaf deuterium enrichment in seasonally dry Tanzania”. Joint European Stable Isotope User group Meeting (JESIUM). Ghent, Belgium.

Poca, M.*; **P. Hervé-Fernández**; D. Gurvich; A. Cingolani; E. Jobbágy; P. Boeckx. (2016). “Evidence for the two water worlds hypothesis from highland seasonal ecosystems of central Argentina”. AGU Chapman conference: Emerging issues in tropical Ecohydrology. Cuenca, Ecuador.

De Wispelaere, L.*; S. Bodé; **P. Hervé-Fernández**; A. Hemp; D. Verschuren and P. Boeckx. (2016). “Temporal and Spatial Partitioning of Water Resources in a Seasonal Dry Tropical Climate”. AGU Chapman conference: Emerging issues in tropical Ecohydrology. Cuenca, Ecuador.

Hervé-Fernández, P.*; Oyarzún, C.; Huyghens, D.; N.E.C. Verhoest and P. Boeckx. (2016). “Assessing the "two water worlds hypothesis" and water sources for native and exotic evergreen species in south-central Chile”. European Geoscience Union (EGU), Vienna, Austria.

De Deurwaerder, H.*; **P. Hervé-Fernández**; C. Stahl; D. Bonal; B. Burban; P. Boeckx and H. Verbeeck. (2016). “Tapping another water source: lianas’ and trees’ below ground competition for water”. European Geoscience Union (EGU), Vienna, Austria.

De Wispelaere, L.; S. Bodé*; **P. Hervé-Fernández**; A. Hemp; D. Verschuren and P. Boeckx. (2016). “Toward a better δD-alkanes paleoclimate proxy; Partitioning of seasonal water sources and xylem-leaf deuterium enrichment according to plant growth form and phenology”. European Geoscience Union (EGU), Vienna, Austria.

Hervé-Fernández, P*; Oyarzún, C.; Huyghens, D.; Boeckx, P. and N.E.C. Verhoest. (2015). “Evaporation losses and sources of water vapor in old-growth native evergreen forest and *Eucalyptus nitens* covered catchments in South-Central, Chile (40°S)”. Boussinesq lecture. Amsterdam, The Netherlands.

Hervé-Fernández, P.*; Oyarzún, C.; Boeckx, P. and N. E. C. Verhoest. (2014). “Water sources during storm events for old growth native evergreen forest and *Eucalyptus nitens* plantation covered catchments, in south central Chile (40°S)”. BIOGEOMON2014. Bayreuth, Germany.

Oyarzún, C. & **P. Hervé-Fernández*.** (2014). "N and P balance from catchments with different land cover, and exportation of nutrients during storm events, in south central Chile (40°S)". BIOGEOMON2014. Bayreuth, Germany.

Hervé-Fernández, P.*; Oyarzún, C.; Boeckx, P. and N. E. C. Verhoest. (2014). "Water sources for native old growth and fast growing exotic plantation ecosystems in southern Chile". Benelux Association of Stable Isotope Scientists (BASIS). Neijmegen, The Netherlands.

Hervé-Fernández, P.*; Oyarzún, C.; Boeckx, P. and N. E. C. Verhoest. (2013). "Hydrological control over nutrient exports in catchments with different land cover in southern Chile". 18th National Symposium on Applied Biological Sciences (NSABS). Ghent, Belgium.

Hervé-Fernández, P.* and C. Oyarzún. (2012). "Transpiration and water use efficiency in native Chilean and exotic species, a useful tool for catchment management?". European Geophysical Union (EGU). Vienna, Austria.

Oyarzún, C*. and **P. Hervé-Fernández**. (2010). Control Hidrologico y Exportacion de Nutrientes en bosques del sur de Chile. Reunion EcoProductos forestales no madereros. Esquel, Argentina.

Hervé-Fernández, P.*; Oyarzún, C. and S. Mulsow. (2010). "Effects of land use conversion over nutrients exportation on catchments from the Cordillera de la Costa, South of Chile". VI Southern Connection Congress. Bariloche, Argentina.